THE UNIVERSITY
of EDINBURGH

Monomer Driven Design of Aromatic-Aliphatic Polyesters Built Through Ring-Opening Polymerisation

THE UNIVERSITY *of* EDINBURGH

Vishalkumar Makwana

A thesis submitted for the Doctor of Philosophy

University of Edinburgh in the School of Chemistry

Year of Submission 2020

Signed Declaration

I declare that this thesis has been composed solely by myself and that it has not been submitted, in whole or in part, in any previous application for a degree. Except where states otherwise by reference or acknowledgment, the work presented is entirely my own.

Parts of this work have been published in the following journals:

- Lizundia, E., Makwana, V. A., Larrañaga, A., Vilas, J. L. and Shaver, M. P., Polym. Chem., 2017, **8**, 3530-3538
- Makwana, V. A., Lizundia, E., Larrañaga, A., Vilas, J. L. and Shaver, M. P., Green Materials, 2018, **6:3**, 85-96

02/02/2020

Abstract

The growing environmental impact of plastic waste has led to extensive research into the life-cycle of polymeric materials. Reduction in the build-up of commodity plastics, such as poly(ethylene terephthalate), has been a hot topic. However, recycling poly(ethylene terephthalate) requires energy intensive conditions and further purification to obtain the starting material phthalic acid after polycondensation. Advances in monomer design have expanded the range of biodegradable polymers accessible to mimic the properties of commercial plastics, whilst giving the advantage of greener recycling methods. Benzodioxepinones with varying *meta*-substituents were subjected to ring-opening polymerisation, using an aluminium salen catalyst to afford a series of novel aromatic-aliphatic polyesters. The polymerisation, catalytic degradation, and thermal behaviours of the polyesters were explored along with their crystallographic structure. The characteristic degradation of poly(2-(2-hydroxyethoxy))benzoate back to its cyclic monomer, through exploitation of the monomer-polymer equilibrium, outweighed the poor thermal properties (T_g (27 °C)) of the polyester. The unique degradability and thermal properties of this polyester gave potential as use in copolymers and blends with poly(lactic acid). Copolymerisation with poly(lactic acid) improved the thermal properties of poly(2-(2-hydroxyethoxy)benzoate) and introduced UV-vis absorbing properties to poly(lactic acid). The copolymers were shown to catalytically degrade, via the use of aluminum salen complexes, and enzymatically degrade, via proteinase K. Altering the electron donating and withdrawing properties of the *meta*-substituents from hydrogen has been shown to tune the rate of degradation and the thermal properties and stability of the polyester. The polymerisation and depolymerisation kinetics

showed faster rates for electron withdrawing groups with selective depolymerisation back to their cyclic monomers in 10 minutes at 110 °C. The thermal characterisation showed varying glass transition temperatures from 29.7 °C to 60.7 °C, with electron withdrawing groups exhibiting higher values. An increase in the melting temperatures and the thermal degradation activation energies of the polyesters were also observed. The tunability and characteristics of this class of aromatic-aliphatic polyesters gives insight into replacing commodity plastics with polyesters that have the ability to be recycled selectively back to their monomers, thus minimising the amount of starting material required to reprocess the plastic.

Lay Summary

The increasing environmental impact of plastic waste has led to research into the possibilities of biodegradable plastics. Poly(ethylene terephthalate) is widely used in plastic bottles and packaging due to its excellent properties. However, poly(ethylene terephthalate) requires harsh conditions to be fully recycled back to its original starting material, without contributing to greenhouse gases. Therefore, extensive research is being done to replace plastics such as poly(ethylene terephthalate) with greener alternatives. The starting materials of the greener alternatives have been carefully designed to give a series of plastics with different properties and different chemical reactivities. The chemical structure of the plastic poly(2-(2-hydroxyethoxy))benzoate was modified to monitor how change in the structure would affect the properties. In addition, the chemical reactivity of the modifications were studied to monitor the effect of modification on the degradation of the plastics through chemical and enzymatic degradation. Poly(2-(2-hydroxyethoxy))benzoate was also combined with the commercially available plastic poly(lactic acid) to improve its properties. The tunability and properties of the synthesised plastics give insight into replacing commercially available plastics with greener alternatives that have the ability to be recycled selectively back to their starting materials and thus minimising the amount of starting materials required to reprocess the plastic.

Acknowledgements

I would like to start off by thanking the Shaver group for helping me settle in during my early days and for their continuous support during the ups and downs of my PhD. Even after the split, into various other groups and those who progressed on to jobs, I have always been able to count on them for academic and moral support.

I would also like to thank the McKeown group for welcoming me in and supporting me through the final hurdle of the roller-coaster that was a PhD.

In addition, I would like to thank Dr Lorna Murray and Mr Juraj Bella with NMR spectroscopy and Dr. Logan Mackay with Mass Spectrometry. I would also like to thank Simon Cummings, Tim Calder and Mark Forrest, who without even knowing made the journey that much easier.

My deepest gratitude goes to Dr Erlantz Lizundia who hosted me at the Univeristy of the Basque Country. Here I was able to progress my research and learn invaluable skills as well as make connections.

Outside of my research I have been extremely fortunate to have my partner in crime, my wife, and amazing parents who not only supported me during the emotionally challenging times, but gave me strength to always see the positive in every situation and to never give up trying.

Lastly I would like to thank the SOFI team for giving me the opportunity to learn in unique ways and giving me the skills I need to be successful in my future career.

Contents

1 Introduction **1**

1.1 Plastics 1

1.2 Biodegradable Polymers 3

1.3 Ring-opening Polymerisation 6

1.4 A Closed Loop - Monomer ⇌ Polymers 15

1.4.1 Poly(lactic acid) 15

1.4.2 Polystyrene and Potential Alternatives 21

1.4.3 Poly(ethylene terephthalate) 24

1.4.4 Benzodioxepinones 29

1.5 Aims 32

2 Monomer Design **33**

2.1 Introduction 33

2.2 Results and Discussion 45

2.2.1 α-Phenyl-β-Propiolactone 45

2.2.2 Substituted Benzodioxepinones 47

3 Polymerisation **52**

3.1 Introduction 52

3.2 Results and Discussion 52

3.2.1 Screening of Polymerisation Conditions for 2,3-DHB 53

3.2.2 Screening of Polymerisation Conditions for Monomer **2** 54

3.2.3 Screening of Polymerisation Conditions for Monomer **1** 57

3.2.4 Screening of Polymerisation Conditions for Monomer **3** 58

3.2.5 Screening of Polymerisation Conditions for Monomer **4** 60
3.2.6 Polymerisation Kinetics 61
3.2.7 Catalysed Degradation Studies 70
3.2.8 Copolymers 79
3.2.9 Block Copolymer Catalytic Degradation 86
3.2.10 Enzymatic Degradation 88

4 Characterisation **94**
4.0.1 Introduction 94
4.1 Results and Discussion 95
4.1.1 Thermal Analysis 95
4.1.2 Dynamic Mechanical Analysis 112
4.1.3 Wide Angle X-Ray Diffraction 115
4.1.4 Copolymers: Thermal Analysis 122
4.1.5 Copolymers: Dynamic Mechanical Analysis 125
4.1.6 Copolymers: Wide Angle X-Ray Diffraction 127
4.1.7 Copolymers: Optical Properties 128
4.1.8 Copolymers: Morphology 129
4.1.9 Blends: Thermal Analysis 132
4.1.10 Blends: Dynamic Mechanical Analysis 137
4.1.11 Blends: Optical Properties 139
4.1.12 Blends: Morphology 140

5 Conclusion and Future Work **143**
5.1 Future Work 146

6 Experimental **148**
6.1 General considerations and materials 148
6.2 MeAl[salen] 149
6.2.1 Synthesis of 2,4-di-tert-butylsalicylaldehyde 149
6.2.2 Synthesis of salen 149
6.2.3 Synthesis of MeAl[salen] 150

6.3 Synthesis of thiazolium catalyst . . . 151
6.4 α-phenyl-β-propiolactone . . . 152
6.4.1 Synthesis of 2-bromo-2-phenylethanol . . . 152
6.4.2 Synthesis of α-phenyl-β-propiolactone via a palladium catalyst 152
6.4.3 Synthesis of α-phenyl-β-propiolactone via a rhodium catalyst . 153
6.5 ROP of α-phenyl-β-propiolactone . . . 153
6.5.1 ROP using MeAl[salen] . . . 153
6.5.2 ROP using TBD . . . 154
6.6 Synthesis of 2-(2-hydroxyethoxy)-5-R-benzaldehyde . . . 154
6.6.1 2-(2-hydroxyethoxy)-5-methyl-benzaldehyde . . . 155
6.6.2 2-(2-hydroxyethoxy)-5-methoxy-benzaldehyde . . . 155
6.6.3 2-(2-hydroxyethoxy)-5-fluoro-benzaldehyde . . . 155
6.6.4 2-(2-hydroxyethoxy)-5-bromo-benzaldehyde . . . 156
6.6.5 2-(2-hydroxyethoxy)-5-nitro-benzaldehyde . . . 156
6.7 Synthesis of 2-hydroxy-4-trifluoromethyl-benzaldehyde via *ortho*-formylation 156
6.8 Synthesis of 2-hydroxy-4-cyano-benzaldehyde using the Duff reaction 157
6.9 Synthesis of 2-hydroxy-4-trifluoromethyl-benzaldehyde using the Duff reaction . . . 157
6.10 Synthesis of Monomers **1** to **4** . . . 158
6.10.1 Monomer 1 . . . 158
6.10.2 Monomer 2 . . . 159
6.10.3 Monomer 3 . . . 159
6.10.4 Monomer 4 . . . 159
6.11 Synthesis of P2HEB . . . 159
6.12 Synthesis of Polymers **1** to **4** . . . 160
6.12.1 Polymer 1 . . . 160
6.12.2 Polymer 2 . . . 161
6.12.3 Polymer 3 . . . 161
6.12.4 Polymer 4 . . . 161
6.13 Synthesis of BnOH-initiated PLLA . . . 161

6.14 Synthesis of 1,3-propanediol initiated PLLA 162
6.15 Synthesis of P2HEB-PLLA diblock copolymer 163
6.16 Synthesis of P2HEB-PLLA-P2HEB triblock copolymer 164
6.17 Degradation Studies 165
6.17.1 Preparation of P2HEB polymer films 165
6.17.2 Enzymatic degradation of P2HEB 165
6.17.3 Catalytic degradation of P2HEB 165
6.18 Blend preparation 165
6.19 Characterisation 166
6.19.1 Differential scanning calorimetry (DSC) 166
6.19.2 Thermogravimetric analysis (TGA) 166
6.19.3 Dynamic Mechanical Analysis (DMA) 166
6.19.4 UV-Vis spectroscopy (UV-Vis) 167
6.19.5 Wide angle X-Ray diffraction (WAXD) 167
6.19.6 Morphology 167

List of Figures

1.1 Plastic production 2

3.1 Monitoring the ring-opening polymerisation of monomers **1** to **4** . . . 63

3.2 Combined plot of the ring-opening polymerisations to afford polymers **1** to **4** 64

3.3 Natural log of the conversion of monomer to polymer against time . . 65

3.4 Rate of polymerisation in relation to the Hammett Constant 66

3.5 DOSY NMR spectrum of monomer **2** and MeAl[salen] 69

3.6 DOSY NMR spectrum of monomer **8** and MeAl[salen] 69

3.7 Depolymerisation of P2HEB 71

3.8 Depolymerisation of polymers **1** to **4** 72

3.9 Depolymerisation of polymers **1** to **4** at 70 °C 73

3.10 Depolymerisation of polymers **1** to **4** at 110 °C 74

3.11 Depolymerisation of polymers **1** to **4** and P2HEB at 110 °C by ^{1}H NMR 75

3.12 Combined depolymerisation plots and rates of depolymerisation of polymers **1** to **4** and P2HEB 77

3.13 Types of copolymers 79

3.14 DOSY NMR spectrum of the diblock copolymber **1** synthesised with $Sn(oct)_2$ 82

3.15 Diblock copolymer **1** and triblock copolymer**2** 83

3.16 ^{13}C and DOSY NMR spectra of the diblock copolymer **1** 84

3.17 ^{13}C and DOSY NMR spectra of the triblock copolymer **2** 85

3.18 Degradation of the diblock copolymer **1** and triblock copolymer **2** using MeAl(salen) (0.0045 mol) 87
3.19 Degradation of the diblock copolymer **1** and triblock copolymer **2** using MeAl(salen) (0.045 mol) 88
3.20 Enzymatic degradation of P2HEB monitored by GPC 89
3.21 Enzymatic degradation of P2HEB monitored by ^{1}H NMR spectroscopy 91
3.22 Enzymatic degradation of the diblock copolymer **1** and the triblock copolymer **2** monitored by GPC 92
3.23 DOSY NMR of the degradation of diblock copolymer **1** and triblock copolymer **2** 93

4.1 DSC scans of P2HEB of molecular weight 11,000 g mol^{-1} 96
4.2 DSC scans of P2HEB of molecular weight 11,000, 40,000 and 80,000 g mol^{-1} 96
4.3 DSC scans of polymer **1** 97
4.4 DSC scans of polymer **2** 97
4.5 DSC scans of polymer **3** 98
4.6 DSC scans of polymer **4** 98
4.7 Isothermal treatments of P2HEB 99
4.8 Isothermal treatment of polymers **1** to **4** 100
4.9 Isothermal treatment of polymer **4** at 90 °C 101
4.10 Second DSC scan of polymers **1** to **4** after isothermal treatment . . . 101
4.11 Isothermal treatment of polymer **4** at 140 °C 102
4.12 DSC of P2HEB at different heating rates 103
4.13 First DSC scans of polymers **1** to **4** and P2HEB 104
4.14 Second DSC scans of polymers **1** to **4** and P2HEB 105
4.15 TGA traces of P2HEB 106
4.16 TGA traces of polymers **1** to **4** 107
4.17 TGA traces of polymers **2** and **4** under O_2 108
4.18 DTG traces of polymers **1** to **4** and P2HEB 110

4.19 Kissinger plot to calculate the activation energy of polymers **1** to **4** and P2HEB 111
4.20 Liner Viscoelastic Region of P2HEB 113
4.21 DMA trace of P2HEB 113
4.22 WAXD patterns of polymers **1** to **4** and P2HEB 115
4.23 Cartoon representation of the configurations of polymers **1** to **4** and P2HEB 118
4.24 Cartoon representation of parallel and anti-parallel polymer chains in polymer **1** 119
4.25 High temperature WAXD of polymers **1** to **4** and P2HEB 121
4.26 DSC traces of the diblock copolymer **1** and the triblock copolymer **2** 122
4.27 Isothermal treatments of the diblock copolymer **1** and the triblock copolymer **2** 124
4.28 TGA traces of the diblock copolymer **1** and triblock copolymer **2** . . 124
4.29 Liner Viscoelastic Region of the diblock copolymer **1** 126
4.30 DMA traces of the diblock copolymer **1** and the triblock copolymer **2** 126
4.31 WAXD for the diblock copolymer **1** and triblock copolymer **2** 127
4.32 High temperature WAXD for the diblock copolymer **1** and triblock copolymer **2** 128
4.33 UV-Vis transmittance of the diblock copolymer **1** and triblock copolymer **2** 128
4.34 SEM of the diblock copolymer **1** and triblock copolymer **2** 130
4.35 SEM of the diblock copolymer **1** and triblock copolymer **2** 131
4.36 DSC traces of the PLLA/P2HEB blends 132
4.37 DSC traces of PLLA blended with polymers **1** to **4** 134
4.38 TGA traces of the PLLA/P2HEB blends 136
4.39 TGA traces of PLLA blended with polymers **1** to **4** 136
4.40 DMA traces of the PLLA/P2HEB blends 138
4.41 DMA traces of PLLA blended with polymers **1** to **4** 138
4.42 UV-Vis of polymers **1** to **4** and their respective blends with PLLA . . 139

4.43 SEM of the PLLA/P2HEB blends 141
4.44 SEM of PLLA blended with polymers **1** to **4** 141

List of Schemes

1.1 Polycondensation 4
1.2 Chain growth polymerisation 5
1.3 Example of lactones 7
1.4 Cationic ring-opening polymerisation 7
1.5 Anionic ring-opening polymerisation 8
1.6 Coordination-insertion ring-opening polymerisation 9
1.7 ROP using the organocatalysts TBD 10
1.8 Transesterification 12
1.9 Synthesis of salen 13
1.10 Aluminium complex 15
1.11 Life cycle of PLA 16
1.12 Tacicity of PLA 17
1.13 Catalysts used to tune tacticity 18
1.14 Catalytic mechanism of Proteinase K 20
1.15 Synthesis of polystyrene 22
1.16 Polystyrene mimics 23
1.17 Synthesis of PET 25
1.18 Catalytic mechanism of PETase 28
1.19 P2HEB monomer-polymer equilibrium 31

2.1 Methodologies to afford β-lactones 34
2.2 Carbonylation of an epoxide using a lewis acid-cobalt catalyst 36
2.3 Aluminum salen complexes for carbonylation 37
2.4 Carbonylation of epoxides using a rhodium catalyst 38

2.5 Carbonylation of epoxides using a palladium catalyst 39
2.6 Synthesis of benzodioxepinones via styrene oxide 39
2.7 *Ortho*-formylation of phenols to afford salicylaldehydes 41
2.8 Synthesis of benzodioxepinone derivatives 42
2.9 Monomers chosen 43
2.10 Conformations of π-π interactions 44
2.11 Offset parallel interaction of two adjacent aromatic rings 45
2.12 Synthesis of α-phenyl-β-propiolactone using a palladium catalyst . . . 46
2.13 Synthesis of α-phenyl-β-propiolactone using a rhodium catalyst . . . 47
2.14 Reaction scheme of the synthesis of a benzodioxepinone derivative . . 48
2.15 Monomers with increasing electron withdrawing properties 49
2.16 Duff reaction mechanism 51

3.1 Ring-opening polymerisation of the benzodioxepinone derivatives . . . 53
3.2 Coordination of THF to MeAl(salen) 55

Abbreviations

2,3-DHB 2,3-dihydro-5H-1,4-benzodioxepin-5-one

AFM Atomic force microscopy

AROP Anionic ring-opening polymerisation

BHET Bis(2-hydroxyethyl) terephthalic acid

binap 2,2'-bis(diphenylphosphino)-1,1'-binaphthyl)

β-BL β-butyrolactone

BnOH Benzyl alcohol

CCDC Cambridge Crystallographic Data Centre

CH_2 Methine group

ϵ-CL ϵ-caprolactone

CO Carbon monoxide

CROP Cationic ring-opening polymerisation

$Đ$ Dispersity

DBU 1,8-diazabicyclo [5.4.0]undec-7-ene

DMA Dynamic mechanical analysis

DMF Dimethylformamide

DOSY Diffusion-ordered spectroscopy

DOX 1,3-dioxolan-4-one

DPP Diphenyl phosphate

DSC Differential scanning calorimetry

DTG$_{max}$ Maximum degradation rate

E$_a$ Activation energy

E' Storage modulus

E" Loss modulus

EDG Electron donating group

EWG Electron withdrawing group

GPC Gel permeation chromatography

Δ**H**$_{cc}$ Enthalpy of cold crystallisation

Δ**H**$_m$ Enthalpy of fusion

HTMA Hexamethylenetetramine

L-manOCA O-carboxyanhydride

LVR Linear viscoelastic region

MHET Mono(2-hydroxyethyl) terephthalic acid

NHC N-heterocyclic carbenes

NMR Nuclear magnetic resonance

OMe Methoxy

P2HEB Poly(2-(2-hydroxyethoxy)benzoate)

P3HB Poly(3-hydroxybutyrate)

PBS Poly(butylene succinate)

PCL Polycaprolactone

PDF Powder diffraction file

PDLA Poly(D-lactic acid)

PEP Poly(ethylene phthalate)

PET Poly(ethylene terephthalate)

PHBV Poly(3-hydroxybutyrate-co-3-hydroxyvalerate)

PLA Poly(lactic acid)

PLLA Poly(L-lactic acid)

PMMA Poly(methyl methacrylate)

Poly(PhPL) Poly(phenyl propiolactone)

ROP Ring-opening polymerisation

Salen N,N'-bis(salicylidene)-1,2-ethanediimine

Salen N,N'-bis(salicylidene)-1,2-ethanediamine

SEM Scanning electron microscopy

σ Electronic substituent parameter

Sn(oct)$_2$ Tin(II) octanoate

$\mathbf{T}_{5\%}$ The first 5 % weight loss

$\mathbf{T}_g$ Glass transition temperature

$\mathbf{T}_m$ Melting point temperature

$\mathbf{T}_{cc}$ Cold-crystallisation temperature

$\mathbf{T}_{peak}$ Maximum degradation

TBD 1,5,7-triazabicyclo[4.4.0]dec-5-ene

TEA Triethylamine

TGA Thermogravimetric analysis

THF Tetrahydrofuran

TLC Thin layer chromatography

WAXD Wide angle X-ray diffraction

$\boldsymbol{M}_n$ Number average molecular weight

$\boldsymbol{M}_w$ Weight average molecular weight

Chapter 1

Introduction

1.1 Plastics

A plastic is a type of material that is typically synthetically synthesised and has the ability to be moulded into various shapes above a certain temperature and the capability to hold that shape when cooled back down. Plastics are defined by their characteristic ability to deform irreversibly without breaking. Research and manufacturing of plastics has been on an exponential incline since the early 19^{th} century. Originating from the accidental discovery of polystyrene, through distillation of storax resin obtained from Sweetgum tree, by Eduard Simon in 1839[1] and the accidental synthesis of poly(vinyl chloride) by Eugen Baumann in 1872.[2] It wasn't until the early 20^{th} century the first ever fully synthetic plastic was introduced.[3] Bakelite™was synthesised by Leo Baekeland in 1907 through polycondensation of phenol and formaldehyde.[4] The facile synthesis of Bakelite made it ideal for industrial scale production. Bakelite was extensively produced due to its ability to be moulded for a wide range of applications, in addition to its electrical insulating and heat resistance properties.[4] The versatility of synthetic and natural plastics observed through the 20^{th} century has led to the reliance of plastics in modern society. Plastics have become a foundation to performing everyday tasks, from polyethylene in carrier bags to polystyrene and poly(ethylene terephthalate) (PET) in packaging and disposable cutlery.[5,6]

The driving force behind the increase in production and use of plastics is the characteristic ability to adapt them to a range of applications by exploiting the synthetic pathways to tune the thermal and mechanical properties. Plastics can behave as a glassy solid with a rigid body below a certain temperature, denoted as its glass transition temperature (T_g), and behave rubber-like with the ability to be molded or shaped above that temperature. The T_g influences the ability of a plastic to take strain when subjected to stress. Above the T_g the plastic is typically able to withstand more strain than below the T_g.[7] The facile tuning of the T_g, along with the mechanical properties, through selection and design of the starting materials, have increased the scope of applications for plastics.

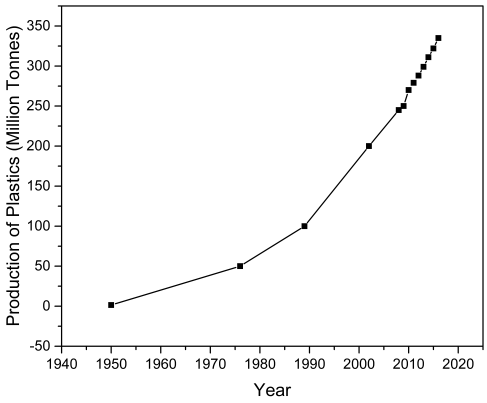

Figure 1.1: Modified graph of the plastic production since 1950.[8]

The global production of plastics from the 1950's to 2016 has rapidly increased from 2 million tonnes to 380 million tonnes (Figure 1.1).[8] The attractiveness of plastics is rapidly being offset due to the increased awareness of the impact plastics can inflict on land and aquatic ecosystems due to their lack of degradation into carbon dioxide, water, methane and other simple organic molecules.[9] Over a period of 65 years approximately 8300 million tonnes of plastics have been produced, with only 9% recycled into single-use items; 12% incinerated, contributing significantly to global warming through emission of methane gas; and 60% deposited into landfill.[9] In addition, marine life is suffering due to plastic contributing to 70% of total litter deposited in the ocean.[10] The expectation by 2050 is that the amount of plastic in

landfill or in marine ecosystems will reach 12 billion tonnes.[9] This is an alarming figure and is detrimental to the environment unless the concern of production and degradation of plastic is addressed.

The recycling and reprocessing of plastics to obtain identical or similar thermal and mechanical properties to the original material is ideal to prevent single-use plastics. However, this is challenging due to the method of separation of plastics. The process of melting and extruding removes the original morphology and properties of the plastic and typically leads to inferior properties if repeated.[11] This is further affected by the presence of other plastics acting as impurities and therefore separation of plastics by type is ideal. Separation methods exist in industrial sites and work by exploiting the hydrophobicity, mass, density, and functionality of plastics. However, this is an energy intensive and inefficient process.[12]

The European Union targets approved in April 2018[13] to recycle 50% of plastics produced by 2025 and 55% by 2030, are being implemented.[14] This will not only drive industry to increase their efficiency in separation and recycling but also discourage deposition of plastics into landfill and marine ecosystems.

Despite the current methods of separation and the advances in recycling targets, the forever increasing demand for plastics along with their diminishing thermal and mechanical properties per cycle of reprocessing has led to extensive research into the life-cycle of biodegradable polymeric materials.[15]

1.2 Biodegradable Polymers

Polymers that eventually degrade into natural by-products such as CO_2 and H_2O are classed as biodegradable irrespective of the origin of the starting material.[16,17] Degradation is not limited to microorganisms or enzymes but also includes chemical[18], thermal[19], photolytic[20] and hydrolytic degradation[21]. In addition to the naturally occurring biodegradable polymers such as proteins, polysaccharides and poly(hydroxyalkanoate)s;[17,22] synthetic biodegradable polymers predominantly contain amide, ether and ester linkages in their backbone.[23] Polyesters have received great interest due to their characteristic ability to be degraded through hydrolytic

cleavage of the ester linkages.[24] Their limited thermal and mechanical properties are outweighed by their reduced environmental impact, non-toxic degradation products and potential to be functionalised.[25,26]

Polyesters are separated into two subclasses, aliphatic polyesters and aromatic polyesters. Aliphatic polyesters, such as poly(β-hydroxy acid) or poly(lactic acid) (PLA), contain no aromaticity in the polymer backbone. Aromatic polyesters on the other hand do and the widely used PET is a classic example of an aromatic polyester.[27]

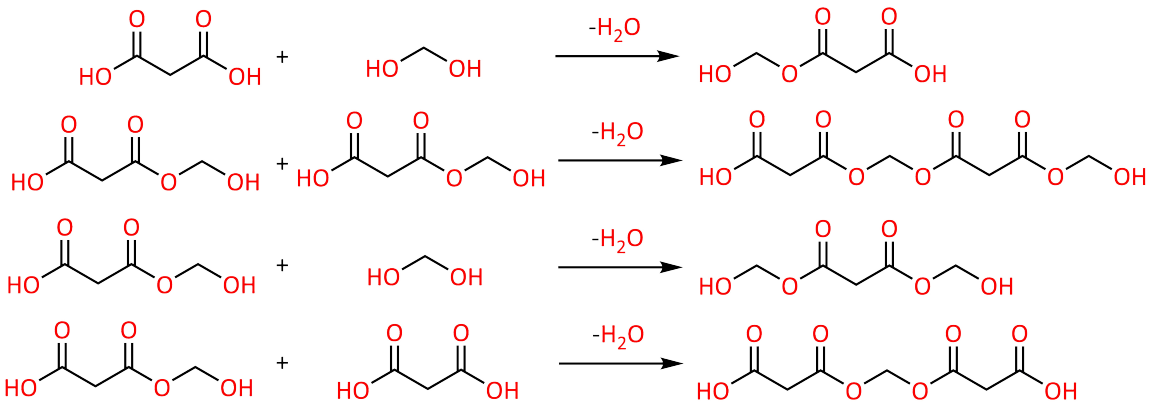

Scheme 1.1: Condensation reaction between a diol and dicarboxylic acid to afford dimers with subsequent condensation reactions to form trimers, tetramers and oligomers.[28]

Traditional polyesters were obtained by polycondensation, a subclass of step-growth polymerisation. Step-growth polymerisation allows the reaction of two bi-functional monomers containing nucleophilic (diol) and electrophilic (dicarboxylic acid) components.[29] These monomers react, expelling water, to form a dimer, which then reacts with another dimer to form a tetramer or with another monomer to form a trimer. The trimers and tetramers can subsequently react with unreacted monomers, dimers, trimers or tetramers to eventually form oligomers and polymers (Scheme 1.1).[27,30] In order to drive the reaction to form polymers it was found that the elimination of water was vital, either through distillation under vacuum or specialist equipment such as the Dean-Stark apparatus.[31] Challenges with achieving high molecular weights were observed due to the poor degree of polymerisation.

This is determined by the Carothers equations (1.1 and 1.2), where $\overline{X}_n$ is the number average value of the degree of polymerisation, p is the extent of polymerisation, N_0 is the amount of monomer in moles and N is the amount of monomer left after a certain time in moles.[32] Furthermore, broad molecular weight distributions (poor dispersity) are observed due to the random nature of the polycondensation. This reflects in the thermal and mechanical properties of the resultant polymers and hence limits their applications range.[33,34]

$$\overline{X_n} = \frac{1}{1-p} \tag{1.1}$$

$$p = \frac{N_0 - N}{N_0} \tag{1.2}$$

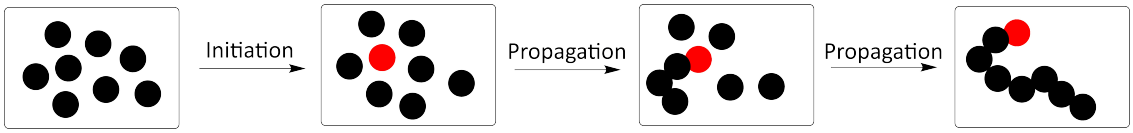

Scheme 1.2: Initiation and propagation at the active chain end.

An alternative type of polymerisation is chain-growth polymerisation, which unlike step-growth where any molecule can react, only permits the reaction at the active chain end of one molecule. Chain-growth polymerisation occurs through initiation to generate a reactive species, followed by propagation leading to growth of the chain. The polymerisation is terminated when the active site is quenched (Scheme 1.2). This leads to the molecular weight of the resultant polymer increasing rapidly at low monomer conversions compared to step-growth polymerisation.[29] Research into well-controlled polymerisation techniques, utilising chain-growth polymerisation, have been widely explored. Ring-opening polymerisation (ROP) is a particular subset of chain-growth polymerisation that has sparked great interest. ROP utilises the ring strain of cyclic monomers to produce higher molecular weight polyesters with narrow dispersities with the additional advantage of being functional group tolerant.[35,36] Dispersity ($Đ$) is the measure of the molecular weight range of a polymeric material. It is ratio of the weight average molecular weight (M_w) and the

number average molecular weight (M_n) (Equation 1.3). M_w and M_n are derived from Equation 1.4 and 1.5, where N_i is the number of molecules and M_i is the molar mass.[27]

$$Đ = \frac{M_w}{M_n} \tag{1.3}$$

$$M_w = \frac{\sigma_i N_i M_i^2}{\sigma_i N_i M_i} \tag{1.4}$$

$$M_n = \frac{\sigma_i N_i M_i}{\sigma_i N_i} \tag{1.5}$$

Polyesters derived from ROP of cyclic esters have been widely used as biomedical[37], agricultural[38], pharmalogical[39] and ecological[40] plastics. The mechanistic approach of ROP is typically governed by the type of catalyst present in the system but can also be influenced by the type of initiator and monomer present. Extensive research into catalytic design has allowed access to well-controlled higher molecular weight polyesters with potential for functionalisation.

1.3 Ring-opening Polymerisation

ROP is considered to be a type of living polymerisation where termination by the coupling of two growing chains in typical chain growth polymerisation does not occur. Termination in the case of a living polymerisation is a result of two factors, the source of monomers is depleted, or the reaction is externally quenched. The molecular weight of the resultant polymer can be controlled through the ratio of initiator to monomer, where a large amount of monomer or small amount of initiator would lead to a higher molecular weight as a result of fewer reactive end chains resulting in longer chains. Addition of further monomer to the reaction vessel would continue propagation without termination. This characteristic can be exploited to afford various architectures of polymers including gradient, random and block copolymers. ROP has the potential to expand the monomer scope to access a range of polymers with characteristic properties.[41]

There are several sub-classes of ROP which are denoted by the type of catalyst present in the system. Cyclic esters (lactones) such as lactide, β-butyrolactone (β-BL), ϵ-caprolactone (ϵ-CL) and glycolide, as well as cyclic carbonates and cyclic phosphoesters are well known to undergo ROP either via anionic, cationic or coordination-insertion depending on the nature of the catalyst (Scheme 1.3).[42]

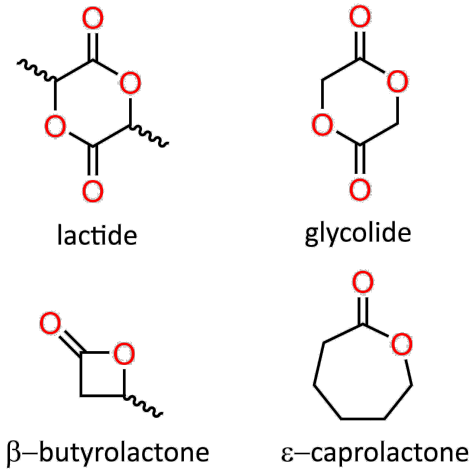

Scheme 1.3: Examples of cyclic esters (lactones).

Organocatalysts were widely explored and further developed in ROP due to their commercial availability and tolerance to bench conditions. Organocatalysts exploit different mechanistic approaches to ROP based on their chemical properties. Organocatalysts that act as Brønsted acids undergo cationic ring-opening polymerisation (CROP) and those that act as Brønsted bases undergo anionic ring-opening polymerisation (AROP).[43]

In CROP, positively charged ions or acids activate the monomer to initiate polymerisation[44] via transfer of a proton to the monomer to generate an electrophilic centre (Scheme 1.4).[41] Common Brønsted acids include dry HCl, H_2SO_4, carboxylic acids, sulfonic acids, and phosphoric acids.[45]

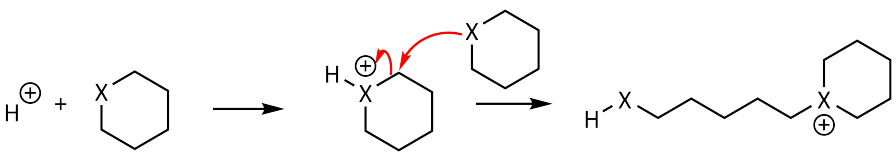

Scheme 1.4: Brønsted acid initiation with a positively charged intermediate.[41]

In contrast, the initiation step in AROP is attributed to the deprotonation of the initiator, thus affording a nucleophilic centre.[44] The position at which ring-opening of the cyclic systems occurs depends upon the substituents attached to the system as well as the catalyst (Scheme 1.5).[41] A wider range of Brønsted bases, such as N-heterocyclic carbenes, have been explored due to their exceptional catalytic activity.[43] However, Brønsted bases have the potential to contribute to transesterification due to their basicity and the exposed negative charge on the active chain-end if the reaction is not monitored.

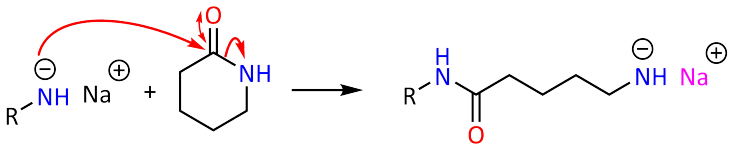

Scheme 1.5: ring-opening of a cyclic system with a negatively charged initiator.[41]

Another category of catalysts are metal-based Lewis acid catalysts. These catalysts can be easily regenerated, however are relatively sensitive depending on the nature of the metal centre used. Certain metal centres are deactivated by oxygen and water thus require anhydrous and inert experimental conditions.[41] Lewis acid catalysts were discovered to undergo a coordination-insertion ring-opening polymerisation via three steps (Scheme 1.6).[46,47] The Lewis acid alkoxide (the metal centre already bound to the alcohol initiator) coordinates to the carbonyl oxygen of the monomer. The carbonyl undergoes nucleophilic attack by the metal-alkoxide bond followed by the bond cleavage of the C-O bond opening the cyclic ester. The Lewis acid catalyst can then be cleaved from the chain end by simple displacement of the metal-alkoxide bond by another OR group such as methoxy from methanol.[48] Traditional early Lewis acid catalysts such as tin(II) octanoate ($Sn(oct)_2$) or early aluminium alkoxides such as $AlEt_3/H_2O$[49,50] and $Al(O^iPr)_3$[51] have limitations due to their toxicity.[52]

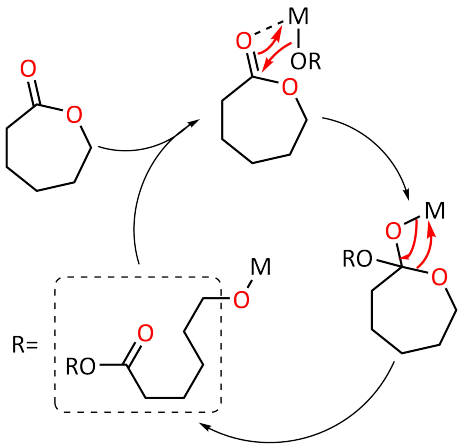

Scheme 1.6: Coordination-insertion mechanism using a metal-based Lewis acid catalyst.[46]

$Sn(oct)_2$ was among the first catalysts to provide control over ROP,[53] demonstrating excellent catalytic activity, giving high conversions and producing high molecular weight polymers. $Sn(oct)_2$ is stable and highly soluble in organic solvents, however the challenge in removal from the resultant polymer and its toxicity raises concerns. In addition, limited monomer scope, high experimental temperatures and tendency for transesterification has led research into alternative catalysts.[54]

Organocatalysts such as 1,5,7-triazabicyclo[4.4.0]dec-5-ene (TBD), 1,8-diazabicyclo [5.4.0] undec-7-ene (DBU) and thiourea-based bifunctional organocatalysts are known to be less toxic and can act as super bases to afford polymers in a fraction of time compared to the early traditional ROP catalysts.[55]

TBD is a Brønsted base that has an unusual ROP mechanism (Scheme 1.7). It acts as a bifunctional catalyst that activates the initiator and monomer simultaneously via two different mechanistic approaches.[55] It can either act as a nucleophile and activate the carbonyl group of the monomer (Scheme 1.7, Mechanism A) or act as a Lewis acid-base catalyst and form hydrogen bonds with the carbonyl oxygen of the monomer and the hydroxyl group of the initiator/chain end (Scheme 1.7, Mechanism B).

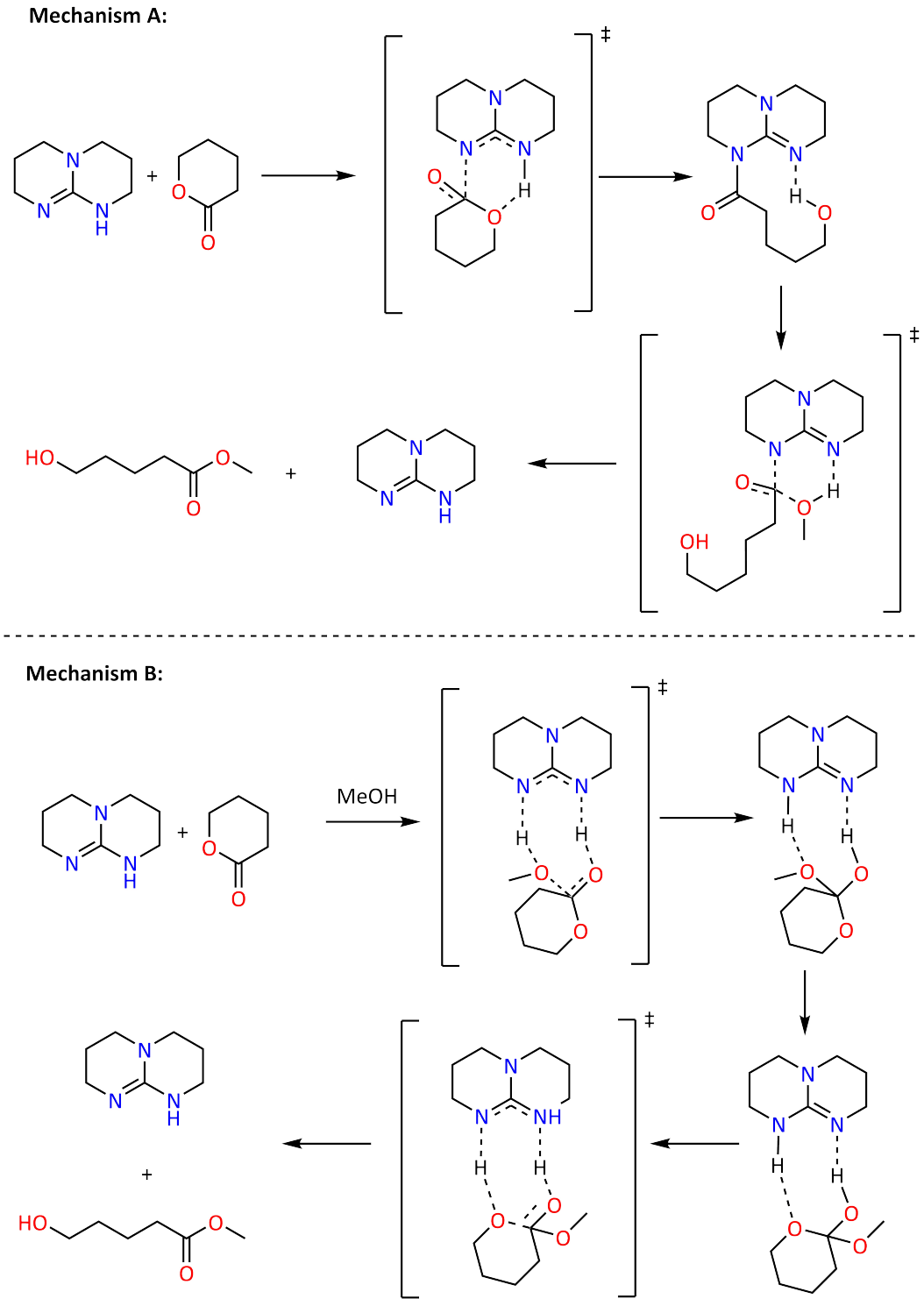

Scheme 1.7: Mechanism A: nucleophilic catalytic mechanism, Mechanism B: acid-base catalytic mechanism.[55]

TBD has demonstrated high reactivity for the ROP of the monomer lactide, affording PLA with conversions above 95% in just one minute at room temperature.[43] TBD, being a strong base, has the potential to cause transesterification of PLA and other polymers if the reaction is not monitored and therefore a balance between rates of polymerisation and control is vitial. Transesterification results in broader molecular weight distributions, loss in tacticity and poorer thermal and mechanical properties. Transesterification is promoted by long reaction times and high reaction temperatures.[55]

Transesterification is unfavourable and arises from the reaction of a catalytic centre on the end of a propagating chain with either a carbonyl along itself (intramolecular) or with a carbonyl on another polymer chain (intermolecular) (Scheme 1.8). The result of intramolecular transesterification is shorter or cyclic chains and the result of intermolecular transesterification is polymer chains of different lengths and thus unpredictable molecular weights with a broad dispersity.[56]

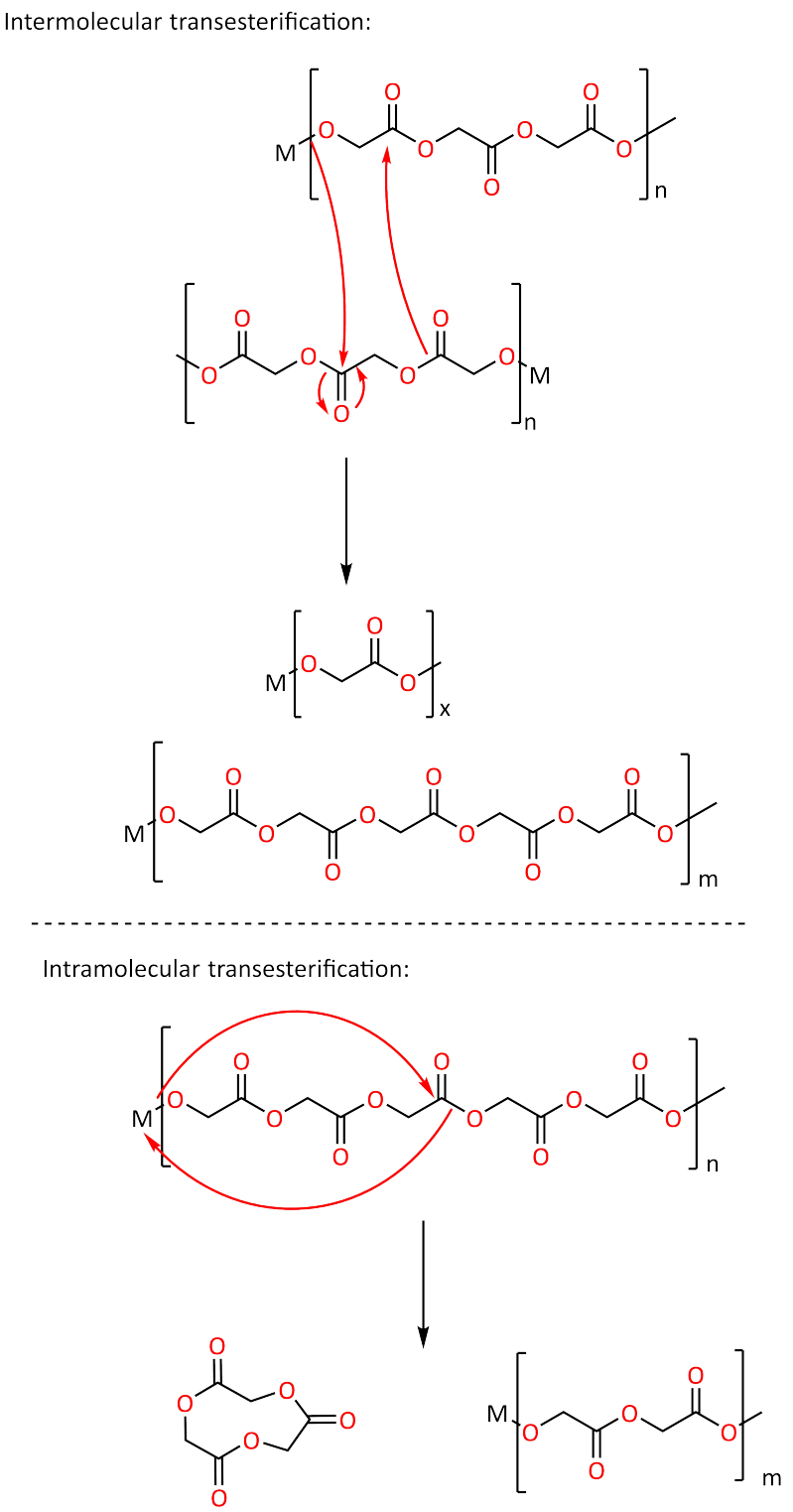

Scheme 1.8: Intermolecular and Intramolecular transesterification, where M is the catalyst.[56]

Introducing selectivity and minimising transesterification compromises on the rate of polymerisation. Aluminium-based catalysts have been extensively studied and developed to demonstrate minimal transesterification with excellent control over polymerisation.[57] The first ligand based aluminium complex with a single site for activity was discovered by Spassky in 1989.[58] Spassky utilised the aluminium complex, derived from the reaction of the ligand (R)-3,3-dimethyl-1,2-butanediol and trialkyl aluminium, in the ROP of β-butyrolactone. The polymerisation yielded low conversions (18%) even after 18 days at 20°C indicating poor catalytic activity.[59] After investigation into the activity, Spassky discovered that the use of a bridged ligand such as (N,N'-bis(salicylidene)-1,2-ethanediamine) (salen), derived from the condensation reaction of two equivalents of a substituted 2-hydroxybenzaldehyde and one equivalent of a diamine (Scheme 1.9),[60] improved the polymerisation conversion up to 70%. However, this was still being considered as low activity compared to literature catalysts at the time such as $Al(O^iPr)_3$. Alternative bridged ligands such as cyclohexyl and binaphthyl diimine also exist with the disadvantages of transesterification at higher conversions leading to poor control.[59,61]

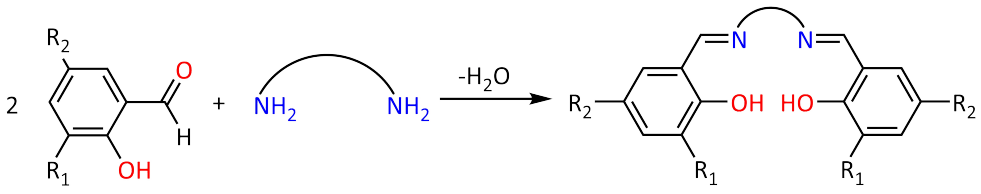

Scheme 1.9: Synthesis of salen from the substituted 2-hydroxybenzaldehyde and the chosen diamine.[60]

Salen based ligands attached to an aluminium core were further explored by altering the electron withdrawing and electron donating groups on various positions on the ligand (Scheme 1.10). Gibson screened a wide range of variations of the salen ligand for the polymerisation of *rac*-lactide. It was experimentally found that room temperature polymerisations of both the enantiomerically pure L-lactide and the *rac*-lactide were accessible through introduction of electron withdrawing groups on the salen ligand. Well controlled polymerisations with narrow dispersities were achieved due to the inhibition of transesterification at lower temperatures. How-

ever, the rate of polymerisation was extremely low with only 24% conversion after 24 hours.[62] Gibson explored the consequences of altering the diimine bridge and electronic and steric properties of the phenoxide substituents on the polymerisations. Increasing the size of substituents on the aromatic rings (R3) (Scheme 1.10) led to the increase in control over tacticity with slower polymerisation rates compared to the hydrogen substituent. In addition, electron withdrawing groups, such as replacement of ^{t}butyl with chlorine, increased rate of polymerisation and the temperature range at which they could occur, with the dichloride substituant being the fastest. The rate of polymerisation followed the trend of ^{t}Bu$<$ H $<$ Cl $<$ Cl_2 for the phenoxide substituents.[57,63] Changing the nature of the diimine bridge (R1) on the ligand was also shown to influence the rate of polymerisation and have tacticity control. Increasing the length of the bridge by a CH_2 group (methine) showed an increase in rate of polymerisation.[64] Further modification to the bridge by replacing the ethylene bridge with either a 2,2-dimethyl substituted propylene linker or a phenylene group showed a dramatic increase to the rate of polymerisation. Gibson concluded that the length of the linker determined the flexibility and accessibility of the metal coordination sphere to the respective initiator and monomer for ROP.[62] Al[salen] along with [salan], where in salan the diamine bridge is replaced with a diimine bridge, were further explored by the Shaver group.[64] Further study on the basic ligand frame work of salen gave insight to the point of saturation of the catalyst, showing that that high molecular weight PLA was achievable where the catalyst would only be saturated if 1000 equivalents of monomer was present.[64] The Shaver group investigated the monomer scope of these catalysts starting with lactide, ϵ-CL, and β-BL. Although previous polymerisations of β-BL with Al[salen] had shown poor conversions, the ^{t}Bu substituted Al[salen] showed excellent conversions with tolerance to a range of solvents and temperatures, for up to 500 equivalents of β-BL. The same catalyst is able to polymerise ϵ-CL, in under 15 minutes, and lactide in three hours, with narrow dispersities.[64] Although other variations of Al[salen] were investigated, in terms of monomer scope, the ^{t}Bu variation was chosen for the ROP of our monomers due to the versatility and the ability to have control of the

polymerisation by altering the time and temperature.

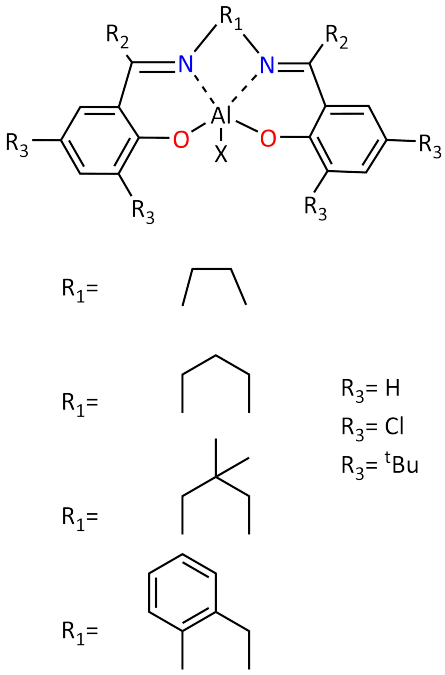

Scheme 1.10: Altering the substituents on an aluminium core to tune polymerisation.[57]

1.4 A Closed Loop - Monomer ⇌ Polymers

1.4.1 Poly(lactic acid)

The transition from lactic acid to lactide as the building block of PLA originated from Wallace Hume Carothers *et al.* in 1932 and later patented by Du Pont in 1954.[65] It wasn't until the 1990's where L-lactide was subjected to ROP to afford high molecular weight PLLA, exhibiting potential to replace commodity plastics due to its characteristic biodegradability, biocompatibility and high mechanical properties.[66] This revolution led to the use of PLA in not only industrial scale packaging or disposable cutlery but also in the biomedical field including drug delivery systems,[67,68] tissue engineering and coatings.[69]

The early synthesis of PLA involved polycondensation of lactic acid under high temperatures (180-200 °C) and low pressures (5 mmHg) to achieve high molecular weights.[70] Upon method development due to the attractiveness of PLA, the cyclic

diester lactide was used to afford high molecular weight PLA at lower temperatures and shorter reaction times. PLA originates from harvested corn starch where the corn is processed to obtain sugars that are fermented via bacteria producing lactic acid. Lactic acid then undergoes step-growth polymerisation and back biting to form the cyclic dimer lactide.[54] The back-biting process is facilitated through metal complexes such as Sn, Al, and Zn that form a metal-alkoxide bond with the hydroxyl group on the end of the oligomer/polymer chain. Due to the equilibrium between oligomeric PLA and lactide, recrystallisation or sublimation is required to obtain pure lactide (Scheme 1.11).[54,71]

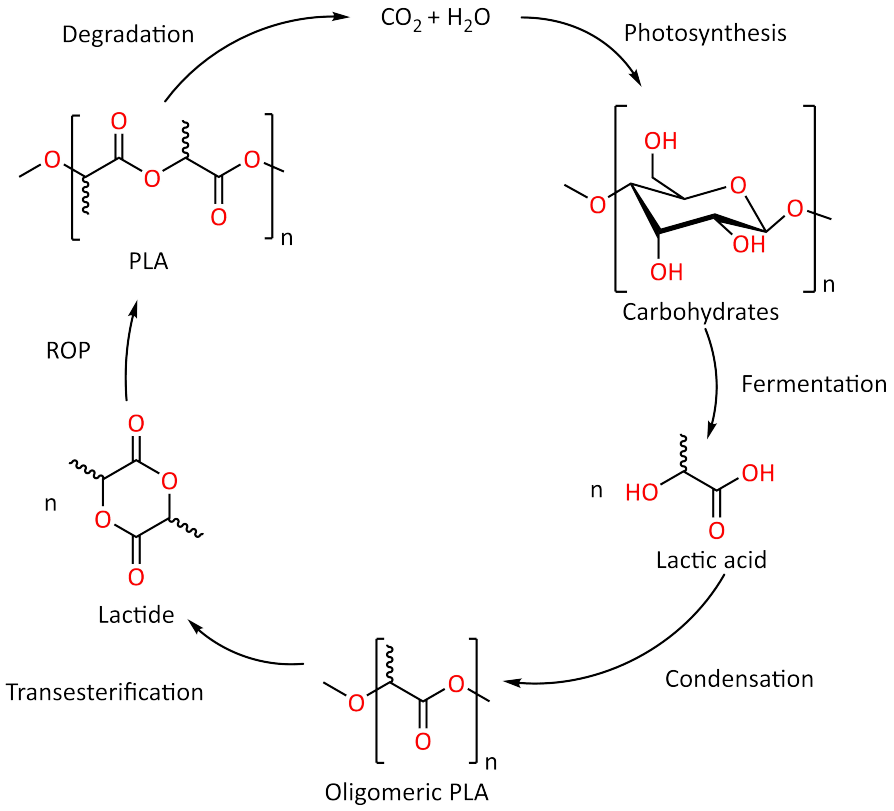

Scheme 1.11: Life cycle of PLA, from natural sugars to the widely used polymeric material.[71]

Lactic acid has a chiral centre, giving rise to three stereoisomeric forms of lactide. The isomeric forms result in stereoregular polymers that determine the macrostructure of the resultant PLA (Scheme 1.12). The exception to this is *meso*-lactide, which predominately undergoes ROP to from syndiotactic PLA. The tacticity of the polymer defines the regularity of the orientation of the side groups. An isotactic poly-

mer has the side groups in the same orientation, a syndiotactic polymer has the side groups alternating in orientation and an atactic polymer has the side groups with random orientations. Optically pure PLA derived from either pure L- or D-lactides give rise to crystalline PLLA or PDLA respectively with melting point temperatures (T_m) of approximately 180 °C and T_g of 60 °C.[72] As the optical purity decreases towards syndiotactic, atactic or racemic PLA, the crystallinity, T_m and T_g decreases. For example the T_m and T_g for syndiotactic PLA is 155 °C and 45 °C respectively.[73] Mixing of isotactic PLLA and PDLA to from stereo-complex crystals interestingly results in a T_m of 230 °C.[72] Being able to tune the degree of crystallinity increases the thermal and mechanical range of PLA and thus its application scope.

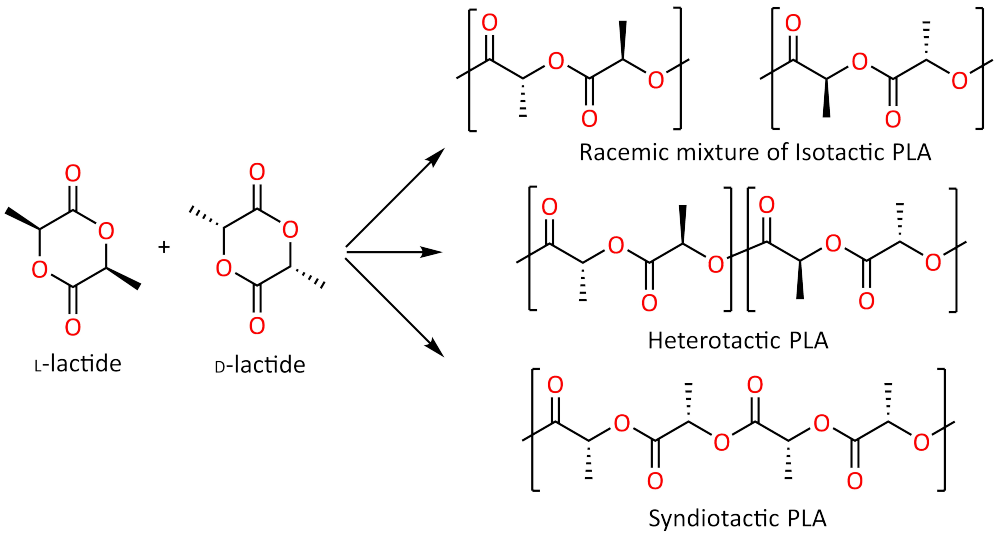

Scheme 1.12: Stereoisomers of lactide along with the potential macrostructures of PLA.[57]

Having control over tacticity starts from the optical purity of the monomer and the choice of catalyst used. Preference of one isomeric monomer over the other was observed by Spassky using the binapthylene imine bridge where there was a strong preference to D-lactide resulting in a gradient stereo block polymer.[61] Other groups expanded on this finding to produce stereo blocks in shorter reactions times.[74] The Shaver group investigated the selectivity of ROP of *rac*-lactide to produce isotactic PLA using the aluminium salen catalysts and found the opposite to that of Spassky where L-lactide undergoes ROP faster than D-lactide hence giving rise

to isotactic PLLA from *rac*-lactide.[75] The Shaver group, along with Chen and co-workers, underwent further studies to investigate the tuning of the tacticity based on the type of catalysts used, for example catalyst **3**, where $R_3 = {}^t$Bu, led to PLA with 88 % isotactic enchainment (highly isotactic) compared to catalyst **4**, where R_2 = Benzyl and $R_3 = {}^t$Bu, leading to more of a heterotactic PLA (Scheme 1.13 and Scheme 1.10).[75] It was concluded that carefully choosing the catalyst would give control over tacticity and that tacticity was chain-end controlled where the previous attached unit would influence the orientation of the next monomer unit.

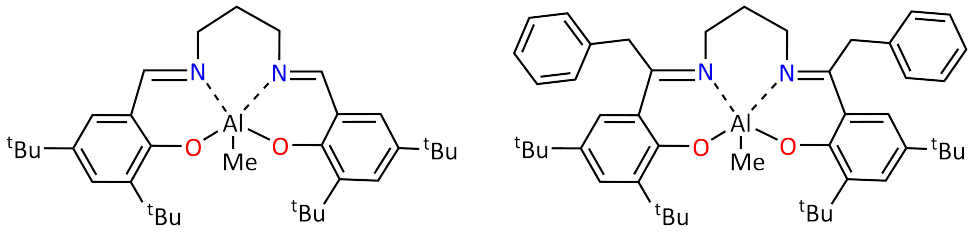

Catalyst **3** Catalyst **4**

Scheme 1.13: Variation of catalysts used to control tacticity of the resultant PLA polymerised from *rac*-lactide.[76]

The advantage of PLA is that degradation is feasible and can include biodegradation through enzymes[16], oxidative degradation[77], photodegradation[78] and hydrolytic degradation[79]. Photodegradation and oxidative degradation are the least efficient due to the inability of light to penetrate into the soil and the pollution caused as a result of oxidative degradation. Biodegradation and hydrolytic degradation are more efficient in the case of PLA.[80] In this work biodegradation is chosen to be discussed in more detail as this was the degradation that was carried out on PLA. Details of the other types of degradation such as hydrolytic degradation can be found in the review written by Jamshidian *et al.*.[81] Biodegradation involves degradation through microorganisms or enzymes in soil into carbon dioxide, water and biomass.[82]

Biodegradation via microbial attack in soil has shown to be extremely slow and inefficient due to the tolerance of PLA to degradation over other biodegradable material in soil. Therefore, extensive research has been carried out for the isolation

of microorganisms that selectively degrade PLA. The first reported microorganisms to degrade PLA pellets after 14 days were strains of the bacteria actinomycetes such as *Amycolatopsis*, by Pranamuda *et al.* in 1997.[83] The strains were predominantly isolated from soils, rivers and ponds. Through development of molecular biological techniques with time and better understanding of the specific strains that degrade PLA, a series of actinomycetes were tabulated and studied for their efficiency on the degradation of PLA by several groups such as, but not limited to, Ikura *et al.*, Nakamura *et al.* and Jarerat *et al.*.[84–87] Similar studies were done on other bacterial and fungal strains and these are highlighted in a review written by Qi *et al.* in 2017.[88]

Biodegradation by bacteria such as *Penicillium roquefort*, *Fusarium moniliform* and *Bacillus brevis* are only efficient at degrading oligomeric PLA. However, enzymatic degradation of PLA has shown the ability to degrade low molecular weight polymeric PLA through hydrolases such as the hog pancreatic lipase and carboxylic esterase.[89] Enzymatic degradation of higher molecular weight PLA was first discovered in 1981 by William *et al.* through proteinase K, a serine protease from the fungus *Tritirachium album.*[90] Since then, Oda *et al.* worked on testing commercially available proteases against PLA and concluded that acidic and neutral proteases showed poor degradation of PLA due to their sensitivity to pH and temperature.[91] The serine proteases such as α-chymotrypsin, trypsin, elastase, in addition to proteinase K, showed the greatest potential for degradation of PLA. As with degradation using bacteria and hydrolases, degradation with proteinase K is dependent on the tacticity (crystallinity) and molecular weight of PLA, as well as external factors such as temperature and pH. The cycle of degradation is initiated by binding of the substrate to the active site on the enzyme followed by nucleophilic attack of the carbonyl, simultaneously with the protonation, and then ended with hydrolysis of the ester bond (Scheme 1.14).[88]

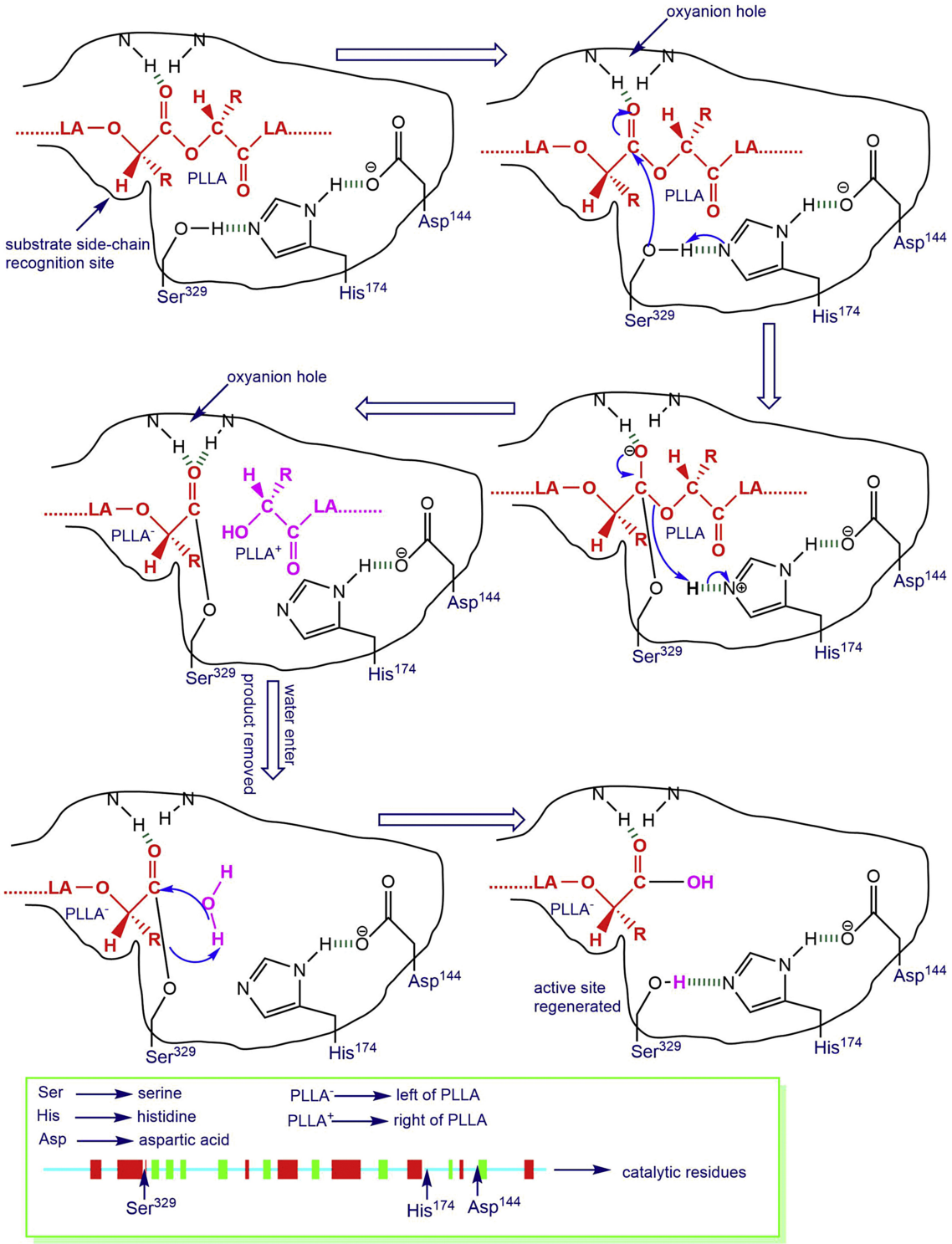

Scheme 1.14: Catalytic mechanism of proteinase K for the degradation of PLA. Taken from an article published by Qi *et al.*[88] License Number 4514200549705.

The certainty of biodegradation of PLA, irrespective of the time taken, along with its renewable source, makes PLA an attractive replacement for commodity plastics. However, challenges exist in the application of linear chains of PLA in the biomedical and pharmacological field because *in vitro* and *in vivo* degradation rates are often not well controlled, bioactive loading is low, and products have a high hydrophobicity.[92] In addition, challenges of obtaining biodegradable polyesters with optimal thermal and mechanical properties values has led to research into introduction of branching and functional groups.

1.4.2 Polystyrene and Potential Alternatives

The inexpensive polystyrene has been developed as an everyday polymer due to its excellent thermal and mechanical properties. Polystyrene has a T_g of 107 °C and a T_m of 240 °C making it rigid at room temperature with a Youngs modulus of 3.73 GPa and thus it is particularly useful in protective packaging, hot drink cups, and disposable plates.[93,94]

Polystyrene is derived from the commercially available and inexpensive monomer styrene. Styrene is the product of a three-step synthesis, involving acetylation of benzene with acetic anhydride, reduction of the acetyl group to phenylmethyl carbinol (1-phenylethanol) with sodium borohydride and dehydration of the phenylmethyl carbinol with potassium hydrogen sulphate. Styrene is then refluxed between 80 -90 °C in the presence of the radical initiator, dibenzoyl peroxide, to afford polystyrene through free radical polymerisation (Scheme 1.15).[95]

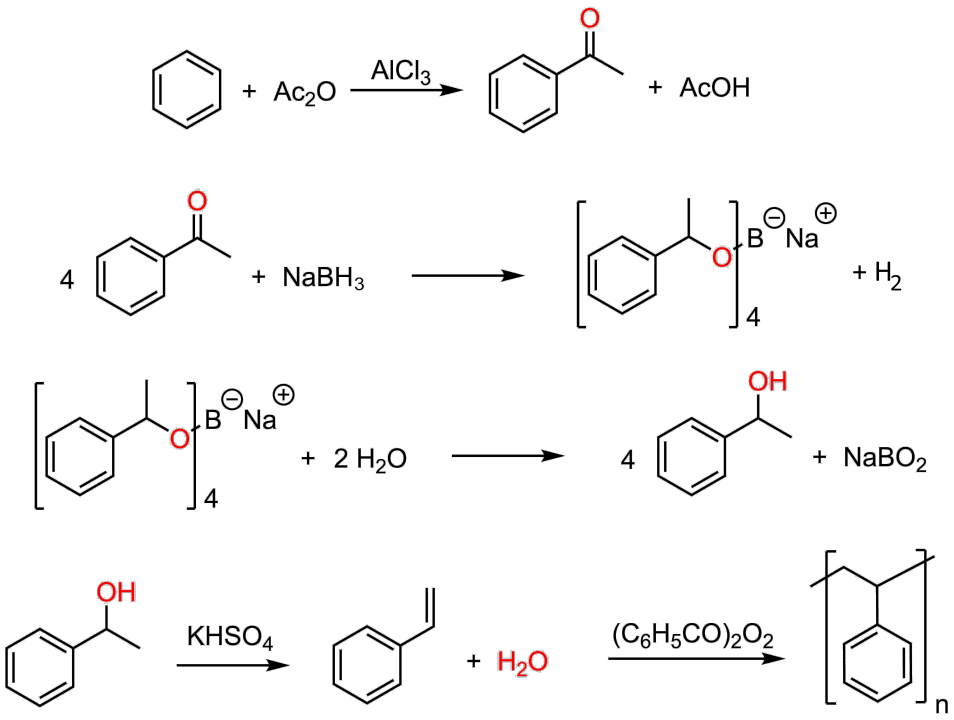

Scheme 1.15: Synthesis and polymerisation of styrene to afford polystyrene, modified from the paper published by Wilen *et al.*[95]

The main disadvantage of polystyrene is its extended life time and inability to easily degrade, causing accumulation in the environment. Thermal degradation studies have been carried out by a process known as cracking. The cracking process takes place in the liquid phase at temperatures above 390 °C and contributes to pollution due to the degraded products being released as volatiles. Long term studies on the biodegradation of polystyrene has been reported by Otake *et al.*, concluding that after 32 years of polystyrene sheets embedded into soil, no degradation was observed.[96] Blends and copolymers of polystyrene have been shown to degrade in controlled conditions over 6 months with isolated microorganisms, however polystyrene degradation in natural environments such as soil and landfill remains a concern.[6]

Baker and his group were pioneers in the research of achieving a biodegradable polymer with a T_g similar to that of polystyrene. Baker's early work focused on the simple substitution of the methyl group in PLA, demonstrating a dramatic increase in the thermal and mechanical properties of the resultant polymer.[92] It was shown that introduction of a benzyl group slightly increased the T_g of the resultant

polymer to 50 °C. The methylene group linking the aromatic ring to the polyester backbone provided flexibility and inhibited a further increase in T_g. Further research was carried out to remove this CH_2 group to provide a more restricted polyester, polymandelide, originating from cyclic L-mandelide (Scheme 1.16). The polymer shared many thermal and mechanical properties with polystyrene.[93,97] Obtaining high molecular weight isotactic poly(mandelide) with a T_g of 100 °C proved challenging due to the α-proton (on the same carbon as the phenyl ring) in the monomer being susceptible to racemisation under basic conditions.[92] Extension of this work was carried out by Buchard *et al.* to afford isotactic poly(mandelide) under milder conditions from a cyclic O-carboxyanhydride (L-manOCA). A pyridine-mandelic acid adduct was used as an organocatalyst to ensure retention of stereochemistry. It was found that reducing the basicity of the catalyst produced isotactic poly(mandelide) with a T_g of 105.5 °C.[98] The work carried out by Baker and Buchard *et al.* showed potential, with room for improvement.

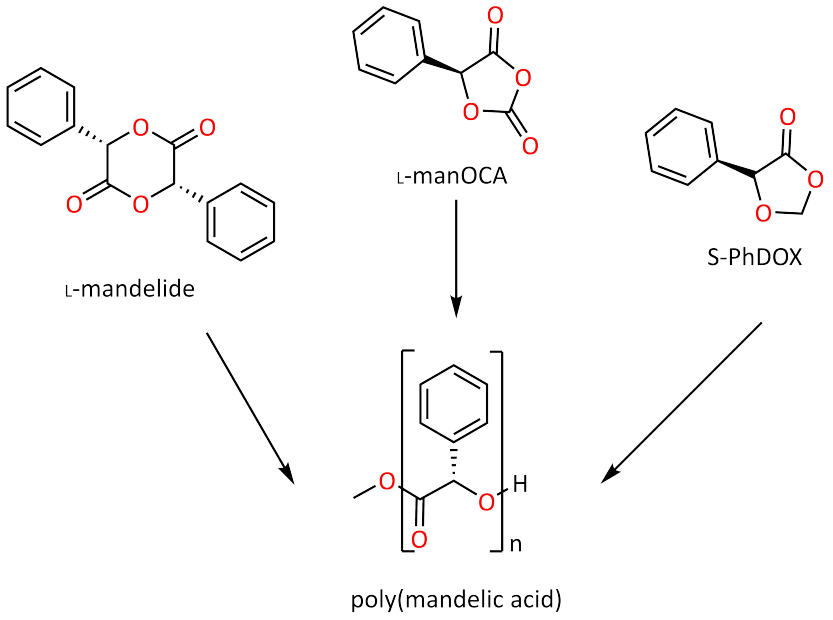

Scheme 1.16: Introducing an aromatic ring pendent to the polymer backbone to afford a polystyrene mimic.[92,98]

Shaver *et al.* developed a greener alternative to isotactic poly(mandelic acid) with the renewable, five membered 1,3-dioxolan-4-ones (DOX). A series of DOX monomers were synthesised and subjected to ROP using metal-based and organocat-

alysts. Of interest in this text is the phenyl substituted DOX (PhDOX), racemic and enantiomerically pure monomers were synthesised via the Dean-Stark apparatus at 110 °C over 6 hours from the reaction between their parent α-hydroxy acid, paraformaldehyde and p-toluenesulfonic acid in benzene. After work up and distillation, the respective monomers were subjected to ROP using the aluminium salen catalyst to yield, in the case of R- or S-PhDOX, isotactic poly(mandelic acid) in the absence of the expensive and toxic diphosgene.[99]

ROP of mandelide and PhDOX to afford poly(mandelic acid) as a biodegradable and recyclable polymer that mimics the thermal properties of polystyrene has been successfully achieved, however does not mimic the core structure of polystyrene. The CH_2 group, along with the pendent aryl group, in polystyrene can be retained through the ROP of four membered cyclic esters (lactones). The lactones pose synthetic challenges due to its characteristic ring strain, however, this ring strain allows the synthesis of otherwise inaccessible polyesters.

1.4.3 Poly(ethylene terephthalate)

PET is an aromatic polyester with the aryl ring along the polymer backbone. Its uses since it was first patented in 1941 by John Whinfield and James Dickson, and trademarked as Mylar in 1951,[100] have exponentially increased from packaging, such as bottles to replacing steel and aluminium in electronic components. PET has exceptional thermal and mechanical properties, with a T_g of 69 °C, a T_m of 260 °C and a Youngs modulus of 1700 MPa. The excellent thermal and mechanical properties similar to polystyrene are attributed to the aryl ring providing rigidity to the polymer chains, preventing free rotation and along with intramolecular interactions, such as the inherent π-π interactions with aryl rings, leading to a greater degree of packing and crystallinity.[101,102]

Industrial synthesis of PET involves the reaction of ethylene glycol and terephthalic acid at 240-260 °C and 3-5 bar to afford bis(2-hydroxyethyl) terephthalic acid (BHET). BHET then undergoes transesterification with other BHET molecules at 250-280 °C and 0.02-0.03 bar whilst eliminating ethylene glycol to afford oligomeric

PET. This is further reacted via polycondensation to afford polymeric PET at 200-240 °C and 1 bar (Scheme 1.17). The energy consuming conditions required to afford PET is overlooked due to the accessibility of the relatively inexpensive starting materials.[101]

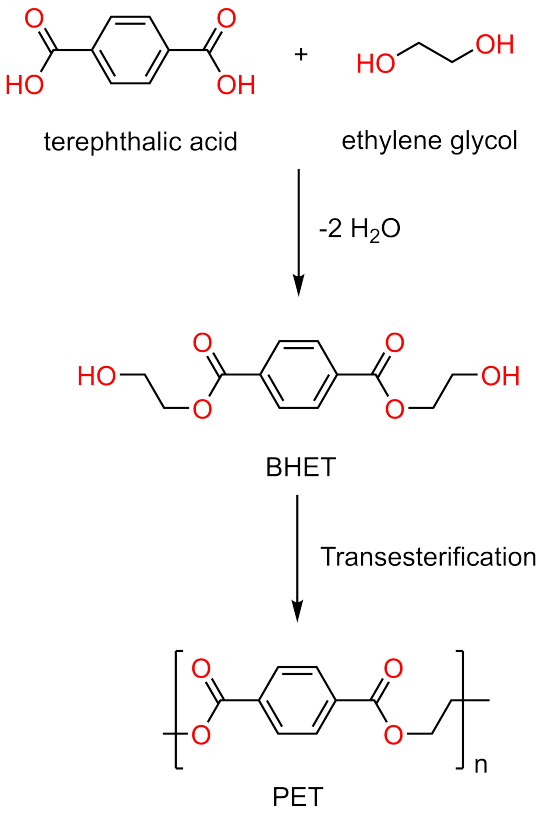

Scheme 1.17: Production of PET via BHET at temperatures above 200 °C and below 5 bar of pressure, modified from the paper published by Webb *et al.*[101]

The thermal and mechanical properties, in addition to the inexpensive starting materials, makes PET attractive for a wide range of applications and this comes with a cost. According to the European plastic demand, approximately 3.5 million tonnes of PET is in demand, which comprises a total of 7.4 % of total plastics in 2016. Since 2006 Europe have reduced the amount of plastic reaching landfill by 43 % and increased the amount recycled by 80 %. Although this is promising, the demand for plastics is still on the rise with the waste being collected increasing. Plastics at the end of their use are either deposited into landfill, where they remain for over 20 years, incinerated, to release toxic carbon and oxygen based free radicals and greenhouses gases into the atmosphere, or recycled.[103]

Similar to PLA, the recycling process can include various categories of degradation with the most common in the case of PET being thermal, chemical and hydrolytic degradation. Thermal degradation occurs at high temperatures in an inert atmosphere through the formation of vinyl ester and carboxyl end groups via random scission of the ester linkages. The vinyl ester end groups then undergo transesterification to afford acetaldehyde via the vinyl alcohol and shorter PET chains.[102]

Chemical degradation is divided into the following commercial processes: methanolysis, glycolysis and hydrolysis, with other processes reported. Methanolysis is the degradation of PET via methanol in a three-step process involving temperatures above 190 °C and an autoclave with pressures of 0.3 MPa to afford dimethyl terephthalate and ethylene glycol. The second most commercially used degradation process is glycolysis, which involves degradation of PET at 190-240 °C and 0.1-0.6 MPa via ethylene glycol. Hydrolysis of PET is the third most common and affords terephthalic acid and ethylene glycol via either acidic conditions such as phosphoric, nitric acid or sulfuric acid, alkaline conditions such as sodium hydroxide or neutral conditions with steam or water. All three processes require corrosive reagents or relatively high temperatures.[102,104]

Due to the increasing demand for PET and the need to efficiently recycle plastics, studies into the degradation of PET have led to the discovery of the enzyme PETase in 2017 by Han *et al.*.[105] The serine proteases have been reported to show activity in the hydrolysis of PET. However, the hydrolysis is not as efficient for PET due to it being structurally different to the other polyesters that fit in the enzyme active site.[105] The discovery of PETase originated from the isolation of a strain of bacteria, *Ideonella sakainsis* 201-F6, in 2016 by Yoshida *et al.*[106] Through screening studies it was concluded that *I. sakaiensis* was vital for PET degradation, with it showing the highest activity for degradation at 30 °C for 18 hours, releasing predominantly mono(2-hydroxyethyl) terephthalic acid (MHET) with trace amounts of terephthalic acid and BHET. *I. sakaiensis* attaches to PET and releases PETase for degradation which was confirmed through expression studies where transcription of the PETase coding gene was highest when *I. sakaiensis* was attached to a PET film. Enzymatic

degradation is influenced by the degree of crystallinity and chain mobility.[106] Han *et al.* further studied this enzyme to gain mechanistic and structural information.

The proposed catalytic mechanism of PETase involves predominately the amino acid tryptophan (W156) which is adjacent to catalytic triad, serine-histidine-asparagine (S131-H208-D177), all found on the protein surface. H208 acts as a base, stabilised by the acid D177, to polarise the nucleophile S131. Upon substrate (PET) binding, W156 fixes the position of the substrate through T-stacked π-π interactions with the first benzene ring whilst the carbonyl group undergoes nucleophilic attack from the catalytic triad, the intermediate being stabilised by the oxyanion hole. The release of the hydrolytic product leaves a more planar substrate which undergoes the stronger sandwich π-π interactions before it is released (Scheme 1.18).[105]

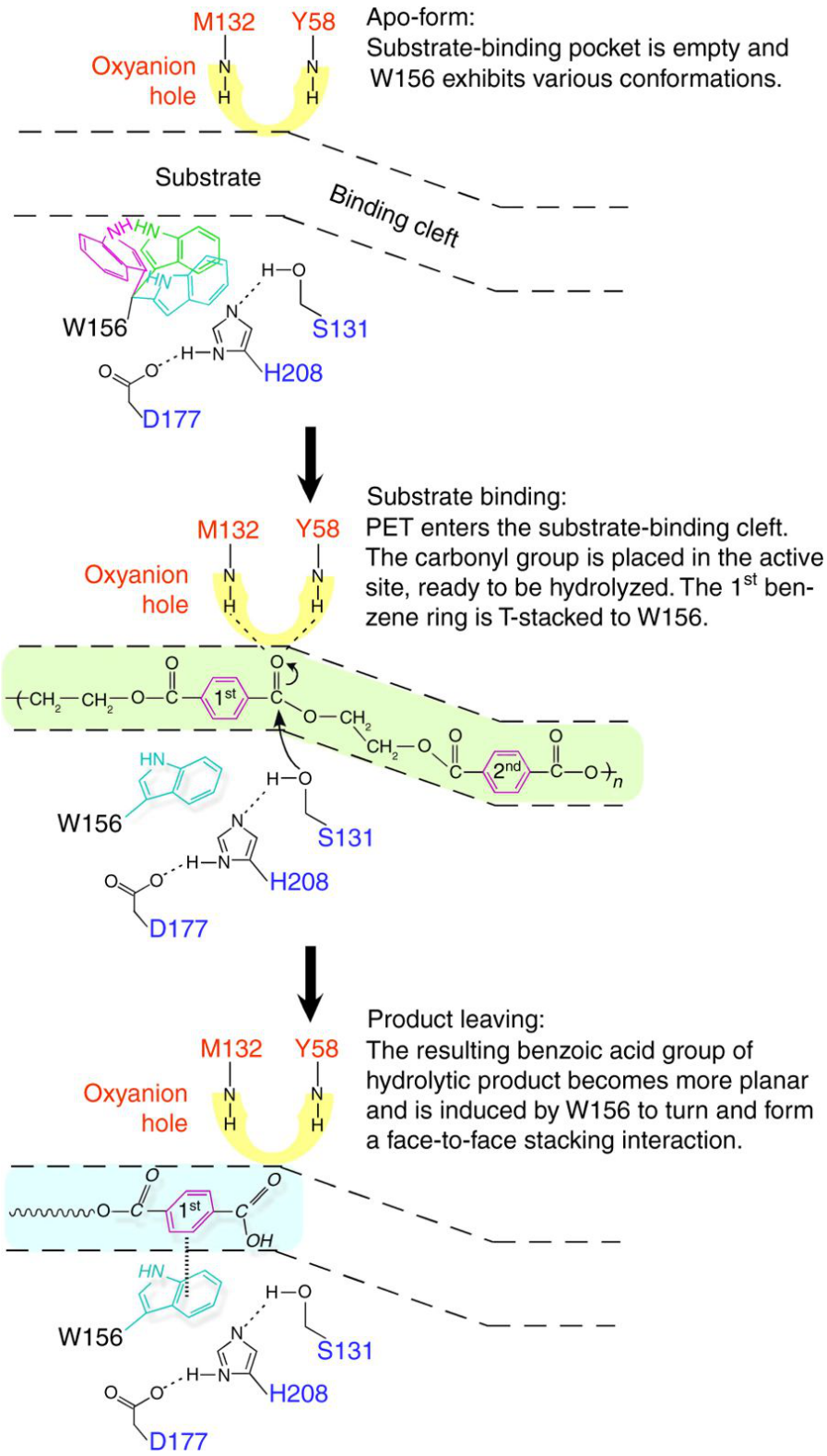

Scheme 1.18: Catalytic mechanism of PETase proposed by Han *et al.* in Nature Communications in 2017. Scheme taken from the communication.[105]

Early studies of PET degradation through PETase showed almost complete degradation after 6 weeks of incubation of the PET film with the enzyme at 30 °C. Austin *et al.* utilised the previous studies on PETase to engineer an enzyme with a double mutant PETase to show a slight increase in performance compared to the wild type, PETase. The degradation efficiency was compared with regards to the change in crystallinity, where the original study used only a 1.9 % crystalline sample and this study used a PET sample of 14.8 % crystallinity typically found in bottles.[107]

The research conducted by Han *et al.* and Yoshida *et al.* sparked great interest in the PETase enzyme. Seo *et al.*[108] reported in 2019 the successful production of an extracellular PETase through extracellular translocation using a Sec-dependent pathway in *E.coli*. Upon testing the expressed enzyme on PET films it was concluded that PETase showed PET-degrading activity.[108]

The *ortho*-linked poly(ethylene phthalate) (PEP) has a lower T_g (38.2 °C)[109] and a lower degree of crystallinity due to the kinked chain induced by the *ortho* ester linkages.[110] Even though PEP hasn't made its breakthrough as a commodity plastic, it has advantages as a copolymer (poly(ethylene isophthalate-co-terephthalate)) to alter thermal and mechanical properties of PET.[109] While non-industrial ROP of cyclic PET and PEP oligomers has accessed PET or PEP polymers and copolymers,[36] simple monomers remain elusive as feedstocks for PET. Although PET has desirable manufacturing properties and there have been advances on recycling of PET with enzymes such as PETase (showing great promise with low crystalline PET), high temperatures or long reactions times are required.[37]

1.4.4 Benzodioxepinones

The motivation for synthesis of polyesters that contain aromaticity in the polymer backbone stems from the excellent thermal and mechanical properties observed for PET and polystyrene. However, the need for polymers that degrade faster under milder conditions leads to the research conducted in this thesis. ROP of cyclic esters containing aromaticity in the polymer backbone is an under-explored area

and the reason for this is the challenge in the monomer synthesis. Four to five membered lactones such as benzpropiolactone, a β-lactone derivative of salicylic acid and phthalide, have been unsuccessful in ROP due to their stability.[111,112]

Benzodioxepinones are a class of aromatic cyclic esters containing one phenyl ring and a seven-membered ring with a carbonyl and two oxygen atoms. The benzodioxepinones, 2,3-dihydro-5H-1,4-benzodioxepin-5-one (2,3-DHB), was explored by MacDonald *et al.* due to its commercial availability and facile synthesis (Scheme 1.19).[113] MacDonald *et al.* screened the ROP of 2,3-DHB with various catalysts and showed that $Sn(oct)_2$ gave no conversion of 2,3-DHB to poly(2-(2-hydroxyethoxy)benzoate) (P2HEB) at 70 °C and low conversions of 58-61 % at 120 °C for 3 to 6 hours respectively. ROP using $Sn(oct)_2$ suggested transesterification which increased with reaction time as evident by the dispersity after 6 hours being 1.44. To address the issue with transesterification an aluminium salen catalyst was used, specifically MeAl[salen]. Under the same conditions as with $Sn(oct)_2$, toluene as the solvent at 120 °C for 3 hours, the conversion was 56 %, although the dispersity was significantly higher at 1.76. Through optimisation it was concluded that a lower temperature and a high initial concentration of 2,3-DHB was required to reach high conversions. Carrying out the polymerisation at 70 °C neat or in toluene for one hour increased the conversion to 64 % and 75 % with dispersities of 1.13 and 1.16 respectively. Further decreasing the temperature to 60 °C minimised transesterification with dispersities less than 1.09 and conversions over 92 %. The polymerisation at 50 °C or room temperature led to lower conversions than at 60 °C but higher than at 70 °C with conversions of 91 % and 80 % respectively.[113]

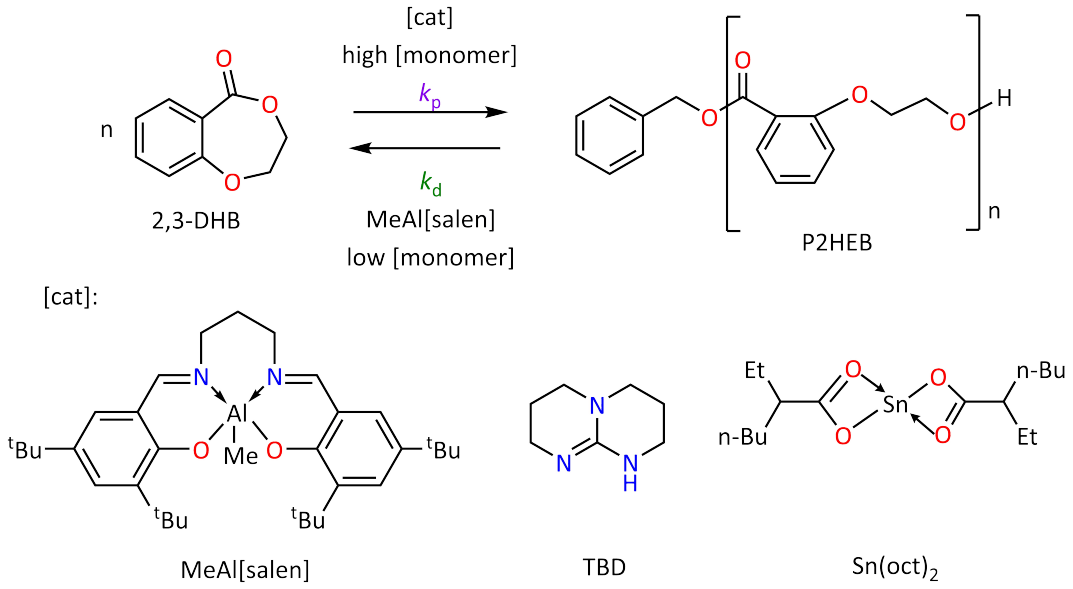

Scheme 1.19: ROP of 2,3-DHB to afford P2HEB via inorganic and organic catalysts. Depolymerisation was shown to be characteristic of the aluminium salen catalyst.[113]

Shaver *et al.* explored the trends observed with lower conversions at higher temperatures and explained it through the monomer-polymer equilibrium. Through variable temperature NMR scale polymerisation and change in concentration it was concluded that the rate of depolymerisation (k_d) was faster than the rate of polymerisation (k_p) at higher temperatures and lower monomer concentrations. At 4.1 M for 6 hours at 60 °C in toluene the equilibrium shifted to the right with 82 % monomer conversion. Decreasing the concentration to 0.2 M led to depolymerisation of the polymer with a conversion of 94 %. This was shown to be reversible whilst maintaining narrow dispersities of 1.07-1.08.[113]

This monomer-polymer equilibrium stood true for MeAl[salen] as the catalyst, however when moving on to organocatalysts such DBU and diphenyl phosphate (DPP), no activity for the ROP of 2,3-DHB was observed. TBD however, catalysed the polymerisation to 89 % monomer conversion in just 30 minutes with a dispersity of 1.19. It was also noted that concentration did not influence the equilibrium in the case of TBD, as subjecting TBD to similar depolymerisation conditions as MeAl[salen] led to less than 5 % depolymerisation and instead to transesterified products.[113] Preliminary thermal studies were carried out on P2HEB using ther-

mogravimetric analysis showing thermal degradation at 219.3 °C and a T_m at 78.2 °C.[113]

MacDonald *et al.* took the work further by copolymerising P2HEB with PLA and poly(3-hydroxybutyrate) (P3HB) to form AB block copolymers. Challenges in forming blocks with PLA were observed due to the monomer-equilibrium where with P3HB AB block copolymers were successfully synthesised and underwent depolymerisation studies to show selective depolymerisation of the P2HEB block.[113]

1.5 Aims

The research here focuses on developing a system to replace commodity plastics, whether it be a polystyrene mimic (through synthesis of a β-lactone) or a PET mimic (through synthesis of a series of novel aromatic-aliphatic polyesters), with functionalised polyesters that have the ability to be recycled selectively back to their monomers in a "closed loop" fashion.

The polymerisation and depolymerisation behaviour of P2HEB through *meta*-substitution of the benzodioxepinone with electron donating and electron withdrawing groups, in addition to the electronic effects of the *meta*-substituent on the thermal transitions, stability and crystallinity of the resultant aromatic-aliphatic polyesters will be explored to afford a polyester with thermal properties close to that of PET.

P2HEB will be further utilised to tune the thermal, mechanical and degradation behaviour of the commercially available PLA through copolymerisation.

Chapter 2

Monomer Design

2.1 Introduction

β-Lactones have been exploited in not only chemical syntheses as intermediates but also in the pharmaceutical industry and as biodegradable polyesters.[114] Synthetic routes including aldol reactions, [2+2]-cycloadditions, epoxide carbonylations and complex multi-step reactions exist to afford β-lactones (Scheme 2.1). Aldol reactions require enantiopure auxiliaries or catalysts to form the enantioenriched β-lactones through aldol moieties and cyclisation. Although it gives access to a range of products, which are desirable as intermediates for synthesis and industrial process that are otherwise inaccessible, the chemistry can be costly and is a non-direct approach to the formation of β-lactones.[115]

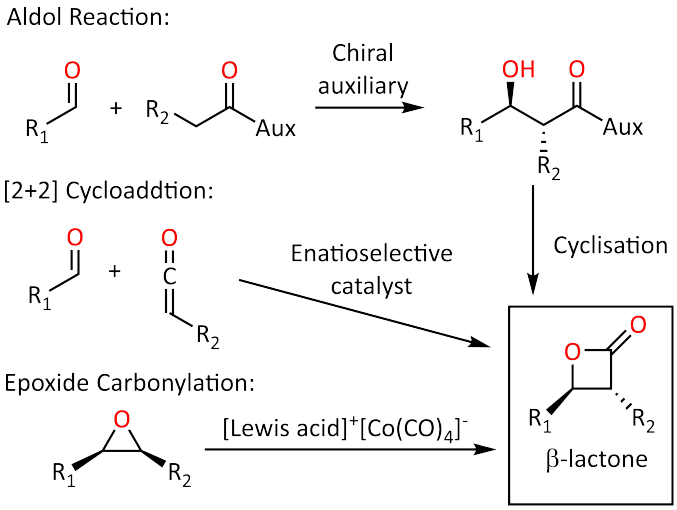

Scheme 2.1: Synthesis of β-lactones via different methods and starting materials.[115]

[2+2]-cycloadditions of ketenes to carbonyl compounds is an attractive way to afford β-lactones. Various catalytic systems have been explored to access β-lactones, however a significant amount of typically expensive catalysts are required to produce the β-lactone in respectable yields.[115] In the 1990's research was done to expand the scope of β-lactones by using palladium (Pd) and aluminium catalysts with high loadings of up to 10 mol %. Tamai *et al.* were the first to report asymmetric [2+2]-cycloaddition of ketenes with aldehydes using the aluminium complex, Al[3,3'-bis(triphenyl-silyl)-1,1'-binapthalene-2,2'-diol-Me_3]. Tamai *et al.* observed deactivation of the catalyst due to acylation of the diolate ligand by the ketene and therefore investigated other Lewis acids, specifically bissulfonamide-aluminium complexes, with lower pK_a's to prevent this deactivation. These catalysts showed activity for a range of aldehydes and demonstrated higher enantioselectivity with sterically bulky aldehydes.[116] In 1999 Hattori *et al.* further explored the potential for Lewis acids to catalyse [2+2] cycloadditions by utilising cationic palladium(II) complexes, Pd[L_2(PhCN)$_2$](BF_4)$_2$]. Using the some of the same substituted aldehydes as Tamai *et al.*, it was shown that with the phosphine ligand, 1,1'-bis(diphenylphosphino)ferrocene (dppf), the activity increased dramatically with yields over 97 % with the exception of the ^{t}Bu showing similar yields.[117] Research to further expand the scope of aldehydes has been done however there has been limited reports on the synthesis of the phenyl substituted β-lactone, propiolactone,

due to difficulty in isolation. It most cases the isolated product is the 1,3-diol derivate.[116,117]

Hmamouchi *et al.* utilised various areas of chemistry to afford the lactone with reasonable yield after seven steps and successfully preformed ROP to afford the polyester, poly(phenyl propiolactone) (poly(PhPL)) in order to study the thermal and mechanical properties.[118] ROP was carried out using a CH_3COOK/dibenzo-18-crown-6-ether complex to yield poly(PhPL) with a range of optical purities (0, 18, 21 and 50 %). It was assumed that the optical purity of the lactone was equivalent to the optical purity of the polymer. Thermal and mechanical analysis showed that the crystallinity and T_g were affected by optical purity. Poly(PhPL) of 0 % optical purity had a T_g of 41 °C and a lower degree of crystallinity compared to poly(PhPL) of 50 % optical purity with a T_g of 50 °C .[118]

An alternative direct approach to the synthesis of β-lactones is carbonylation. Aumann *et al.* was the first to report the successful carbonylation of isoprene oxide with carbon monoxide (CO) via the $[Rh(cod)]Cl_2$ in 1977.[119] Coates *et al.* extensively studied the field of carbonylation, using enantioselective catalysts in the form of $[\text{Lewis acid}]^+[Co(CO)_4]^-$ to improve the catalytic range giving higher yields and selectivities. Through screening and optimisation of catalyst, Coates *et al.* concluded that the Lewis acid component was vital for regioselectivity and reactivity. The proposed mechanism (Scheme 2.2) showed the importance of the Lewis acid in the coordination and activation of the epoxide followed by an S_N2 reaction with $[Co(CO)_4]^-$ to afford the ring-opened species. The insertion of carbon monoxide to the C-Co bond followed by migration of the O-M bond for CO-Lewis acid coordination afforded the β-lactone.[114]

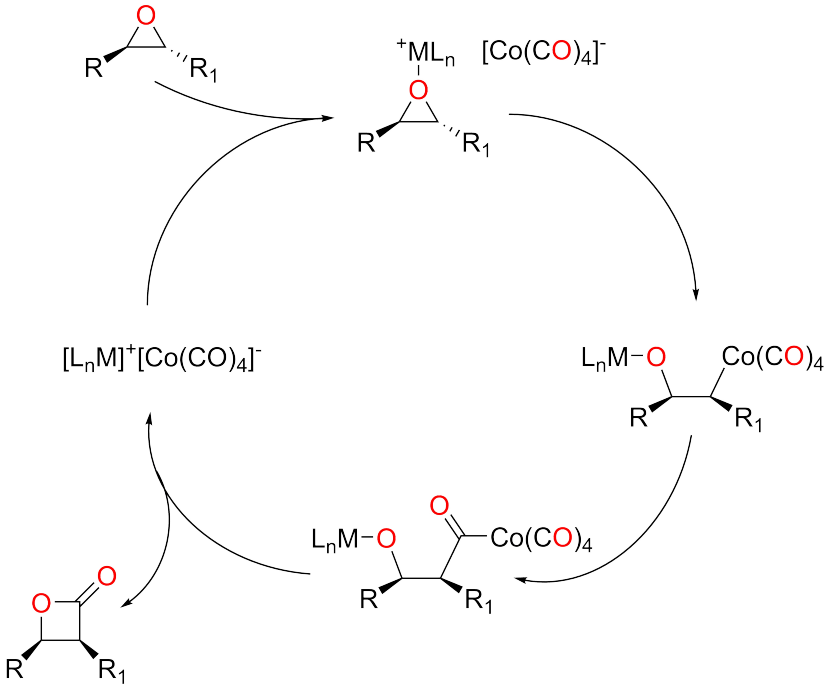

Scheme 2.2: Proposed mechanism for the carbonylation of an epoxide using a [Lewis acid]$^{+}$[Co(CO)$_4$]$^{-}$ catalyst, modified from the paper published by Coates *et al.*[114]

Coates *et al.* were able to access a wide range of β-lactones through optimised aluminium salen complexes (Scheme 2.3), such as monosubstituted and disubstituted β-lactones varying in the carbon chain length as well as more complex substitutions such as benzyl. Excellent yields of the enantioenriched benzyl substituted β-lactone were achieved, however proposed the same issue as observed by Baker in his early work where the methylene group would provide flexibility and hinder high thermal properties.[120] Limited research has been reported on the carbonylation of styrene oxide (to eliminate this flexibility) since 1970 due to low yields and difficulty in the isolation of the lactone. Kamiya *et al.* and Cowell *et al.* however reported the carbonylation of styrene oxide using Rh[Cl(CO(PPh$_3$)$_2$)] and Pd[(PPh$_3$)$_2$Cl$_2$] respectively in 1980.[121,122]

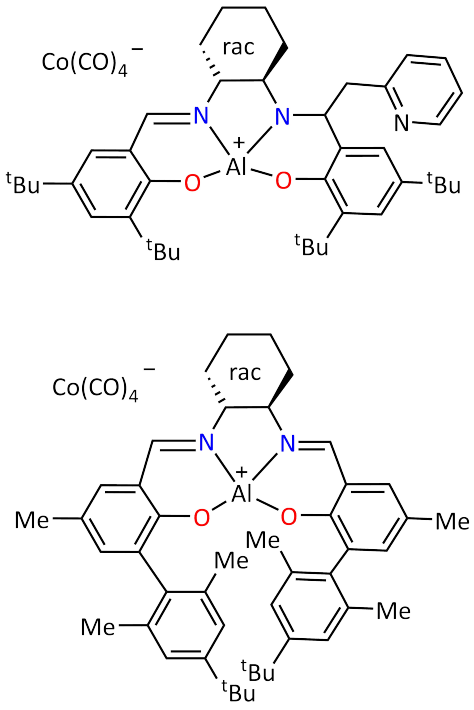

Scheme 2.3: Aluminum salen complexes used for the carbonylation of an epoxide to afford monosubstituted and disubstituted β-lactones.[114]

Kamiya *et al.* reported the synthesis of α-phenyl-β-propiolactone via Rh[Cl(CO)$(PPh_3)_2$]. Conditions of carbonylation were screened by varying the CO pressure from 27.5 to 98 bar, temperature from 60 to 100 °C, and time from 2 to 20 hours. The optimum conditions to obtain isolated lactone were 98 bar CO pressure and 110 °C for 20 hours, although with poor yields of 3.2 %. Kamiya *et al.* observed the formation of the hydroxy ester along with the β-lactone at elevated temperatures, thus lowering the yields; this was also the case with other catalysts studied. Two mechanisms were proposed for the formation of the β-lactone, the first (Mechanism A) involving the rhodium catalyst acting as a Lewis acid and the second (Mechanism B) involving the oxidative addition of the rhodium catalyst to the C-O bond of the epoxide (Scheme 2.4).[121]

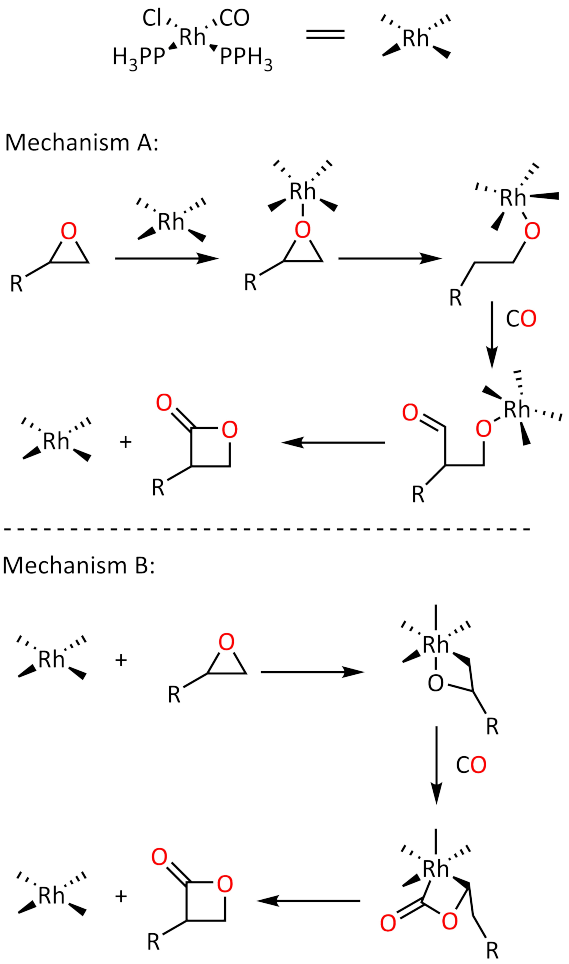

Scheme 2.4: Proposed mechanism of carbonylation of epoxides using a rhodium catalyst, with Mechanism A using the catalyst as a Lewis acid and Mechanism B manipulating the oxidation state of the catalyst, modified from Kamiya *et al.*[121]

Cowell *et al.* reported an alternative synthesis of β-lactones via halo alcohols using pallidum catalysts. Through catalyst screening, $Pd[(PPh_3)_2Cl_2]$ was chosen for the synthesis of α-phenyl-β-propiolactone. The synthesis involved two steps (Scheme 2.5).[122] Styrene oxide was first converted to the halo alcohol, 2-bromo-2-phenylethanol, the $Pd[(PPh_3)_2Cl_2]$ catalyst then utilised the halo alcohol to undergo ligand dissociation and oxidative addition followed by insertion of carbon monoxide into the palladium-carbon bond to afford α-phenyl-β-propiolactone with yields of 63 %.[122]

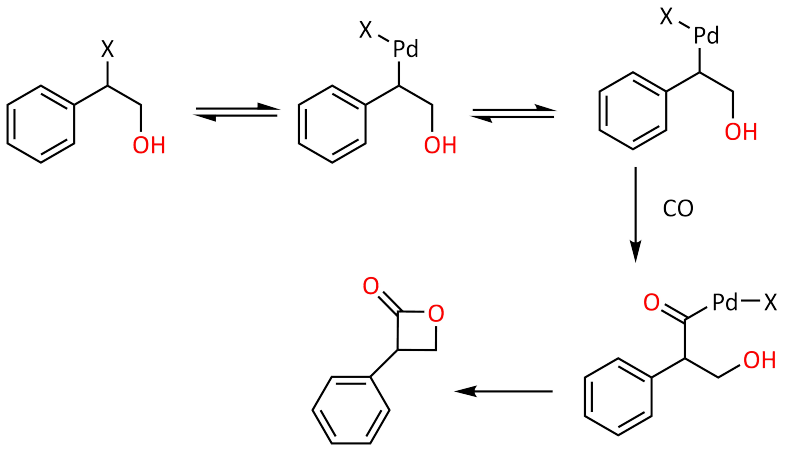

Scheme 2.5: Proposed mechanism of the formation of β-lactones via halo alcohols, where X is a halide, modified from Cowell *et al.*[122]

Palladium catalysed carbonylation reactions have been studied and developed over time. However, carbonylative cross-coupling reactions with epoxides were unexplored until 2013, where Beller *et al.* reported the synthesis of benzodioxepinones (Scheme 2.6).[123]

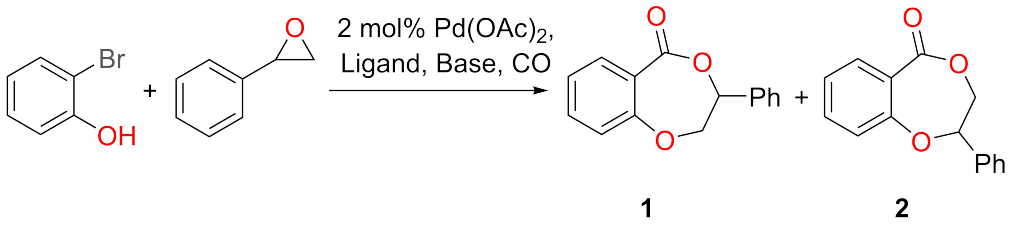

Scheme 2.6: Synthesis of two benzodioxepinones from styrene oxide and 2-bromophenol, modified from Beller *et al.*[123]

In the attempt to synthesise the benzodioxepinone Beller *et al.* observed the formation of 2-bromophenoxy-phenyl-ethanol, from the reaction with 2-bromophenol and styrene oxide using $Pd(OAc)_2$, suggesting the rate-determining step to be the carbonylation. Through screening of ligands, 2,2'-bis(diphenylphosphino)-1,1'- binaphthyl) (binap) was shown to be most promising for further optimisation. It was also observed that the use of a base increased the selectivity between the two products with K_3PO_4 yielding 90 % product with a 90:10 ratio of product **1**:**2**, this was reversed when using $ZnBr_2$ as the catalyst to a ratio of 15:85 of product **1**:**2**. Beller *et al.* synthesised a library of benzodioxepinones by altering the epoxide used.[123]

The 3-methyl and 3-phenyl substituted benzodioxepinones were synthesised by the Shaver group and were subjected to ROP, however were unsuccessful in obtaining the respective polymers.

An alternative metal-free approach to benzodioxepinone derivatives was reported by Rose *et al.* via the use of N-heterocyclic carbenes (NHC). Benzodioxepinones were products of the cyclisation of their respective *meta*-hydroxyethoxy benzaldehydes synthesised from salicylaldehyde derivatives and 2-chloroethanol. The salicylaldehyde derivatives were synthesised via *meta*-formylation of substituted phenols through various methodologies.[124] Hofsløkken *et al.* reported the *meta*-formylation of a range of substituted phenols using anhydrous $MgCl_2$, triethylamine (TEA) and a large excess of paraformaldehyde in acetonitrile under reflux for 2-4 hours. A clear trend was observed with the electronic nature of the substituents, where electron withdrawing groups (EWG) inhibited the reaction and electron donating groups (EDG) promoted the reaction.[125] The mechanism proposed by both Hofsløkken *et al.*[125] and by Casiraghi *et al.*[126] (Scheme 2.7), involved the phenol being initiated by TEA giving rise to the salt, phenoxymagnesium chloride. Formaldehyde, the more reactive species of paraformaldehyde, reacts with the salt through a cyclohexanediene structural intermediate to produce the magnesium salt of salicyl alcohol as the major product. This then undergoes a redox reaction with formaldehyde to afford the salicylaldehyde with the elimination of methanol.[125] The meta-hydroxyethoxy benzaldehydes are then accessed via an S_N2 reaction with the salicylaldehyde derivative and 2-chloroethanol.[124]

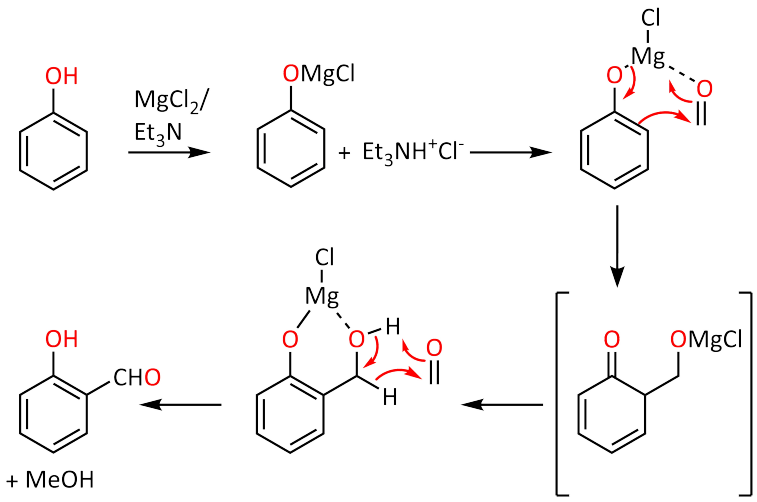

Scheme 2.7: Proposed mechanism of the *ortho*-formylation of phenols, modified from Hofsløkken *et al.*[125]

Rose *et al.* investigated a range of heterazolium salt/base combinations for cyclisation *meta*-hydroxyethoxy benzaldehydes to selectively form the benzodioxepinone monomer over the dimer. The mesitylene-substituted thiazolium perchlorate with azobenzene and TEA in THF at 80 °C for 20 hours exhibited excellent activity with 94 % yield and traces of the 14-membered diolide (dimer). Azobenzene and TEA were found to aid in the cyclisation. Replacing azobenzene with MnO_2 reduced the yield by 10 %, highlighting the influence of azobenzene as the oxidising agent. The benzyl-substituted thiazolium catalyst demonstrated high yields (93 %) however with slightly less selectivity. This is overlooked due to the facile synthesis of the catalyst from commercially available 4,5-dimethylthiazole and benzylbromide in acetonitrile under reflux for 24 hours followed by recrystallisation from ethyl acetate. Rose *et al.* confirmed the catalytic role of the NHCs by control experiments in their absence to show no conversions. The proposed mechanism of the catalytic oxidative lactonisation involves the heterazolium derived carbene acting as an acyl transfer agent followed by oxidation via azobenzene to then undergo cyclisation by deprotonation of the hydroxy end group and displacement of the acyl transfer agent (Scheme 2.8).[124]

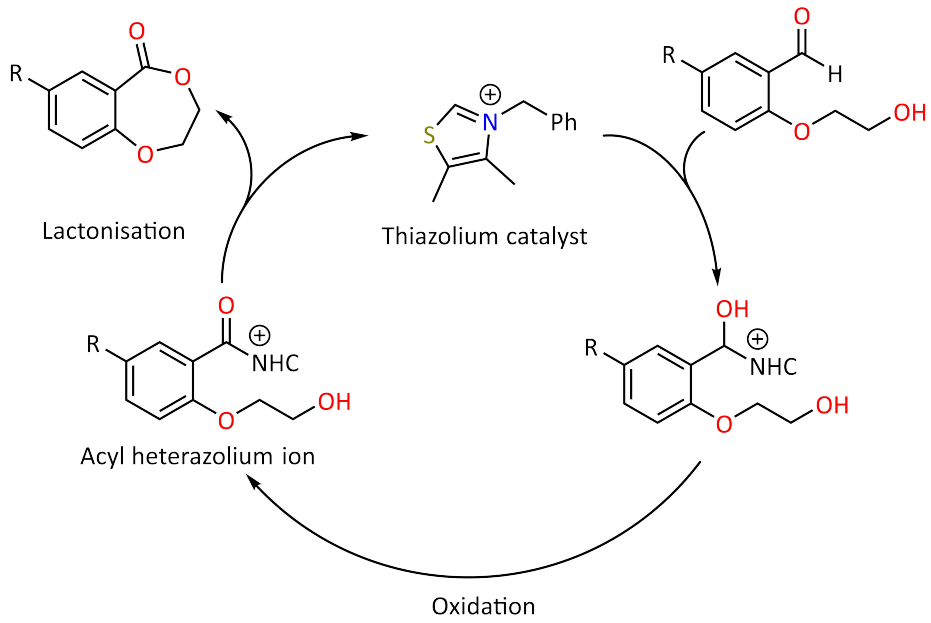

Scheme 2.8: Proposed mechanism for the synthesis of benzodioxepinone derivatives using a N-heterocyclic carbene.[124]

Rose *et al.* synthesised a library of benzodioxepinone derivatives with electron withdrawing and donating substituents due to their bespoke biological activity in potassium channels and their application in perfumery.[124]

The reported benzodioxepinone derivatives have not yet been subjected to ROP to afford aliphatic-aromatic polyesters, with the exception of the hydrogen substituted benzodioxepinone, 2,3-DHB.[113] The benzodioxepinone derivatives were chosen to exploit the electronic density, eliminating steric effects, in the aromatic ring on the rationale that the electron density would influence the reactivity and thermal and mechanical properties of the resultant polyester (Scheme 2.9).

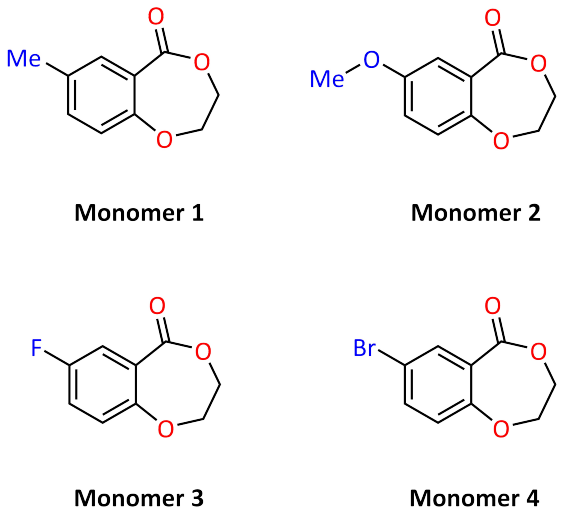

Scheme 2.9: Chosen benzodioxepinone derivatives varying in electronic parameters.

The benzodioxepinone derivatives were chosen upon research into the extent which the substituent's electronic properties effected the reactivity of the aromatic ring through the Hammett constant. Louis Plack Hammett, in 1937, quantitatively studied the effect of substituents on the reaction rate constants through pH titration curves, using the acidity constants of substituted benzoic acids to define the electronic substituent parameter (σ).[127]

The Hammett equation (Equation 2.1) defines σ from the ionisation constants of benzoic acid, where K_X is the rate constant for an aromatic compound with para or meta substitution, K_H is the rate constant for benzoic acid, and p is the reaction constant. To solve for σ, the ionisation of benzoic acid at 25 °C in water is used as the reference reaction for constant p to equate to 1.00.[128,129]

$$\sigma p = log \frac{K_X}{K_H} \tag{2.1}$$

The constant p is governed by the ability of a substituent to stabilise charge during the reaction and is influenced by the type of reaction, solvent and temperature. Substituents with p greater than 0 stabilise negative charges and are classed as EWG's whereas substituents with p less than 0 typically stabilise positive charges and are classed as EDG's. σ correlates with p, where the magnitude of σ defines the extent of a substituent to be electron withdrawing or donating. σ is positive

for EWG's and negative for EDG's. The electronic substituent constants have been determined for substituents meta (σ_{meta}) and para (σ_{para}) to the reactive centre. This was due to the additional influence of resonance as well as inductive effects on the stabilisation of the charges in σ_{para}.[129]

The Hammett constant is known to influence reaction rates as well as noncovalent interactions such as those between adjacent aromatic rings. Noncovalent interactions, specifically π-π interactions, are well known to influence chemical, thermal and mechanical properties in addition to the structure and function of a range of aromatic systems. It has been reported that electron donating substituents, with a negative σ, cause aromatic π-π stacking destabilisation through pushing of electron density into the aromatic ring, leading to electrostatic repulsion. On the other hand, electron withdrawing substituents, with a positive σ, enhance the π-π stacking by drawing electron density out of the aromatic ring. This is known as the Hunter-Sanders model and can be correlated to the electronic substituent parameter.[130]

The Hunter-Sanders model explains the existence of π-π stacking by the interaction of the positively charged σ bond framework with the adjacent negatively charged π electron density (Scheme 2.11). This explains why out of the four proposed conformations of π-π stacking, face-to-face is the least stable (Scheme 2.10).[130]

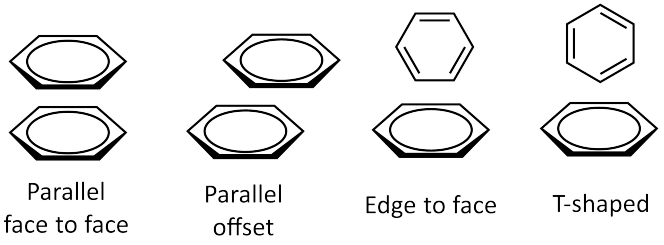

Scheme 2.10: Typical conformations of π-π interactions in aromatic rings.[130]

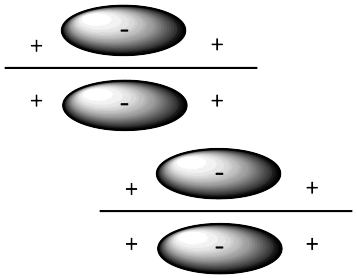

Scheme 2.11: A proposed offset parallel conformation of two adjacent rings interacting.[130]

Focusing on the inductive effects of substituents, tuning the group on the *meta* position of the reactive centre, based on σ, can influence the extent of π-π stacking and lead to tuneable thermal and mechanical properties of the resultant polyesters and their reactivities.

2.2 Results and Discussion

2.2.1 α-Phenyl-β-Propiolactone

The synthesis of α-phenyl-β-propiolactone via the palladium catalyst, $Pd[(PPh_3)_2Cl_2]$, was carried out following literature procedure.[122] Styrene oxide was reacted with hydrobromic acid in chloroform for 30 minutes at room temperature to afford 2-bromo-2-phenylethanol. The ^1H NMR showed traces of impurities and therefore column chromatography was carried out to obtain a pure sample. This was then reacted in an ampoule with the catalyst in the presence of hydrazine, to activate the catalyst through reduction, in dimethylformide (DMF) for 24 hours at room temperature under 1 bar CO pressure, to saturate the ampoule via a balloon (Scheme 2.12). The crude mixture was filtered to yield 7.1 % of α-phenyl-β-propiolactone. NMR analysis of the filtered brown oil showed several peaks in the aromatic region indicating the oil obtained was impure.

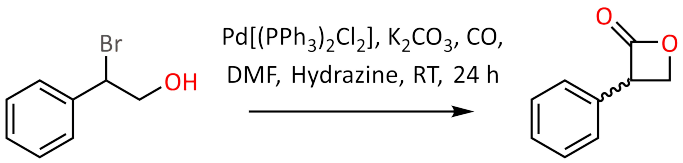

Scheme 2.12: Reaction steps to afford α-phenyl-β-propiolactone using a palladium catalyst.

The insufficient yield led to the optimisation of the reaction set up. A high-pressure vessel, Parr reactor, was used in the presence of 100 bar CO. The reaction yield (9.8 %) indicated no improvement through the adjusted set up. It has been known for the presence of oxygen or water in air to influence the reactivity of many catalysts. For successful carbonylation, CO coordination to palladium requires a free coordination site; water or oxygen could block this site. Therefore, the reaction was set up in the glove box, where an inert atmosphere was achieved. 2-bromo-2-phenylethanol was distilled under vacuum to eliminate traces of water or oxygen and the catalyst and other reagents were dried under vacuum for 16 hours prior to cycling them into the glove box. The reaction yield was similar to the previous reaction set up indicating that the Pd catalyst was more robust that predicted.

The purity of the solvent (through the amount of water present) was also investigated, standard, anhydrous and dried dimethylformide were used. Two consecutive reactions were performed with one yielding product and the other with no reaction, where the only difference was the batches of DMF used. The purity of the solvent was tested via ^{1}H NMR spectroscopy and showed no traces of impurities, the pH of the solvent was also tested and showed that the standard DMF was slightly acidic. Standard DMF was then dried via calcium hydride and distilled before use and showed an increase in yield (21.4 %). The purity of the lactone was analysed via ^{1}H NMR spectroscopy to show several peaks in the aromatic region, similar as to before. The crude oil was subjected to flash chromatography using dichloromethane in attempt to remove the impurities and to yield 14 mg (4.7%) of a yellow oil. ^{1}H NMR spectroscopy confirmed the yellow oil was pure lactone. The reaction was repeated several times to obtain sufficient monomer for ROP. This indicates that

under acidic environments the reaction does not proceed, predictably due to the open form of the lactone being the major product but also counter-acting the base hydrazine for the activation of the catalyst.

The alternative route to α-phenyl-β-propiolactone using the rhodium catalyst, $Rh[Cl(CO)(PPh_3)_2]$, was attempted. The reaction required a higher catalyst loading (2.1 mol%). The oxidative addition reaction between the $Rh[Cl(CO)(PPh_3)_2]$ catalyst and styrene oxide in methanol in the presence of carbon monoxide yielded no product with signs of the starting material observed (Scheme 2.13).

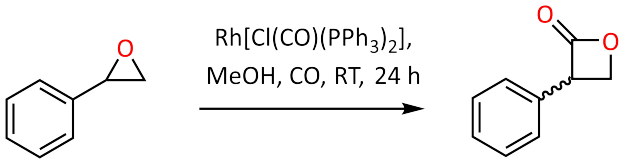

Scheme 2.13: Synthesis of α-phenyl-β-propiolactone via styrene oxide using a rhodium catalyst.

Accessing α-phenyl-β-propiolactone was challenging due to the reactive hydrogen atom on the α-carbon.[118] The phenyl ring can act as an electron rich source as well as a point of resonance to stabilise any intermediates. In addition, the electron-withdrawing effect of the phenyl ring could lower the pK_a of the α-hydrogen atom to 20.8. Consequently, addition of a reagent with a pK_a higher than 20.8, for example a strong base, will result in abstraction of the proton leading to by-products.

The electronic and steric effects of the phenyl ring also decreases the basicity of the hydroxyl group making it less nucleophilic to attack the carbonyl group and thus closing the ring to form the lactone becomes even more challenging.[122] Scaling up the reaction was not feasible due to the high loading of the expensive catalyst.

2.2.2 Substituted Benzodioxepinones

Monomers **1** to **4** were accessed via a two-step synthesis involving an S_N2 reaction to form the 2-(2-hydroxyethoxy)-5-R-benzaldehydes, which were then subjected to lactonisation via a thiazolium catalyst (Scheme 2.14).

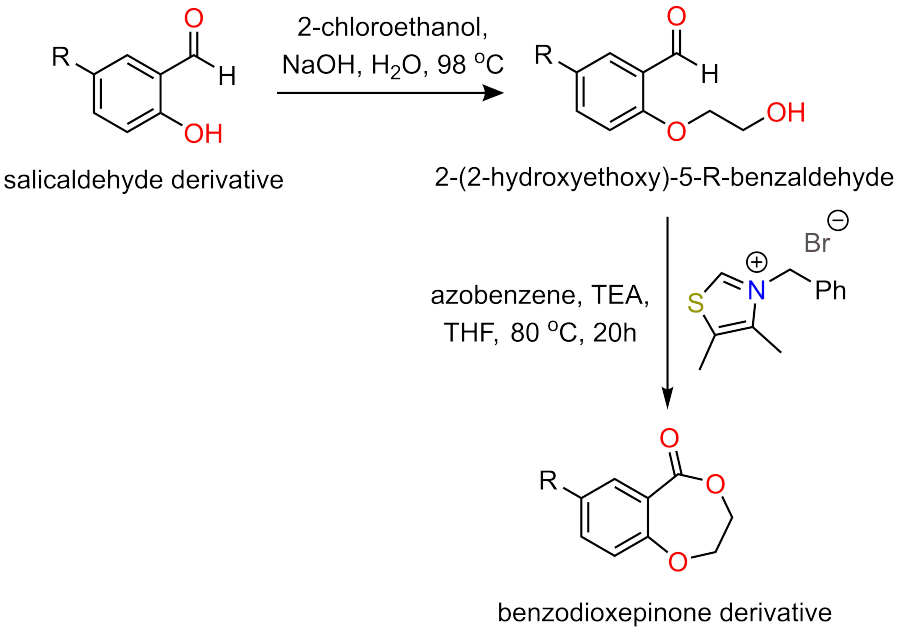

Scheme 2.14: Synthesis of substituted benzodioxepinone derivatives using a thiazolium catalyst derived from salicylaldehyde derivatives and 2-chloroethanol.

The bromine substituted benzodioxepinone was the first to be synthesised and was used to optimise the synthesis for subsequent monomers. 5-bromosalicaldehyde was reacted with 2-chloroethanol in the presence of sodium hydroxide in water to form 5-bromo-hydroxyethanol benzaldehyde, with the elimination of hydrochloric acid. The reaction mixture was stirred at 98 °C for 16 hours followed by extraction with ethyl acetate. The ^{1}H NMR spectrum prior to extraction showed chemical shifts relating to the starting material and product, however the ^{1}H NMR spectrum after extraction only showed 5-bromosalicaldehyde; the product was absent in both the organic and aqueous layer.

The procedure was modified to avoid work-up. The reaction solution after 16 hours was measured to be pH 11, due to the presence of sodium hydroxide, suggesting that the hydroxy proton could be deprotonated and thus charged, making it more soluble in water. As both starting materials were soluble in water, dilute hydrochloric acid was added dropwise to protonate the hydroxyl group and precipitate out the product. The ^{1}H NMR spectrum of the precipitate showed 5-bromosalicaldehyde, unlike the ^{1}H NMR spectrum before addition of HCl, showing both starting materials and product.

The reaction progress was then monitored by thin layer chromatography (TLC). The TLC of the reaction after 16 hours revealed the presence of two compounds, one being the starting material, 5-bromosalicaldehyde. The work-up process was avoided, and the crude mixture was concentrated under vacuum, with 50 % toluene to form an isotrope. The second spot was isolated via column chromatography in a 5:1 petroleum ether:ethyl acetate eluent system to afford 2-(2-hydroxyethoxy)-5-bromo-benzaldehyde (88.6 % yield), confirmed by ^{1}H and ^{13}C NMR spectroscopy.

2-(2-hydroxyethoxy)-5-bromo-benzaldehyde was reacted with trans-azobenzene under inert conditions with the thiazolium catalyst and anhydrous TEA in anhydrous tetrahydrofuran (THF) at 80 °C for 20 hours. TLC of the crude mixture showed presence of starting material, product and several by-products of trans-azobenzene. Column chromatography with a gradient hexane:ethyl acetate eluent system yielded 88.6 % of monomer **4**. Increasing the equivalents of trans-azobenzene from 1 to 1.5, increased the yield of the lactonisation.

Monomers **1**, **2** and the novel monomer **3** were synthesised from the optimised conditions and purification methods as per monomer **4**. Exploring the electronic substituent parameter, higher values of σ_{meta} were selected to investigate the extent to which the π-π interactions of the resultant polymers could be enhanced (Scheme 2.15).

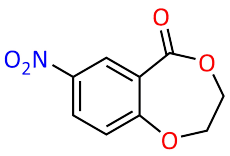

Monomer 5

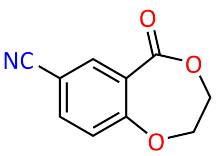

Monomer 6

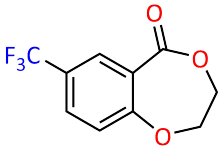

Monomer 7

Scheme 2.15: Monomers with substituents of increasing electron withdrawing properties, denoted by their higher values of σ_{meta}.

Synthesis of monomer **5** was attempted following the previously optimised procedure. 5-nitro-hydroxyethanol benzaldehyde was synthesised and purified via column chromatography, through dry loading due to poor solubility, to yield 46.6 % of a brown solid. This was subjected to lactonisation under the same conditions. However, poor solubility of the starting material was observed, leading to poor conversions. Changing the solvent from THF to toluene, in accordance with Rose *et al.*,[124] decreased the solubility even further. The ^{1}H NMR spectrum of the novel compound, 5-nitro-hydroxyethanol benzaldehyde, suggested no impurities to cause solubility issues. The ^{1}H NMR spectrum of the crude mixture from the lactonisation showed chemical shifts relating to the product and the starting material, indicating some conversion. Several purification methods such as recrystallisation, extraction, column chromatography and distillation were attempted to isolate the product. The poor solubility of the starting material and the resultant lactone led to the theory that even if the lactone was isolated, homogenous polymerisation would not be possible.

Monomers **6** and **7** required *ortho*-formylation of the substituted phenols to access their respective salicaldehydes. Hofsløkken *et al.* synthesised an array of substituted salicaldehydes from the reaction of paraformaldehyde, magnesium dichloride and TEA in acetonitrile under reflux. Hofsløkken *et al.* observed that EWG's inhibited the reaction, leading to lower yields, where EDG's promoted the reaction. Methyl, tert-butyl, and methoxy substituents accessed the aldehydes with excellent yields. When attempting the synthesis of EWG's such as cyano reduced the reactivity of the phenol significantly and increased the tendency for the by-product, 4-methoxymethoxybenzonitrile, to be formed. It was observed that elongated reaction times or changing the solvent had no improvement on the yields.[125]

The electronic substituent parameter for the cyano group in the meta position is 0.56 where as for the trifluoromethyl σ_{meta} is 0.43, indicating that trifluoromethyl is less electron withdrawing. This substituent was not attempted by Hofsløkken *et al.* under those conditions. Therefore, 4-trifluromethylphenol was reacted following literature procedure for 4 hours.[125] Monitoring the reaction through TLC and ^{1}H

NMR spectroscopy, no reaction was observed.

An alternative method for *ortho*-formylation using an organic reagent in the Duff formylation reaction was explored. The Duff formylation reaction involves the hexamine, hexamethylenetetramine (HTMA), as the formyl carbon source instead of paraformaldehyde. The accepted mechanism involves the protonation and ring-opening of the hexamine to give rise to the intermediate, β-aminoketone-type Mannich base. The intermediate then undergoes oxidation, rearrangement and re-aromatisation followed by hydrolysis to afford the respective salicylaldehyde (Scheme 2.16).[131]

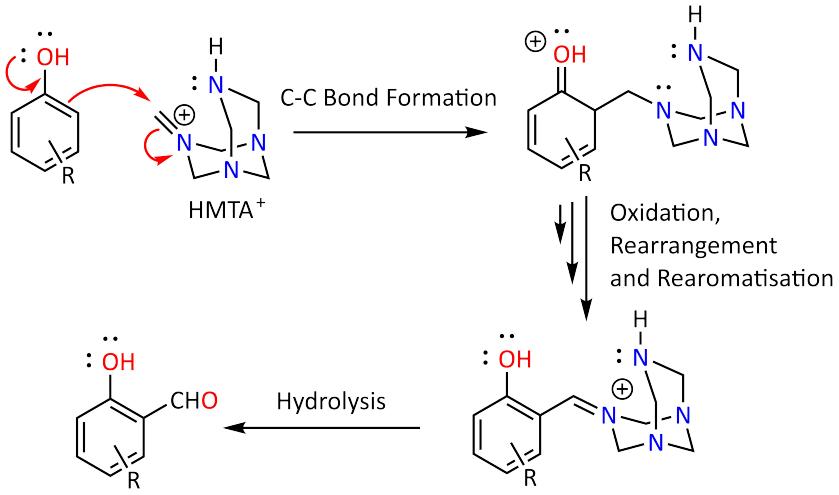

Scheme 2.16: Accepted mechanism of the Duff reaction to afford salicylaldehyde derivatives, modified from Grimblat *et al.*[131]

The reaction of 4-trifluoromethylphenol and 4-cyanophenol with HMTA in trifluoracetic acid for 18 hours under reflux yielded no product. This is predicted to be due to insufficient electron density around the hydroxyl oxygen to form the first intermediate.

The reactivities of monomers **1** to **4** upon ROP were investigated along with the thermal and mechanical properties of their resultant polyesters. Unfortunately, the poor solubility and the challenges in synthesising the more electron withdrawing substituents, monomers **5** to **7** were disregarded.

Chapter 3

Polymerisation

3.1 Introduction

A series of benzodioxepinones have been synthesised by Rose *et al.*,[124] with the unsubstituted 2,3-DHB being subjected to ROP by MacDonald *et al.* to afford P2HEB with a molecular weight of up to 52,050 g mol^{-1}.[113] The driving force behind the synthesis of P2HEB was the desire to replace commodity plastics such as PET. P2HEB and PET are both aromatic-aliphatic polyesters, however there are structural differences. The aromatic group in PET is *para*-linked where as in P2HEB the aromatic group is *ortho*-linked, similar to that of PEP. The orientation of the aromatic group has an influence on the packing efficiency of the polymer and hence the thermal and mechanical properties as seen with PET and PEP. The discovery of the monomer-polymer equilibrium led to expansion of this research to target P2HEB of different molecular weights, in addition to the ROP of monomers **1**, **2**, **4** and the novel monomer **3**, to investigate the thermal, mechanical and degradation characteristics of the novel aromatic-aliphatic polyesters.

3.2 Results and Discussion

MacDonald *et al.* screened catalysts for the ROP of 2,3-DHB and concluded that the optimal catalysts were the aluminium salen catalyst and the organocatalyst TBD.[113] The conditions for these catalysts were further tuned to probe the monomer-polymer

equilibrium and investigate the effect of substituents on equilibrium rate constants, k_p and k_d (Scheme 3.1).

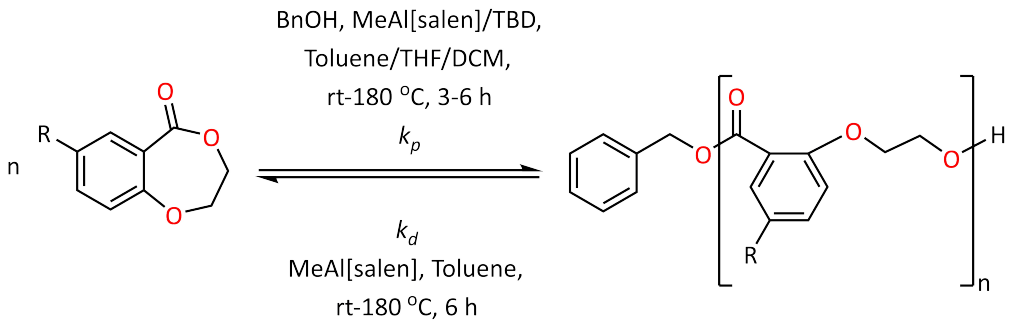

R = H (P2HEB), Me (**1**), OMe (**2**), F (**3**), Br (**4**)

Scheme 3.1: General ROP scheme of Monomers **1** to **4** and 2,3-DHB using MeAl[salen] or TBD as a catalyst.

3.2.1 Screening of Polymerisation Conditions for 2,3-DHB

Table 3.1: [a]Determined by ^{1}H NMR, [b]Determined by gel permeation chromatography (GPC), dn/dc value used to calculate M_n was 0.115.

M:I:C	Cat.	Solv.	Temp. (°C)	Time (h)	Conver.[a] (%)	Target M_w (g mol^{-1})	M_n[b] (g mol^{-1})	Đ
100:1:1	Al	Tol.	60	6	99.3	11,000	11600	1.14
500:1:1	Al	Tol.	60	6	93.4	40,000	40300	1.23
1000:1:1	Al	Tol.	60	6	95.1	80,000	78600	1.20

The aromatic-aliphatic polyester, P2HEB, of higher molecular weights was targeted to explore the effects of molecular weight on the polyester's thermal, mechanical and degradation behaviours. P2HEB was accessed through the ROP of 2,3-DHB, catalysed by aluminium salen with a benzyl alcohol (BnOH) initiator in toluene. The polymerisation showed excellent control with narrow dispersities and predictable molecular weights without compromising conversion, even at higher molecular weights (Table 3.1). P2HEB with molecular weights of 11,600, 40,300 and 78,600 g mol^{-1} were afforded by altering the monomer to initiator to catalyst

ratio (M:I:C - $[2,3\text{-DHB}]_0$: $[BnOH]_0$: $[Al]_0$) from 100:1:1 to 500:1:1 and 1000:1:1 respectively. The concentration of the polymerisation played a vital role in the successful conversion of 2,3-DHB. In order to shift the monomer-polymer equilibrium to the right the concentration of monomer had to be high, which was achieved through minimal solvent use. Increasing the temperature to 70 °C and having a dilute concentration was shown to increase the rate of transesterification leading to depolymerisation (k_d).[113] The optimum conditions to reduce this during polymerisation was found to be 60 °C with minimal amount of solvent.

3.2.2 Screening of Polymerisation Conditions for Monomer 2

Table 3.2: [a]Determined by ^{1}H NMR, [b]Determined by GPC, dn/dc value used was that of polystyrene standards (0.185).

No.	M:I:C	Cat.	Solv.	Temp. (°C)	Time (h)	Conc. (M)	Conver.[a] (%)	M_w[a] (g mol^{-1})	Đ[b]	M_n[b] (g mol^{-1})	M_w[b] (g mol^{-1})
1	65:1:1	TBD	DCM	22	1	5.15	95.7	4470	1.24	3920	4850
2	65:1:1	TBD	DCM	50	1	5.15	95.3	6020	1.52	4480	6800
3	65:1:1	Al	Tol.	60	3	2.03	32.1	3880	1.41	3630	5110
4	65:1:1	Al	Tol.	60	6	2.03	60.8	6800	1.32	4850	6380
5	65:1:1	Al	THF	60	6	2.15	42.8	6020	1.36	4300	5840
6	65:1:1	Al	Tol.	60	6	6.08	63.5	5830	1.41	4600	6460
7	65:1:1	Al	Tol.	60	6	12.15	72.3	7570	1.29	5770	7420
8	100:1:1	Al	Tol.	60	6	3.04	52.8	10100	1.23	5360	6600
9	100:1:1	Al	Tol.	60	6	5.15	65.5	11260	1.24	7130	8830
10	65:1:1	Al	Tol.	50	6	3.04	54.7	5830	1.31	4450	5830
11	65:1:1	Al	Tol.	22	6	3.04	35.1	4080	1.17	2790	3280
12	65:1:1	Al	-	110	6	neat	0	-	-	-	-
13	65:1:1	Al	-	180	6	neat	0	-	-	-	-

The conditions for the ROP of monomer **2** were screened with TBD and aluminium salen to study the monomer-polymer equilibrium and afford the aromatic-aliphatic polyester **2** with a target molecular weight of 11,000 g mol^{-1} (Table 3.2). Entry 1 and 2 show the rapid conversion of monomer **2** to polymer **2** with the organocatalyst TBD in just 1 hour. In both cases the target molecular weight of

11,000 g mol^{-1} was not achieved. Altering the temperature of the polymerisation from 22 °C to 50 °C showed no change in conversion, however the molecular weight increased as observed by ^{1}H NMR spectroscopy. The dispersity of the polymerisation also increased significantly indicating poor control over the polymerisation. The inability to afford polymer **2** with a molecular weight of 11,000 g mol^{-1}, albeit the high conversions, was an indication of transesterification leading to shorter polymer chains and a higher dispersity.[55,113]

Following literature procedure,[113] the polymerisation was catalysed by aluminium salen in toluene at 60 °C. Monitoring the conversion at 3 hours (Entry 3) and 6 hours (Entry 4) a two-fold increase in conversion and molecular weight were observed with Entry 4 having a lower dispersity. Subliming monomer **2** under vacuum using a Schlenk flask to further purify the monomer showed no further improvement to the conversion.

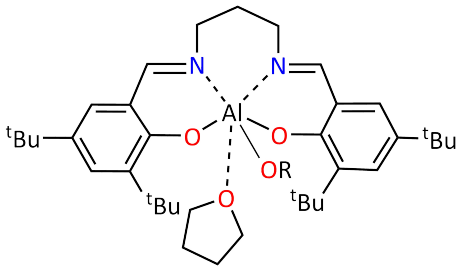

Scheme 3.2: Rapid equilibrium of the weak coordination of the oxygen in a THF molecule to aluminium salen.[132]

Increasing the polarity of the solvent to THF (Entry 5) showed a slight decrease in conversion and molecular weight with a similar dispersity to Entry 4. The weak Lewis base coordination ability of THF suggests possible hindrance on the catalytic activity of aluminium salen due to the rapid equilibrium between the active catalyst and the Al-THF complex (Scheme 3.2)[132]

Through increasing the initial monomer concentration in Entry 4 from 2.03 M to 6.08 M and 12.15 M in Entry 6 and 7 respectively, an increase in the conversion and molecular weight was observed. The experimental data agrees with the monomer-polymer equilibrium, where increasing the initial monomer concentration would shift the equilibrium to the right, with k_p dominating, leading to higher conversions.

ROP of monomer **2** to achieve a target molecular weight of 11,000 g mol^{-1} was challenging as seen from Entries 1 to 7, however increasing the M:I:C to 100:1:1 (Entry 8) a higher molecular weight was achieved with a similar dispersity, although no improvement in the conversion was observed. Increasing the concentration (Entry 9) led to a higher conversion and the target molecular weight whilst maintaining a narrow dispersity for this system.

Probing the monomer-polymer equilibrium further, ROP was carried out at varying temperatures. Decreasing the temperature to 50 °C (Entry 10) and comparing with Entry 8, both at a concentration of 3.04 M of initial monomer, no significant difference was observed in the conversion. Performing the polymerisation at 22 °C with aluminium salen (Entry 11) showed a significant decrease in conversion, however a decrease in the dispersity was also observed. It is well known that transesterification can be minimised through decrease in temperature and reaction time.[55]

Carrying out the polymerisation in the absence of solvent (Entry 12 and 13) showed no conversion. At 110 °C monomer **2** was still a solid, therefore no reaction was observed. The temperature was increased to 180 °C in order for monomer **2** to be in the melt phase for polymerisation to occur, however the polymerisation was still unsuccessful.

The discrepancy in the molecular weights analysed by ^{1}H NMR and GPC was due to the poor solubility of the polymer in THF, therefore the molecular weights reported in publications of this work are those by ^{1}H NMR spectroscopy.

3.2.3 Screening of Polymerisation Conditions for Monomer 1

Table 3.3: [a]Determined by ^{1}H NMR Spectroscopy, [b]Determined by GPC, dn/dc value used was that of polystyrene standards (0.185).

No.	M:I:C	Cat.	Solv.	Temp. (°C)	Time (h)	Conc. (M)	Conv.[a] (%)	M_w[a] (g mol^{-1}	Đ[b]	M_n[b] (g mol^{-1})	M_w[b] (g mol^{-1})
1	100:1:1	TBD	DCM	22	1	4.9087	97.2	5350	1.19	8100	9620
2	100:1:1	TBD	DCM	50	1	4.9087	84.3	4450	1.27	5800	7330
3	100:1:1	Al	Tol.	60	6	4.2355	60.5	9270	1.26	8770	11080
4	100:1:1	Al	THF	60	6	4.9085	56.9	6590	1.23	6670	8210
5	115:1:1	Al	Tol.	60	6	5.74118	73.2	11050	1.23	9230	11340
6	65:1:1	Al	Tol.	22	6	3.04	63.3	6240	-	-	-
7	65:1:1	Al	-	110	6	neat	0	0	-	-	-
8	65:1:1	Al	-	180	6	neat	0	0	-	-	-

The data obtained from the ROP of monomer **2** was used as a foundation for the further optimisation of monomer **1** to afford polymer **1** (Table 3.3). As predicted, the polymerisation catalysed by TBD was rapid with high conversions and in the case of Entry 1, at 22 °C, a narrow dispersity. The polymerisation at 50 °C (Entry 2) led to a slightly broader dispersity with a lower conversion and molecular weight. The high conversions did not translate to the target molecular weight of 11,000 g mol^{-1}, whilst also disagreeing with the GPC molecular weights due to transesterification with TBD and the poor solubility in the GPC solvent (THF). It is evident from the dispersity that the degree of transesterification of monomer **1** was lower than that of monomer **2**.

Using a M:I:C of 100:1:1 with aluminium salen in toluene at 60 °C for 6 hours, afforded the aromatic-aliphatic polyester **1** with a molecular weight close to that of the target molecular weight whilst maintaining an acceptable dispersity (Entry 3). Altering the solvent from to toluene to THF (Entry 4), showed a decrease in conversion and molecular weight, again due to the weak coordination of THF to aluminium salen even though the polymer was soluble in THF at the polymerisation temperature of 60 °C.

The polymerisations catalysed by aluminium salen for monomer **1** were reaching

approximately 60 % conversion, therefore the M:I:C was increased to 115:1:1 along with the initial monomer concentration (Entry 5). A higher conversion was observed after 6 hours, attributed to the increase in concentration of monomer, with the target molecular weight of 11,000 g mol^{-1} achieved.

Decreasing the temperature for the ROP of monomer **1** (Entry 6) showed no difference in conversion, even at a lower initial monomer concentration. The conversion at 22 °C suggested that 60 °C was not required, however the balance between solubility of the monomer and polymer in toluene as well as the temperature to drive the polymerisation led to the conclusion that the optimal conditions for polymerisation of monomer **1** was 60 °C in toluene.

The opposite was observed when increasing the temperature to 110 and 180 °C (Entry 7 and 8 respectively) where in the absence of solvent no polymerisation was observed.

3.2.4 Screening of Polymerisation Conditions for Monomer 3

Table 3.4: [a]Determined by ^{1}H NMR Spectroscopy, [b]Determined by GPC, dn/dc value used was that of polystyrene standards (0.185).

No.	M:I:C	Cat.	Solv.	Temp. (°C)	Time (h)	Conc. (M)	Conv.[a] (%)	M_w[a] (g mol^{-1})	Đ[b]	M_n[b] (g mol^{-1})	M_w[b] (g mol^{-1})
1	100:1:1	Al	THF	60	6	5.48	64.6	9470	1.39	7020	9730
2	150:1:1	Al	Tol.	60	6	5.48	63.2	12020	-	-	-
3	65:1:1	Al	THF	22	6	2.75	71.5	5830	1.20	4950	5920
4	65:1:1	Al	-	110	6	neat	66.9	7290	-	-	-
5	65:1:1	Al	-	180	6	neat	58.4	2190	-	-	-

The ROP of monomers **3** and **4** were catalysed by aluminium salen due to the degree of transesterification caused by TBD, observed in monomers **1** and **2**. The initial ROP of monomer **3** to afford polymer **3** was done in THF due to the poor solubility of the monomer in toluene (Table 3.4, Entry 1). The polymerisation was poorly controlled with a dispersity of 1.38, however with good conversion. Changing the solvent to toluene (Entry 2) led to similar conversions, with greater control, and

the target molecular weight. Precipitation of the polymer was observed in both Entry 1 and 2 after approximately three hours, indicating the poor solubility of the polymers in THF and toluene after a certain molecular weight. The polymerisations were no longer homogenous and unable to proceed, therefore producing a lower molecular weight polymer. The M:I:C was increased in Entry 2 to 150:1:1, whilst maintaining the concentration, in order to drive the polymerisation to reach the target molecular weight.

A higher conversion was achieved at 22 °C (Entry 3) for monomer **3** than for monomer **1** and **2**. Several factors can affect the degree of polymerisation and for this system specifically, the electronic substituent parameter and the solubility of the monomer and polymer can influence the rate and extent of polymerisation. Monomer **3** has a higher σ_{meta} value than monomers **1** and **2**, denoting that monomer **3** is more electron withdrawing. The electronic nature of monomer **3** suggests that the rate of polymerisation would be higher. In this case, solubility has not greatly affected the trend as monomer **3** is soluble in THF and partially soluble in toluene.

Increasing the polymerisation temperature to 110 °C and 180 °C (Entry 4 and 5 respectively) showed similar conversions to the polymerisations at 60 °C, with Entry 5 showing a slight decrease in conversion. The inability to obtain a GPC chromatogram for Entry 4 and 5 indicated the formation of oligomers, which by ^{1}H NMR spectroscopy would show as polymeric chemical shifts.

3.2.5 Screening of Polymerisation Conditions for Monomer 4

Table 3.5: [a]Determined by ^{1}H NMR Spectroscopy, [b]Determined by GPC, dn/dc value used was that of polystyrene standards (0.18).

No.	M:I:C	Cat.	Solv.	Temp. (°C)	Time (h)	Conc. (M)	Conv.[a] (%)	M_w[a] (g mol^{-1})	Đ[b]	M_n[b] (g mol^{-1})	M_w[b] (g mol^{-1})
1	30:1:1	Al	Tol.	60	3	3.16	73.2	6960	-	-	-
2	80:1:1	Al	THF	60	6	3.125	44.8	6240	1.389	4416	6132
3	100:1:1	Al	THF	60	6	3.958	75.3	6720	-	-	-
4	100:1:1	Al	THF	60	6	5.15	50.3	7680	1.426	4109	5861
5	65:1:1	Al	THF	22	6	3.04	44.3	6240	1.254	3563	4436
6	50:01:01	Al	Tol.	180	6	7.81	-	-	1.444	1325	1953
7	80:1:1	Al	Tol.	180	0.5	4.85	-	-	1.267	1390	1760
8	150:1:1	Al	Tol.	60	6	4.16	36.2	10320	-	-	-

Challenges in solubility of monomer **4** were observed in THF and toluene even at low concentrations (Table 3.5). A low M:I:C ratio was initially used (Entry 1) showing a good conversion after just three hours in toluene to polymer **4**. Increasing this ratio to 80:1:1 with a longer reaction time in THF (Entry 2) whilst maintaining the concentration, showed a significant decrease in conversion and with a dispersity of 1.38, indicating poor control over the polymerisation. The lower conversion was due to the poor solubility of the monomer and polymer THF and the weak coordination of THF to aluminium salen.

A further increase to 100:1:1 (Entry 3) in THF with a slightly higher concentration compared to Entry 1 and 2 led to an increase in conversion with a similar molecular weight. Increasing the concentration from 3.98 M to 5.15 M (Entry 4) led to an increase in molecular weight, albeit with a decrease in conversion. ROP in THF compared to toluene showed the general trend of poorer control and lower conversions.

The polymerisation at 22 °C (Entry 5) showed only 44.3 % conversion, similar to monomer **2**, this is surprising as due to the electronic nature of monomer **4**, where the electronic substituent parameter is the highest, it is predicted to have the highest rate and degree of polymerisation. It was clearly observed that solubility

had an influence in the rates.

Monomer **4** was not soluble in the melt phase at 110 °C and therefore the polymerisations in the absent of solvent were done at 180 °C. Entry 6 and 7 with different M:I:C ratio showed an insignificant conversion with poor control over the polymerisations.

Due to the inability to reach the target molecular weight of 11,000 g mol^{-1}, the M:I:C ratio, similarly to monomer **3**, was increased to 150:1:1 (Entry 8). Even though the conversions were poor, a molecular weight close to the target molecular weight was achieved.

3.2.6 Polymerisation Kinetics

The influence of the electronic substituent parameter on the rate of polymerisation was investigated in toluene at 60 °C. The solubility of the monomers and polymers were tested in THF, toluene and DCM prior to studying the polymerisation kinetics (Table 3.6).

Table 3.6: Solubility tests of monomers **1** to **4** and polymers **1** to **4** in THF, DCM and toluene.

Monomer	**Solvent**	**Solubility (mg mL^{-1})**
1	THF	210.8
	DCM	799.4
	Toluene	161.7
2	THF	142.8
	DCM	220.5
	Toluene	75.1
3	THF	137.5
	DCM	216.7
	Toluene	85.7
4	THF	90.7
	DCM	128.6
	Toluene	74.9
Polymer	**Solvent**	**Solubility (mg mL^{-1})**
1	THF	33.2
	DCM	200.8
	Toluene	<1
2	THF	<1
	DCM	160.6
	Toluene	<1
3	THF	<1
	DCM	<1
	Toluene	<1
4	THF	<1
	DCM	<1
	Toluene	<1

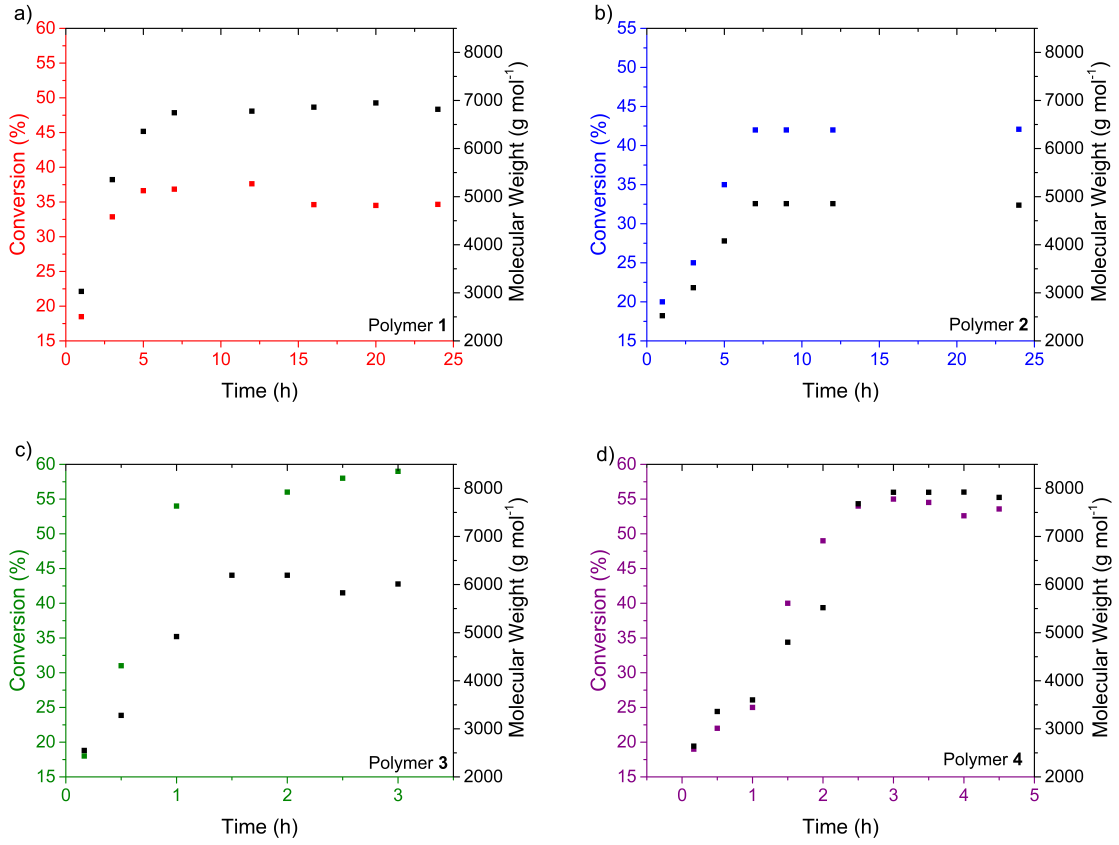

Figure 3.1: Converison of monomer to polymer and change in molecular weight with time. A close correlation between the two are indicative of a well controlled polymerisation. a) Conversion of monomer **1** to polymer **1**, b) Conversion of monomer **2** to polymer **2**, c) Conversion of monomer **3** to polymer **3** and d) Conversion of monomer **4** to polymer **4**.

The polymerisation kinetics for monomers **1** and **2** were studied over 24 hours with 2 to 3 hour intervals, whilst monomer **3** was studied over 3 hours at 30 minute intervals due to precipitation of the polymer after 3 hours and monomer **4** was studied over 6 hours with 30 minute intervals (Figure 3.1). The aliquots were taken and quenched with a few drops of 10 % dichloromethane in methanol to prevent further polymerisation during transfer to analysis by ^{1}H NMR spectroscopy.

The polymerisation of monomers **1** to **4** proceeded in a linear fashion up to the point of maximum conversion were the polymerisations plateaued. The analysed molecular weights closely matched the trend observed for the conversions of each monomer to polymer. The maximum conversions did not correlate to the conver-

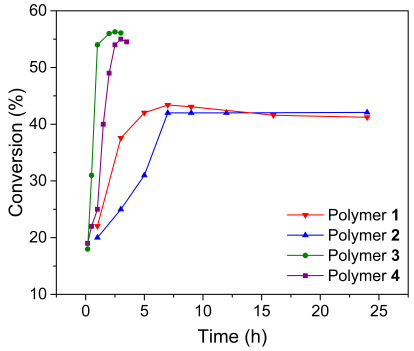

Figure 3.2: Combined plot of polymers **1** to **4** showing the monomer conversion with time.

sions observed during polymer condition screening due to more solvent needed for monomer **4**, and thus less concentrated solutions for all four monomers.

Maximum conversions of monomers **3** and **4** were similar to one another and higher than that of monomers **1** and **2**. This arises from the EWG's on monomers **3** and **4** increasing the rate of polymerisation and shifting the monomer-polymer equilibrium in favour of k_p in a significantly shorter time than monomers **1** and **2**.

A closer look at monomers **1** and **2** (Figure 3.2) shows that monomer **1** reached maximum conversion of 42.5 % in 5 hours where monomer **2** reached a similar maximum conversion at 7 hours. According to the σ_{meta} values, where monomer **1** is -0.069 and monomer **2** is 0.0115,[129] monomer **2** is less electron donating and therefore is predicted to have a higher conversion and a slightly faster rate of polymerisation. The disagreement between prediction and experimental data was investigated further and is discussed later in this chapter.

Careful analysis of the maximum conversions of monomers **3** and **4** (Figure 3.2) reveals that monomer **3** had a rapid conversion to 55.1 % within the first hour followed by a further, slower, increase from 1 hour to 3 hours to 58.4 %. Monomer **4** on the other hand reaches a maximum conversion of 55.2 % in 2 $\frac{1}{2}$ hours and plateaus. The data suggests that the rate of polymerisation is higher for monomer **3**, this is the opposite to the predicted trend from the σ_{meta} values, where monomer **3** is 0.337 and monomer **4** is 0.391.[129] In the case of these two monomers, solubility is the overriding factor, where monomer **4** has a lower solubility in toluene at room

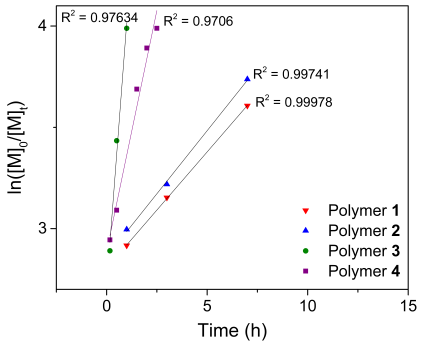

Figure 3.3: Conversion of monomer to polymer in the form of $\ln([M]_0/[M]_t)$ vs time in order to calculate the rate of polymerisation.

temperature, when the solution is prepared, and therefore until the inside of the reaction vessel reaches 60 °C the rate of polymerisation is significantly slower. This is evident by the conversion only being 22.5 % after 30 minutes whereas with monomer **3** the conversion was 32.6 %.

The rates of polymerisation, k_p, for each of the monomers were calculated from the linear regions of the polymerisation curves to gain further insight into the polymerisation. Plotting the linear regions of the conversion as $\ln([M]_0/[M]_t)$ vs time, showed pseudo-first order kinetics with respect to monomer concentration (Figure 3.3), indicating that the ROP of the monomers proceeded in a controlled manner.

Table 3.7: The trend observed between the σ_{meta} and the rates of polymerisation. [a]Rate of polymerisation calculated by MacDonald *et al.*[113]

Monomer	σ_{meta}	**Rate (h^{-1})**	**Rate (min^{-1})**
1	-0.069	0.11	0.0018
2	0.115	0.12	0.0020
3	0.337	1.3	0.0217
4	0.391	0.48	0.0080
2,3-DHB	0	0.6[a]	0.01[a]

The gradient of each monomer in the plot of $\ln([M]_0/[M]_t)$ vs time equates to k_p. Tabulating the σ_{meta} values along with the rates calculated and the rate previously

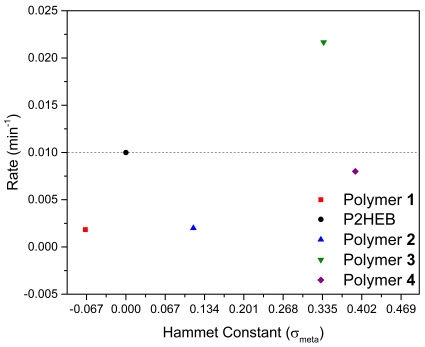

Figure 3.4: Rate of polymerisation in correlation with σ_{meta}, the dotted line represents the reference point in which σ_{meta} is zero.

calculated for 2,3-DHB under the same conditions,[113] shows a clear influence of the electronic substituent parameter on the rate constant (Table 3.7). A visual representation of the rate vs σ_{meta} shows the general trend that larger σ_{meta} values correlate to higher polymerisation rates (Figure 3.4).

According to the σ_{meta} values and the black dotted line (the reference point where σ_{meta} is zero) it is clear that monomers **2** and **4** do not follow that trend. Monomer **4**, theoretically, should have the fastest rate of polymerisation, however the theoretical and experimental data disagree due to the additional factor of solubility as previously discussed, where the poor solubility of monomer **4** in toluene decreases the rate of polymerisation, even below that of 2,3-DHB. Albeit the polymerisation rate of monomer **4** was faster than that of the electron donating substituents in monomers **1** and **2**.

Solubility was not an issue with monomer **2**, therefore the value of k_p was surprising. The methoxy (OMe) substituent is one of the few that can either be electron donating or electron withdrawing in respect to the hydrogen substituent depending on its position on the aromatic ring. In the *meta* position, only the electron withdrawing inductive effects of OMe are taking place, whereas in the *para* position both electron withdrawing inductive and the more dominating electron donating resonance effects are taking place, hence the negative σ_{para} value of -0.268.[129] With regards to monomer **2** the OMe substituent is *meta* to the reactive centre and is more electron withdrawing than the hydrogen substituent and thus should have a

higher rate constant.

This was further investigated by the synthesis of the *para* substituted methoxy (monomer **8**) in order to understand the anomaly observed with monomer **2**. Monomer **8** was synthesised in the same fashion as monomers **1** to **4** (57.9 % yield) and subjected to ROP.

Table 3.8: [a]Determined by ^{1}H NMR Spectroscopy, [b]Determined by GPC, dn/dc value used was that of polystyrene standards (0.185).

No.	M:I:C	Cat.	Solv.	Temp. (°C)	Time (h)	Conc. (M)	Conv.[a] (%)	M_w[a] (g mol^{-1})	Đ[b]	M_n [b] (g mol^{-1})	M_w [b] (g mol^{-1})
1	65:1:1	Al	Tol.	60	6	2.03	20.8	2130	-	-	-
2	65:1:1	Al	Tol.	60	6	6.08	16.6	1550	-	-	-
3	65:1:1	Al	Tol.	60	6	12.15	10.2	970	-	-	-
4	100:1:1	Al	Tol.	60	6	5.15	5.7	1160	-	-	-
5	65:1:1	Al	Tol.	50	6	3.04	29.7	3100	-	-	-
6	65:1:1	Al	Tol.	22	6	3.04	6.3	780	-	-	-

Low conversions were observed with the ROP of monomer **8**, even at higher concentrations (Table 3.8). The decrease in conversion upon increase in concentration (Entries 1-3) along with a decrease in conversion with an increase of monomer (Entry 4) suggested that the presence of more monomer **8** hindered the polymerisation. Decreasing the polymerisation temperature to 50 °C (Entry 5) gave the highest conversion at 29.7 %. This decreased significantly when performing the polymerisation at 22 °C (Entry 6).

The reason behind the unusual behaviour of monomer **8** was further investigated. It is known that hydroxyl and amine groups have a tendency to inhibit or adversely effect ROP catalysed by metal-based catalysts such as aluminium salen through "nonproductive" coordination.[133]

The coordination ability of the methoxy substituent in the *para* and *meta* position was studied using diffusion-ordered spectroscopy (DOSY), where NMR signals of different species are separated by their molecular volume and thus their diffusion constants. A 1:1 stoichiometric amount of MeAl[salen] and monomer **2** was added

to a Youngs tap NMR tube in deuterated toluene. The DOSY analysis (Figure 3.5) was manipulated to obtain the Log-D values of the two diffusion constants shown. The Log-D value was used to calculate the estimated molar mass of the components using a calibration curve developed by Weronika Gruszka from the Garden group at the University of Edinburgh. The DOSY NMR spectrum showed that the chemical signals from MeAl[salen], in the region of 2.19 ppm to 3.71 ppm, had the same diffusion constant (1.31 $\times 10^{-5}$ cm^2/sec) as the chemical shift relating to the methoxy protons on monomer **2** at 3.27 ppm. In addition to this, the methine protons at 3.54 ppm and 3.61 ppm also had the same diffusion constant (1.31 $\times 10^{-5}$ cm^2/sec). The estimated molar masses, based on their diffusion constant, were 281.84 g mol^{-1} for the chemical signals from MeAl[salen] (Log-D value of 8.93) and 145.89 g mol^{-1} for the chemical signals relating to monomer **2** (Log-D value of 8.67).

Upon decreasing the MeAl[salen]:monomer **2** ratio to 0.5:1 the molar mass increased for MeAl[salen] to 354.81 g mol^{-1} and decreased for monomer **2** to 125.73 g mol^{-1}. The change in molar mass may tentatively suggest that the level of coordination is dependent upon the ratio between MeAl[salen] and monomer **2**. However, all molar masses calculated are significantly different from the individual molar masses, where MeAl[salen] is 546.67 g mol^{-1} and monomer **2** is 194.19 g mol^{-1}. DOSY NMR typically can have up to 20 % error which partly arises from the fact that the calibration is done using molecular weight where diffusion is dependent on molecular volume instead of weight. This could explain the variation in the calculated molecular weights. While the molecular weights calculated are all significantly lower than expected, this data may tentatively suggest that two MeAl[salen] units coordinate one monomer, for example through the carbonyl oxygen and the methoxy oxygen[134,135]. This could explain the unexpected polymerisation behaviour and kinetics of monomer **2**.

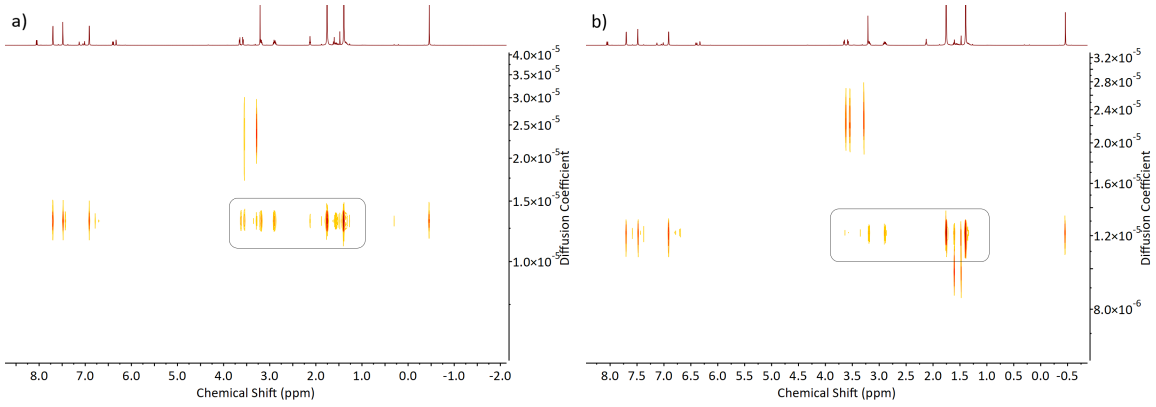

Figure 3.5: DOSY NMR of a) 1:1 MeAl[salen]:monomer **2** and b) 0.5:1 MeAl[salen]:monomer **2**.

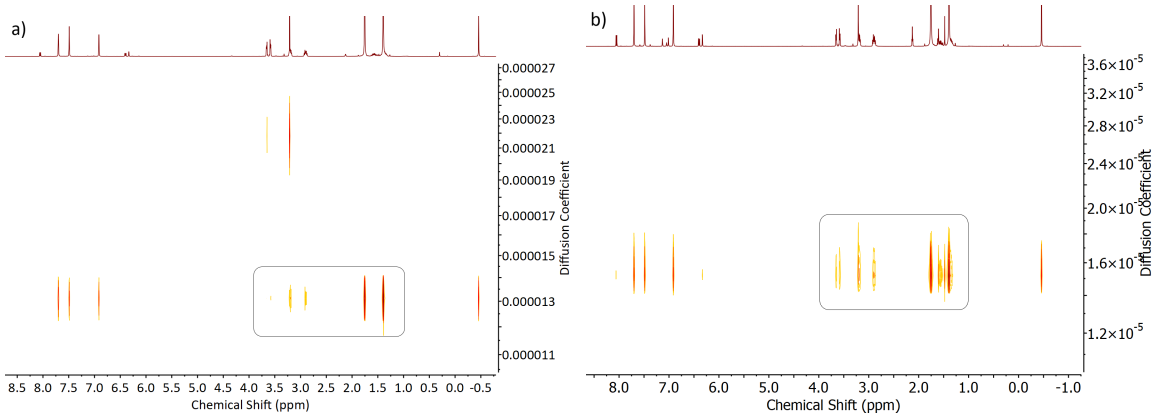

Figure 3.6: DOSY NMR of a) 1:1 MeAl[salen]:monomer **8** and b) 2:1 MeAl[salen]:monomer **8**.

When subjecting monomer **8** to a 1:1 stoichiometric amount of MeAl[salen], the calculated molar masses of the chemical signals in the region of 2.19 ppm to 3.71 ppm for MeAl[salen] was 316.23 g mol^{-1} and 112.20 g mol^{-1} for the chemical signal at 3.27 ppm for monomer **8**. The methine protons at 3.54 ppm and 3.61 ppm for monomer **8** were on a different diffusion constant as the methoxy protons and the MeAl[salen] protons. Increasing amount of MeAl[salen] to 2:1, showed an increase in molar mass for MeAl[salen] to 380.198 g mol^{-1} and a decrease in molar mass for monomer **8** to 100 g mol^{-1} (Figure 3.6). This could be a result of coordination of the monomer bridging between two aluminum metals suggesting the monomer may be coordinating to aluminum through both the carbonyl oxygen and the methoxy oxygen.

The observations from DOSY suggested that catalyst loading may influence the degree of coordination. The effect on catalyst concentration on the ROP of monomer **8** was studied (Table 3.9), however the polymerisation showed a reverse trend, where an increase in catalyst loading led to an increase in the rate of depolymerisation, k_d.

Table 3.9: ROP of monomer **8** for 6 hours at 60 °C in toluene with increasing molar equivalents of MeAl[salen] with respect to the initiator, BnOH. Monomer **8**:BnOH:MeAl[salen] = 100:1:1, 100:1:2, 100:1:5, 100:1:10, 100:1:20.

Molar Equivalents of MeAl[salen]	Conversion (%)
1	16.6
2	17.3
5	15.3
10	13.7
20	5.2

The lower polymerisation conversions and rates observed for monomers **2** and **8** are potentially explained by the possible coordination of aluminium salen to the methoxy oxygen as well as the carbonyl oxygen, supported by the differences in molar masses and the similarity in the diffusion constants of the catalyst and monomers.

3.2.7 Catalysed Degradation Studies

Catalytic degradation kinetics

P2HEB has previously demonstrated the ability to selectively depolymerise back to its cyclic monomer, 2,3-DHB, where k_d dominates. The depolymerisation is induced by the aluminium salen catalyst, at elevated temperatures and dilute concentrations.[113] Following literature findings, the catalytic degradation of P2HEB, in film form, via aluminium salen, of molecular weights 11,000, 40,000, and 80,000 g mol^{-1} were investigated.

Preliminary studies on the conditions for degradation were done on P2HEB with a molecular weight of 11,000 g mol^{-1}. While P2HEB degradation is insignificant at room temperature due to poor solubility in organic solvents, decreasing the concentration of the solution to 0.003 M at 70 °C with a stoichiometric amount of

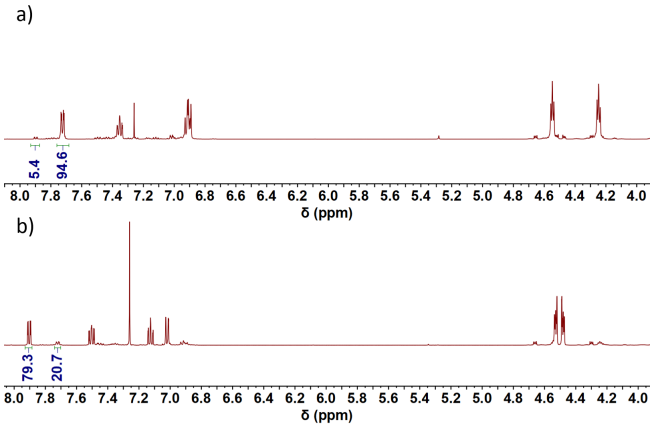

Figure 3.7: ^{1}H NMR spectra of a) P2HEB and b) 2,3-DHB.[136]

aluminium salen for one hour showed the chemical shift for one of the aryl protons in P2HEB at 7.72 ppm rapidly disappearing with the same proton chemical shift at 7.90 ppm reappearing for the monomer (Figure 3.7). Integration of both peaks after one hour showed 79.3 % of catalytic degradation. Under the same conditions, P2HEB of 40,000 and 80,000 g mol^{-1} showed a similar extent of degradation at 81.7 % and 80.4 % respectively, indicating the degree of depolymerisation was independent of molecular weight.[136] The extent of degradation was also independent of whether P2HEB was in the form of a film, isolated powders, or if degradation was conducted in situ after polymerisation, supporting the findings in literature.[113]

The catalytic degradation of purified and dried P2HEB and polymers **1** to **4** was studied in more detail to understand the kinetics of the depolymerisation and the effect of the substituents on these kinetics. Polymers **1** to **4** were subjected to depolymerisation studies under the same conditions and concentration as the P2HEB at 70 °C for 1 hour (Figure 3.8). Depolymerisation was shown to take place predominately in the first 10 minutes upon taking aliquots at 10 minutes intervals. Polymer **1** exhibited an increase in depolymerisation up to 30 minutes where it plateaued to reached a maximum degradation of 65.2 % after one hour. Polymer **2** on the other hand reached a maximum degradation of 85.8 % in 20 minutes and then plateaued to 82.1 % degradation after one hour. This observed plateau is attributed to the reaction being in equilibrium between monomer and polymer.

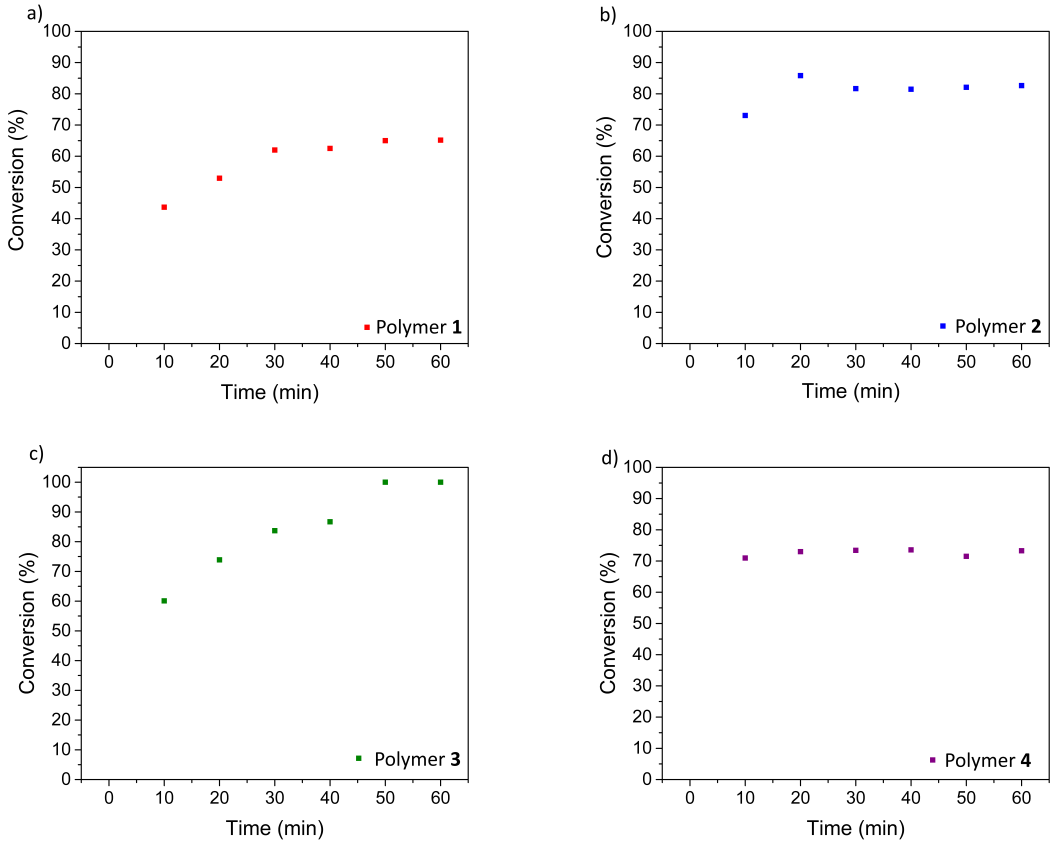

Figure 3.8: Depolymerisation of a) polymer **1**, b) polymer **2**, c) polymer **3** and d) polymer **4** over 60 minutes.

Polymer **3** showed a rapid increase in conversion from polymer to monomer, denoted by the 60.1 % depolymerisation at 10 minutes, which decreased in rate to give 100 % depolymerisation after one hour. Polymer **4** reached a maximum degradation of 74.9 % in 10 minutes and remained in equilibrium with the degradation being 73.3 % after one hour.

The first 10 minutes of depolymerisation was investigated further as it was clear that it showed the greatest depolymerisation activity (Figure 3.9). Individual ampoules were set up for each time point to eliminate the possibility of air entering the ampoule during sampling. Polymer **1** showed 45.2 % degradation after 10 minutes, matching the previous kinetic study, however plateaued to 45.3 %, unlike the previous kinetic study. Polymer **2** reached a lower degree of depolymerisation after 10 minutes compared to the previous study at only 61.9 %. Polymers **3** and **4** were significantly slower with depolymerisation after 10 minutes of 37.8 % and 28.3 %

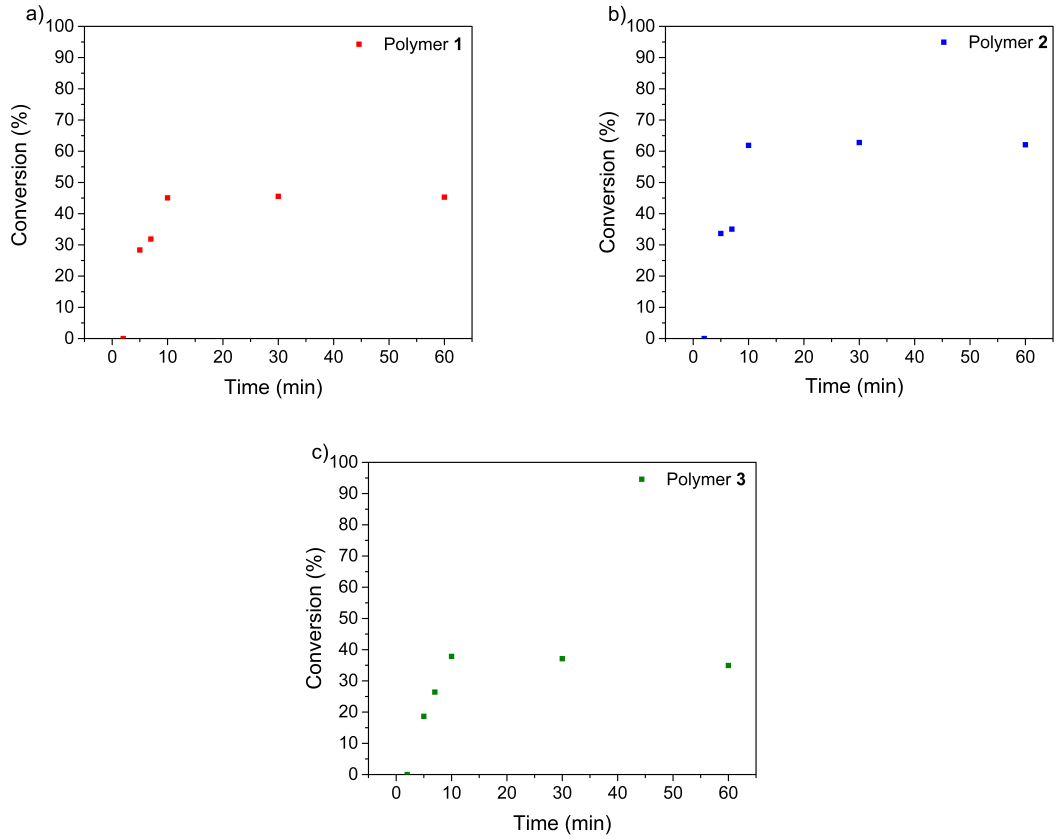

Figure 3.9: Depolymerisation of a) polymer **1**, b) polymer **2** and c) polymer **3** at 70°C.

respectively. Polymer **4** reached an equilibrium at 28.1 % for the remaining hour, indicating that the limiting factor of depolymerisation was solubility at 70 °C.

The disagreement between the initial study and the study with aliquots every 2-3 minutes was due to the poor solubility of the polymers in organic solvent, meaning every batch under study would have a different degree of solubility until the temperature inside the reaction vessel (ampoule) reached the experimental temperature of 70 °C.

The depolymerisation of the polymers were therefore studied at room temperature to monitor the degree of depolymerisation upon transferring the ampoule from the glovebox to the hotplate. No sign of depolymerisation was observed for polymers **3** and **4** due to the poor solubility of the polymers in toluene. However, polymers **1** and **2** showed a small degree of depolymerisation at approximately 5.7 %, note that the poor signal to noise ratio from the NMR spectra reduced the accuracy of

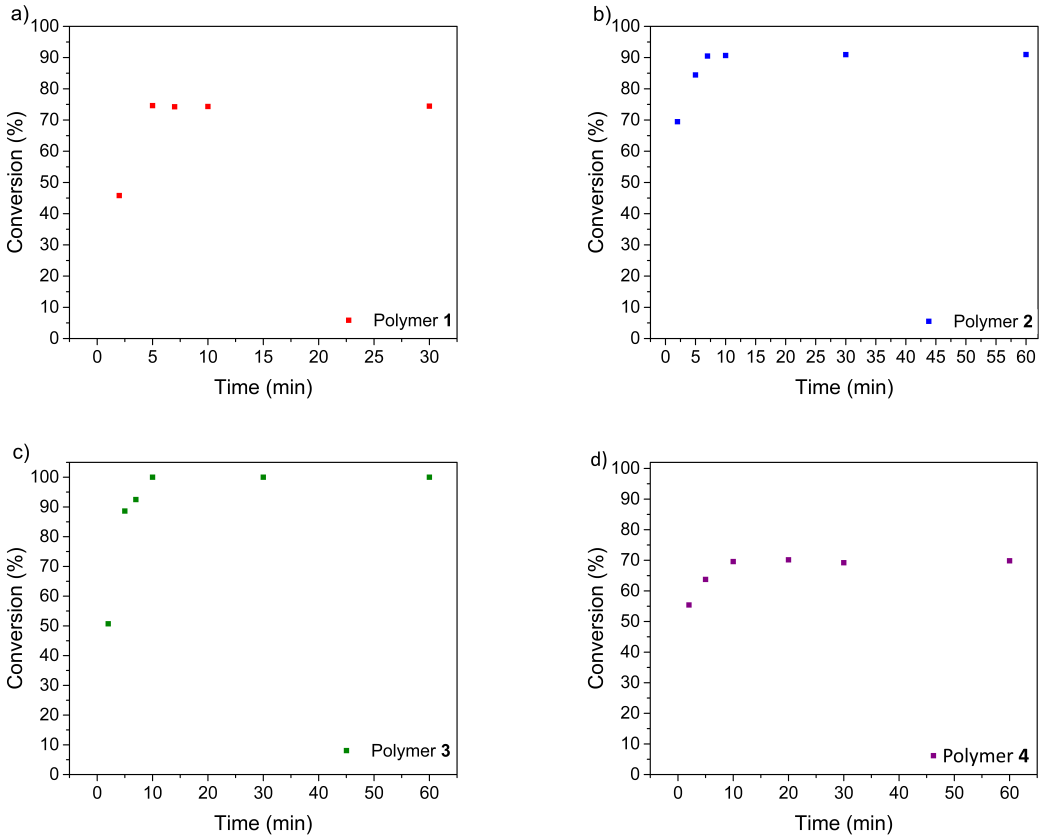

Figure 3.10: Depolymerisation of a) polymer **1**, b) polymer **2**, c) polymer **3** and d) polymer **4** at 110 °C

integration. To ensure that the time taken in transfer was not an affecting factor the ampoules were kept on ice until they were cycled on to the Schlenk line prior to subjecting them to heat.

The catalytic degradation of polymers **1** to **4** was investigated at 110 °C, due to the poor solubility of polymers **3** and **4** at 70 °C in toluene (Figure 3.10). After 2 minutes, polymer **1** showed a conversion of 45.8 % back to monomer with a further increase to 74.6 % after 5 minutes, before plateauing. A similar behaviour was observed for polymer **2** where a plateau was reached after 7 minutes at 90.5 %. Polymer **3** showed 100 % depolymerisation in 10 minutes, whereas polymer **4** showed the least degree of depolymerisation even after one hour only being 69.8 %. The slower depolymerisation of polymer **4** was associated with the time taken for the polymer to dissolve in toluene at 110 °C, albeit being faster than that at 70 °C.

Both depolymerisation at 70 °C and 110 °C reiterated the initial studies, that

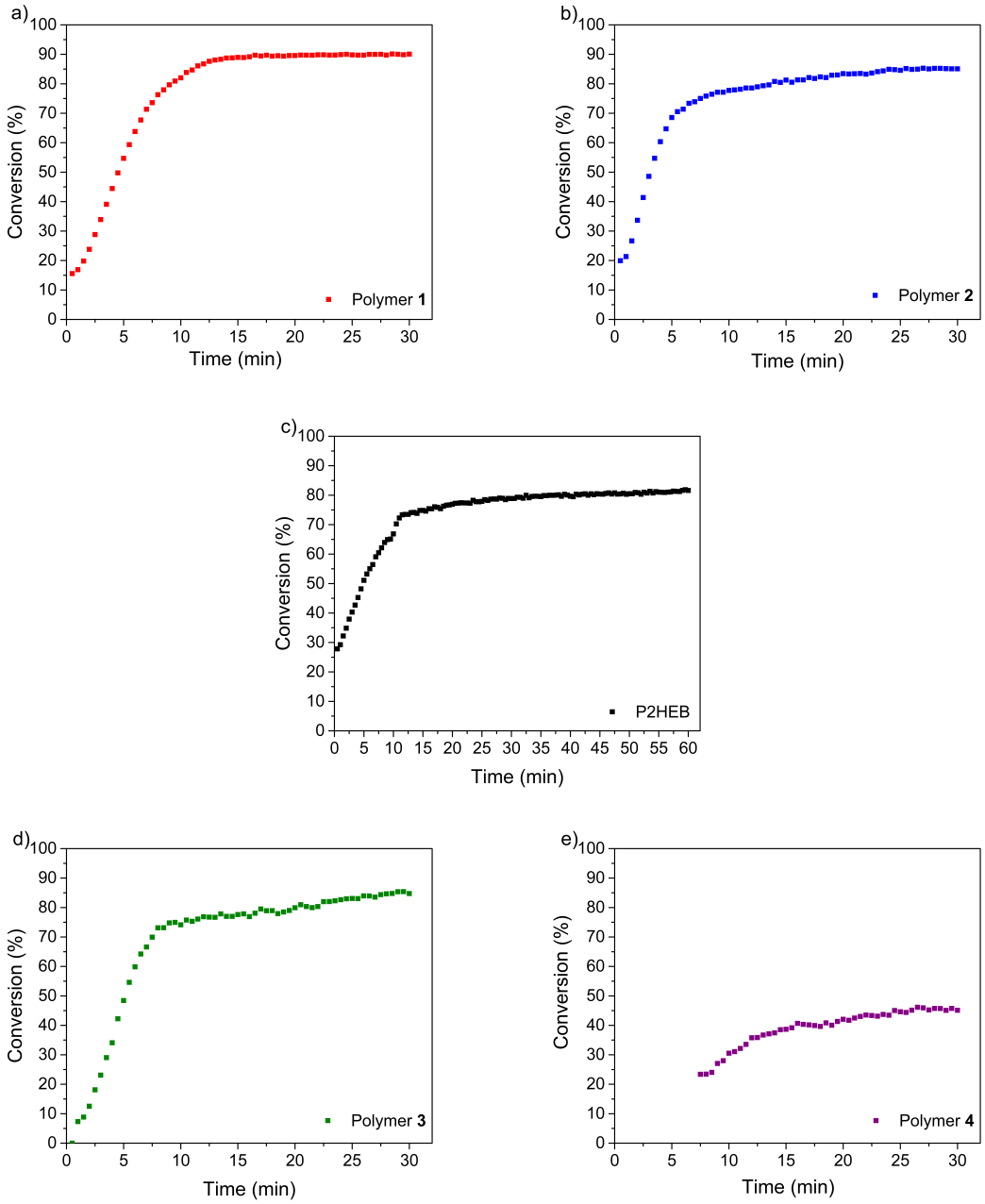

Figure 3.11: Depolymerisation of a) polymer **1**, b) polymer **2**, c) P2HEB, d) polymer **3** and e) polymer **4** at 110 °C probed by ^{1}H NMR in a Youngs tap NMR tube.

the majority of catalytic degradation was occurring within the first 10 minutes and in the case of 110 °C in the first 2 minutes. The early stages of depolymerisation at 110 °C was probed through ^{1}H NMR in deuterated toluene in a Youngs tap NMR tube (Figure 3.11). Note that 110 °C was close to the temperature limit of the NMR machine when using deuterated toluene as the solvent as well as being close the to limit for the specification of the NMR machine used for this study.

Polymer **1** showed a maximum degradation of 89.7 % in 16 minutes where an equilibrium was then reached. Polymer **2** exhibited two different rates of depolymerisation where in the first 7 minutes the rate was higher, which plateaued to 85.4 % after 30 minutes. A similar behaviour was observed for polymer **3** where a maximum degradation of 84.8 % degradation was observed. Polymer **4** was an exception to the studies as no sign of depolymerisation was observed until 7 minutes where a slow increase in polymer to monomer conversion occurred to a maximum degradation of 45.9 %. P2HEB displayed a rapid increase in polymer to monomer conversion with 72.7 % depolymerisation after 10 minutes and then plateauing to 81.5 %.

The discrepancy between the maximum degradations at 110 °C in an ampoule vs a Youngs tap NMR tube is proposed to be due to the absence of stirring in the NMR tube, suggesting that the polymers would take longer to dissolve in deuterated toluene.

The rates of depolymerisation, k_d, were calculated from the linear regions of the data obtained at 70 °C and 110 °C in both the ampoule and the Youngs tap NMR tube in addition to the catalytic degradation of P2HEB at 110 °C in a Youngs tap NMR tube (Figure 3.12).

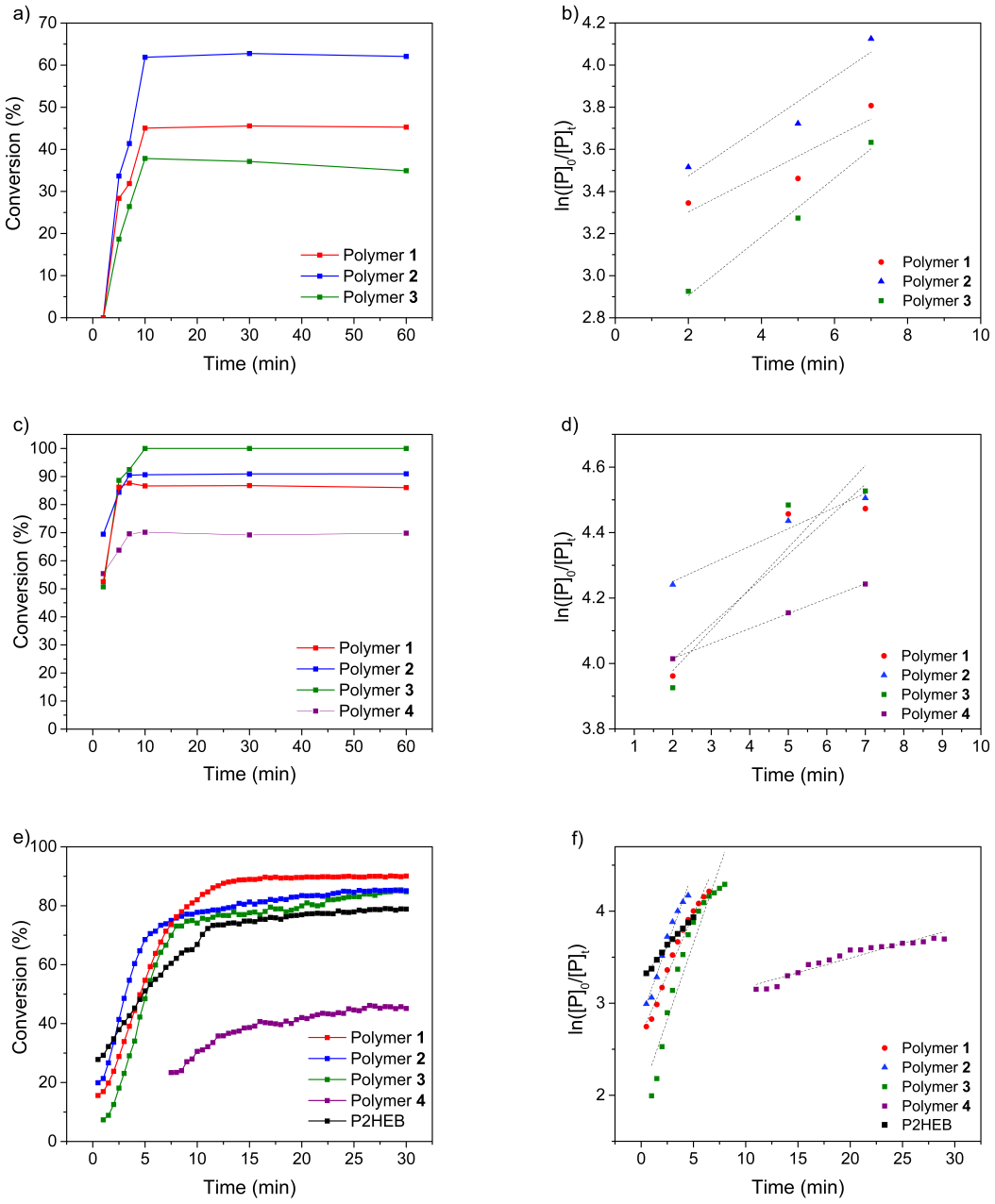

Figure 3.12: Combined plots of depolymerisation at a) 70°C, c) 110 °C, e) 110 °C probed by ^{1}H NMR, and their respective ln([P]$_0$//[P]$_t$) vs time at b) 70°C, d) 110 °C and e) 110 °C by ^{1}H NMR spectroscopy.

The catalytic degradation rate of P2HEB at 60 °C was previously calculated to be 0.01 min^{-1}.[113] The slope of each of the polymers when the change in conversion over time is plotted as ln([P]$_0$/[P]$_t$) vs time, equates to k_d. The kinetics for the depolymerisation at 70 °C were only studied for polymers **1** to **3** due to the poor solubility of polymer **4**. Polymer **1** showed a depolymerisation rate of 0.09 min^{-1},

this was increased to 0.12 min^{-1} and 0.14 min^{-1} for polymer **2** and **3** respectively. As predicted, the increase in k_d, correlates well with the increase in the electronic substituent parameter, indicating that the more electron withdrawing substituents depolymerise at a faster rate at 70 °C.

The depolymerisation study at 110 °C in an ampoule, analysing aliquots every two minutes, demonstrated that the linear region of the curve was within the first 7 minutes with only a maximum of three time points. The disadvantage of attempting to calculate k_d from this data is that polymers **1** to **3** start to plateau after 5 minutes, resulting in inaccurate k_d values. Polymers **1** and **3** demonstrated a depolymerisation rate of 0.11 min^{-1} and 0.13 min^{-1} respectively, this decreased by half to 0.054 min^{-1} for polymer **2** and 0.046 min^{-1} for polymer **4**. The rates calculated at 110°C were surprising due to the trends observed at 70 °C, where there was a clear increase in rate with increase in the electronic substituent parameter.

More reliable depolymerisation rates at 110 °C were calculated through the data obtained from ^{1}H NMR spectroscopy. The k_d values obtained in the first 7 minutes for polymers **1** to **3** correlated with the trends observed at 70 °C and the electronic substituent parameter, where k_d was 0.26 min^{-1} for polymer **1**, 0.32 min^{-1} for polymer **2** and 0.33 min^{-1} for polymer **3**. The exception to this trend was polymer **4** which is predicted to have the fastest rate of depolymerisation, with a k_d value of 0.032 min^{-1}. This was attributed to the solubility issues with the polymer **4**, where in a Youngs tap NMR tube there was no stirring and there was evidently an incubation period in which the polymer was dissolving before being subjected to depolymerisation. The hydrogen substituted P2HEB with a σ_{meta} value of 0,[129] is predicted to have a k_d value higher than polymer **1** and lower than polymer **2**, however the observed rate of depolymerisation was 0.14 min^{-1}, lower than both polymers **1** and **2**.

The additional influence of solubility was observed in the depolymerisation rates, as with the polymerisation rates. Although the electronic nature of the substituents influences the monomer-polymer equilibrium and their kinetic behavior, the solubility of the monomers/polymers is a limiting factor that also needs to be considered

to achieve optimal kinetic profiles. The balance was well achieved with monomer **3**/polymer **3**, with the fastest rates of polymerisation and depolymerisation to afford a novel aromatic-aliphatic polyester that rapidly degrades in a "closed loop" fashion.

3.2.8 Copolymers

Copolymers are a result of the polymerisation of two or more monomers either simultaneously or sequentially. There are two classes of copolymers, containing their own subclasses, branched copolymers, including graft and star copolymers, and linear copolymers, including gradient, random, alternating and block copolymers (Figure 3.13).[137,138]

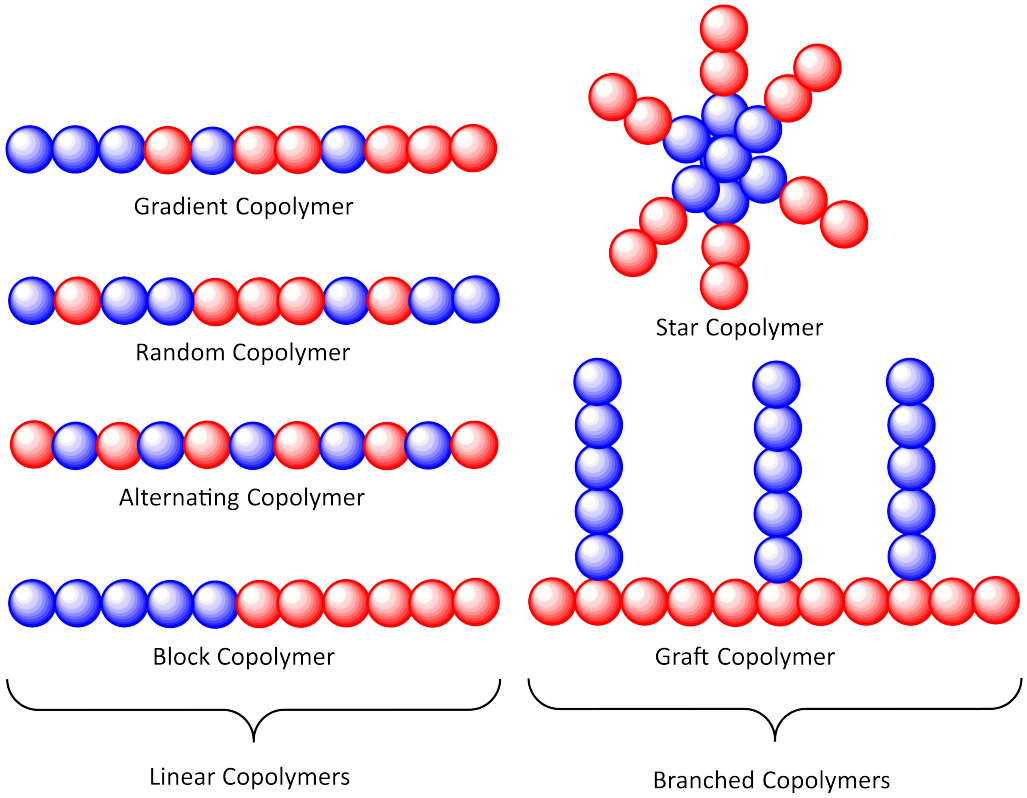

Figure 3.13: A cartoon representation of the types of linear and branched copolymers.

Block copolymers tend to have a higher degree of architectures that encompass linear, branched and cyclic architectures, depending on the nature and length of the second block. Block copolymers are accessed through the addition of a second monomer to the existing polymer (of the first monomer), thus resulting in a diblock.

Further addition of another monomer to the existing diblock copolymer would result in a triblock copolymer.[139]

The advantage of copolymerisation is the ability to tune the macrostructure of the resultant copolymer. The macrostructure influences the thermal and mechanical properties of a copolymer as well as its morphology and degradation profiles. Random and gradient copolymers tend to behave close to that of blends, which is a cost-effective method for the mixing of two homopolymers. However, block copolymers, due to their nature, can lead to more interesting properties and morphologies.[140]

The increasing attractiveness of PLA, due to its characteristic biocompatibility and biodegradability, has led to research into the improvement of the thermal and mechanical properties of PLA.[141] Copolymerisation of PLA[142,143] with monomers such as ϵ-caprolactone, by ROP of the second cyclic monomer using the end hydroxyl group from PLA as a macroinitiator,[144] led to a change in thermal properties and crystallinity to improve the brittleness of the PLA copolymer by increasing the percentage strain at which it breaks.[145,146] The hydrocarbon polymer backbone of polycaprolactone (PCL) and its significantly lower T_g (-60 °C),[147] adds flexibility to the copolymer and thus increasing the elongation of the copolymer. This allows the copolymer to take more strain before breaking of the material.[148] Other examples of monomers that have been copolymerised with PLA include glycolic acid, dipropargyl glycolide, allyl glycidyl ether and cyclic carbonates.[144]Alternative methods such as fabrication,[149,150] stereocomplexation[151–153] and blending[154,155] also exist to tune the thermal and mechanical properties of PLA.

While copolymerisation typically requires air-sensitive techniques, blending is a facile alternative to tune the properties of a particular homopolymer. Blending of PLA with poly(3-hydroxybutyrate-co-3-hydroxyvalerate) (PHBV),[156] poly(butylene succinate) (PBS),[157] PCL[158] and polyolefins such as poly(methyl methacrylate) (PMMA),[159] can offer improvement on the brittleness of PLA as well interesting morphologies.[157] However, blending of two immiscible polymers can often lead to macro-separation and consequently inferior properties compared to that of their

homopolymers.

Copolymerisation of P2HEB on the other hand, has only once been previously reported by MacDonald *et al.*,[113] by utilising the hydroxyl end group of P2HEB as a macroinitiator in the ROP of L-lactide. The result of this was gradient copolymers due to the monomer-polymer equilibrium of P2HEB. As the lactide monomer units were being added to the chain end, there was a degree of depolymerisation and repolymerisation of P2HEB leading to a gradient copolymer. Using the monomer 2,3-DHB and subjecting it to ROP by poly(3-hydroxybutyrate) (P3HB) led to a diblock copolymer.

This unique observation on the order of addition of 2,3-DHB was further investigated in this work to afford diblock and triblock copolymers of P2HEB and PLLA. The copolymers were also subjected to catalytical and enzymatic degradation along with their homopolymers to further investigate the selective degradation of the P2HEB block as was previously observed by Shaver *et al.*[113]

Synthsis of diblock copolymer 1 and triblock copolymer 2

The reactivity of 2,3-DHB and L-lactide towards ROP via aluminium salen was investigated by a one pot polymerisation in the presence of aluminium salen and the initiator BnOH, in toluene at 60 °C for 6 hours. The ^{1}H NMR spectrum showed successful polymerisation of L-lactide to PLLA with no incorporation of P2HEB, evident by the absence of aromatic peaks in the spectrum. This suggested that the consumption of L-lactide occurred at a faster rate than that of P2HEB.[147]

The ROP of 2,3-DHB and L-lactide catalysed by $Sn(oct)_2$, according to ^{1}H NMR spectroscopy, was successful, with a 1:0.62 ratio of PLLA:P2HEB. To determine the type of copolymer that was synthesised the ^{13}C NMR and DOSY spectra were analysed. The ^{13}C NMR spectrum of a homopolymer of PLLA has a signal attributed to the carbonyl at 169.7 ppm, this carbon is predicted to shift upon copolymerisation due to the presence of P2HEB. The ^{13}C NMR spectrum analysed showed three chemical shifts in the region of 170 to 150 ppm, the chemical shift at 169.6 ppm correlates to the carbonyl on the lactic acid repeat unit, the chemical shift at 165.9

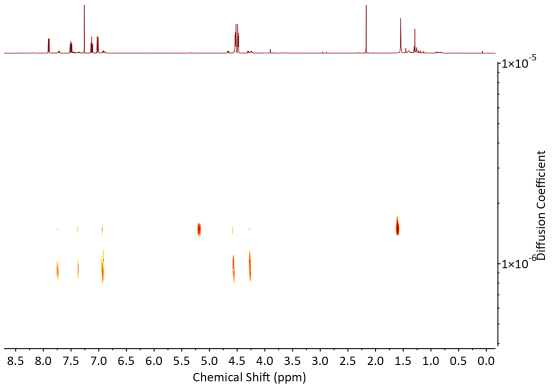

Figure 3.14: DOSY NMR of the attempted synthesis of the diblock copolymber **1** with $Sn(oct)_2$.

ppm correlates to the carbonyl on the P2HEB repeat unit and the last chemical shift at 158.2 ppm correlates to the aromatic carbon in P2HEB. An additional carbonyl shift should normally be observed, attributed to the point at which both monomers link, however in the case of these polymers the signal:noise was too low for it to be detected. This data suggests that due to the presence of two carbonyl chemical shifts the resultant copolymer is a block whereas the presence of multiple carbonyl chemical shifts would indicate several different chemical environments as a result of a random or gradient copolymer. For example, a carbonyl from a lactic acid unit next to another lactic acid unit would have a different chemical shift to one next to a 2,3-DHB unit. Further investigation into this via DOSY NMR spectroscopy (Figure 3.14) contradicted this finding and led to the conclusion that no copolymerisation had occurred, rather two homopolymers with different diffusion constants were present. The PLLA with the methine at 5.2 ppm and the methyl at 1.6 ppm had a different diffusion constant to that of the chemical shifts relating to aromatic protons in P2HEB from 6.94 ppm to 7.74 ppm.

Using P2HEB as a macroinitiator to afford block polymers was previously attempted. This study was unsuccessful due to the monomer-polymer equilibrium leading to a gradient copolymer.[113] Therefore, PLLA was used as a macroinitiator to afford the diblock copolymer **1** (PLLA:P2HEB) and triblock copolymer **2** (P2HEB:PLLA:P2HEB) (Figure 3.15).

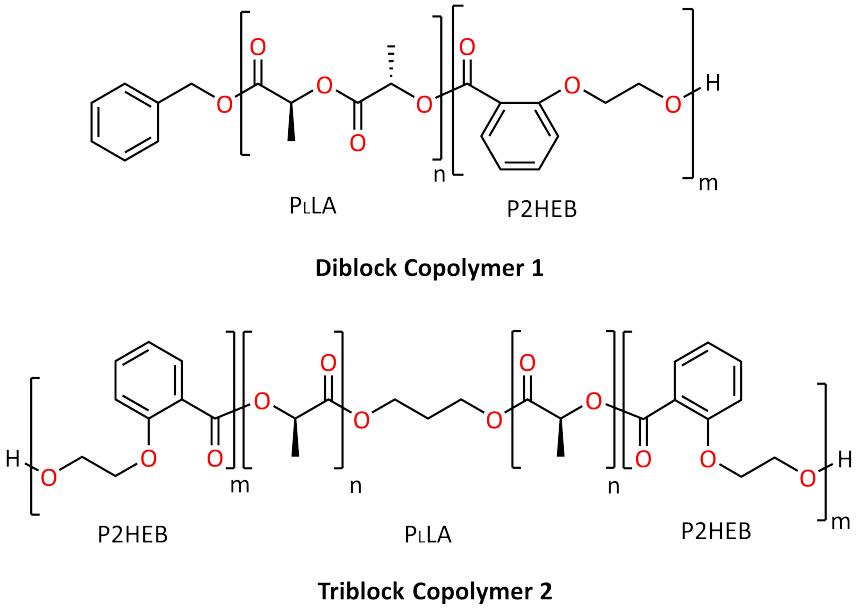

Figure 3.15: Schematic of the diblock and triblock copolymer using PLLA cores.

L-lactide was subjected to ROP via MeAl[salen] with BnOH as the initiator in toluene at 85 °C for 3 hours to afford PLLA. The synthesised PLLA was used as a macroinitiator in the ROP of 2,3-DHB. The poor solubility of PLLA in toluene at 60 °C (the polymerisation temperature of 2,3-DHB) meant that the polymerisation was carried out at 85 °C for 6 hours, with an initial 2,3-DHB concentration of 2.4 M. Integration of the ^{1}H NMR spectrum showed chemical shifts corresponding to the methine protons in PLLA and the aromatic protons in P2HEB against the benzyl chemical shift for the initiator at 5.29 ppm resulting in a PLLA:P2HEB block length of 1:0.0125,indicating only 1.25 % incorporation of 2,3-DHB. Decreasing the temperature of ROP of 2,3-DHB to 66 °C and increasing the polarity of the solvent to THF, which was effective at dissolving PLLA, led to the same result.

Through exploiting the monomer-polymer equilibrium of 2,3-DHB, the concentration was increased significantly to 50 M to drive the equilibrium towards polymer. After 6 hours in THF at 66 °C with PLLA as the macroinitiator, a PLLA:P2HEB block length of 115:46 was observed. To confirm that a block copolymer was produced, the ^{13}C NMR and DOSY spectra were analysed. The ^{13}C NMR spectrum showed only a chemical shift at 169.8 ppm, correlating to the carbonyl on the lactic acid repeat unit, and a chemical shift at 166.1 ppm, correlating to the carbonyl on

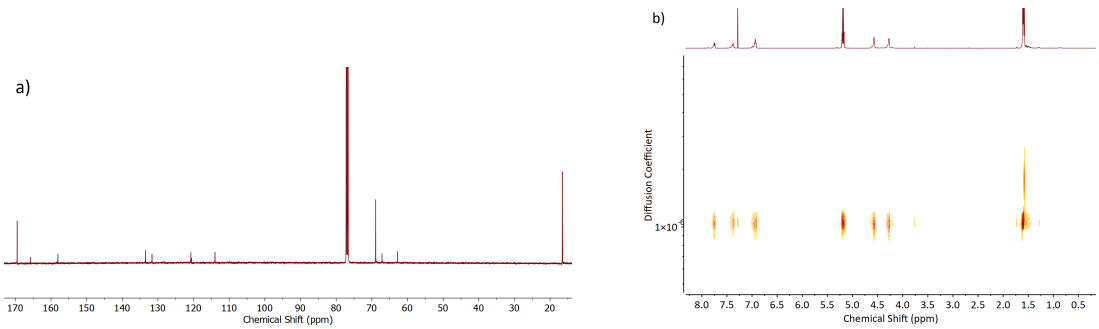

Figure 3.16: a) ^{13}C NMR spectrum of the diblock copolymer **1** showing two carbonyl peaks indicating only two environments for a block copolymer and b) DOSY NMR spectrum of the diblock copolymer **1** with the same diffusion constant suggesting a copolymer.

the P2HEB repeat unit. This indicates a block copolymer which was further confirmed by the DOSY spectrum showing the methine and methyl of PLLA and the aromatics of P2HEB to have a similar diffusion constant, suggesting the successful synthesis of diblock copolymer **1** (Figure 3.16).

The triblock copolymer **2** was synthesised using 1,3-propanediol as an initiator in the ROP of L-lactide in toluene at 85 °C for 3 hours with MeAl[salen] to afford PLLA with two end hydroxyl groups as macroinitiators for the ROP of 2,3-DHB. Similar to the diblock, maintaining a high concentration of 2,3-DHB, whilst ensuring a homogenous solution, was important due to the monomer-polymer equilibrium. However, lower conversions of 2,3-DHB were observed for the triblock copolymer **2**, due to the monomer-polymer equilibrium, with a P2HEB:PLLA:P2HEB block length of 15:100:15. The integration ratio was determined by integrating the methine chemical shift of PLLA at 5.16 ppm against the aromatic chemical shift of P2HEB at 7.76 ppm. The nature of the block copolymer was confirmed with the ^{13}C NMR spectrum showing a chemical shift at 169.8 ppm, correlating to the carbonyl on the lactic acid repeat unit, and a chemical shift at 166.1 ppm, correlating to the carbonyl on the P2HEB repeat unit, in addition to the presence of one diffusion constant in the DOSY spectrum (Figure 3.17).

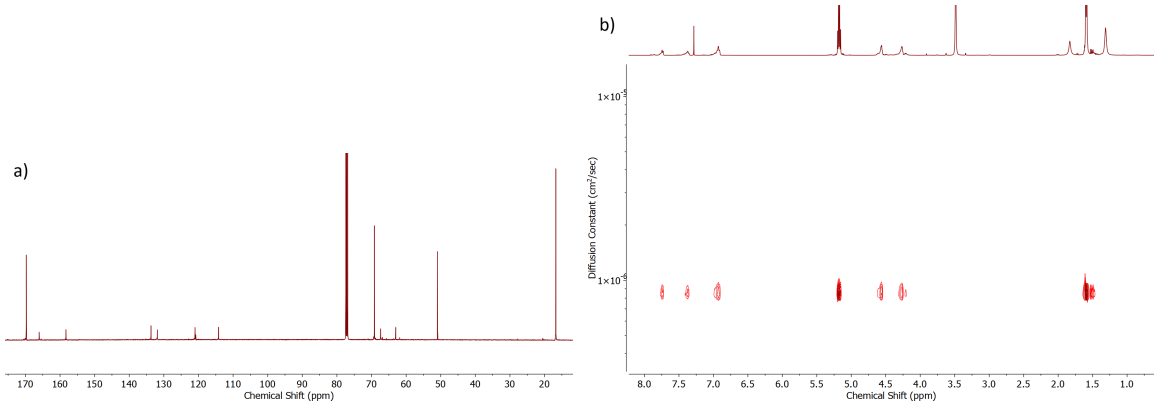

Figure 3.17: a) ^{13}C NMR spectrum of the triblock copolymer **2** showing two carbonyl peaks indicating only two environments for a block copolymer and b) DOSY NMR spectrum of the triblock copolymer **2** with the same diffusion constant suggesting a copolymer.

The diblock and triblock copolymers had narrow dispersities and similar molecular weights of 16,932 g mol^{-1} and 16,304 g mol^{-1} respectively (Table 3.10). The narrow dispersity of the triblock copolymer **2** suggested an even split on both ends of the PLLA core.[160]

Table 3.10: ^{a}[L-lactide]$_0$:[MeAl[salen]]$_0$:[BnOH]$_0$=70:1:1; ^{b}[L-lactide]$_0$:[MeAl[salen]]$_0$:[1,3-propanediol]$_0$=70:2:1; ^{c}[2,3-DHB]$_0$:[MeAl[salen]]$_0$:[**1**]$_0$=70:1:1; ^{d}[2,3-DHB]$_0$:[MeAl[salen]]$_0$:[**2**]$_0$= 70:1:1; ^{e}determined by ^{1}H NMR spectroscopy; ^{f}determined by GPC, dn/dc=0.05; ^{g}$M_{n,th}$ = ([M]/[ini]) × M_W(M)×(% conv.) + M_W(end group).

Polymer	**Conversion (%)**^{e}	**M_n (g mol^{-1})**^{f}	**$M_{n,th}$ (g mol^{-1})**^{g}	**Đ**
PLLA, with BnOH (1)^{a}	95	9500	10200	1.05
PLLA, with 1,3-propanediol (2)^{b}	98	9470	10170	1.07
Diblock Copolymer 1^{c}	20	16930	21680	1.15
Triblock Copolymer 2^{d}	22	16300	21660	1.14

The potential of diblock copolymer **1** and the triblock copolymer **2** in improving the thermal, mechanical and degradation profile of PLLA was investigated further.

3.2.9 Block Copolymer Catalytic Degradation

It has previously been shown that the P2HEB block of a copolymer of P2HEB with P3HB was able to undergo more than 90% selective depolymerisation back to the cyclic monomer, 2,3-DHB, in the presence of MeAl[salen].[113]

The homopolymer of P2HEB as previously discussed demonstrated greater than 80 % depolymerisation within one hour at 70 °C in toluene in the presence of MeAl[salen]. Due to the monomer-polymer equilibrium, it is understood and experimentally shown that concentration is vital in determining where the equilibrium sits. Dilute conditions promote depolymerisation and the equilibrium shifting to the monomer, where the opposite is true for concentrated conditions. Therefore, dilute conditions of the homopolymer were mimicked for the depolymerisation of the diblock copolymer **1** and the triblock copolymer **2** with THF as the solvent, due to the poor solubility of the copolymers in toluene. As THF is able to weakly coordinate to the aluminium salen catalyst, the conversions of polymer to monomer are expected to be lower.[132]

The degradation of the copolymers were monitored by ^{1}H NMR over 5 hours, taking aliquots every hour (Figure 3.18). The ^{1}H NMR spectrum showed the reappearance of the chemical shifts correlating to the monomer 2,3-DHB, as expected, however the reappearance of the chemical shift at 5.04 ppm correlating to the monomer L-lactide was also observed. In all cases the extent of depolymerisation of P2HEB was significantly lower than that of its homopolymer. This suggested that the depolymerisation of P2HEB was competing with the transesterification of PLLA, the presence of the lactide monomer suggested intramolecular transesterification.

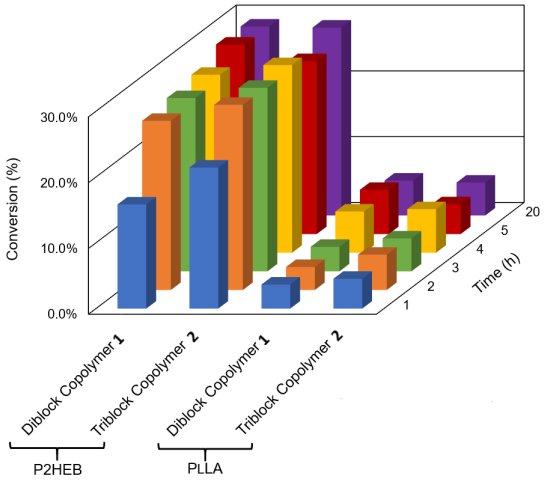

Figure 3.18: Degradation of the diblock copolymer **1** and triblock copolymer **2** monitored by ^{1}H NMR spectroscopy over 20 hours in the presence of MeAl[salen] (0.0045 mol).

Integration of the monomer and polymer peaks from the ^{1}H NMR spectrum revealed that the diblock copolymer **1** showed 28.8 % degradation of the P2HEB block after 5 hours, with 6.7 % degradation of the PLLA block. Similar results were observed for the triblock copolymer **2**, with 26.3 % degradation of the P2HEB block and 4.5 % of the PLLA block. Subjecting the copolymers to 20 hours of degradation showed no further increase in depolymerisation of either block.

Increasing the catalyst loading by ten times led to an increase in the degree of depolymerisation of the P2HEB and PLLA blocks (Figure 3.19). The diblock copolymer **1** showed a maximum degradation of the P2HEB block of 46.8 % after 5 hours, this was further increased to 52.8 % after 20 hours. The P2HEB block of the triblock copolymer **2** showed a maximum degradation of 62.2 % after 5 hours and 88.9 % after 20 hours. Close analysis of the ^{1}H NMR spectrum also showed after 5 hours 12.9 % and 25.4 % degradation of the PLLA block in the diblock copolymer **1** and the triblock copolymer **2** respectively, which was increased to 34 % and 59.9 % after 20 hours. The homopolymer of PLLA was also subjected to the higher catalyst loading degradation and showed a maximum degradation of 10.4 % after 5 hours and 33.2 % after 20 hours.

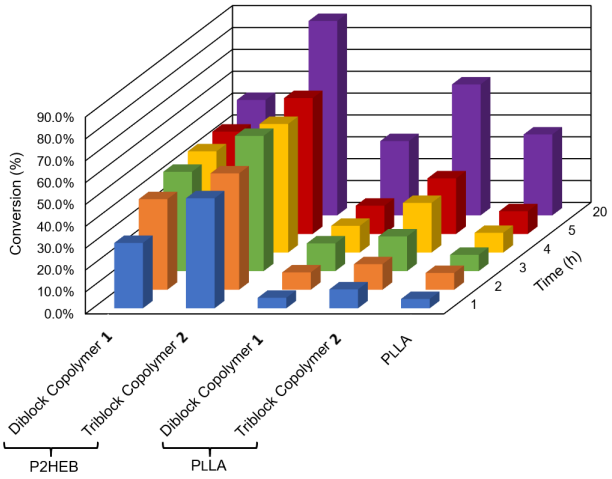

Figure 3.19: Degradation of the diblock copolymer **1** and triblock copolymer **2** monitored by ^{1}H NMR spectroscopy over 20 hours in the presence of MeAl[salen] (0.045 mol).

Comparing the PLLA fraction of the diblock copolymer **1** and the homopolymer of PLLA, it can be observed that the maximum degradations were similar after 5 hours and 20 hours, suggesting that the transesterification of PLLA was dominating over the catalytic degradation of P2HEB. Whereas, the triblock copolymer **2** promoted the degradation of the PLLA block.

It is clear that the degree of depolymerisation of the P2HEB block was affected by the catalyst concentration and the competing transesterification of the PLLA block. The maximum degradation of the PLLA block in the copolymers was significantly higher than the maximum degradation of the homopolymer, this suggests that the degradation of PLLA was promoted by the presence of the P2HEB block. The influence of the P2HEB block on the PLLA block and vice versa on the degradation of the copolymers give potential to encourage research into alternative chemical recycling strategies.

3.2.10 Enzymatic Degradation

Enzymatic degradation studies were carried on polymer films of the P2HEB homopolymer, the diblock copolymer **1** and the triblock copolymer **2** to investigate the extent of enzymatic degradation of P2HEB compared to previously studied

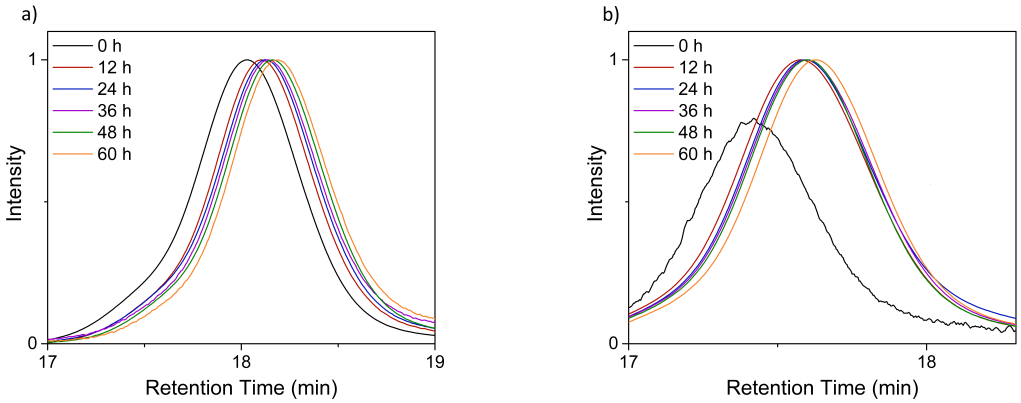

Figure 3.20: GPC traces of P2HEB of molecular weight a) 40,000 g mol^{-1} and b) 80,000 g mol^{-1} over 60 hours showing a shift towards lower hydrodynamic volumes.

PLLA.[161]

P2HEB with molecular weights of 40,000 g mol^{-1} and 80,000 g mol^{-1} were dissolved in chloroform and placed on PTFE plates to allow the solvent to evaporate, via solvent casting, leaving behind a film with a thickness of 100 μm. P2HEB of molecular weight 11,000 g mol^{-1} demonstrated challenges in affording a consistent film. The polymer films were cut into 1 cm^2, where the polymer films of the copolymers, prepared in the same fashion, were cut into fractions with a weight of 12 mg. The polymer films of the copolymers were brittle and difficult to handle due to their low molecular weight and the presence of PLLA. The films were then subjected to enzymatic degradation via proteinase K in a tris-HCl buffer. The loss of molecular weight was monitored by GPC over 60 hours at 12 hour intervals (Figure 3.20). Control experiments were also set up in the following manner; tris-HCl buffer with proteinase K, and tri-HCl buffer with the polymer films (specifically P2HEB with molecular weight of 40,000 g mol $^{-1}$).

A decrease in molecular weight was observed for P2HEB of molecular weight 40,000 g mol^{-1} and 80,000 g mol^{-1}, as evident by the GPC traces shifting towards lower hydrodynamic volumes (higher retention times). In addition to the extent of enzymatic degradation being similar for both P2HEB polymers, the dispersity of the analysed fractions remained narrow, suggesting that enzymatic degradation was independent of molecular weight (Table 3.11 and Table 3.12).

Table 3.11: Enzymatic degradation of P2HEB of molecular weight 40,000 g mol^{-1} monitored by GPC (dn/dc=0.05).

Time (h)	**M_n (g mol^{-1})**	**Đ**
0	40,300	1.23
12	39,400	1.26
24	39,000	1.25
36	38,600	1.23
48	37,500	1.26
60	36,100	1.27

Table 3.12: Enzymatic degradation of P2HEB of molecular weight 80,000 g mol^{-1} monitored by GPC (dn/dc=0.05).

Time (h)	**M_n (g mol^{-1})**	**Đ**
0	78,600	1.22
12	76,800	1.23
24	74,400	1.24
36	73,200	1.23
48	72,500	1.25
60	70,100	1.24

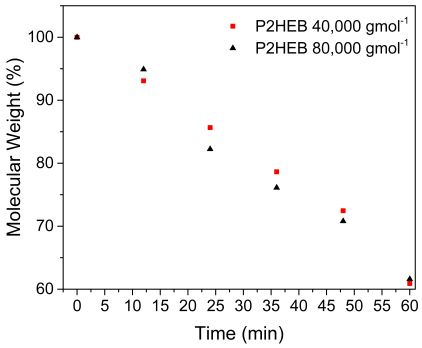

Figure 3.21: Enzymatic degradation monitored by ^{1}H NMR spectroscopy for P2HEB showing the independence of molecular weight on degree of degradation.

The enzymatic degradation was also studied with ^{1}H NMR spectroscopy (Figure 3.21) due to the partial solubility of P2HEB in THF leading to inaccurate dn/dc values and thus inaccurate molecular weights. The enzymatic degradation behaviour of both molecular weights were similar, as with the result from the GPC data, showing 39 % decrease in molecular weight over 60 hours in both cases. This suggests that the rate of enzymatic degradation was independent of the molecular weight. Other factors such as surface area and degree of crystallinity may influence the degree of degradation.

The triblock copolymer **2** showed a similar degradation profile to P2HEB, where a clear shift towards lower hydrodynamic volumes was observed over 60 hours. However, the diblock copolymer **1** exhibited a unique bimodal GPC trace (Figure 3.22). A decrease in the weight fraction of the higher hydrodynamic volume peak and the increase in weight fraction of the lower hydrodynamic volume was observed over 60 hours. This suggested nonuniform degradation of the diblock copolymer **1**. It has been previously shown that the amorphous region of the polymer matrix is favoured over the crystalline region for enzymatic degradation, specifically in the case of PLLA, where high surface areas and low molecular weights promote enzymatic degradation.[16,162] The diblock copolymer **1** is predicted to have different regions of crystallinity, suggesting that the bimodal trace is a result of the preferred degradation of the P2HEB blocks with lower degree of crystallinity, in addition to amorphous regions of PLLA, thus leading to low molecular weight PLLA segments

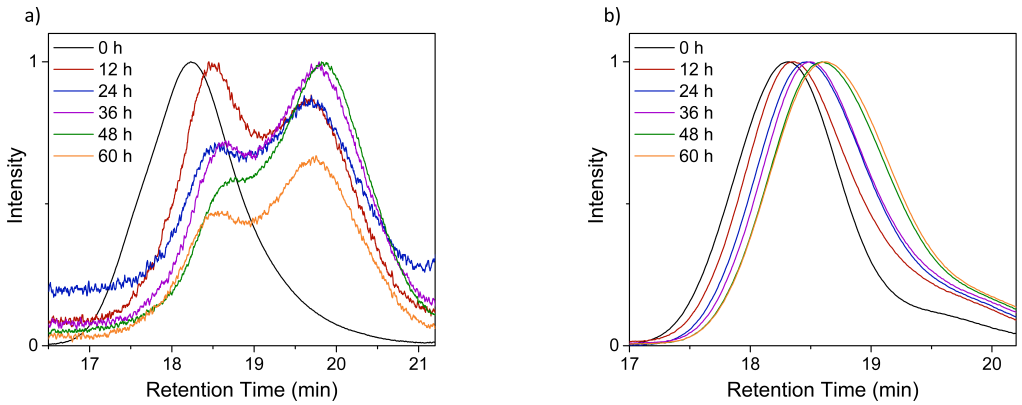

Figure 3.22: GPC traces of a) the diblock copolymer **1** and b) the triblock copolymer **2** over 60 hours showing a shift towards lower hydrodynamic volumes

with a broad dispersity.

To understand the enzymatic degradation behaviour in more detail, the DOSY spectra were analysed (Figure 3.23). The DOSY spectrum of the diblock copolymer **1** prior to degradation showed the chemical shifts correlating to P2HEB and PLLA having the same diffusion constant. After enzymatic degradation the chemical shifts correlating to P2HEB and PLLA showed different diffusion constants, where the chemical shifts for the PLLA were observed to have more than the one diffusion constant, suggesting that shorter PLLA fragments were being formed from the original copolymer. This supports the bimodal GPC trace observed for the diblock copolymer **1**.

The DOSY spectrum for the triblock copolymer **2** suggested degradation occurred through random chain scission, evident by the chemical shifts relating to P2HEB (between 7.76-6.93 ppm and 4.57-4.28 ppm) and PLLA (5.16 ppm) still having the same diffusion constant, albeit more than one was observed. Chain scission is the degradation or cutting of a polymer backbone into two fragments of shorter length.[163] This data supports the gaussian peak observed by GPC.

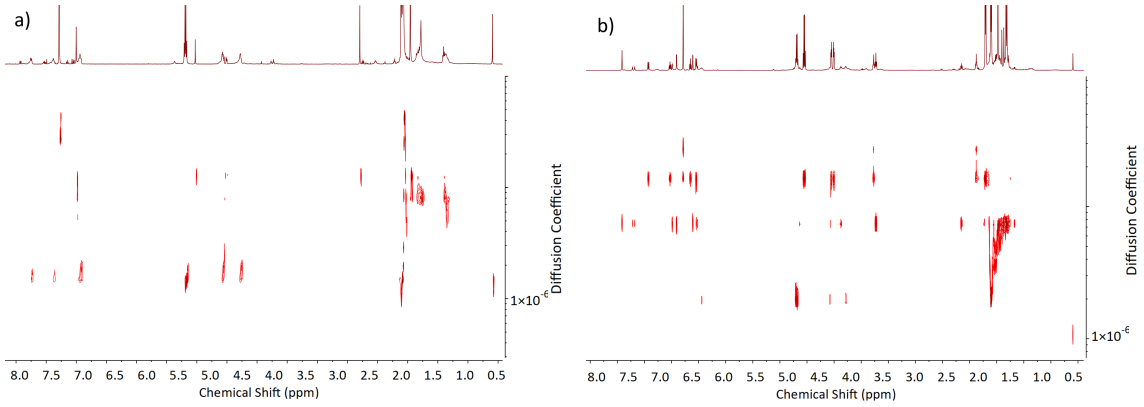

Figure 3.23: DOSY NMR of a) the diblock copolymer **1** and b) the triblock copolymer **2** showing degradation of the copolymers by multiple diffusion constants

The degree of crystallinity in the polymer matrix influences the rate and extent of enzymatic degradation.[16,162] The enzymatic degradation of P2HEB was observed to be significantly faster than that for PET,[164] due to the ester linkages in P2HEB and orientating themselves 90 ° to the *ortho* linked aromatic rings along the polymer backbone.[110] This orientation allows for increased chain mobility and a lower degree of crystallinity, thus a faster rate of enzymatic degradation. The opposite was observed when comparing to atactic PLA where the enzymatic degradation of P2HEB was significantly slower, due to the presence of aromatic rings in P2HEB. The enzyme active site is specifically designed and orientated to maximize efficiency and therefore changing the substrate, for example aromatic rings, hinders enzymatic activity.

In the case of the copolymers, P2HEB is predicted to lower the crystallinity of the polymer matrix due to the orientation of the aromatic rings. However, P2HEB may promote the crystallisation of PLLA to increase the overall crystallinity of the polymer matrix. This phenomenon has been previously observed in copolymers of PLA and PCL. Therefore, the enzymatic degradation of the copolymers were slower than that of the homopolymers.[136,161,162]

The catalytic and enzymatic degradation profiles of PLLA were tuned by copolymerisation with P2HEB with the catalytic degradation being significantly faster.

Chapter 4

Characterisation

4.0.1 Introduction

P2HEB, polymers **1** to **4** and the diblock and triblock copolymers were characterised to determine their thermal and mechanical properties in addition to identifying their crystal structures and morphologies.

Differential scanning calorimetry and thermogravimetric analysis was used to understand the thermal transitions and degradation limits of the studied polymers. The mechanical properties of the polymers, specifically the storage modulus, was measured through dynamic mechanical analysis. In addition to obtaining the thermal and mechanical properties of the polymers, the morphologies were also studied under scanning electron microscopy and atomic force microscopy.

The work presented in this chapter was part of a collaboration with Dr Erlantz Lizundia at the University of Basque Country. The thermal and mechanical characterisation of P2HEB homopolymers, diblock copolymer **1**, triblock copolymer **2** and the PLLA/P2HEB blends, were carried out by Dr Erlantz Lizundia. Their morphologies and crystal structures were characterised by Dr Aitor Larrañaga (from the University of Basque Country). The work here is presented in the following two publications:

1. Thermal, structural and degradation properties of an aromatic–aliphatic polyester built through ring-opening polymerisation, Lizundia, E., Makwana, V. A., Larrañaga, A., Vilas, J. L. and Shaver, M. P., Polym. Chem., 2017, **8**, 3530-3538

2. Thermal, optical and structural properties of blocks and blends of PLA and P2HEB, Makwana, V. A., Lizundia, E., Larrañaga, A., Vilas, J. L. and Shaver, M. P., Green Materials, 2018, **6:3**, 85-96

The thermal and mechanical property and morphology studies of polymers **1** to **4** and their blends were carried out by myself on my placement visit to the University of Basque Country and resulted in the following publication:

Kinetic, thermal, structural and degradation studies on the effect of *meta*-substituted aromatic-aliphatic polyesters built through ring-opening polymerisation, Makwana, V. A., Lizundia, E., Larrañaga, A. and Vilas, J. L., Polym. Degrad. Stab., 2019, **169**, 108984

4.1 Results and Discussion

4.1.1 Thermal Analysis

Differential Scanning Caliometry

The thermal transitions of P2HEB of the different molecular weights were probed using differential scanning caliometry (DSC). Upon heating P2HEB of 11,000 g mol^{-1} at a heating rate of 10 °C min^{-1} two endothermic events were observed (Figure 4.1); the second order transition at 26.5 °C, denoted as the T_g, and the well-defined first order transition centred at 68.8 °C, denoted as T_m. The narrow melting curve suggested a narrow distribution of crystals within the polymer matrix.[165] The absence of an exothermic event typically between the T_g and the T_m, correlating to the cold-crystallisation temperature (T_{cc}), suggested that further crystallisation of the polymer did not occur.

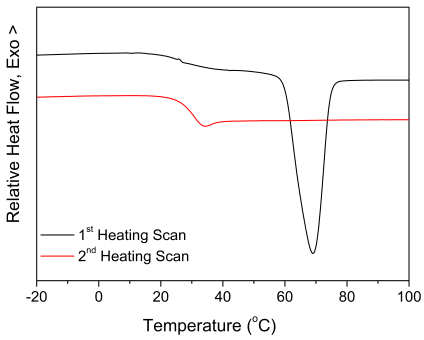

Figure 4.1: First and second heating scans of P2HEB of molecular weight 11,000 g mol^{-1}.

Upon cooling the polymer and applying a second heat scan, a T_g at 30.8 °C without a T_m was observed (Figure 4.1). The T_g is a result of the vibrational energy in the amorphous region of the polymer matrix, whereas the T_m is a result of the melting of the crystalline region. The absence of a T_m in the second heating scans indicated that P2HEB was unable to crystallise upon cooling, once previously melted above the T_m into a fully amorphous matrix.

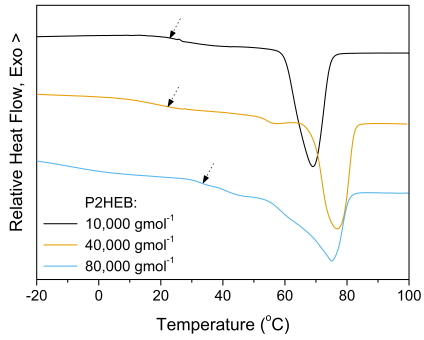

Figure 4.2: First heating scan of P2HEB of molecular weight 11,000, 40,000 and 80,000 g mol^{-1}.

The effect of the molecular weight on the thermal transitions of P2HEB was investigated (Figure 4.2). P2HEB of molecular weight 40,000 and 80,000 g mol^{-1} exhibited slightly higher T_g's of 27.9 °C and 33.4 °C respectively. The T_m's also increased to 76.8 °C and 74.9 °C respectively.

Polymer **1** demonstrated similar thermal transitions, where the first heating scan

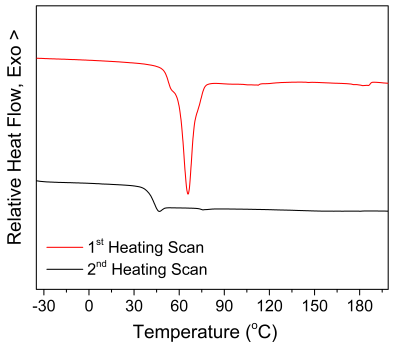

Figure 4.3: First and second heating scans of polymer **1**.

showed a T_m centred at 65.8 °C. However, unlike P2HEB there was no clear presence of a T_g in the first scan, this could be due to the overlapping of the T_g and the T_m or a highly crystalline sample (Figure 4.3). Applying a second heating scan, after cooling down from melt, showed a T_g at 42.5 °C with the absence of a T_m, indicating poor crystallisation ability, similar to P2HEB.

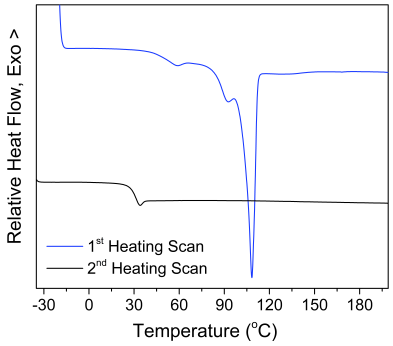

Figure 4.4: First and second heating scans of polymer **2**.

Polymer **2** (Figure 4.4) and **3** (Figure 4.5) followed the same trend where the first heating scans showed a T_g at 52.3 °C and 55.6 °C and a T_m at 108.5 °C and 130.6 °C respectively. Upon cooling and applying a second heat scan, both polymer **2** and **3** showed poor crystallisation ability with the absence of a T_m, however exhibited a T_g at 29.7 °C and 39.4 °C respectively.

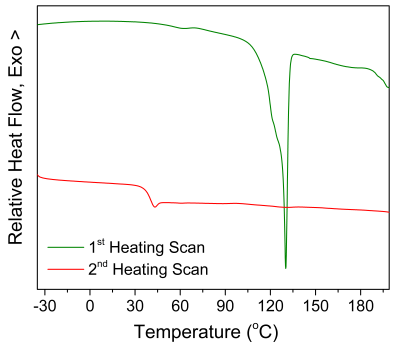

Figure 4.5: First and second heating scans of polymer **3**.

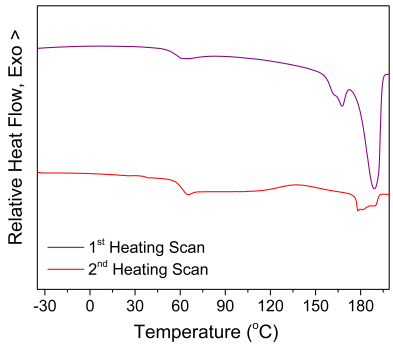

Figure 4.6: First and second heating scans of polymer **4**.

Polymer **4** however, showed good crystallisation ability, where a T_m centred at 182.6 °C was observed in the second heating scan with a T_g at 60.7 °C (Figure 4.6). A closer look at the second heating scan revealed an exothermic event centred at 136.4 °C, denoted as T_{cc}, suggesting the polymer matrix was undergoing crystallisation to a new crystalline state, hence the presence of a T_m in the second heating scan. The values of thermal transitions in the first heating scan were similar to that of the second heating scan with the T_g at 57.5 °C and the T_m at 189.1 °C. The melting curves of polymers **1** to **4** show either a shoulder or more than one distinct melting curve. This suggests that more than one degree of crystallinity is present in the polymer matrix.

The nature and degree of crystallinity in polymer **1** to **4** and P2HEB differs in the nascent form and after melting above their respective T_m. This has previously been observed for materials such as ultra-high molecular weight polyethylene,[166] poly-

oxymethylene,[167], and heterotactic polylactide,[168] where upon melting and cooling the polymer chains entangle and order themselves to a state with an energy minimum typically higher than that of the original state. Polymer **1** to **4** and P2HEB are obtained as powders and exhibit a high degree of crystallinity, as evident by the presence of the melting curve in the first heating scan. ROP to afford these polymers aid in crystalline growth, where the polymer chains are organised into regular segments through dynamic chain sliding diffusion via disentanglement and rearrangement into larger regular crystals.[169] Several factors such as temperature, concentration, pressure and solvent influence the crystallisation process, albeit the presence of a catalyst typically lowers the energy barrier to crystallisation.[170] When polymer **1** to **4** and P2HEB are heated above their respective T_m, the nascent crystalline structure is lost and only in the case of polymer **4** does recrystallisation into a new crystalline structure occur.

To gain more information on the thermal transitions, isothermal treatments at different temperatures were carried out, with the attempt to induce crystallisation at an optimum temperature between T_g and T_m.

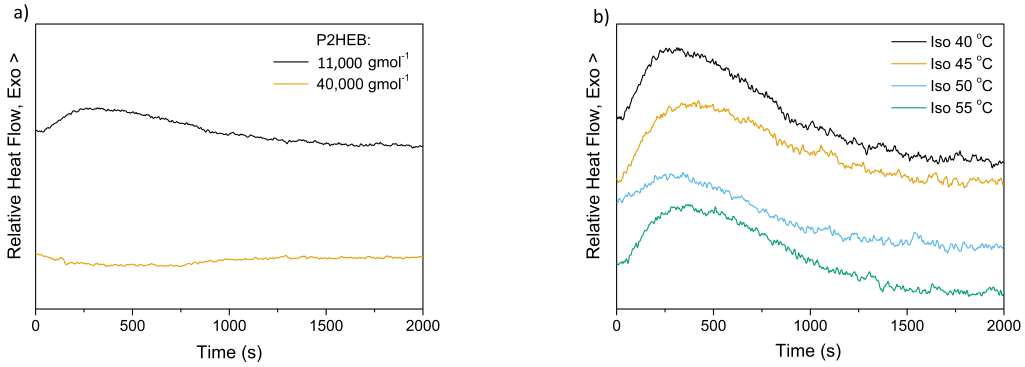

Figure 4.7: Isothermal treatment of a) P2HEB of molecular weight 11,000 and 40,000 g mol^{-1} at 40 °C and b) P2HEB of molecular weight 11,000 g mol^{-1} at different temperatures.

P2HEB of 11,000 and 40,000 g mol^{-1} were isothermally treated at 40 °C for 200 minutes to show a subtle exothermic crystallisation event after 18 minutes for P2HEB of 11,000 g mol^{-1}. The absence of the exothermic peak with P2HEB of 40,000 g mol^{-1} indicated that higher molecular weight P2HEB has a lower degree

of crystallisation ability, due to the decreased chain mobility of the longer chains being unable to rearrange and reorder with ease and thus a lower crystallisation capacity.[171,172] P2HEB of molecular weight 11,000 g mol^{-1} was also isothermally treated at 45, 50 and 55 °C showing that 40 °C was the most efficient at recrystalising the polymer (Figure 4.7).

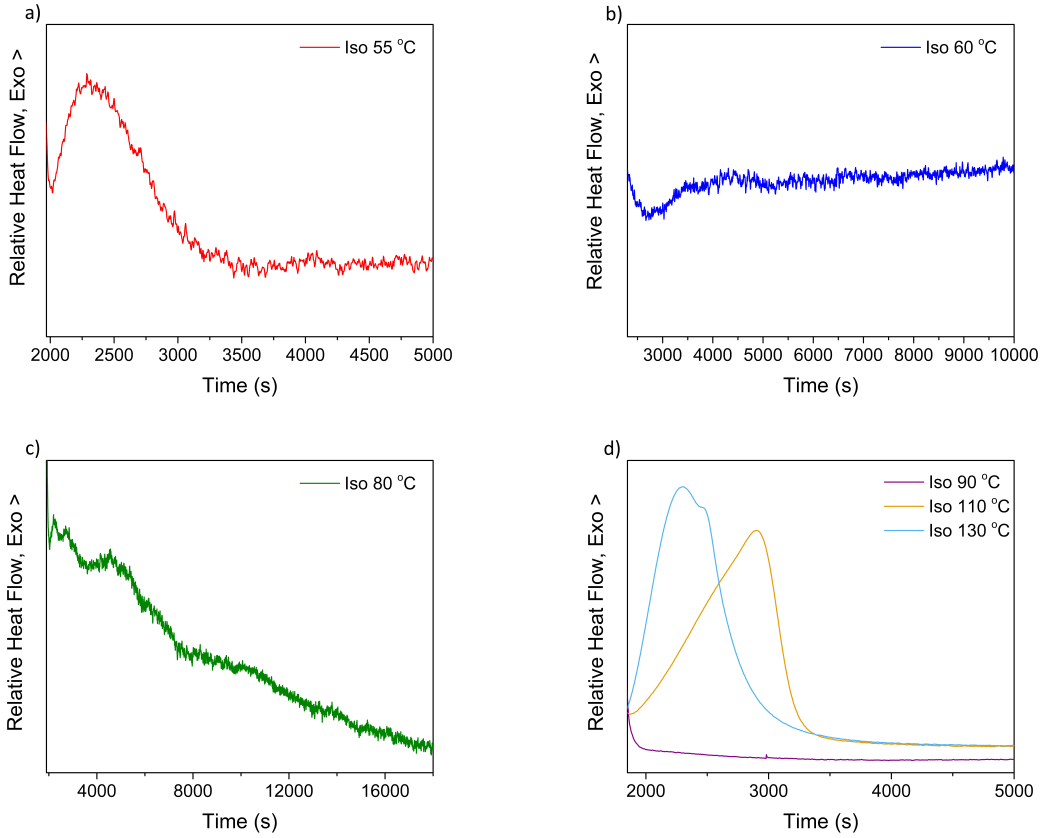

Figure 4.8: Isothermal treatments of a) polymer **1** at 55 °C, b) polymer **2** at 60 °C, c) polymer **3** at 80 °C and d) polymer **4** at 90, 110 and 130 °C.

Polymer **1** was subjected to isothermal treatment at 55 °C to show an exothermic crystallisation event within 25 minutes. Similar was observed for polymer **4**, where after being isothermally treated at 110 °C and 130 °C , an exothermic crystallisation event was observed after 25 minutes and 20 minutes respectively. Isothermal treatment of polymer **4** at 90 °C however showed no sign of crystallisation in the time frame of the first plot (Figure 4.8).

A closer look at the isothermally treated polymer **4** at 90 ° showed crystallisation taking place over a time scale of 3 hours and 3 minutes (183 minutes) (Figure 4.9).

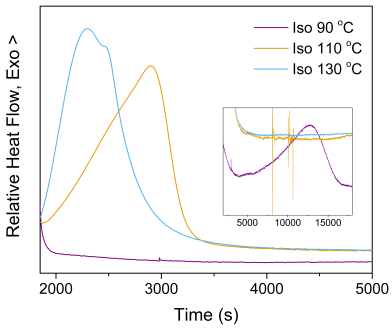

Figure 4.9: A Closer analysis of polymer **4** isothermally treated at 90 °C.

Polymer **2** and **3** also showed no sign of crystallisation, even after 300 minutes, indicating these two polymers had the lowest crystallisation ability (Figure 4.8).

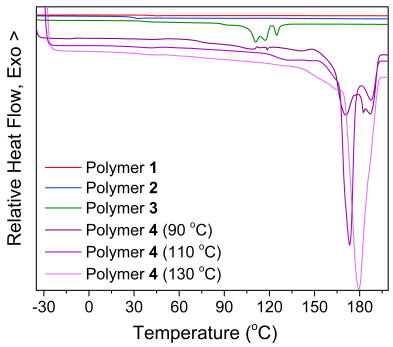

Figure 4.10: Second heating scan of polymers **1** to **4** after isothermal treatment.

Analysing the second heating scans of polymers **1** to **4** after isothermal treatment showed no T_m for polymer **2** due to the lack of an exothermic crystallisation event (Figure 4.10). Polymer **1** also showed no T_m, albeit the observed crystallisation event, suggesting the energy of T_{cc} was insufficient to induce crystallisation in the polymer matrix (Table 4.1). Polymer **3** and **4** both showed T_m's, even though polymer **3** had no exothermic crystallisation event. Multiple melting curves of polymer **3** and **4** in the second heating scan were observed, supporting the idea of more than one degree of crystallinity being present in the polymer matrix.

Table 4.1: Main thermal transition temperatures of polymers **1** to **4** when subjected to isothermal treatments. Enthalpy of cold crystallisation (ΔH_{cc}) and enthalpy of fusion (ΔH_m).

	First Heating Scan	**Second Heating Scan**	
	ΔH_m (Jg^{-1})	ΔH_m (Jg^{-1})	ΔH_{cc} (Jg^{-1})
Polymer **1**	29.3	-0.89	-
Polymer **2**	44.6	-	-
Polymer **3**	46.2	-0.44	1^{st} Peak = 23.7, 2^{nd} Peak = 3.9
Polymer **4** at 90 °C	1^{st} Peak = 3.2, 2^{nd} Peak = 28.9	-28.7	1^{st} Peak = 5.8, 2^{nd} Peak = 6.9
Polymer **4** at 110 °C	29.9	-38.9	39.2
Polymer **4** at 130 °C	29.7	-43.3	55.7

A closer look at polymer **4** shows the fastest crystallisation occurring at 130 °C, this is the optimum temperature for crystallisation as increasing the isothermal treatment to 140 °C decreased the rate at which crystallisation was occurring to 33 minutes (Figure 4.11).

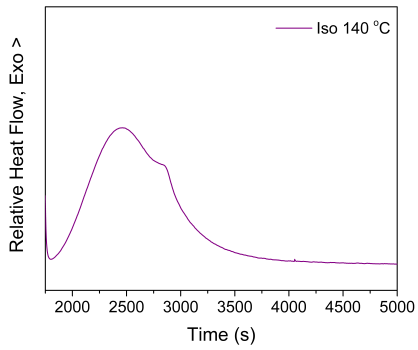

Figure 4.11: Isothermal treatment of polymer **4** at 140 °C.

Different heating rates were also applied to P2HEB to study the effect on the rate of heating on the thermal transitions (Figure 4.12), as it was predicted that an increase in the rate of heating would lead to increased values of the thermal transitions. The values of T_m were not significantly different, however the melting curves were more well-defined due to the rate at which thermal energy was being transferred to the pan and the sample.[173]

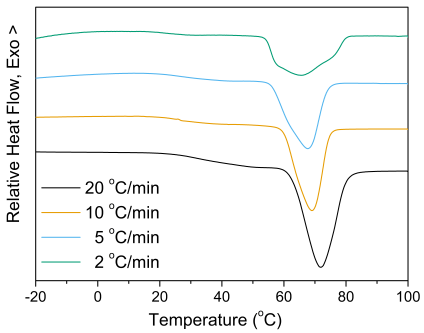

Figure 4.12: First heating scans of P2HEB of molecular weight 11,000 g mol^{-1} at different heating rates.

The area under the melting curve and the cold-crystallisation curve provides information on the energy, specifically the enthalpy of fusion, ΔH_m, and the enthalpy of cold-crystallisation, ΔH_{cc}, of each polymer system. As only polymer **4** recrystallised, the energy between T_m from the first and second scans were compared (Table 4.2). A significant reduction in energy during the second heating scan was observed, suggesting that the new crystalline state formed had a notably lower degree of crystallinity.

Table 4.2: Main thermal transition temperatures of polymers **1** to **4** and P2HEB.

	First Heating Scan	**Second Heating Scan**	
	ΔH_m (Jg^{-1})	ΔH_m (Jg^{-1})	ΔH_{cc} (Jg^{-1})
Polymer **1**	29.4	-	-
Polymer **2**	45.5	-	-
Polymer **3**	41.9	-	-
Polymer **4**	1^{st} Peak = 3.0, 2^{nd} Peak = 29.7	5.34	-6.4
P2HEB	29.8	-	-

Analysing the energies obtained from the isothermal studies, indicated that the exothermic and endothermic events in the second scan were significantly less than that of the first heating scans, due to the loss of the nascent crystalline structures.

The thermal transitions of polymer **1** to **4** and P2HEB of 11,000 g mol^{-1} were compared (Figure 4.13). The substituent effects on the thermal transitions of the polymers are hidden in the intermolecular interactions. Comparing the first heating

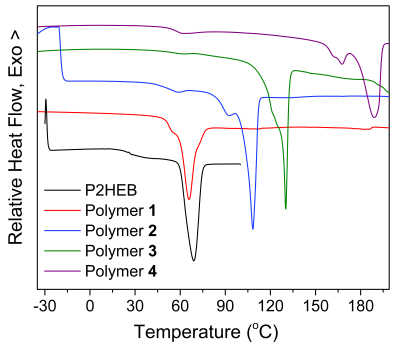

Figure 4.13: Combined plot of the first heating scans for polymers **1** to **4** and P2HEB.

scans of polymers **1** to **4** and P2HEB, it can be seen that as the σ_{meta} increases, the T_m's also increase in the same fashion. σ_{meta} influences the electron density in the aromatic ring, where a smaller σ_{meta} from an electron donating group would lead to an increase in electron density in the aromatic ring and repel adjacent aromatic rings, thus destabilising the π-π interactions and effecting the packing of the polymer matrix, the opposite is true for the electron withdrawing groups. The differences in electron density in the aromatic ring influences the strength of interactions between adjacent rings as well as the degree of packing and the degree of crystallinity. This is a common concept which has been explained through the Hunter-Sanders model.[130] Polymer **1**, with the lowest σ_{meta} value of -0.069, displayed a T_m at 65.9 °C. The T_m increased to 68.9 °C for P2HEB where σ_{meta} also increases to 0. A further increase in the σ_{meta} value to 0.115 for polymer **2** led to an increase in the T_m to 108.5 °C. The same trend is observed for polymer **3** and **4**, with σ_{meta} values of 0.337 and 0.391 respectively, showing T_m at 130.6 °C and 189.1 °C respectively.[129] It is worth noting that the σ_{meta} values associated with the packing and crystallinity of the sample affect the melting points of the resultant polymers, allowing one to tune the thermal properties of the polymers through altering the substituents.

Comparing the T_g's of polymers **1** to **4** and P2HEB in the second heating scan, it can be seen that the T_g does not follow the same trend as the T_m (Figure 4.14). Polymers **2** to **4** and P2HEB follow the predicted trend, where increasing in the electronic substituent parameter leads to an increase in the T_g. However, polymer

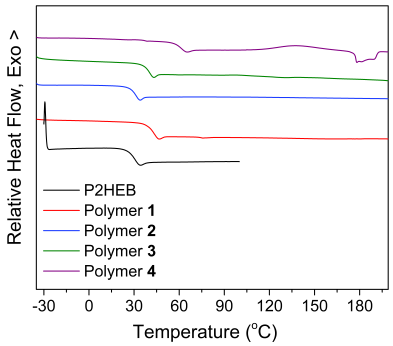

Figure 4.14: Combined plot of the second heating scans for polymers **1** to **4** and P2HEB

1 had the second highest T_g. Other factors in addition to the degree of packing influence the value of T_g, where chain mobility, flexibility and other interactions including hydrogen bonding and halogen bonding play a larger role. These interactions also influence the T_m however to a lesser extent. The more immobile and restricted the polymer chain is the higher the T_g and this can be introduced in the form of sterics and intermolecular forces.[174]

Thermogravimetric Analysis

Thermogravimetric analysis (TGA) was performed on polymers **1** to **4** and P2HEB of all three molecular weights to understand the thermal stability and the processing window of the polymers. The change in weight of the sample over a temperature period of 25 °C to 500 °C under a N_2 atmosphere was recorded at different heating rates and the data was analysed to give the thermal degradation behaviour of the polymers.

At a heating rate of 1 °C min^{-1} the onset of thermal degradation for P2HEB of 11,000 g mol^{-1}, denoted by the first 5 % weight loss ($T_{5\%}$), occurred at 145.6 °C, where 91 % weight loss was observed. This increased to 165.4 °C with an increase in heating rate to 5 °C min^{-1} and a further increase to 183.2 °C and 196.4 °C for heating rates of 10 °C min^{-1} and 20 °C min^{-1} respectively (Figure 4.15). The same trends are observed for polymers **1** to **4**, where an increase in the heating rate led to an increase in $T_{5\%}$ (Figure 4.16).

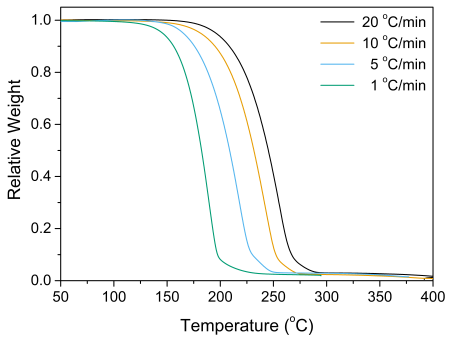

Figure 4.15: Thermogravimetric traces of P2HEB at different heating rates.

Polymer **1** showed an onset thermal degradation increase from 212.9 °C to 271.7 °C at a heating rate of 2 °C min^{-1} and 20 °C min^{-1} respectively. Polymer **2** showed an increase in onset of thermal degradation from 210.3 °C at a heating rate of 2 °C min^{-1} to 263.4 °C at a heating rate of 20 °C min^{-1}.

Polymer **3** and **4** followed the same trend, where increasing the heating rate from 2 °C min^{-1} to 20 °C min^{-1} led to an increase in the onset of thermal degradation from 209.5 °C to 262.3 °C for polymer **3** and from 199.3 °C to 253.5 °C for polymer **4**.

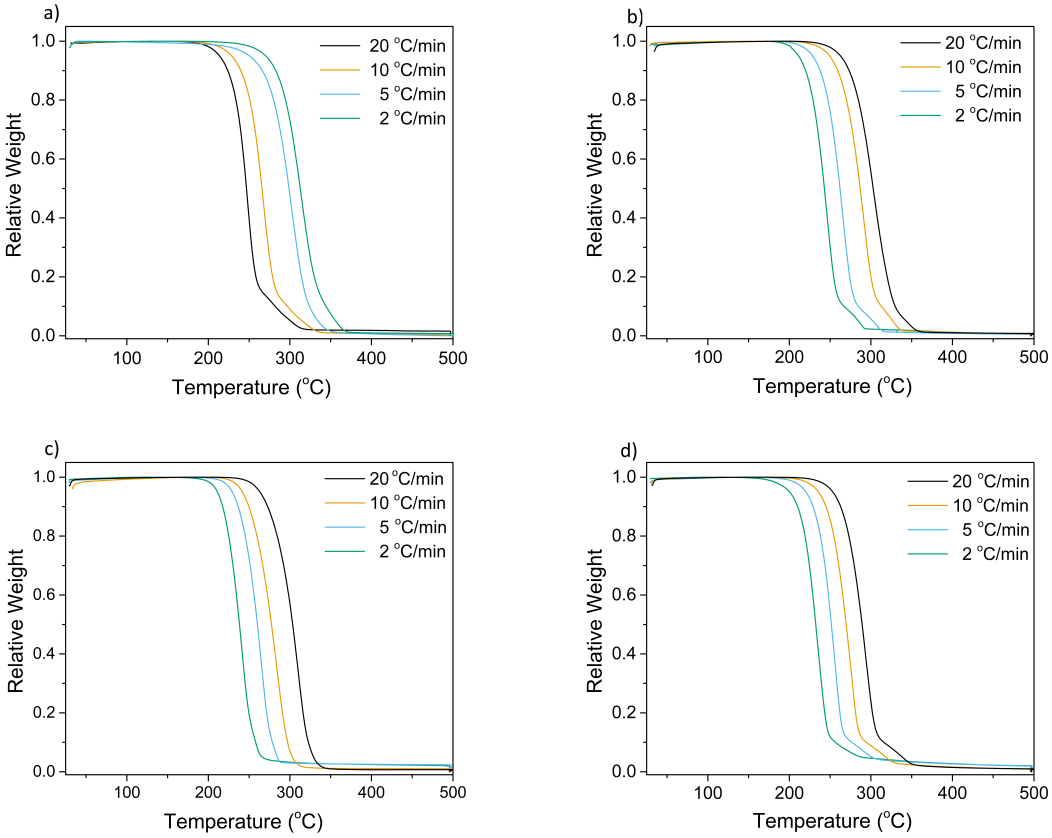

Figure 4.16: Thermogravimetric traces of a) polymer **1**, b) polymer **2**, c) polymer **3** and d) polymer **4** at different heating rates.

Upon increasing the molecular weight of P2HEB to 40,000 and 80,000 g mol^{-1} the onset of thermal degradation increased from 183.2 °C for 11,000 g mol^{-1} to 185.2 °C for 40,000 g mol^{-1} and to 191.3 °C for 80,000 g mol^{-1} at a heating rate of 10 °C min^{-1}. A shift of the onset of thermal degradation of approximately 9 °C from P2HEB of 11,000 g mol^{-1} to 80,000 g mol^{-1} suggests the independence of molecular weight on the thermal stability of this particular polymeric system.

A closer look at the degradation profiles of polymer **2** and **4** showed an increase in sample weight during the early temperatures, typically indicative of oxidation occurring in a sample. To monitor the possibility of oxidation, polymer **2** and **4** were subjected to thermal degradation studies under an O_2 atmosphere to encourage any oxidation processes (Figure 4.17). It can be seen upon analysis that no oxidation occurred as evident by no further increase in the sample weight.

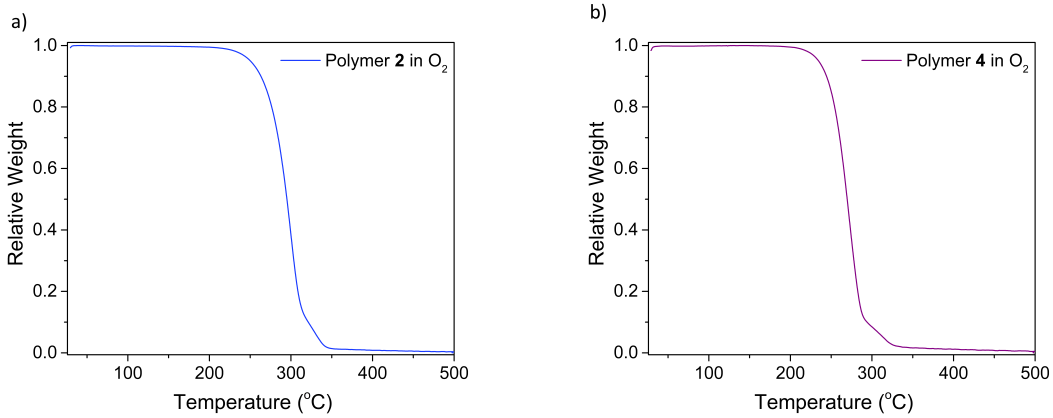

(a) Polymer **2** under O_2

(b) Polymer **4** under O_2

Figure 4.17: Thermogravimetric traces of a) polymer **2** and b) polymer **4** under O_2.

The thermal degradation of polymers **1** to **4** and P2HEB occurred at significantly lower temperatures than for other polyesters such as PLLA, where at a heating rate of 10 °C min^{-1} $T_{5\%}$ was observed at 290.5 °C.[149], and for PCL and poly(lactide-co-caprolactone) (PLCL), where $T_{5\%}$ was observed at 339.8 °C and 274.5 °C respectively.[175]

The rate of change of the sample weight was investigated for the polymers under a N_2 atmosphere by taking the first derivatives of each thermal degradation analysis (Figure 4.18). The maximum degradation (T_{peak}) was influenced by the heating rate showing an increase from 188.9 °C to 256 °C for heating rates of 1 °C min^{-1} and 20 °C min^{-1} for P2HEB of 11,000 g mol^{-1}. A similar trend was observed for polymers **1** to **4**, the values of T_{peak} are expressed in Table 4.3.

Table 4.3: $T_{5\%}$, T_{peak} and DTG_{max} (maximum degradation rate) values for polymers **1** to **4** at heating rates of 2, 5, 10 and 20 °C min^{-1}.

Polymer	**Heating Rate (°C min^{-1})**	**T$_{5\%}$ (°C)**	**T$_{peak}$ (°C)**	**DTG$_{max}$**
1	2	213.8	248.3	-0.0325
	5	228.7	267.7	-0.0271
	10	255.4	302.8	-0.0209
	20	268.4	314.3	-0.0201
2	2	211.2	245.5	-0.0285
	5	288.7	265.5	-0.0272
	10	251.9	292.5	-0.0244
	20	259.6	303.7	-0.0195
3	2	210.1	241.7	-0.0294
	5	229.9	265.5	-0.0208
	10	243.2	283.9	-0.0230
	20	261.8	308.1	-0.0237
4	2	200.8	234.4	-0.0291
	5	220.4	256.6	-0.0305
	10	234.9	275.8	-0.0274
	20	252.2	293.2	-0.0246

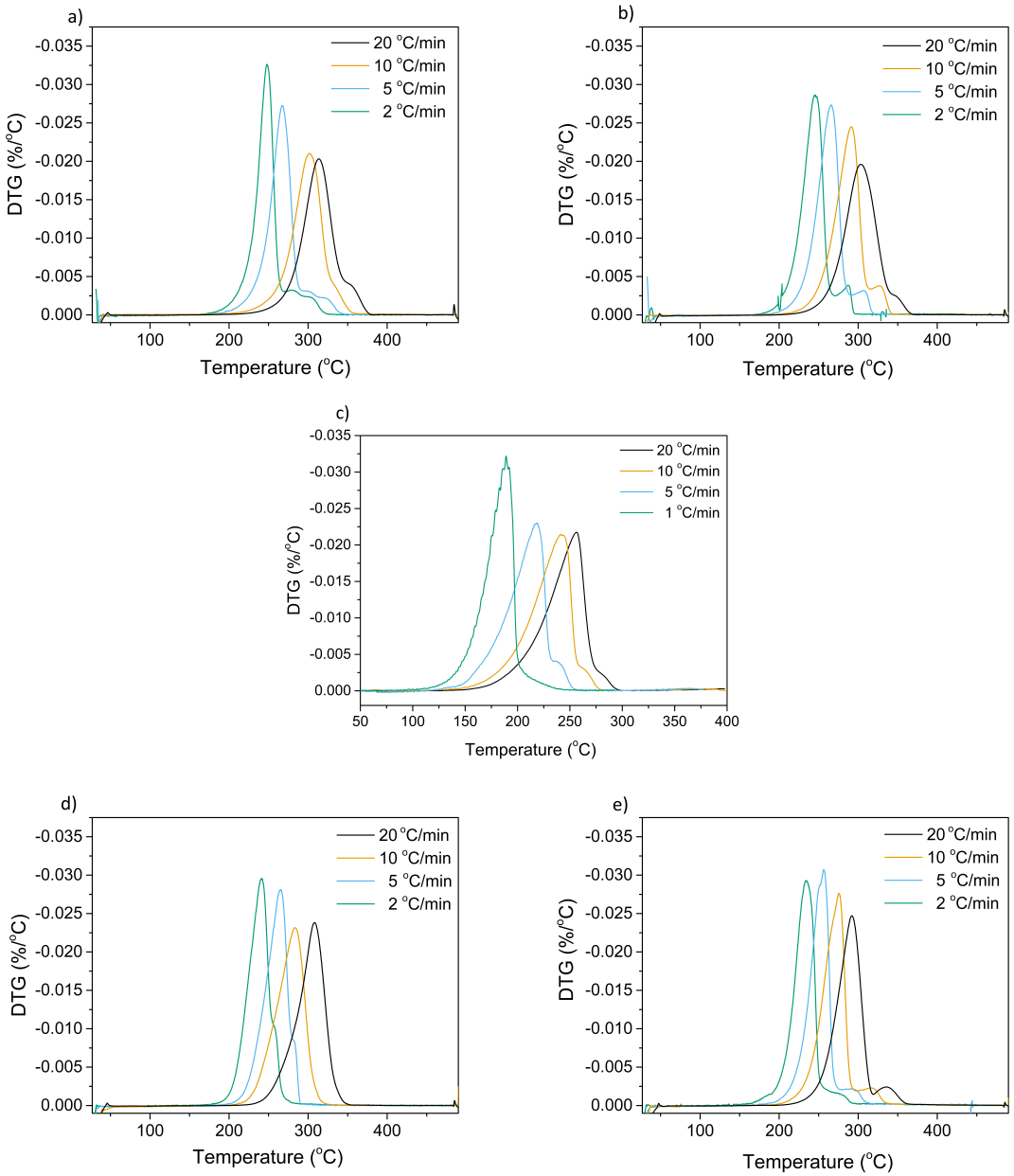

Figure 4.18: First derivatives of the thermogravimetric traces of a) polymer **1**, b) polymer **2**, c) P2HEB, d) polymer **3** and e) polymer **4** at different heating rates.

The T_{peak} values obtained for each polymer at different heating rates from the first derivative plots allows information about the energies in the polymeric system and their behaviour to be studied. The activation energy (E_a), of the system, gives an insight into the reactivity of the polymers to degradation. E_a can be calculated using the Kissinger equation. The Kissinger equation calculates the average activation energy of the polymeric system, whereas the Ozawa equation calculates the

activation energy profile of the polymeric system. The Kissinger equation utilises the T_{peak} obtained from the first derivatives of the different heating rates and plots $\ln(\beta/T^2_{max})$ as a function of $1/T_{max}$. The activation energy was calculated from the slopes in Figure 4.19 using Equation 4.1, where β is the heating rate, A is the pre-exponential factor, α is the maximum conversion, n is the reaction order and R is the universal gas constant (8.314 $JK^{-1}mol^{-1}$).

$$ln\frac{\beta}{T^2} = [ln\frac{AE_a}{R(\alpha)}] - \frac{E_a}{RT} \tag{4.1}$$

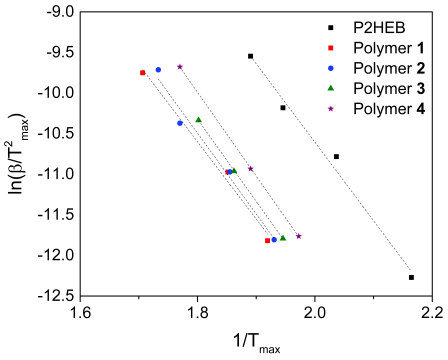

Figure 4.19: A plot of $\ln(\beta/T^2_{peak})$ vs $1/T_{peak}$ to calculate the activation energy for polymers **1** to **4** and P2HEB.

The average activation energies obtained for polymers **1** to **4** and P2HEB correlate well with their respective Hammett constants, where polymer **1** with a σ_{meta} value of -0.069 had the lowest activation energy of 78.9 ± 0.7 kJ mol^{-1}. An increase in the σ_{meta} value of P2HEB to 0, resulted in an increase in the activation energy to 79.7 ± 6.5 kJ mol^{-1} from 78.9 ± 0.7 kJ mol^{-1} . The trend followed for polymers **2**, **3** and **4**, where the σ_{meta} values of 0.115, 0.337 and 0.391 respectively led to activation energies of 82.7 ± 1.1 kJ mol^{-1}, 84.1 ± 0.1 kJ mol^{-1} and 85.7 ± 0.1 kJ mol^{-1} respectively. The increase in activation energy with σ_{meta} is evident, however it is important to note that the differences in activation energy are small with overlapping standard deviations.

Increasing the molecular weight of P2HEB to 80,000 g mol^{-1} resulted in a slight increase in activation energy to 84.1 ± 9.3 kJ mol^{-1}, this is observed in other poly-

meric systems such as polystyrene and poly(phenylene sulphide ether) where an increase in molecular weight leads to an increase in thermal stability and E_a.[176,177]

The calculated activation energies remain well below the calculated activation energies found for other polyesters such as PCL (228.9 kJ mol^{-1}) or PLCL (136.3 kJ mol^{-1}),[175] PLLA (100.8-163.8 kJ mol^{-1})[149,175] and PET (120 $\pm$ 12 kJ mol^{-1}).[178] The lower activation energies obtained for polymer **1** to **4** and P2HEB confirm their relatively low thermal stability. The thermal stability of polymer is influenced by the degree of crystallinty, molecular weight and chemical structure, where aromaticity increases thermal stability through π-π interactions and the amount of oxygen atoms present decreases thermal stability.[179] In the case of polymer **1** to **4** and P2HEB the aromatic rings are *ortho* linked, leading to a less efficient form of π-π interactions compared to that of PET. It is also important to note that the molecular weights of polymer **1** to **4** and P2HEB differ from the other polyesters reported in literature.

Considering the relatively low thermal stability of these polymers, when processing the material careful attention needs to be paid to ensure that the working temperature is in the narrow processing window.

4.1.2 Dynamic Mechanical Analysis

Dynamic mechanical analysis (DMA) is a powerful technique that allows the storage and loss modulus as well the stress and strain of a polymeric material to be probed as a function of temperature. In order for successful analysis of the polymeric materials, they need to be processed into films, via solvent casting using chloroform, to a known thickness of 200 μm. However, polymers **1** to **4** and P2HEB of molecular weight 11,000 and 40,000 g mol^{-1} demonstrated difficulty in forming a uniform film due to the brittleness observed. The low molecular weights contribute to the difficulty in forming films due to the lack of chain entanglement which typically aids in film formation.

A P2HEB film of molecular weight 80,000 g mol^{-1} was subjected to DMA in tensile mode (stretching of the polymer film under stress with varying temperature). Prior to probing the dynamic mechanical properties as a function of temperature, the

linear viscoelastic region (LVR) of the film was studied via a dynamic strain sweep experiment over the 0.001-10 % range (Figure 4.29). The importance of studying the LVR of a polymer system is to determine the strain range where the observed viscoelastic properties remain independent of imposed forces.

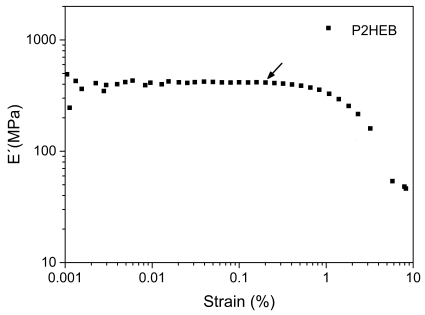

Figure 4.20: Stress strain sweep to determine the linear viscoelastic region of P2HEB of molecular weight 80,000 g mol^{-1}.

The LVR of P2HEB was studied at 0 °C, below the T_g, and the percentage strain in which the storage modulus (E') dropped due to overstrain was observed at 0.4 %, indicating the elastic structure of P2HEB would be lost if the film was subjected to further strain. Therefore, the chosen displacement to carry out further experiments on the P2HEB film was set at 0.4 %.

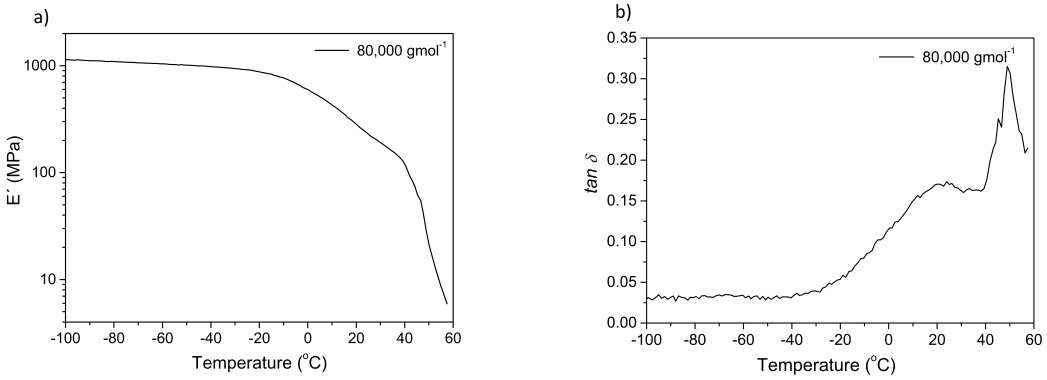

Figure 4.21: DMA of P2HEB of molecular weight 80,000 g mol^{-1} with a) the storage modulus and b) the tan δ against temperature.

At temperatures below the T_g of P2HEB it demonstrates a storage modulus of 1050 MPa with a rigid, glassy behaviour independent of the applied temperature.

Below T_g the maximum tan δ value is 0.17, which is ten times smaller than that observed for PLLA,[180] indicating the material would be elastic, where the storage modulus is high, and the loss modulus is low (Figure 4.21). Tan δ is the damping factor and is a ratio between the loss modulus (E") and the storage modulus (E'), where the storage modulus is related to the elasticity in the material and the loss modulus is related to the viscous part of the material. Tan δ monitors the way energy is lost in a material due to internal friction and molecular rearrangements.

Upon increasing the temperature from -20 °C to 40 °C, the storage modulus decreases, leading to an increase in tan δ, indicating that the polymer is exhibiting a rubber-like behaviour which is indicative of a highly viscous material. The storage modulus decreases even further when the temperature reaches 42 °C, above the T_g, this is due to the increase in molecular mobility and is denoted as the α relaxation mode. The low tan δ below T_g suggests the presence of highly ordered domains, providing stiffness to the whole material, having poor energy dissipation.[181,182] Tan δ is highest at T_g where the contribution of the loss modulus is higher than that of the storage modulus. Tan δ maximum is centred at 23 °C, correlating well with the T_g value obtained via DSC.

Further increasing the temperature resulted in the dramatic decrease in the storage modulus correlating to the melting of the polymer. The temperatures of the T_g and T_m being in close proximity to each other eliminate the possibility of observing a rubbery plateau that is typically found in other polyesters. The rubbery plateau is observed between the T_g and T_m and is a result of chain entanglement. The entanglement of the polymer chains in this temperature range allows the polymer to enter a rubbery state where there is sufficient vibrational energy in the system to rotate the polymer chains without causing translational motion, corresponding to the T_m.[174,183]

The storage modulus of P2HEB below T_g of 1050 MPa is still more than half of traditional petro-based polymers such as PMMA or other polyesters such as PLLA.[180,184] The marked decrease in storage modulus near physiological temperature (37 °C) highlights the potential of P2HEB to be used for biomedical applica-

tions.

4.1.3 Wide Angle X-Ray Diffraction

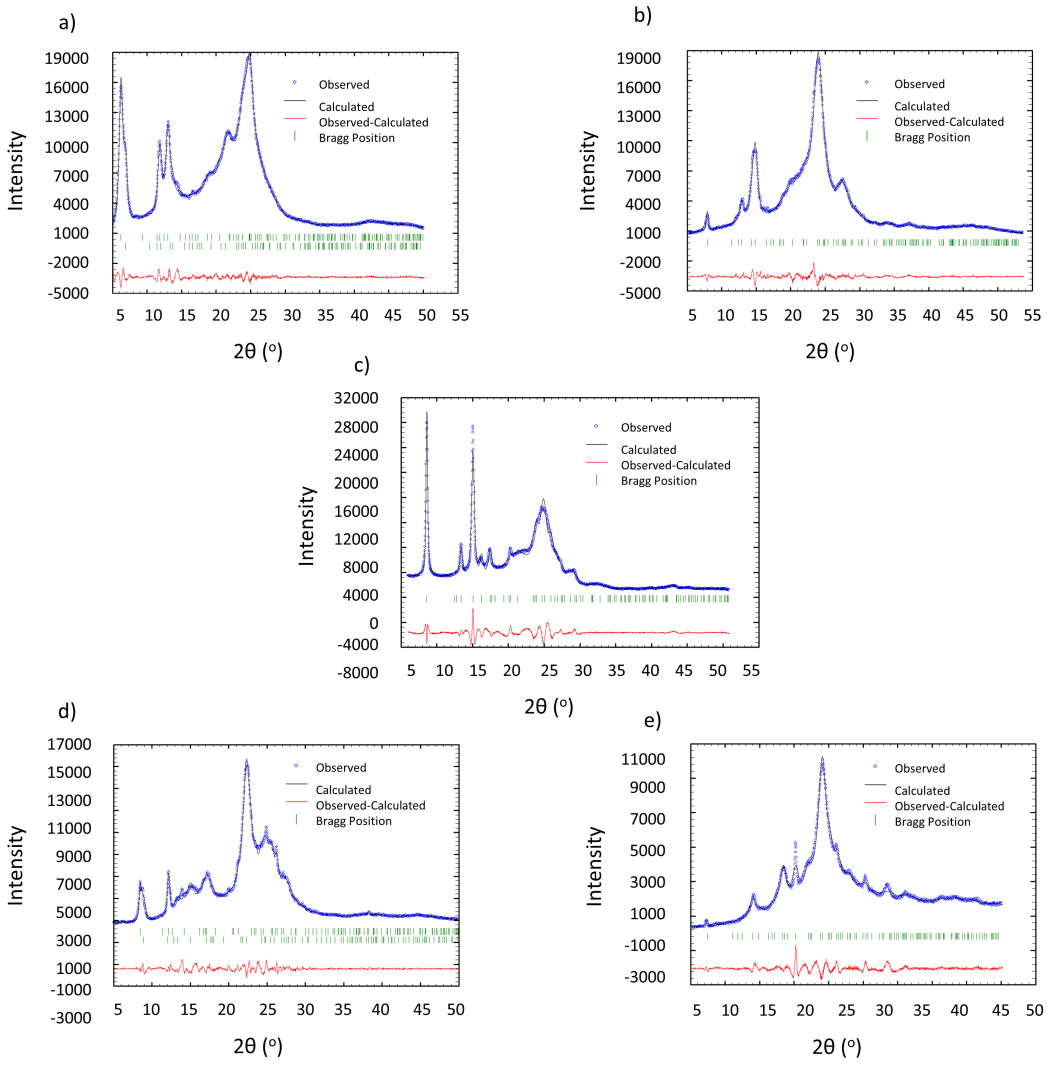

Figure 4.22: Wide angle X-ray scattering of a) polymer **1**, b) polymer **2**, c) P2HEB, d) polymer **3** and e) polymer **4** from a 2θ range of 5θ to 55θ.

The crystalline structure of polymers **1** to **4** and P2HEB were studied using wide angle X-ray diffraction (WAXD) (Figure 4.22). WAXD utilises the diffraction pattern caused by the polymer sample, where the scattering intensity as a function of the angle at which the X-ray source is positioned gives information about the degree of crystallinity of the polymer sample as well as information about the symmetry

and unit cell parameters.

Powder forms of polymer **1** to **4** and P2HEB were placed on a sample holder, typically made from a single crystal of silicone which displays one distinct refraction peak and placed on a plate inside of the instrument. The plate rotates 360 ° to ensure an accurate representation of the sample can be obtained. The X-ray source and the detector are positioned at angle, θ, and each measurement or scan is taken at every 0.02626 θ from a range of 5θ to 60θ, where 2θ is the overall angle of the X-ray source and detector combined.

The scattering intensity of the polymer sample is plotted as a function of 2θ and the peaks are mathematically deconvoluted to obtain the exact 2θ values of each peak using the peak fit option in WinPLOTr. A simulated trace that closely matches that of the original plotted data is then generated. These 2θ values are then evaluated using the software TREOR and DICVOL to index the powder diffraction patterns and generate unit cell parameters from the peak positions, denoted by 2θ. The trace is simulated again using the cell parameters generated by the software, this process is repeated, and each parameter is optimised until the observed data and the calculated/simulated data are in good agreement.

The unit cell parameters are determined through Bragg's Law (Equation 4.2), where d is the lattice interplanar spacing of the crystal at angle θ and λ is the wavelength (typically fixed). h,k,l are miller indices and correspond to the size and shape of the unit cell being analysed. The angle at which the peaks appear on the powder pattern can be extracted and used to calculate the miller indicates corresponding to the plane restrictions in the sample and to gain information on the geometry, unit cell size and orientation of the sample for example cubic, tetragonal, orthorhombic, or hexagonal.[185]

$$d = \frac{\lambda}{2sin(\theta)} \tag{4.2}$$

P2HEB is an unexplored polymeric system and therefore previous starting parameters were unknown. Initially the Powder Diffraction File (PDF) database aided in the identification of the phases of P2HEB along with PANalyticalX' Pert

High Score (a search-match program to interpret the raw X-ray data using known databases). However, the results obtained for P2HEB did not correlate to any known phases. Further testing of the chemical configuration using CSD database Cambridge Crystallographic Data Centre (CCDC)[186] also showed no correlation to known data. The data was therefore extracted and manipulated using TREOR and DICVOL with WinPLOTR to gain further information on the unknown powder diffraction patterns.

The results obtained for P2HEB, upon calculation, generated the initial unit cell parameters of a=b=7.48 Å c=23.28 Å, indicating a tetragonal symmetry. Through optimisation and refinement of the unit cell parameters, backgrounds, systematic 2θ shifts, and peak shapes (pseudo-Voigt using a convolution of a Gaussian and Cauchy-Lorentz distribution or Cagliotis using the Cagliotis formula to understand how the full width at half maximum varies with θ) via the program FULLPROF[187–189] the final unit cell parameters were a=b=7.494(2) Å and c=23.19(1) Å. The calculated and experimental data were in good agreement with the final reliability factors being R_p: 12.8, R_{wp}: 13.1, R_{exp}: 3.14, Chi^2: 17.4 and Bragg R-factor: 0.206. The R_p (profile residual), R_{wp} (weighted profile residual) and R_{exp} (expected profile residual) values are the Rietveld refinement parameters that give insight into how well the model data fits the observed data by minimising the difference between the calculated profile and the observed data. The Bragg R-factor is the goodness of fit that encompasses the other Rietveld refinement parameters.[187] It is important to note that molecular weight did not affect these values.

The sharp diffraction signals at low 2θ suggest a highly crystalline sample with long range ordering, however the broad diffraction signals at high 2θ suggests poor short-range ordering and possible molecular conformation disorder. This observation is independent of the molecular weight of P2HEB.

A similar diffraction pattern at high 2θ values was observed in polymer **2** where the broad diffraction signal indicated polymer chain conformation disorder. However, at low 2θ values, the low intensity and high full width at half maximum signals indicated lower degree of crystallinity compared to that of P2HEB, possibly due to

the molecular packing disorder, as supported by the larger unit cell parameters of a=b=7.75 Å and c=25.53 Å.

Polymer **4**, similar to polymer **2** and P2HEB, displayed polymer chain conformation disorder at high 2θ values. At low 2θ values however, the low intensity signals suggest poor or no long-range ordering in the polymeric system. On the other hand, the full width at half maximum signals indicated a degree of anisotropy in the system, due to the asymmetrical peak shape, with unit cell parameters of a=b=7.46 Å and c=23.83 Å.

Polymer **1** and **3** demonstrated unique crystal structures, with splitting of the signals at low 2θ values. This related to the packing distances of the molecules, indicating the presence of more than one type of conformation. Polymer **1** demonstrated two different packing distances in the z plane with two-unit cell parameters varying in lattice constant c where c=25.72 Å and 28.39 Å, whilst a=b=7.29 Å. Polymer **3** on the other hand, showed an average lattice constant c of 20.35 Å and varied lattice constants a and b, where in one a=b=7.32 Å and the other a=b=7.74 Å.

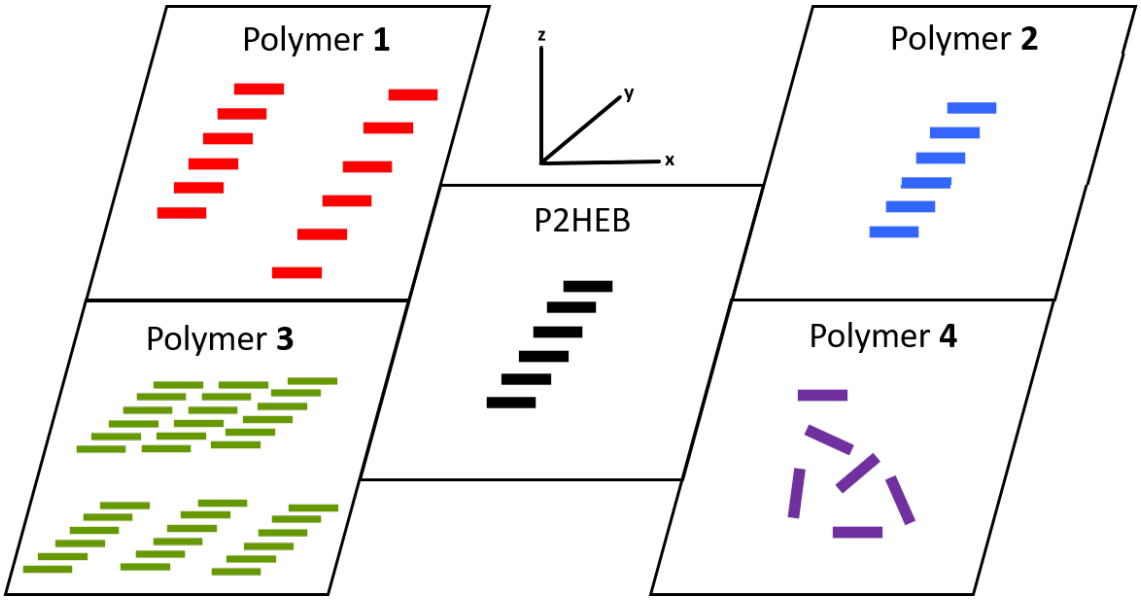

Figure 4.23: Cartoon representation of one of the many possible configurations of the molecules in each polymeric system.

A suggested cartoon representation of one of the many possible conformations

are displayed for each of the polymers in Figure 4.23. The z plane is related to the lattice constant c, where the x and y planes are related to the lattice constants a and b respectively. Polymer **1** had two-unit cell parameters indicating different stacking distances, where one was closer than the other. This could be due to the difference in the orientation of the packing where the larger unit cell parameter is attributed to the steric clashing of the methyl groups. This phenomenon can be explained through parallel and anti-parallel orientation of the polymer chains (Figure 4.24, where anti-parallel would result in a larger unit cell parameter.

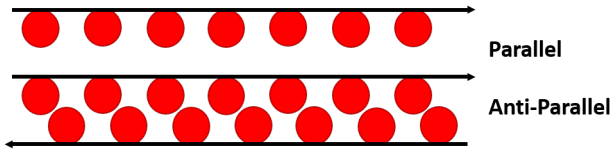

Figure 4.24: Cartoon representation of parallel and anti-parallel polymer chains in polymer **1** where the arrows represent the polymer backbone and the red circles represent the methyl groups causing steric repulsion in the anti-parallel example.

Polymer **2** was very similar to P2HEB, where the stacking was clear and the same distance throughout the analysed sample. However, in polymer **2** the stacking was further apart. Polymer **3** similarly had, on average, the same packing throughout, however the two-unit cell parameters suggested that one region was more ordered and tightly packed than the other. Polymer **4**, unlike the others, had no ordering and was suggested to be anisotropic.

The crystalline behaviour of polymers **1** to **4** and P2HEB were confined to the 00L and 10L planes suggesting a highly crystalline lamellar structure, specifically of 20 x 30 nm for P2HEB. The 00L plane is related to the π-π stacking in the polymeric systems where only the l miller index is changing. Although P2HEB shows a highly crystalline structure, there are amorphous regions in the 0k0 plane that cloud the overall crystallinity of the sample.[167]

Upon a closer look at the lattice constant c for polymers **1** to **4** and P2HEB in relation to their Hammett constants, it is predicted that an increase in σ_{meta} would lead to enhancement in π-π stacking. The exceptions to the trend are polymer **2** and **4** where their lattice constants are 25.53 Å and 23.83 Å respectively. Polymer **1**

with the lowest σ_{meta} value has the largest distant between the stacking of c=28.39 Å and increasing the σ_{meta} values for P2HEB and further for polymer **3**, the distances between the stacking decreases to c= 23.19 Å and 20.35 Å respectively.

The exceptions of polymer **2** and **4** are attributed to the size of the atoms. Fluorine has the smallest atomic radius of 0.42 Å and polymer **3** has the smallest lattice constant c. The trend follows with hydrogen and bromine having an atomic radius of 0.53 Å and 0.94 Å respectively.[190]

Taking the atomic radii into account, the trend observed for the Hammett constant can be better interpreted. Even though polymer **4** is predicted to have the smallest packing distance, the size of the bromine atom being significantly larger than the fluorine atom causes steric repulsion between adjacent aromatic rings as well as adjacent bromine atoms and thus a larger packing distance. The case is the same for the methoxy group in polymer **2** where a packing distance less than P2HEB is predicted, however due to the steric size of the methoxy group over a hydrogen atom, the packing distance was greater.

Polymers **1** to **4** were subjected to high temperature X-ray diffraction to monitor the change in crystallinity upon heating (Figure 4.25). The polymers were heated from 30 °C to 360°C at a heating rate of 10 °C min^{-1}. The disappearance of the normalised intensity area corresponding to the main 002 plane can be observed upon heating. The thermal stability of the crystalline phase of P2HEB was at 55 °C. Further heating resulted in a fully amorphous sample at 90 °C where the relative intensity dropped below 5%.

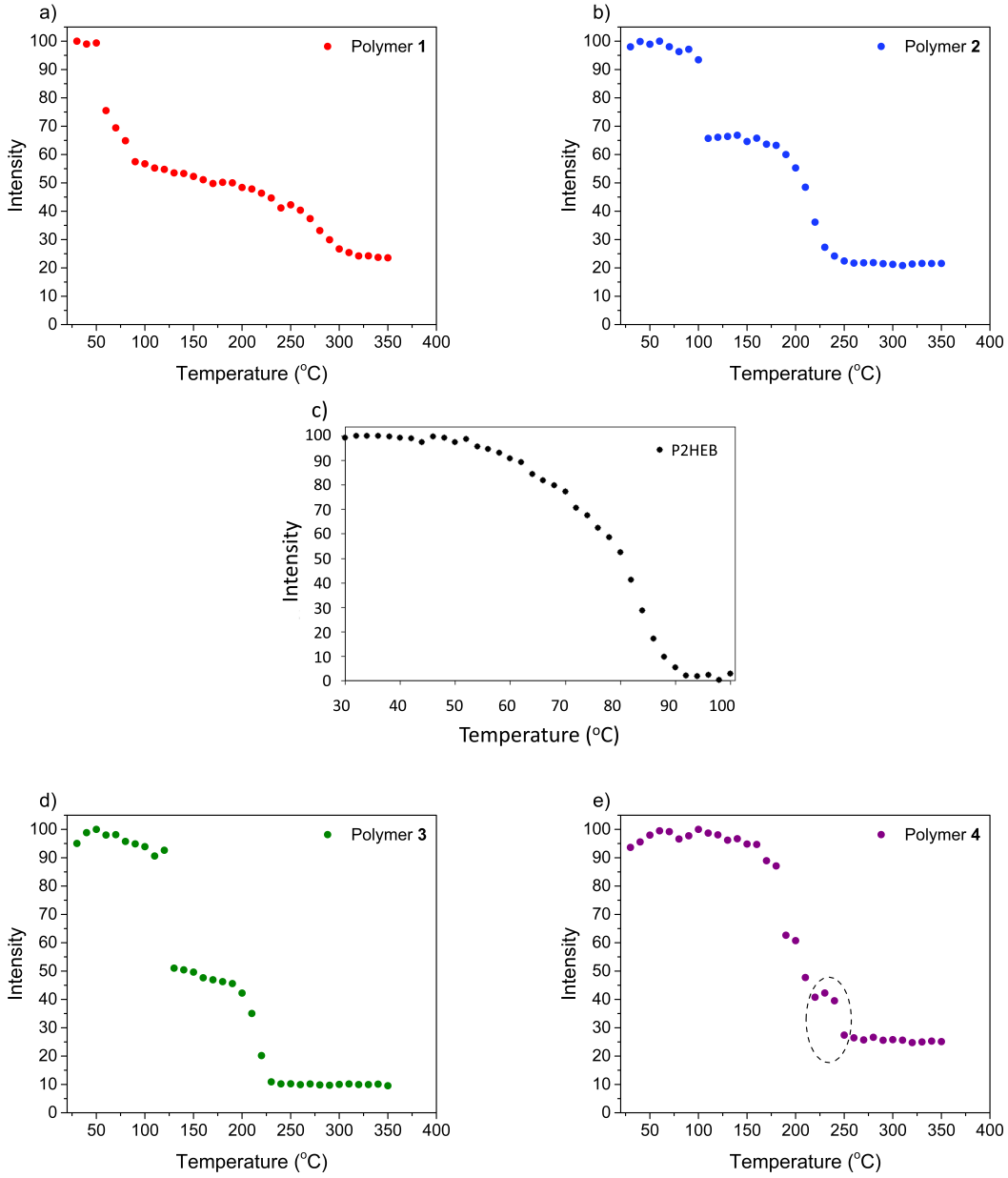

Figure 4.25: X-ray diffraction as a function of temperature to determine the thermal stability of the crystalline phase for a) polymer **1**, b) polymer **2**, c) P2HEB, d) polymer **3** and e) polymer **4** (the dotted circle shows the appearance of a new crystalline structure).

Similar was observed for polymers **1** to **3** where the relative intensities dropped above a certain temperature denoted by the thermal stability of the crystalline phases. The thermal stability observed for polymer **1**, **2** and **3** were 50 °C, 100 °C and 120 °C respectively.

Polymer **4** displayed a thermal stability of 180 °C, however upon further heating there was a small window where another crystal structure was observed (dotted circle in Figure 4.25 e). Integrating the total area of all the signals from this new crystal structure and comparing it to the total area of all the signals from the original observed crystal structure it was concluded that the contribution of the new crystal structure was less than 5 % and was possibly due to defects in the polymeric system.

The thermal stabilities observed for polymers **1** to **4** and P2HEB correlate well with the Hammett constants and the observed T_m values from DSC.

4.1.4 Copolymers: Thermal Analysis

Copolymers: Differential Scanning Calorimetry

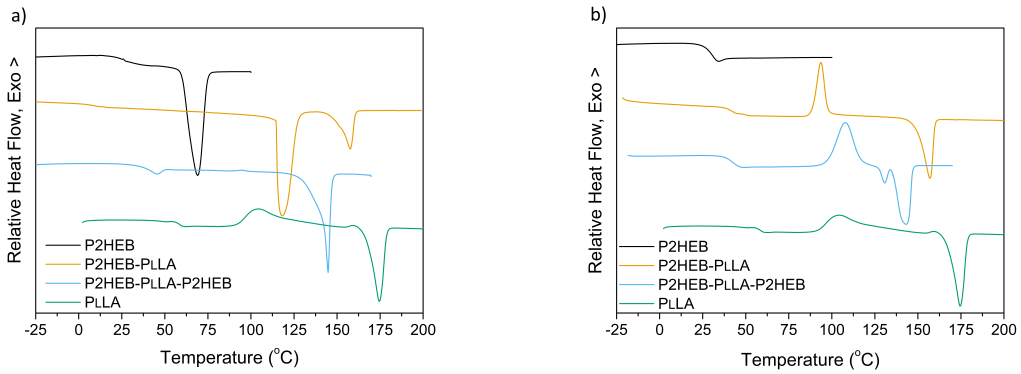

Figure 4.26: a) First and b) second heating scans of the diblock copolymer **1** and the triblock copolymer **2** along with their homopolymers.

DSC was used to study the thermal transitions present in diblock copolymer **1** (P2HEB-PLLA) and the triblock copolymer **2** (P2HEB-PLLA-P2HEB) (Figure 4.26). The first heating scan of the diblock copolymer **1** displayed an endothermic event (T_g) at 15.2 °C. A further increase in the temperature resulted in the double melting behaviour of the diblock copolymer **1** at 118.2 °C and 157.8 °C. The triblock

copolymer **2** on the other hand displayed a single melting curve at 144.6 °C with the presence of a shoulder at earlier temperatures. This is attributed to the apparent overlap between the T_g of the copolymer and the T_m of short P2HEB blocks. The T_g of the triblock copolymer **2** was centred at 39.9 °C. The presence of a single T_g indicated miscibility of the two blocks.

The second heating scan of the diblock copolymer **1** showed a single T_m at 156.9 °C, due to the poor crystallisation ability of the P2HEB blocks, and a dramatic increase in the T_g to 42.3 °C. The second heating scan also displayed an exothermic event at 93.6 °C corresponding to the T_{cc} from the PLLA block. The triblock copolymer **2** showed two melting curves at 130.7 °C and 143 °C and a single T_g at 41.9 °C.

ΔH_{cc} and ΔH_m, determined from the area under the curves, showed the triblock copolymer **2** to have a greater crystallisation event due to the incorporation of a larger amount of PLLA (Table 4.4).

Table 4.4: Main thermal transition temperatures of the diblock copolymer **1** and triblock copolymer **2**.

Diblock Copolymer 1	ΔH_{cc} **(Jg^{-1})**	ΔH_m **Peak 1 (Jg^{-1})**	ΔH_m **Peak 2 (Jg^{-1})**
1^{st} heating	-	79.4	24.8
2^{nd} heating	16.5	-	22.6
Isothermal at 80 °C	-	-	23.6
Triblock Copolymer 2	ΔH_{cc} **(Jg^{-1})**	ΔH_m **Peak 1 (Jg^{-1})**	ΔH_m **Peak 2 (Jg^{-1})**
1^{st} heating	-	-	26.4
2^{nd} heating	21.6	2	18.6
Isothermal at 80 °C	-	-	24.2

The diblock copolymer **1** and the triblock copolymer **2** were subjected to isothermal treatments at 80 °C to induce crystallisation (Figure 4.27). Upon subjection to a second heating scan two well-defined endothermic events were observed at 37.9 °C and 156.7 °C for the diblock copolymer **1** for the T_g and T_m respectively and at 37.1 °C and 141.6 °C for the triblock copolymer **2** for the T_g and T_m respectively. This indicated the recrystallisation of only the PLLA block during isothermal treatment,

supporting previous findings of the poor crystallisation ability of P2HEB.[136]

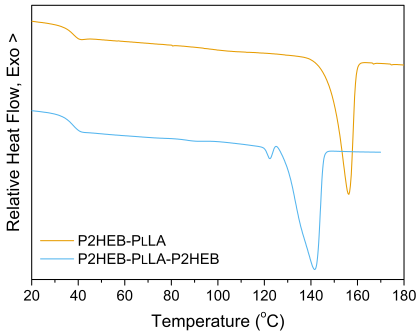

Figure 4.27: Isothermal treatment of the diblock copolymer **1** and the triblock copolymer **2** at 80 °C.

The thermal transitions of the copolymers are lower than that of the PLLA homopolymer (T_g = 55 °C and T_m = 175 °C) but higher than that of the P2HEB homopolymer. The incorporation of P2HEB into PLLA has shown the ability to tune the thermal properties of the resultant copolymers.

Copolymers: Thermogravimetric Analysis

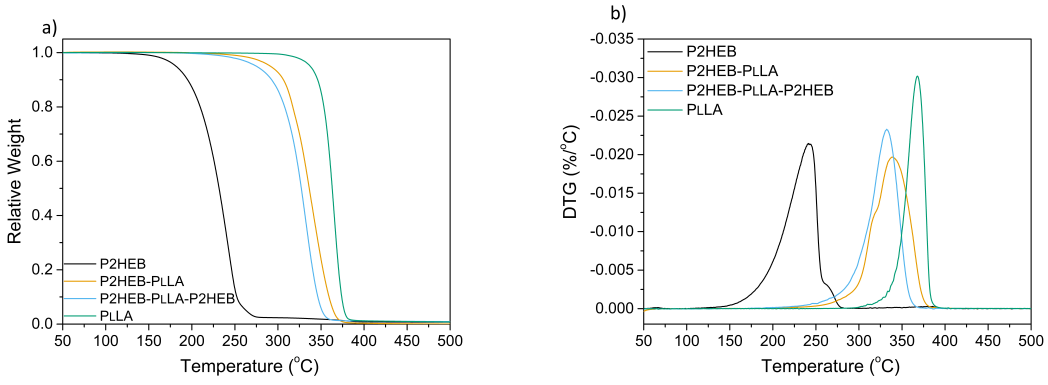

Figure 4.28: a) Thermogravimetric and b) first derivative traces of the diblock copolymer **1** and triblock copolymer **2**.

TGA was used to determine the thermal stability of the diblock copolymer **1** and the triblock copolymer **2**. The thermal stability of the copolymers were considerably higher than that of the P2HEB homopolymer ($T_{5\%}$ = 183.2 °C), with the diblock

copolymer **1** having a $T_{5\%}$ of 291.2 °C and the triblock copolymer **2** having a $T_{5\%}$ of 274.9 °C (Figure 4.28 a).

A closer look at the first derivative of weight loss against temperature (Figure 4.28 b) also showed the T_{peak} of the copolymers being higher than that of the P2HEB homopolymer due to the incorporation of PLLA units. Incorporation of PLLA into P2HEB increased the thermal stability of the copolymers, however incorporation of P2HEB into PLLA decreased the thermal stability of the copolymers when compared to the PLLA homopolymer ($T_{5\%}$ = 337.7 °C and T_{peak} = 368.8 °C) (Table 4.5). The presence of small shoulders at earlier temperatures on the first derivative curve for the copolymers suggested degradation of the less thermally stable P2HEB block followed by the degradation of the PLLA block. The difference in the DTG peaks of the copolymers and the P2HEB homopolymer shows the ability to improve the thermal stability of P2HEB through incorporation of PLLA.

Table 4.5: Main thermodegradation parameters of the diblock copolymer **1** and triblock copolymer **2**.

	P2HEB	**Diblock Copolymer 1**	**Triblock Copolymer 2**	**PLLA**
$\mathbf{T_{5\%}}$ **(°C)**	180.9	291.2	274.9	337.7
$\mathbf{T}peak$ **(°C)**	242.1	340.5	333.2	368.8
$\mathbf{DTG}_{max}$	-0.021	-0.019	-0.23	-0.031

4.1.5 Copolymers: Dynamic Mechanical Analysis

The mechanical properties of the diblock copolymer **1** and the triblock copolymer **2** films of 150 μm thickness (obtained through solvent casting) were studied using DMA in tensile mode. Prior to measurement a dynamic strain sweep experiment over the 0.001-5 % range was studied to obtain the LVR of the diblock copolymer **1**, similar to that of P2HEB (Figure 4.29). The chosen displacement, before the storage modulus dropped due to over strain, was the same as that for P2HEB at 0.4 %.

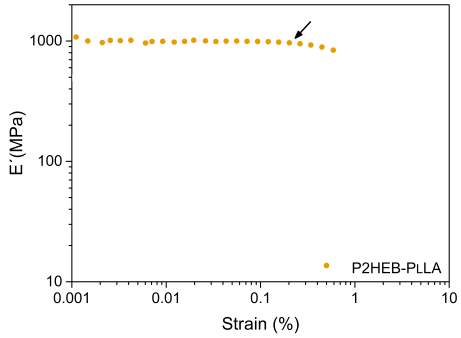

Figure 4.29: Stress strain sweep to determine the linear viscoelastic region of the diblock copolymer **1**.

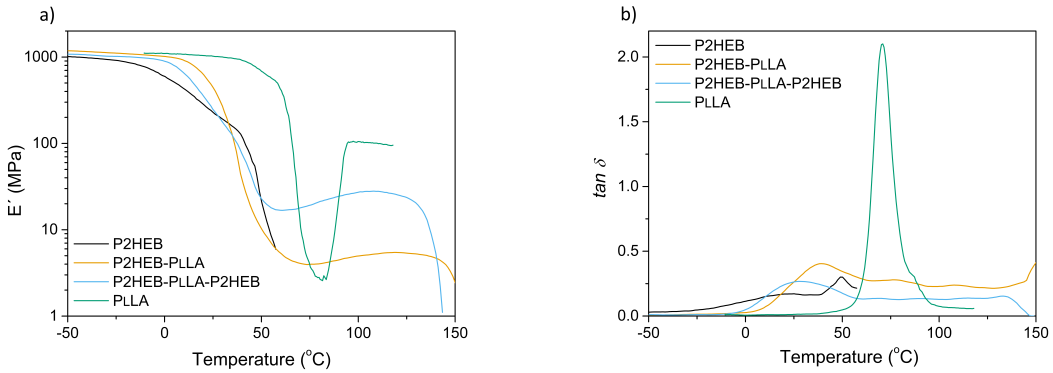

Figure 4.30: a) DMA of the diblock copolymer **1** and the triblock copolymer **2** and b) their respective tan δ traces.

Below T_g the copolymers displayed a rigid, glassy behaviour with a storage modulus of 1178 MPa for the diblock copolymer **1** and 1087 MPa for the triblock copolymer **2** (Figure 4.30). These were similar values to that observed for their respective homopolymers, where P2HEB had a storage modulus of 1013 MPa and PLLA had a storage modulus of 1107 MPa. Increasing the temperature above the T_g led to a dramatic decrease in the storage modulus and an increase in tan δ, attributed to the sudden increase in chain mobility. Unlike the P2HEB homopolymer, the copolymers displayed a rubbery plateau before a further drop in the storage modulus. The PLLA homopolymer displayed an increase in the storage modulus upon further heating, this corresponds to the crystallisation of the PLLA leading to a new crystalline state with a storage modulus of 105.4 MPa. The rubbery plateau

observed in the copolymers could be mistaken for the crystallisation of the PLLA block with the curve being more subtle due to the P2HEB block inhibiting crystallisation of the PLLA block. However, it is worth noting that the tan δ for the copolymers did not decrease back to the baseline during the rubbery plateau, unlike the PLLA homopolymer, suggesting little or no crystallisation was occuring in the copolymers. The incorporation of P2HEB increased the strain at break of the copolymer compared to neat PLLA and therefore shows the potential to improve the inherent brittle nature of PLLA.

4.1.6 Copolymers: Wide Angle X-Ray Diffraction

The observations of the crystallisation of only the PLLA block through DSC and DMA was confirmed using WAXD, where the diffraction pattern for the copolymers predominantly corresponded to the PLLA crystals (Figure 4.31). This was evident through comparing the angle at which each peak occurred to the PDF database and calculating the lattice planes. The peaks at 2θ values of 14.8, 16.5, 19.0 and 22.3° attributed to (010), (110)/(200), (203) and (015) planes respectively in PLLA.[191,192] The crystallisation of only the PLLA block in copolymers has previously been reported by Fernandez *et al.* where the crystal structure of poly(ω-pentadecalactone-co-δ-hexalactone) was not able to be determined by WAXD.[193]

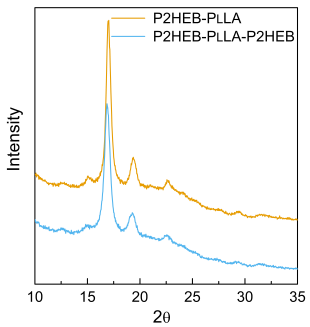

Figure 4.31: Wide angle X-ray scattering for the diblock copolymer **1** and triblock copolymer **2** at room temperature.

The copolymers were subjected to high temperature X-ray to monitor the change

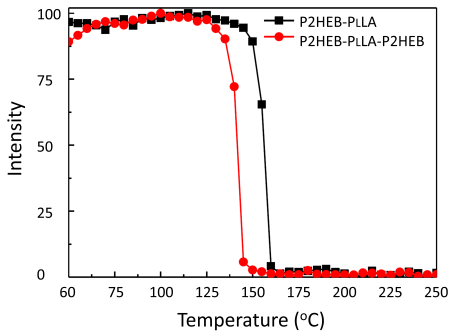

Figure 4.32: X-ray diffraction as a function of temperature to determine the thermal stability of the crystalline phase of the diblock copolymer **1** and triblock copolymer **2**.

in crystallinity upon heating (Figure 4.32). The triblock copolymer **2** displayed a loss of crystallinity in the 110 plane at 145 °C. This increased to 160 °C for the diblock copolymer **2**. No significant changes were observed in the temperature range at which the P2HEB crystals melt (68.8 °C to 76.8 °C)[136], further confirming the crystallisation of only the PLLA block.

4.1.7 Copolymers: Optical Properties

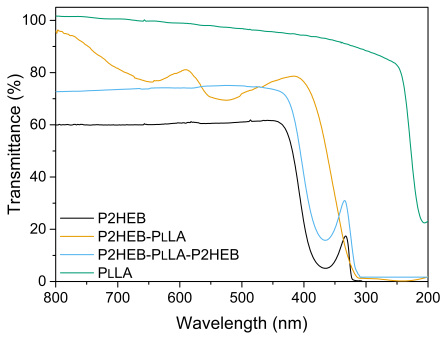

Figure 4.33: UV-Vis transmittance spectra for neat P2HEB, neat PLLA, the diblock copolymer **1** and triblock copolymer **2**.

UV–Vis spectroscopy was used to determine the ability of the diblock copolymer **1** and the triblock copolymer **2** to be used in packaging applications. The optical transparency of PLA is excellent, however the poor UV-absorbing properties of PLA

limits its use in packaging of food due to reduced food quality and shelf life.[194–196] Therefore, in order to prevent food photodegradation, biodegradable polymers with UV-absorbing properties need to be synthesised.

Figure 4.33 shows the transmittance of the diblock copolymer **1** and the triblock copolymer **2**. The diblock copolymer **1** exhibited an optical transparency of 72 %, determined as the transmission of light from 540-560 nm; ASTM D1746-03 (standard test method for transparency of plastic).[197] A closer look at the curve also displayed more than 99 % UV-absorbing characteristics, absorbing both UV-A light (λ=315-400 nm) and UV-B light (λ=280-315 nm). The triblock copolymer **2** displayed similar characteristics with 75 % optical transparency and more than 98 % UV-A and UV-B absorbance.

The copolymers showed both optical transparency and UV-absorbing properties, unlike their respective homopolymers. The PLLA homopolymer had an optical transparency of 98 % with no UV-absorbing properties, whereas the P2HEB homopolymer had strong UV-absorbing characteristics with only 60 % optical transparency. The UV-absorption of P2HEB (λ_{max} = 333 nm) is seen in other polymers containing aromaticity for example poly(4-(2-thiophenyl)styrene) or poly(5- hexyl-5"-(4-vinylphenyl)-2,2':5',2'-terthiophene).[198]

The optical transparency and the UV-absorbing properties of the diblock copolymer **1** and the triblock copolymer **2** show potential as a sustainable alternative in packaging applications. The good transparency suggests no macro-phase separation larger than the studied wavelength of light.[199] This may typically be seen with nanofillers (due to difficulty in nanocomposite processing) or polymer blends (due to incompatibility of blending).[150,200]

4.1.8 Copolymers: Morphology

Scanning electron microscopy (SEM) was used to investigated the extent of macro-phase or micro-phase separation, as a result of self-assembly, in the diblock copolymer **1** and the triblock copolymer **2**.[201]

SEM works by focusing an electron beam on the sample to emit photon and

electron signals, where each emitted signal provides unique information about the sample. X-ray and Auger electrons (emission of a core electron causing an electron from a higher energy level to fall into the core shell) aid in determining areas of contrasting chemical composition; primary backscattered electrons (electrons originating from the beam reflected back) give information on the average atomic number of the area studied; and secondary electrons (emissions of electrons from the sample) provide topographical information.[202]

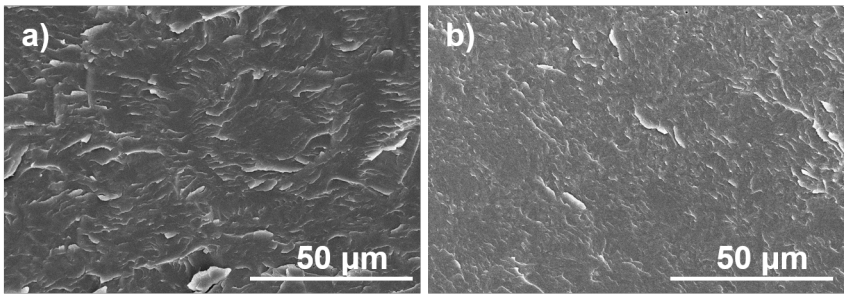

Figure 4.34: SEM images of the cryogenically fractured diblock copolymer **1** and triblock copolymer **2**.

The diblock copolymer **1** and the triblock copolymer **2** display no macro-phase separation, as evident by the single phase analysed (Figure 4.34). This is attributed to the strong interaction between the PLLA and P2HEB blocks.

The formation of lamellar, cylindrical and spherical morphologies on a micro-scale for copolymers is well known and leads to micro-phase separation.[201] Atomic force microscopy (AFM) was used to investigate the presence of micro-phase separation.

AFM uses a cantilever, tip and detector to determine the morphology of a sample. AFM has three modes of function; contact mode, where the tip is in constant contact with the sample surface; tapping mode, where the tip is in contact with the sample surface at set intervals; and non-contact mode where the tip and sample do not touch. The interaction between the tip, attached directly to the cantilever, and the sample causes atomic scale vibrations and motions that are detected in the cantilever on a macro-scale. The movement of the cantilever is detected by the detector and manipulated into an image.[203]

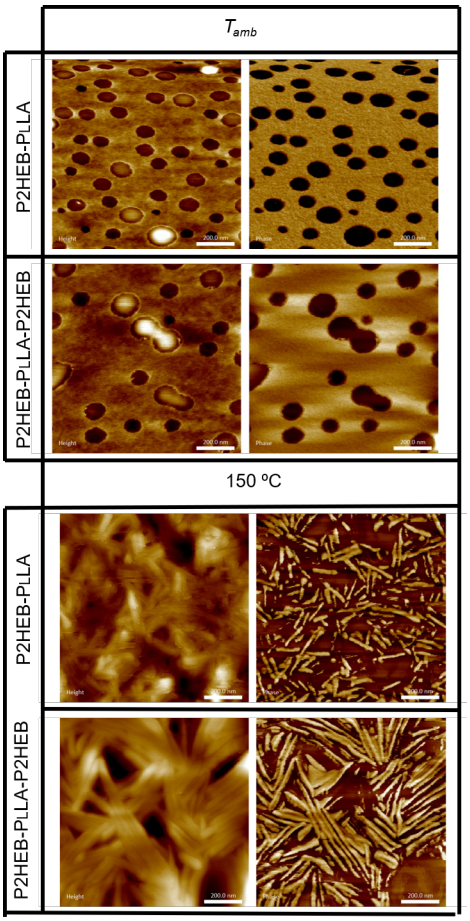

Figure 4.35: AFM height (left image in each box) and phase images (right image in each box) of the diblock copolymer **1** and triblock copolymer **2** at room temperature and 150 °C. Each scale bar represents 200 nm.

In this work, tapping mode AFM was used to better investigate the extent of micro-phase separation. The analysis was also done at two different temperatures to study the effect of temperature on the phase separation (Figure 4.35). It can be seen that at room temperature both the diblock copolymer **1** and the triblock copolymer **2** display characteristic micro-phase separation with domain sizes between 40 to 200 nm.[204] The AFM height images (left image in each box) correspond to mountains (bright) and valleys (dark) in the sample, whereas the AFM phase images (right image in each box) correspond to the hard phase material (bright regions) in the sample.[205]

The AFM phase image at room temperature showed the continuous hard phase (bright) surrounded by soft segments (dark). The hard phase is attributed to the

PLLA block, whereas the soft segments are attributed to the P2HEB block due to its lower modulus at room temperature.

Upon increase in temperature to 150 °C, the formation of well-defined lamellae (15 nm thick) were observed in both the diblock copolymer **1** and the triblock copolymer **2**. These lamellae are due to the recrystallisation of the PLLA block and are surrounded by dark regions of amorphous P2HEB. The formation of a new crystalline domain is supported by the exothermic T_{cc} peak observed during DSC (Figure 4.26).

4.1.9 Blends: Thermal Analysis

Blends: Differential Scanning Caliometry

In addition to copolymers of P2HEB and PLLA, polymers **1** to **4** and P2HEB were processed into films with a 50 % by weight composition of PLLA to afford blends. The PLLA/P2HEB blends were studied in a range of compositions in addition to the 50/50 to determine the effect of the composition on the thermal transitions.

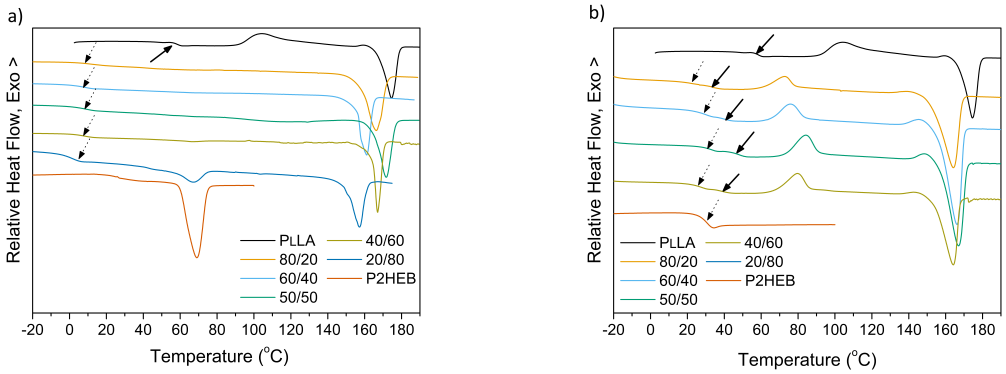

Figure 4.36: a) First and b) second heating scans of the PLLA/P2HEB blends of different composition at a heating rate of 10 °C min^{-1}.

Upon heating the PLLA/P2HEB blends, two endothermic events were observed in the DSC trace corresponding to the T_g of P2HEB (between 0 °C and 9.2 °C) and the T_m (between 157.2 °C and 174.5 °C) of PLLA (Figure 4.36). The absence of a T_g for PLLA suggested high crystallinity of the PLLA fraction, possibly due to the introduction of P2HEB acting as a nucleating agent, and the absence of a T_m for

P2HEB could be due to the overlapping T_{cc} of PLLA or the decrease in crystallinity of the P2HEB fraction upon blending.

The second heating scan exhibited two distinctive T_g's corresponding to the P2HEB and PLLA fractions in addition to the T_m for PLLA (with a similar range to the first heating scan). An exothermic event was also observed corresponding to the T_{cc} of the PLLA fraction between 72.1 °C and 84.3 °C. The presence of two well-defined T_g's suggested the immiscibility of the blends.[206–209] The T_g for P2HEB were significantly higher than that of the first heating scan between 25.1 °C and 31.7 °C, close to that of neat P2HEB (26.5 °C). The T_g for PLLA however were significantly lower than that of neat PLLA (T_g = 59.6 °C), ranging from 32.9 °C to 46.7 °C. The decrease in the T_g and T_m observed for PLLA suggest that although P2HEB may act as a nucleating agent, it could also prevent the formation of lamellae structures of PLLA.[149,180,210,211]

Small differences in the thermal transitions of the blends between compositions was observed and therefore polymers **1** to **4** were blended with a 50/50 composition (Figure 4.37).

Upon blending polymer **1** with PLLA, a well-defined double T_g was observed, close to the T_g values of the neat polymers, at 44.4 °C, for the polymer **1** fraction, and 54.9 °C for the PLLA fraction. A T_m was not observed for polymer **1** in the first heating scan, possibly due to the overlapping T_{cc} for PLLA at 125.5 °C, however a T_m at 151.8 °C was observed for PLLA. The second heating scan showed a similar trace with a T_g at 49.5 °C, for the polymer **1** fraction, and 56.1 °C for the PLLA fraction. A single T_{cc} and T_m was also observed for PLLA at 96.1 °C and 152.8 °C respectively. The DSC traces of the polymer **1**/PLLA blend, similar to P2HEB, indicated an immiscible system.

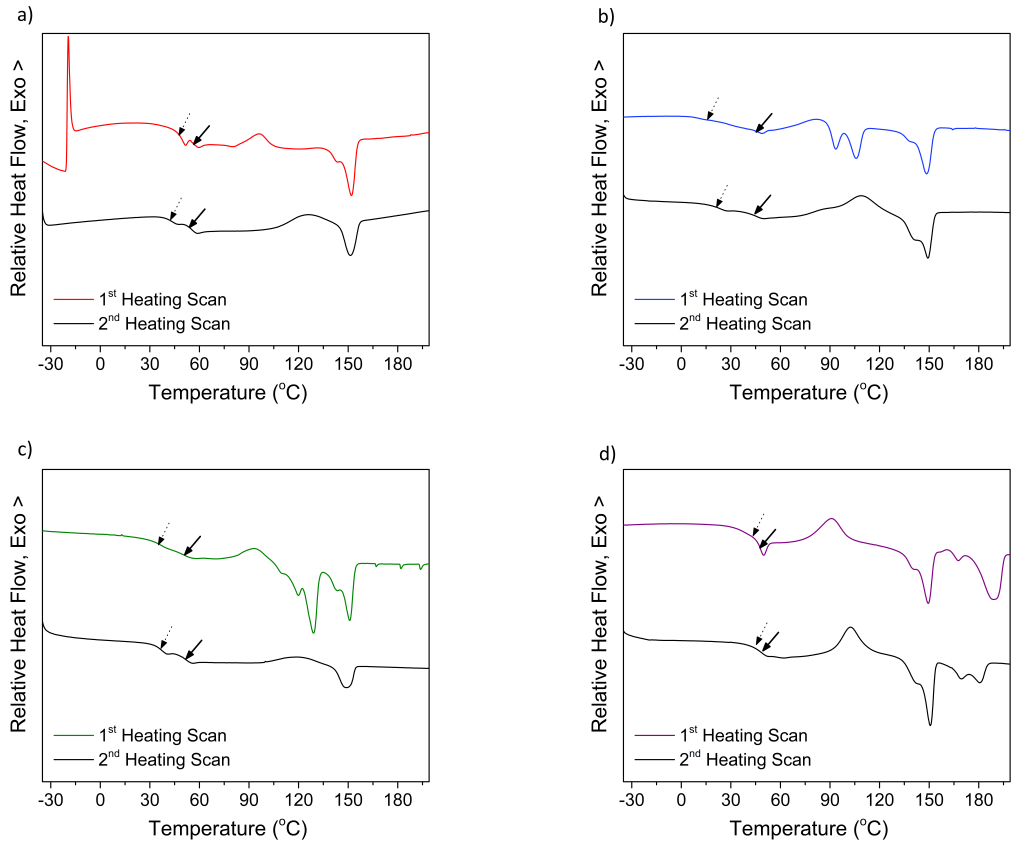

Figure 4.37: DSC traces of PLLA blended with a) polymer **1**, b) polymer **2**, c) polymer **3** and d) polymer **4**

Immiscibility was also was observed for polymer **2**/PLLA, where the first heating scan showed a well-defined double T_g at 22.2 °C, for the polymer **2** fraction, and 44.1 °C for the PLLA fraction. In addition, a T_{cc} and T_m was also observed for PLLA at 109.8 °C and 147.9 °C respectively. The second heating scan, in addition to the T_m for PLLA at 148.7 °C and a T_g at 24.2 °C, for the polymer **2** fraction, and 42.1 °C for the PLLA fraction, displayed a T_m at 93.8 °C and 106.3 °C for polymer **2**. The double melting curve could be due to the overlap of the T_{cc} for PLLA.

For polymers **1** and **2** the T_g values in the first heating scan were distinctively different indicating immiscibility and no interaction with the PLLA counterparts. However, this was not the case for polymers **3** and **4**, where the close proximities of the T_g values indicated a degree of interaction. Upon heating above the T_m of polymer **3** and **4** and cooling and applying a second heating scan, it can be observed that the blend of PLLA with polymer **3** showed a well-defined double T_g at 36.7

°C, for the polymer **3** fraction, and 50.5 °C for the PLLA fraction. However, with polymer **4** the T_g's were again very similar to one another. The second heating scan of the polymer **3**/PLLA blend showed a T_m for the polymer **3** fraction at 129.7 °C, similar to the observation for the polymer**2**/PLLA blend. The polymer **4**/PLLA blend however displayed a T_m for the polymer **4** fraction in both the first and second heating scans at 189.9 °C and 175.6 °C respectively, suggesting the introduction of PLLA did not affect the crystallinity of the polymer **4** fraction upon blending.

The differences in the values of the thermal transitions and the energies of all the blends respective to their neat polymers indicated that blending had an effect on the thermal transitions of the individual polymers (Table 4.6. The extent of immiscibility was investigated futher with SEM, later discussed.

Table 4.6: Main thermal transition temperatures of PLLA blended polymers **1** to **4** and P2HEB.

	Polymer			**PLLA**			
	1st Scan	**2nd Scan**		**1st Scan**		**2nd Scan**	
	ΔH_m (Jg^{-1})	**ΔH_m (Jg^{-1})**	**ΔH_{cc} (Jg^{-1})**	**ΔH_m (Jg^{-1})**	**ΔH_{cc} (Jg^{-1})**	**ΔH_m (Jg^{-1})**	**ΔH_{cc} (Jg^{-1})**
Polymer 1:PLLA	-	-	-	8.9	-4	5.9	-6.5
Polymer 2:PLLA	1st Peak=2.3,						
2nd Peak=3.9	-	-	8.3	-4.2	9.2	-5.2	
Polymer 3:PLLA	1st Peak=0.2,						
2nd Peak=8.1	-	-	9.1	-8.2	4.8	-4.5	
Polymer 4:PLLA	12.5	1st Peak=0.91,					
2nd Peak=0.71	-	10.4	-9.9	12	-8.9		
PLLA	-	-	-	6.3	-	0.3	-

Blends: Thermogravimetric Analysis

Thermogravimetric traces and weight loss rates of the P2HEB/PLLA blends indicated a two-step degradation process, denoted by the broader full width at half maximum of the blends in comparison to the neat polymers (Figure 4.38). A similar two-step degradation is observed for PLLA blends with polymers **1** to **4**, indicating a more complex degradation mechanism when both polymers are blended (Figure 4.39).

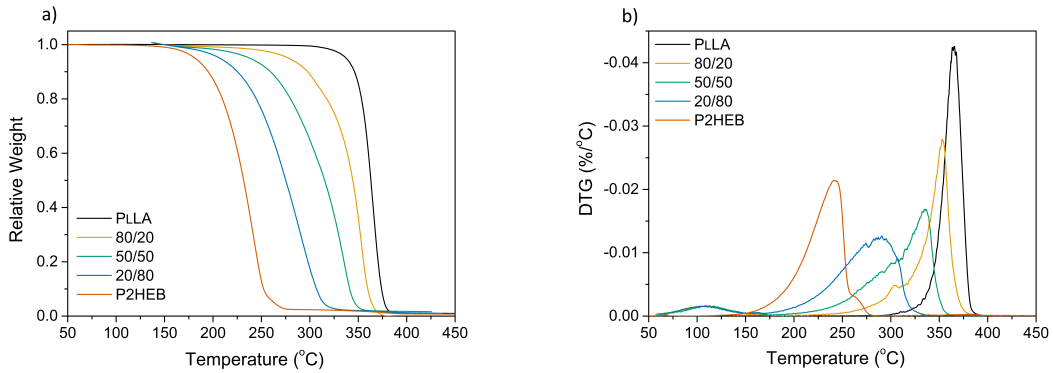

Figure 4.38: a) Thermogravimetric and b) first derivative traces of the PLLA/P2HEB blends of different compositions at a heating rate of 10 °C min^{-1}.

The thermal stability of the P2HEB/PLLA blends, as predicted, decrease with increasing amount of P2HEB. PLLA blends with polymers **1** to **3** show lower stability than the 50/50 blend with P2HEB, whereas PLLA/polymer **4** demonstrates a higher thermal stability (Table 4.7 and Table 4.8).

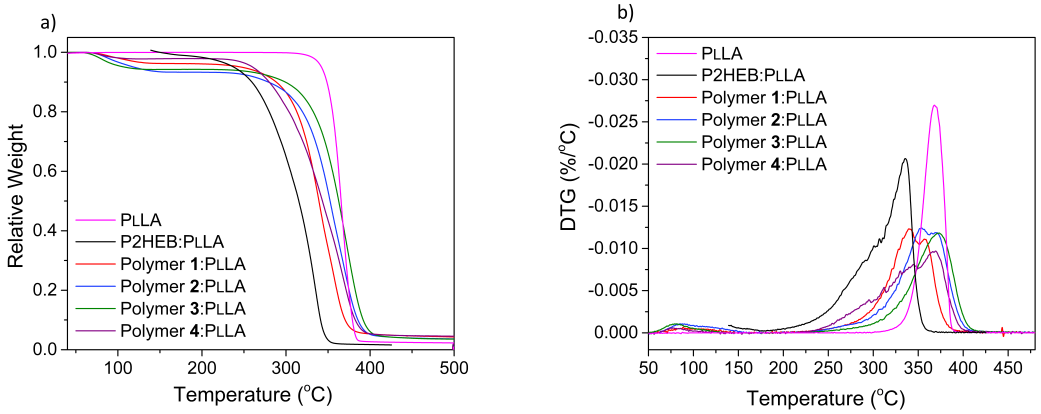

Figure 4.39: a) Thermogravimetric and b) first derivative traces of the PLLA blended with polymers **1** to **4**.

The introduction of polymer **1** to **4** and P2HEB into PLLA dramatically decreases the thermal stability of the blends, leading to a narrower processing window and therefore careful attention needs to be paid during processing of these materials.

Table 4.7: Main thermodegradation parameters for PLLA/P2HEB blends of compositions at a heating rate of 10 °C min^{-1}.

PLLA/P2HEB Blend	$T_{5\%}$ (°C)	T_{peak} (°C)	DTG_{max}
PLLA	332.7	365.7	-0.0421
80/20	266.1	353.7	-0.0277
50/50	222.9	335.5	-0.0167
20/80	196.9	288.9	-0.0122
P2HEB	174.2	241.8	-0.0212

Table 4.8: Main thermodegradation parameters for polymers **1** to **4** blended with a 50 % by weight composition of PLLA at a heating rate of 10 °C min^{-1}.

Polymer:PLLA Blend	$T_{5\%}$ (°C)	T_{peak} (°C)	DTG_{max}
PLLA	340.6	369.1	-0.0268
P2HEB:PLLA	227.9	336.2	-0.0206
1:PLLA	184.8	340.2	-0.0122
2:PLLA	102.6	364.22	-0.0122
3:PLLA	86.8	370.7	-0.0114
4:PLLA	252.5	369.1	-0.009

4.1.10 Blends: Dynamic Mechanical Analysis

As with the copolymers and P2HEB the linear viscoelastic region of the blends were determined, where the optimum percentage strain before dramatic dropping of the storage modulus was observed at 0.4 % (Figure 4.40).

The DMA of the PLLA/P2HEB blends were performed under tensile mode, whereas the PLLA blends with polymers **1** to **4** were done under shear mode (rotation of the polymer film under stress). The PLLA/P2HEB 50/50 blend was also repeated in shear mode for comparison (Figure 4.41).

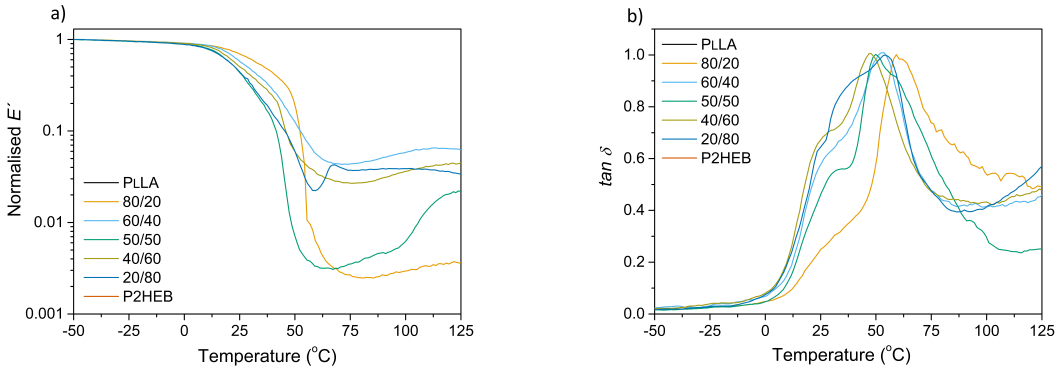

Figure 4.40: a) DMA of the PLLA/P2HEB blends of different composition and b) their respective tan δ traces.

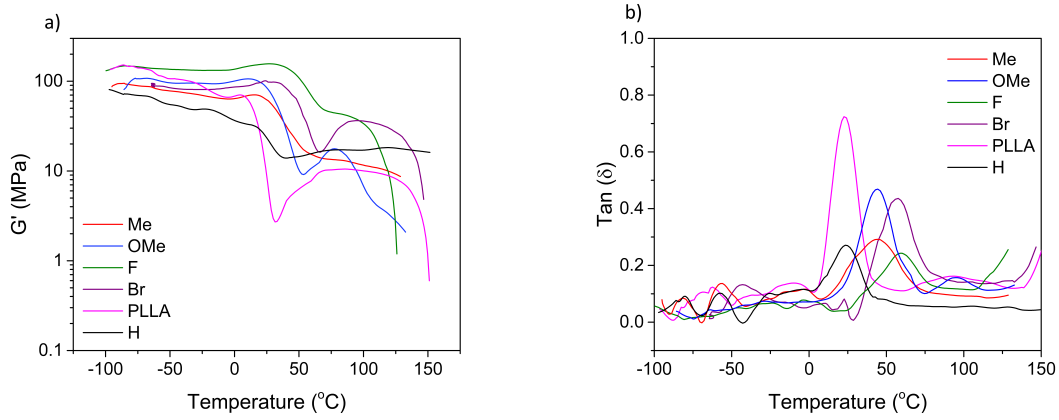

Figure 4.41: a) DMA of PLLA blended with polymers **1** to **4** and b) their respective tan δ traces.

The PLLA/P2HEB blends displayed a similar storage modulus to that of neat PLLA below their respective T_g's. Increasing the temperature to approximately 28 °C led to a decrease in storage modulus, denoted by the increase in tan δ. Further increase in temperature around 62 °C resulted in a larger tan δ and a lower storage modulus. The temperatures in which these α relaxation processes occurred corresponded to the T_g of the P2HEB and PLLA fractions. Introduction of P2HEB increased the percentage strain at break of the PLLA fraction, however the presence of two α relaxation processes, instead of the one observed for the copolymers and P2HEB, confirms the immiscibility of the blends (Figure 4.40).

The PLLA blends with polymers **2** and **4**, showed the storage modulus dropped

at 25 °C and 35 °C respectively. At approximately 50 °C and 60 °C the storage modulus increased, attributed to the crystallisation of the PLLA fraction, after which a rubbery plateau is observed until a final drop upon melting of the blends. The rubbery plateau is denoted by the material being more viscoelastic with a high tan δ and a low storage modulus. The rubbery plateau is also observed in polymers **1**, **3** and P2HEB with the absence of an increase in the storage modulus prior to it.

In the shear mode the presence of two α relaxation processes is less evident however a notable increase in the full width at half maximum is observed indicating immiscibility of the blends.

The differences in the overall storage modulus of the blends were insignificant with PLLA/polymer **3** having the largest storage modulus (153.4 MPa). This suggests that blending PLLA with polymers **1** to **4** and P2HEB have no detrimental impact on the thermal or mechanical stability of PLLA whilst increasing the percentage strain at break of PLLA.

4.1.11 Blends: Optical Properties

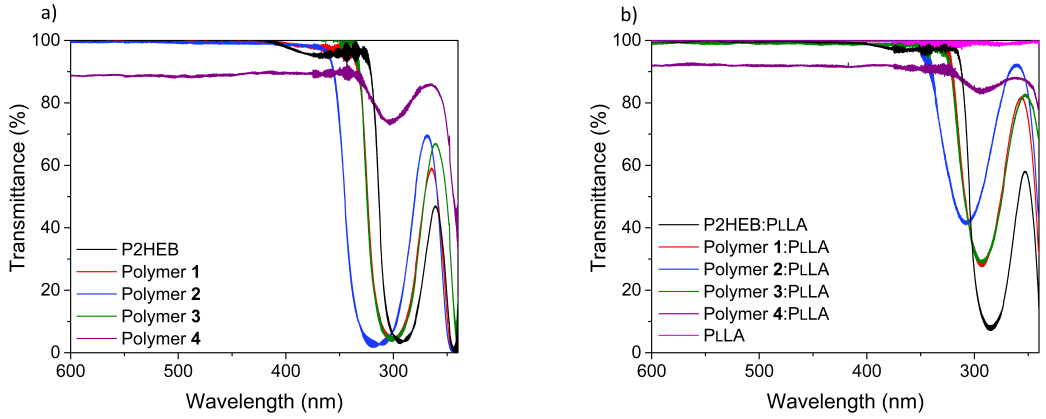

Figure 4.42: UV-Vis transmittance spectra of a) polymers **1** to **4** and P2HEB and b) their respective blends with PLLA.

The optical transparency of the homopolymers were investigated and showed, similar to the copolymers, that polymers **1** to **4** and P2HEB had more than 98 % UV-A and UV-B absorbing properties with optical transparency of 100 % (Figure 4.42 a).

Upon blending PLLA with polymers **1** to **4** and P2HEB it was evident that there was insignificant change in the transmittance values compared to that of the individual polymers (still being 100 %). The UV-A and UV-B absorbing properties of the blends however were reduced with the highest being the PLLA/P2HEB blend at 95 %, followed by PLLA blends with polymers **1** and **3** at 70 % and polymer **2** at 58 % (Figure 4.42 b).

The exception in both cases was polymer **4** which only had an optical transparency of 88 % and UV-A and UV-B absorbing properties of 25%. The optical transparency increased slightly when blended with PLLA to 92 %, however the UV-A and UV-B absorbing properties decreased to 15 %.

This application of the blends are very similar to that of the copolymers, where the strong UV absorbing properties of the aromatic-aliphatic polyesters with the optical transparency of PLLA allows for packaging applications.

4.1.12 Blends: Morphology

SEM was used to investigate the extent of macro-phase or micro-phase separation in PLLA blended with P2HEB and polymers **1** to **4**. As the immiscibility of the blends was suggested by DSC and DMA, the blends were not analysed by AFM.

The PLLA/P2HEB blends of different composition exhibited macro-phase separation with the continuous phase being PLLA and the circular regions being P2HEB (Figure 4.43). The macro-phase separation was unaffected by the introduction of a compatibiliser, in the form of the diblock copolymer **1**. Aggregates of approximately 5-12 μm were observed with the largest being the 80/20 composition of PLLA/P2HEB. This has been previously seen in other PLA based immiscible blends such as poly(*N*-isopropylacrylamide),[212] poly[(butylene succinate)-co-adipate],[213] PCL,[214] or poly(ethylene-co-vinyl acetate).[215]

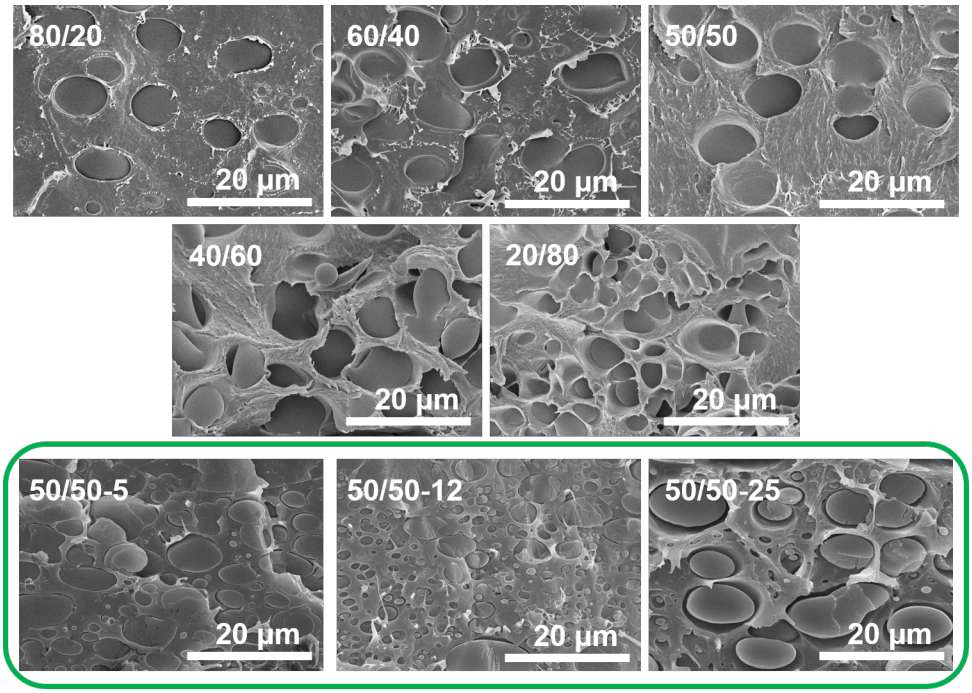

Figure 4.43: SEM images of the cryogenically fractured PLLA/P2HEB blends at 80/20, 50/50 and 20/80 composition. Images in the green box show the morphology of 50/50 blends having 5, 12.5 and 25 % by weight of the diblock copolymer **1** as a compatibiliser.

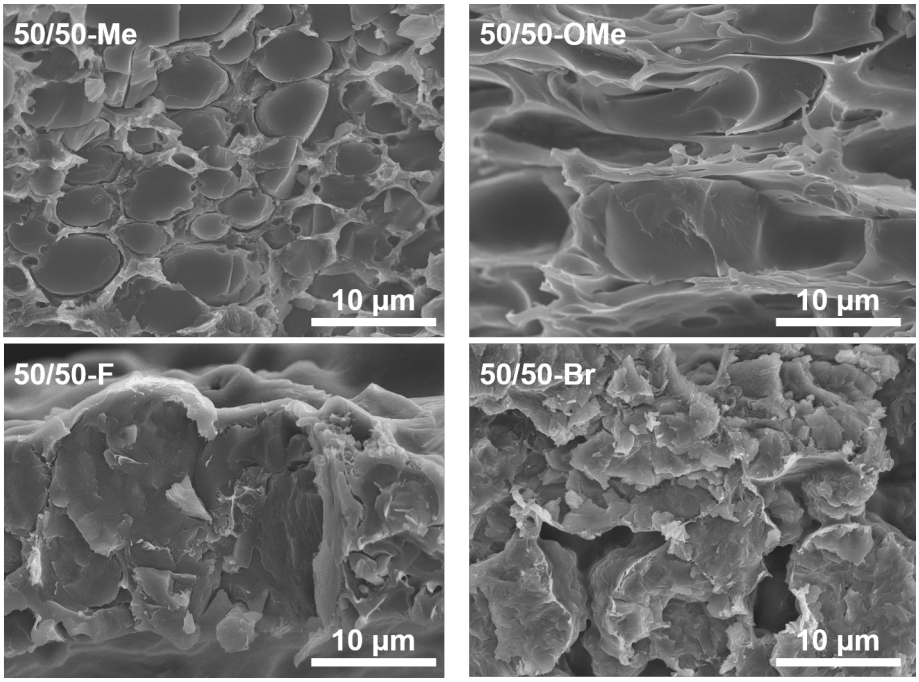

Figure 4.44: SEM images of the cryogenically fractured PLLA blends of polymers **1** to **4**.

Similar morphology was observed for PLLA blends with polymer **1** and **2** with aggregates of approximately 2-6 μm and 3-18 μm respectively. However, polymers **3** and **4** exhibited a degree of interaction with no clear macro-phase separation (Figure 4.44). This is supported by the close proximity of T_g values observed by DSC. The presence of more than one phase confirmed immiscibility of the blends.

Chapter 5

Conclusion and Future Work

This work has demonstrated the potential to afford a "closed loop" system with tunable thermal and mechanical properties to replace commodity plastics.

meta-Substituted benzodioxepinone derivatives, varying in electronic properties, were successfully synthesised and subjected to ROP along with the unsubstituted benzodioxepinone, 2,3-DHB, to afford a series of novel aromatic-aliphatic polyesters. An aluminium salen catalyst and the organocatalyst TBD were used to screen for optimal polymerisation conditions. ROP with TBD was poorly controlled due to transesterification, whereas the aluminum salen catalyst produced well controlled polymerisations, albeit with low monomer to polymer conversions. Probing the system further gave insight into the monomer-polymer equilibrium, demonstrating the importance of solubility and concentration in the position of the equilibrium.

The electronic effects of the *meta*-substituent (denoted by their electronic substituent parameter) on the rate of polymerisation and depolymerisation were investigated. The fastest rate of polymerisation was demonstrated by monomer **3** and the slowest by monomer **1**. Monomer **2** was predicted to have a faster rate of polymerisation than 2,3-DHB due to the larger electronic substituent parameter (more electron withdrawing), however upon further investigation it was found that the polymerisation was being limited due to the presence of a methoxy oxygen coordinating to aluminum salen.

The depolymerisation was carried out at 70 °C and 110 °C due to the poor

solubility of polymer **4**. The studies showed depolymerisation to occur in the first 10 minutes with polymer **3** achieving 100 % depolymerisation selectively back to its cyclic monomer.

It was clear that electronic effects of the *meta*-substituent influenced the polymerisation and depolymerisation behaviour, however solubility was a key limiting factor. A balance between solubility and electronics was achieved with monomer **3** and polymer **3** where a novel aromatic-aliphatic polyester with the ability to degrade in a "closed loop" fashion was synthesised. The electronic effects of the *meta*-substituent on the thermal properties of the resultant polyesters was also investigated through DSC and TGA.

P2HEB, of molecular weight 11,000 g mol^{-1}, displayed similar thermal transitions to that of poly(ethylene phthalate) (T_g's of 38.2 °C) with a T_g at 26.5 °C and a T_m at 60.8 °C. Increasing the molecular weight of P2HEB to 80,000 g mol^{-1} increased the T_g to 38.7 °C and the T_m to 77.2 °C. The second DSC heating scans of P2HEB displayed only a T_g demonstrating poor crystallisation ability, which was more prominent at higher molecular weights.

Polymers **1**, **2** and **3** also showed poor crystallisation ability with T_g's of 42.5 °C, 29.7 °C and 39.4 °C and T_m's of 65.8 °C, 108.5 °C and 130.6 °C respectively. Polymer **4** exhibited a T_{cc} at 136.4 °C, indicating crystallisation in the polymer matrix. Polymer **4**, with the largest electronic substituent parameter, had the highest T_g at 60.7 °C and T_m at 182.6 °C.

An increase in the electronic substituent parameter led to an increase in melting points and activation energies (calculated through the Kissinger equation using their thermal stability from TGA), with polymer **4** showing a glass transition close to that of PET (T_g's of 69 °C).

The crystallinity of the aromatic-aliphatic polyesters were investigated through WAXD. Polymers **1** to **4** and P2HEB displayed a tetragonal symmetry with varying unit cell parameters according to the size of the *meta*-substituent. Polymers **1** to **3** and P2HEB displayed characteristic π-π stacking, with polymer **1** and **3** having more than one unit cell parameter. Polymer **4**, on the other hand, displayed no long

range or short range order. The stability of the crystalline domains, probed via high temperature WAXD, were in agreement with the melting points observed by DSC.

P2HEB was copolymerised with PLLA in the attempt to tune the thermal and mechanical properties of PLLA and increase its application range. A P2HEB-PLLA diblock copolymer **1** and a P2HEB-PLLA-P2HEB triblock copolymer **2** were successfully synthesised through sequential ROP of L-lactide and 2,3-DHB using mono- and bi-functional initiators.

The incorporation of P2HEB into PLLA decreased the T_g from 55 °C to 42.3 °C for the diblock copolymer **1** and to 41.9 °C for the triblock copolymer **2**. The crystallisation ability and thermal stability of PLLA also decreased. However, no effect was observed in the crystallinity of PLLA, with WAXD showing only lattice planes corresponding to PLLA and AFM revealing nano-phase separation of the copolymers.

The effect of P2HEB on the mechanical properties of PLLA was investigated using DMA. Neat P2HEB displayed a storage modulus of 1050 MPa and a glassy rigid behaviour below its T_g. The storage modulus increased upon copolymerisation with PLLA to 1178 MPa for the diblock copolymer **1** and to 1087 MPa for the triblock copolymer **2**. The incorporation of P2HEB led to an increase in the strain at break of the copolymer compared to neat PLLA thus showing the potential to improve the brittleness of PLLA.

The use of PLLA in food packaging is limited due to the absence of UV-vis absorption. Introduction of P2HEB led to almost 100 % UV-A and UV-B absorbance with 75 % optical transparency.

To ensure PLLA was still biodegradable, the copolymers were tested via enzymatic and catalytic degradation. The copolymers exhibited slower degradation compared to that of their respective homopolymers due to the competing transesterification of the PLLA blocks.

PLLA was also blended with polymers **1** to **4** and P2HEB. However, the blends displayed macro-phase separation with SEM, indicating immiscibility. This was confirmed with DSC and TGA with two T_g's and a two-step degradation process.

The advantages of copolymerisation over blending for tuning thermal and mechanical properties of polymers was highlighted with the potential to exploit the characteristic thermal, mechanical and depolymerisation behaviours of P2HEB.

Polymerisation and thermal behaviour of these novel semi-crystalline aromatic-aliphatic polyesters can be tuned through manipulation of the electronic substituent parameter of the *meta*-substituent whilst maintaining a "closed loop" with selective degradation to their cyclic monomers. The characteristic thermal properties and selective depolymerisation of synthesised polyesters give them the potential to be functionalised further, in addition to copolymerisation, thus expanding the scope of monomers and polymers available to replace commodity plastics.

5.1 Future Work

The characteristic thermal properties and selective depolymerisation of synthesised novel aromatic-aliphatic polyesters give them the potential to be functionalised further, thus expanding the scope of monomers and polymers available to replace commodity plastics.

The ROP of monomers **1** to **4** can be further manipulated to achieve block copolymers with PLLA. The block copolymers have the potential to exhibit interesting and complex morphologies due to the poor solubilities of polymers **1** to **4** in organic solvents. The ROP of the second block, being insoluble in the solvent, results in the formation of a block copolymer that has the ability to self-assemble. This is known as polymerisation-induced self-assembly (PISA) and can lead to various morphologies such as spheres, rods, fibers and vesicles depending on the length of the second block.

In addition to PISA, higher molecular weights of polymers **1** to **4** could be targeted through further optimisation of polymerisation conditions to be able to directly measure the storage modulus of the homopolymers, similar to the studies done on P2HEB.

Through copolymerisation and tuning of the kinetics, these novel aromatic-aliphatic polyesters show great promise in applications ranging from packaging to

self-assembled vesicles for biomedical applications.

Chapter 6

Experimental

6.1 General considerations and materials

ROP of the cyclic monomers was carried out under a nitrogen atmosphere in a Vigor glovebox equipped with a -35 °C freezer and [H_2O] and [O_2] detectors. Dispersities were determined using GPC in THF at a flow rate of 1 mL min^{-1} at 35 °C on a Malvern Instruments Viscotek 270 GPC Max triple detection system with 2 x mixed bed styrene/DVB columns (300 × 7.5 mm). Molecular weights were also determined by ^{1}H NMR spectroscopy by integration of polymer vs initiator resonances on a Bruker Asance 500 MHz spectrometer. Benzyl alcohol (BnOH) and 1,3-propanediol, in addition to DMF, were dried for 24 hours under reflux with calcium hydride and distilled, or filtered in the case of DMF, under an inert atmosphere. Toluene, THF and DMF were collected from an Innovative Technologies solvent purification system consisting of columns of alumina and copper catalysts. Toluene, THF, BnOH and 1,3-propanediol were degassed via three freeze-pump-thaw cycles prior to use. 2,3-DHB was recrystallised three times from ethyl acetate: hexanes (50:50) prior to it being dried under vacuum and sublimed at 60 °C for 18 hours.[113]

6.2 MeAl[salen]

6.2.1 Synthesis of 2,4-di-tert-butylsalicylaldehyde

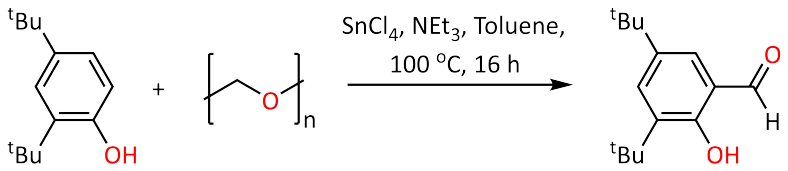

$SnCl_4$ (5.20 g, 19.97 mmol) was dissolved in toluene (342 mL) in a Schlenk flask and transferred to another Schlenk flask with predried 2,4-ditert-butylphenol (41.23 g, 0.20 mol) via a canula. NEt_3 (11.15 mL) was added dropwise via a canula needle under nitrogen and the reaction was left to stir for one hour at room temperature. Paraformaldehyde (19.82 g, 0.66 mol) was rapidly added to the reaction and was heated to 100 °C and left to stir for 16 hours. The solution was cooled to room temperature and diluted with distilled water (500 mL). The solution was adjusted to pH 2 via conc. HCl and extracted three times with diethyl ether. The combined organic extracts were dried over $MgSO_4$ and filtered. The solvent was removed under vacuum to yield 39.76 g (96.4 %) of a yellow solid. ^{1}H NMR (500 MHz, $CDCl_3$) δ 9.88 (s, 1H, $HOC_6H_2[C(CH_3)_3]_2C\mathbf{H}O$), 7.62 (d, 1H, $HOC_6\mathbf{H}_2[C(CH_3)_3]_2CHO$), 7.36 (d, 1H, $HOC_6\mathbf{H}_2[C(CH_3)_3]_2CHO$), 1.45 (s, 9H, $HOC_6H_2[C(\mathbf{H}_3)_3]_2CHO$), 1.35 (s, 9H, $HOC_6H_2[C(C\mathbf{H}_3)_3]_2CHO$).

6.2.2 Synthesis of salen

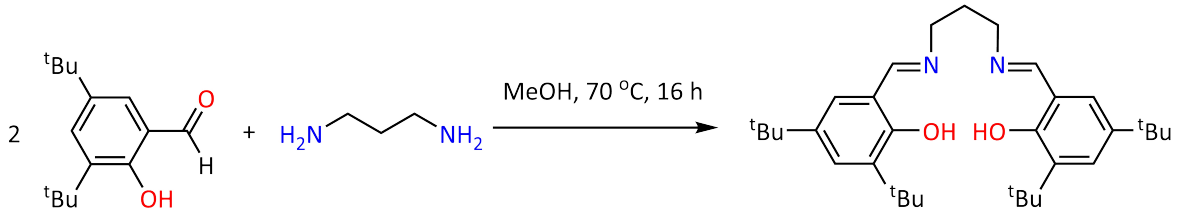

2,4-ditert-butylsalicylaldehyde (21.47 g, 0.1 mol) was dissolved in methanol (600 mL) to which 1,3-diaminopropane (3.83 mL, 0.046 mol) was added dropwise. The reaction was stirred for three hours under reflux at 70 °C prior to stirring at room temperature for 16 hours. The precipitate was filtered and dried to yield

20.3 g (87.1 %) of a yellow solid. ^{1}H NMR (500 MHz, $CDCl_3$) δ 8.39 (d, 2H, $HOC_6H_2[C(CH_3)_3]_2C\mathbf{H}_2N(CH_2)_3N$), 7.39 (d, 2H, $HOC_6\mathbf{H}_2[C(CH_3)_3]_2CH_2N(CH_2)_3N$), 7.09 (d, 2H, $HOC_6\mathbf{H}_2[C(CH_3)_3]_2$ $CH_2N(CH_2)_3N$), 3.71 (td, 1.2 Hz, 2H, $HOC_6H_2[C(CH_3)_3]_2$ $CH_2N(C\mathbf{H}_2)_3N$), 2.13 (m, $HOC_6H_2[C(CH_3)_3]_2$ CH_2 $N(C\mathbf{H}_2)_3N$), 1.46 (s, 2H, HOC_6H_2 $[C(C\mathbf{H}_3)_3]_2CH_2N(CH_2)_3N$), 1.31 (s, 2H, $HOC_6H_2[C(C\mathbf{H}_3)_3]_2CH_2N(CH_2)_3N$). ^{13}C NMR (126 MHz, $CDCl_3$) δ 166.48 ($HOC_6H_2[C(CH_3)_3]_2\mathbf{C}H_2N(CH_2)_3N$), 158.1 ($HO\mathbf{C}_6H_2$ $[C(CH_3)_3]_2CH_2N(CH_2)_3N$), 140.05 ($HO\mathbf{C}_6H_2[C(CH_3)_3]_2CH_2N(CH_2)_3N$), 136.70 ($HO\mathbf{C}_6H_2$ $[C(CH_3)_3]_2CH_2N(CH_2)_3N$), 126.89 ($HO\mathbf{C}_6H_2[C(CH_3)_3]_2CH_2N(CH_2)_3N$), 125.84 ($HO\mathbf{C}_6H_2$ $[C(CH_3)_3]_2CH_2N(CH_2)_3N$), 117.86 ($HO\mathbf{C}_6H_2[C(CH_3)_3]_2CH_2N(CH_2)_3N$), 56.76 ($HOC_6H_2$ $[C(CH_3)_3]_2CH_2N(\mathbf{C}H_2)_3N$), 35.05 ($HOC_6H_2[\mathbf{C}(CH_3)_3]_2CH_2N(CH_2)_3N$), 34.14 ($HOC_6H_2$ $[\mathbf{C}(CH_3)_3]_2CH_2N(CH_2)_3N$), 31.72 ($HOC_6H_2[C(CH_3)_3]_2CH_2N(\mathbf{C}H_2)_3N$) 31.62 ($HOC_6H_2$ $[C(\mathbf{C}H_3)_3]_2CH_2N(CH_2)_3N$), 29.44 ($HOC_6H_2[C(\mathbf{C}H_3)_3]_2CH_2N(CH_2)_3N$).

6.2.3 Synthesis of MeAl[salen]

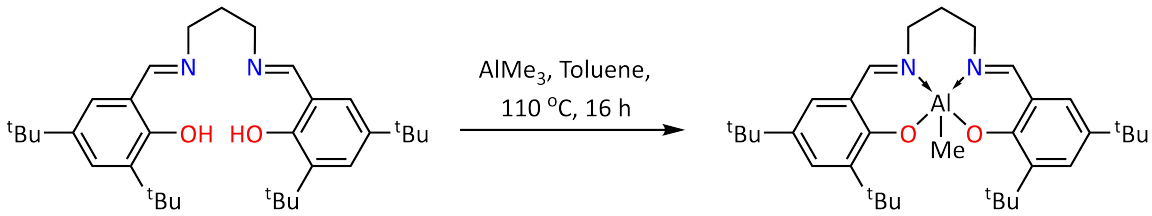

Trimethyl aluminium (7.59 mL, 15.2 mmol) was added dropwise to a Schlenk flask contaning salen (7 g, 13.8 mmol) and anhydrous toluene (0.5 mL) under nitrogen and was stirred for 16 hours at 110 °C. The reaction was concentrated under vacuum and washed three times with anhydrous hexane via a canula and canula filter. The remaining solid was dried under vacuum for four hours to yield 2.5 g (26.5 %) of a pale yellow solid. The reaction was carried out under anhydrous conditions. ^{1}H NMR (500 MHz, C_6D_6) δ 7.73 (d, 2H, $OC_6H_2[C(CH_3)_3]_2C\mathbf{H}_2N(CH_2)_3NAlCH_3$), 7.38 (s, 2H, $OC_6\mathbf{H}_2[C(CH_3)_3]_2CH_2N(CH_2)_3NAlCH_3$), 6.90 (d, 2H, $OC_6\mathbf{H}_2[C(CH_3)_3]_2CH_2$ $N(CH_2)_3NAlCH_3$), 3.06 (m, 2H, $OC_6H_2[C(C\mathbf{H}_3)_3]_2CH_2N(CH_2)_3NAlCH_3$), 2.77 (m, 2H, $OC_6H_2[C(C\mathbf{H}_3)_3]_2$ $CH_2N(CH_2)_3NAlCH_3$), 1.79 (s, 18H, $OC_6H_2[C(C\mathbf{H}_3)_3]_2$ CH_2 $N(CH_2)_3NAlCH_3$), 1.38 (s, 18H, $OC_6H_2[C(C\mathbf{H}_3)_3]_2$ $CH_2N(CH_2)_3NAlCH_3$), -0.34 ($OC_6H_2[C(CH_3)_3]_2$ $CH_2N(CH_2)_3NAlC\mathbf{H}_3$). ^{13}C NMR (126 MHz, $CDCl_3$) δ 163.88

($OC_6H_2[C(CH_3)_3]_2$ **C**H_2 $N(CH_2)_3NAlCH_3$), 140.92 (O**C**$_6H_2[C(CH_3)_3]_2$ CH_2 $N(CH_2)_3$ $NAlCH_3$), 137.15 (O**C**$_6H_2[C(CH_3)_3]_2$ CH_2 $N(CH_2)_3NAlCH_3$), 130.04 (O**C**$_6H_2[C(CH_3)_3]_2$ CH_2 $N(CH_2)_3NAlCH_3$), 126.99 (O**C**$_6H_2$ $[C(CH_3)_3]_2$ CH_2 $N(CH_2)_3NAlCH_3$), 118.71 (O**C**$_6H_2$ $[C(CH_3)_3]_2$ CH_2 $N(CH_2)_3NAlCH_3$), 54.83 (OC_6H_2 $[C(CH_3)_3]_2$ CH_2 $N($**C**$H_2)_3$ $NAlCH_3$), 35.55 ($OC_6H_2[$**C**$(CH_3)_3]_2$ CH_2 $N(CH_2)_3$ $NAlCH_3$), 33.81 ($OC_6H_2[$**C**$(CH_3)_3]_2$ CH_2 $N(CH_2)_3$ $NAlCH_3$), 31.64 ($OC_6H_2[C(CH_3)_3]_2$ CH_2 $N($**C**$H_2)_3$ $NAlCH_3$), 31.50 (OC_6H_2 $[C($**C**$H_3)_3]_2$ CH_2 $N(CH_2)_3$ $NAlCH_3$), 29.77 ($OC_6H_2[C($**C**$H_3)_3]_2$ CH_2 $N(CH_2)_3NAlCH_3$), 1.07 (OC_6H_2 $[C(CH_3)_3]_2$ CH_2 $N(CH_2)_3NAl$**C**H_3).

6.3 Synthesis of thiazolium catalyst

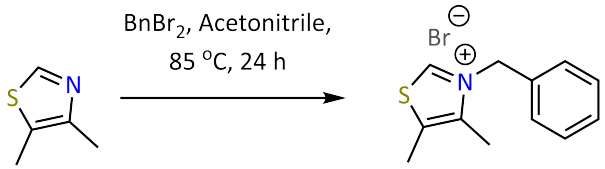

Following a modified literature procedure,[124,216] a solution of 4,5-dimethylthiazole (1.1 mL, 10 mmol) and acetonitrile (5 mL) was treated dropwise with benzylbromide (1.19 mL, 10 mmol) at room temperature. The reaction was stirred for four hours under reflux at 85 °C prior to cooling back to room temperature. The solution was allowed to crystallise in the freezer for 48 hours. The crystals were purified through recrystalliation using ethyl acetate to afford 2.4 g (84.8 %) of an off white powder. m.p = 166 °C - 168 °C, m/z = 283.00. ^{1}H NMR (500 MHz, d_6-DMSO) δ 10.10 (s, 1H, SC**H**N), 7.44 (m, 3H, Ar**H**), 7.31 (m, 2H, Ar**H**) , 5.77 (s, 2H, NC$\mathbf{H}_2$Ar), 2.49 (d, 3H, NCC$\mathbf{H}_3$), 2.31 (d, 3H, SCC$\mathbf{H}_3$). ^{13}C NMR (126 MHz, $_6$-DMSO) δ 156.27 (S**C**HN), 141.65, 133.89, 132.96, 129.20, 128.88, 127.90 (Ar), 55.85 (N**C**H_2Ar), 11.93 (NC**C**H_3), 11.22 (SC**C**H_3).

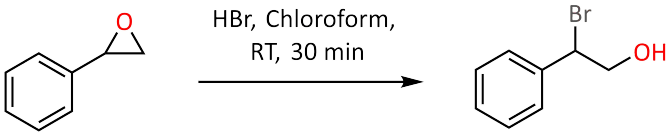

6.4 α-phenyl-β-propiolactone

6.4.1 Synthesis of 2-bromo-2-phenylethanol

Styrene oxide (1.46 mL, 0.013 mol) and hydrobromic acid (33 mL, 0.60 mol, 48 % aq. solution) were dissolved in chloroform (33 mL) and stirred for 30 minutes at room temperature. The biphasic mixture was diluted with distilled water (400 mL) and extracted three times with DCM (200 mL). The combined organic extracts were over $MgSO_4$ and filtered. The solvent was removed under vacuum to yield a yellow oil which which was purifed via column chromatography using a gradient petroleum ether and DCM eluent system followed by distillation at 110 °C to yield 0.402 g (15.6 %) of the product. ^{1}H NMR (500 MHz, $CDCl_3$) δ 7.33 (tdd, 5H, $C_6\mathbf{H}_5CHBrCH_2OH$), 5.11 - 5.05 (m, 1H, $C_6H_5C\mathbf{H}BrCH_2OH$), 4.13 - 4.03 (m, 1H, $C_6H_5CHBrC\mathbf{H}_2OH$), 4.01 - 3.93 (m, 1H, $C_6H_5CHBrC\mathbf{H}_2OH$), 2.04 (s, 1H, $C_6H_5CHBrCH_2O\mathbf{H}$). ^{13}C NMR (126 MHz, $CDCl_3$) δ 138.26 ($\mathbf{C}_6H_5CHBrCH_2OH$), 129.03 ($\mathbf{C}_6H_5CHBrCH_2OH$), 128.93 ($\mathbf{C}_6H_5CHBrCH_2OH$), 127.95 ($\mathbf{C}_6H_5CHBrCH_2OH$), 67.58 ($C_6H_5CHBr\mathbf{C}H_2OH$), 57.02 ($C_6H_5\mathbf{C}HBrCH_2OH$).

6.4.2 Synthesis of α-phenyl-β-propiolactone via a palladium catalyst

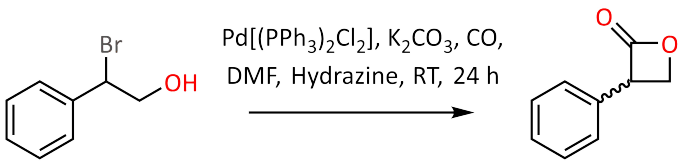

$Pd[(PPh_3)_2Cl_2]$ (23.0 mg, 0.03 mmol), 2-bromo-2-phenylethanol (402.0 mg, 2.00 mmol) and K_2CO_3 (276.4 mg, 2.00 mmol) were added to a Parr reactor and dissolved in DMF (20 mL). One drop of hydrazine was carefully added to the solution prior to filling the Parr reactor with carbon monoxide (100 bar). The reaction was stirred

for 24 hours at room temperature. The reaction was diluted with diethyl ether and extracted three times with distilled water. The combined organic layers were dried with $MgSO_4$ and filtered. The solvent was removed under vacuum to yield a dark brown oil (21.4 %). The crude was subjected to flash chromatography using dichloromethane to yield 14 mg (4.7%) of a yellow oil. ^{1}H NMR (500 MHz, $CDCl_3$) δ 7.49 - 7.39 (m, 5H, $C_6\mathbf{H}_5CHCOOCH_2$), 5.67 (t, 1H, $C_6H_5C\mathbf{H}COOCH_2$), 4.82 - 4.77 (m, 1H, $C_{6s}H_5CHCOOC\mathbf{H}_2$), 4.35 (dd, 7.8 Hz, 1H, $C_6H_5CHCOOC\mathbf{H}_2$). ^{13}C NMR (126 MHz, $CDCl_3$) δ 162.53 ($C_6H_5CH\mathbf{C}OOCH_2$), 128.58 ($\mathbf{C}_6H_5CHCOOCH_2$), 128.19 ($\mathbf{C}_6H_5CHCOOCH_2$), 125.50 ($\mathbf{C}_6H_5CHCOOCH_2$), 71.19 ($C_6H_5\mathbf{C}HCOOCH_2$), 36.47 ($C_6H_5CHCOO\mathbf{C}H_2$).

6.4.3 Synthesis of α-phenyl-β-propiolactone via a rhodium catalyst

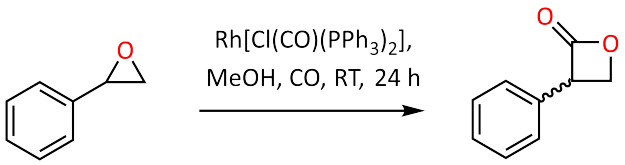

Styrene oxide (1 g, 8.33 mmol), $RhCl(CO)(PPh_3)_2$ (0.12 g 0.17 mmol), and methanol (0.56 mL) were added to a Parr reactor. The Parr reactor was filled with carbon monoxide (27 bar) and stirred for 24 hours are room temperature. Crude ^{1}H NMR spectrum showed the presence of unreacted sytrene oxide.

6.5 ROP of α-phenyl-β-propiolactone

6.5.1 ROP using MeAl[salen]

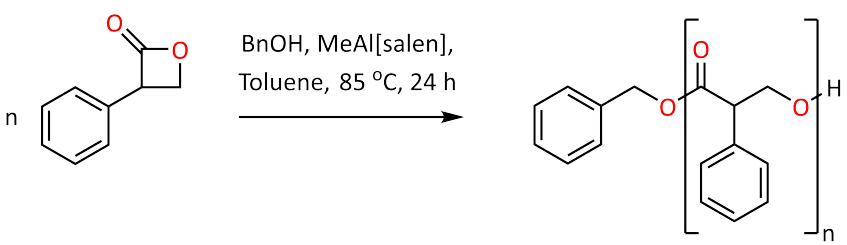

α-phenyl-β-propiolactone (14.0 mg, 0.09 mmol), BnOH (0.2 μL, 1.873 μL), and MeAl[salen] were dissolved in toluene (1 mL) in an ampoule. The reaction was stirred for 24 hours at 85 °C . Crude ^{1}H NMR spectrum showed presence of unreacted α-phenyl-β-propiolactone.

6.5.2 ROP using TBD

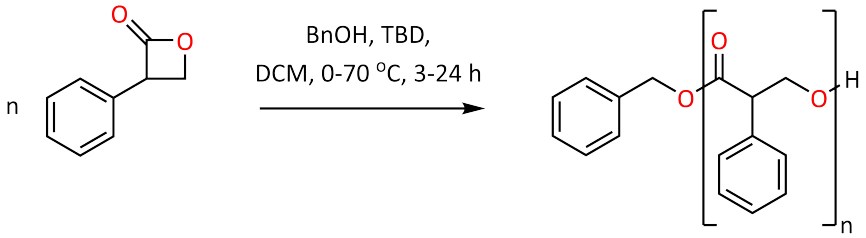

Triazabicyclodecene (TBD) (20 mg, 0.14 mmol) was dissolved in DCM (3 mL) to make a stock solution. Two sets of reactions were attempted where α-phenyl-β-propiolactone (13.0 mg, 0.09 mmol), BnOH (0.19 μL, 0.0018 mmol), and TBD (39 μL from stock solution, 0.0018 mmol) were dissolved in DCM (1 mL) in two ampoules. The first reaction was stirred for 3 hours and the second was stirred for 24 hours. Crude ^{1}H NMR spectrum showed presence of unreacted α-phenyl-β-propiolactone.

6.6 Synthesis of 2-(2-hydroxyethoxy)-5-R-benzaldehyde

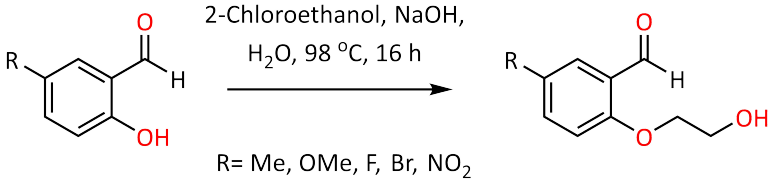

NaOH (0.4 g, 10 mmol) was dissolved in 10 mL of distilled water. The respective salicylaldehyde (10 mmol) was added to this stirring solution over a period of 15 minutes. 2-Chloroethanol (10 mmol, 0.81g) was added dropwise and the solution was heated to 98 °C. The reaction was left to stir under reflux overnight. The solvent was

removed under vacuum at 50 °C to yield a dark brown oil. 2-(2-hydroxyethoxy)-5-R-benzaldehyde was afforded through purification via column chromatography using a 5:1 petroleum ether:ethyl acetate eluent system.

6.6.1 2-(2-hydroxyethoxy)-5-methyl-benzaldehyde

: 1.27 g, 93.4 %, $R_f = 0.20$, m.p. = 52 °C - 56 °C, m/z = 180.08. ^{1}H NMR (500 MHz, $CDCl_3$) δ 10.42 (s, 1H, C**H**O), 7.62 (dd, 1H, Ar**H**), 7.35 (m, 1H Ar**H**), 6.91 (d, 1H, Ar**H**), 4.19 (m, 2H, PhOC**H**$_2$CH$_2$OH), 4.02 (q, 2H, PhOCH$_2$C**H**$_2$OH), 2.33 (d, 3H, ArC**H**$_3$). ^{13}C NMR (126 MHz, $CDCl_3$) δ 190.05 (**C**HO), 158.68, 136.72, 130.94, 129.82, 125.05, 113.35 (Ar), 70.50 (PhOC**H**$_2$CH$_2$OH), 61.45 (PhOCH$_2$**C**H$_2$OH), 20.43 (Ar**C**H$_3$).

6.6.2 2-(2-hydroxyethoxy)-5-methoxy-benzaldehyde

: 1.33g, 87.5 %, $R_f = 0.13$, m.p. = 66 °C - 70 °C, m/z = 196.07. ^{1}H NMR (500 MHz, $CDCl_3$) δ 10.43 (s, 1H, C**H**O), 7.31 (d, 1H, Ar**H**), 7.12 (dd, 1H Ar**H**), 6.97 (d, 1H, Ar**H**), 4.17 (m, 2H, PhOC**H**$_2$CH$_2$OH), 4.01 (q, 2H, PhOCH$_2$C**H**$_2$OH), 3.81 (s, 3H, ArOC**H**$_3$). ^{13}C NMR (126 MHz, $CDCl_3$) δ 189.62 (**C**HO), 155.75, 154.20, 125.63, 123.53, 115.25, 111.40 (Ar), 71.13 (PhOC**H**$_2$CH$_2$OH), 61.50 (PhOCH$_2$**C**H$_2$OH), 55.97 (ArO**C**H$_3$).

6.6.3 2-(2-hydroxyethoxy)-5-fluoro-benzaldehyde

: 1.68 g, 88.4 %, $R_f = 0.19$, m.p. = 64 °C - 68 ∘C, m/z = 184.05. ^{1}H NMR (500 MHz, $CDCl_3$) δ 10.41 (d, 1H, C**H**O), 7.49 (dd, 1H, Ar**H**), 7.25 (ddd, 1H Ar**H**), 6.98 (dd, 1H, Ar**H**), 4.19 (m, 2H, PhOC**H**$_2$CH$_2$OH), 4.02 (q, 2H, PhOCH$_2$C**H**$_2$OH). ^{13}C NMR (126 MHz, $CDCl_3$) δ 188.85 (**C**HO), 158.23, 157.36, 156.31, 126.00, 122.71, 114.90 (Ar), 71.02 (PhO**C**H$_2$CH$_2$OH), 61.31 (PhOCH$_2$**C**H$_2$OH).

6.6.4 2-(2-hydroxyethoxy)-5-bromo-benzaldehyde

: 1.78g, 88.6 %, R_f = 0.12, m.p. = 72 °C - 74 °C, m/z = 243.97. ^{1}H NMR (500 MHz, d_6-DMSO) δ 10.37 (s, 1H, C**H**O), 7.80 (dd, 1H, Ar**H**), 7.73 (d, 1H Ar**H**), 7.24 (dd, 1H, Ar**H**), 4.97 (t, 1H, PhOCH$_2$CH$_2$O**H**), 4.16 (m, 2H, PhOC**H**$_2$CH$_2$OH), 3.76 (td, 2H, PhOCH$_2$C**H**$_2$OH). ^{13}C NMR (126 MHz, d_6-DMSO) δ 188.62 (**C**HO), 160.30, 138.41, 129.41, 125.91, 116.63, 112.42 (Ar), 71.05 (PhO**C**H$_2$CH$_2$OH), 59.35 (PhOCH$_2$**C**H$_2$OH).

6.6.5 2-(2-hydroxyethoxy)-5-nitro-benzaldehyde

: 1.15g, 46.6 %, R_f = 0.07, m.p. = 77 °C - 80 °C, m/z = 211.05. ^{1}H NMR (500 MHz, $CDCl_3$) δ 10.48 (s, 1H, C**H**O), 8.16 (d, 1H, Ar**H**), 7.35 (d, 1H Ar**H**), 7.19 (dd, 1H, Ar**H**), 4.23 (m, 1H, PhOC**H**$_2$CH$_2$OH), 4.04 (m, 2H, PhOCH$_2$C**H**$_2$OH). ^{13}C NMR (126 MHz, $CDCl_3$) δ 188.80 (**C**HO), 163.51, 142.95, 134.69, 127.72, 119.46, 114.24 (Ar), 70.84 (PhO**C**H$_2$CH$_2$OH), 61.36 (PhOCH$_2$**C**H$_2$OH).

6.7 Synthesis of 2-hydroxy-4-trifluoromethyl-benzaldehyde via *ortho*-formylation

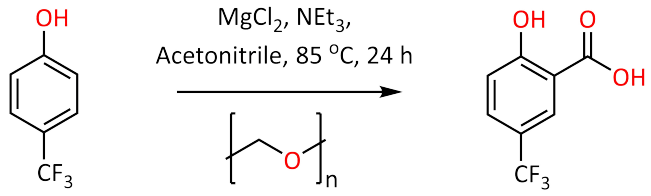

Following a modified literature procedure,[125] 4-trifluoromethylphenol (15 g, 0.093 mol), magnesium dichloride (13.21 g, 0.14 mol) and NEt_3 (45.1 mL, 0.32 mol) were dissolved in acetonitrile (500 mL). Paraformaldehyde (16.66 g, 0.55 mol) was added to the solution and the reaction was stirred under reflux at 85 °C for 24 hours. The reaction was cooled to room temperature prior to adding dilute HCl (50 mL). The mixture was extracted three times with diethyl ether (100 mL) and the organic

layers dried over $MgSO_4$. The crude ^1H NMR spectrum showed no sign of product formation.

6.8 Synthesis of 2-hydroxy-4-cyano-benzaldehyde using the Duff reaction

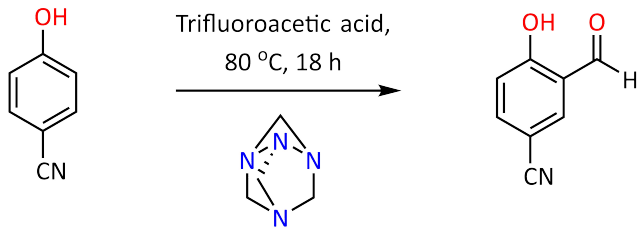

Following a modified literature procedure,[131] anhydrous hexamethylenetetramine (17.65 g, 0.13 mol) was added to a solution of 4-cyanophenol (15 g, 0.13 mol) and trifluoroacetic acid (200 mL) under nitrogen and room temperature. The reaction was heated to 110 °C for three hours and then cooled to room temperature. HCl (50 mL, 6 M) was added over one hour prior to extraction with dichloromethane (three times 200 mL) and drying the organic layers over $MgSO_4$. The crude ^1H NMR spectrum showed no sign of product formation.

6.9 Synthesis of 2-hydroxy-4-trifluoromethyl-benzaldehyde using the Duff reaction

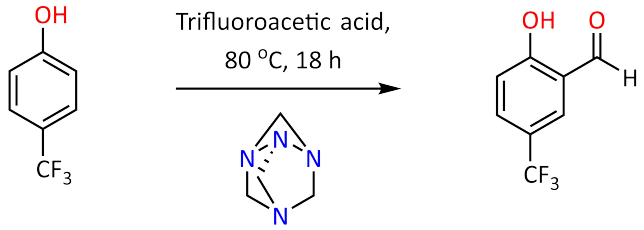

Following a modified literature procedure,[131] anhydrous hexamethylenetetramine (12.97 g, 0.093 mol) was added to a solution of 4-trifluoromethylphenol (15 g, 0.093 mol) and trifluoroacetic acid (200 mL) under nitrogen and room temperature. The

reaction was heated to 110 °C for three hours and then cooled to room temperature. HCl (50 mL, 6 M) was added over one hour prior to extraction with dichloromethane (three times 200 mL) and drying the organic layers over $MgSO_4$. The crude ^{1}H NMR spectrum showed no sign of product formation.

6.10 Synthesis of Monomers 1 to 4

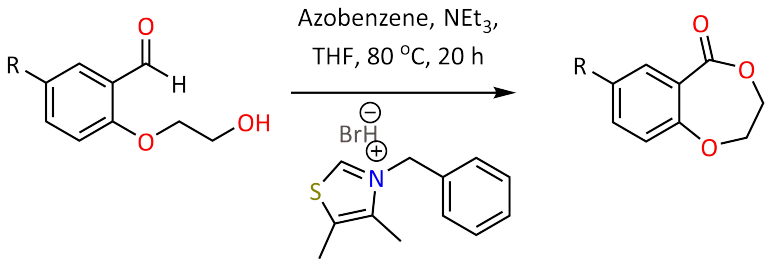

R= Me (Monomer **1**), OMe (Monomer **2**), F (Monomer **3**), Br (Monomer **4**)

2-(2-hydroxyethoxy)-5-R-benzaldehyde (5 mmol) was dissolved in THF (4 mL) in an ampoule under a positive flow of nitrogen and stirred for 5 minutes at room temperature. Azobenzene (7.5 mmol, 1.37 g), 3-benzyl-4,5-dimethyl thiazolium bromide (0.25 mmol, 0.071 g), and triethyl amine (0.4 mmol, 0.056 mL) were added to the stirring solution under nitrogen and the reaction was left to stir for 20 hours at 80 °C. Upon cooling to room temperature, the solvent was removed under vacuum to yield a bright orange oil. The monomers were afforded through purification via column chromatography using a gradient eluent system starting with 5:1 hexanes:ethyl acetate.

6.10.1 Monomer 1

: 0.78 g, 87.6 %, R_f = 0.38, m.p. = 62 °C - 64 °C, m/z = 178.06. ^{1}H NMR (500 MHz, $CDCl_3$) δ 7.67 (dd, 1H, Ar**H**), 7.30 (ddd, 1H Ar**H)**, 6.91 (d, 1H, Ar**H**), 4.46 (m, 4H, C(O)OC**H**$_2$C**H**$_2$O), 2.33 (d, 3H, ArC**H**$_3$). ^{13}C NMR (126 MHz, $CDCl_3$) δ 169.46 (**C**(O)OR), 135.91, 133.28, 132.46, 120.90, 119.26, 112.57 (Ar), 70.79 (C(O)OCH$_2$**C**H$_2$O), 65.49 (C(O)O**C**H$_2$CH$_2$O), 20.29 (Ar**C**H$_3$).

6.10.2 Monomer 2

: 0.89 g, 91.8 %, $R_f = 0.29$, m.p. = 58 °C - 60 °C, m/z = 194.06. ^{1}H NMR (500 MHz, $CDCl_3$) δ 7.30 (d, 1H, Ar**H**), 7.07 (dd, 1H Ar**H**), 6.95 (d, 1H, Ar**H**), 4.44 (s, 4H, C(O)OC$\mathbf{H}_2$C$\mathbf{H}_2$O), 3.81 (s, 3H, ArOC$\mathbf{H}_3$). ^{13}C NMR (126 MHz, $CDCl_3$) δ 169.35 (**C**(O)OR), 155.30, 148.60, 122.73, 120.84, 115.22 (Ar), 70.96 (C(O)OCH_2**C**H_2O), 65.55 (C(O)O**C**H_2CH_2O), 55.99 (ArO**C**H_3).

6.10.3 Monomer 3

: 0.87 g, 95.5 %, $R_f = 0.37$, m.p. = 74 °C - 78 °C, m/z = 182.04. ^{1}H NMR (500 MHz, $CDCl_3$) δ 7.57 (dd, 1H, Ar**H**), 7.22 (ddd, 1H Ar**H**), 7.00 (dd, 1H, Ar**H**), 4.49 (m, 4H, C(O)OC$\mathbf{H}_2$C$\mathbf{H}_2$O). ^{13}C NMR (126 MHz, $CDCl_3$) δ 167.74 (**C**(O)OR), 158.69, 156.75, 150.71, 122.68, 122.26, 118.74 (Ar), 70.79 (C(O)OCH_2**C**H_2O), 65.42 (C(O)O**C**H_2CH_2O).

6.10.4 Monomer 4

: 0.56 g, 46.5 %, $R_f = 0.35$, m.p. = 96 °C - 100 °C, m/z = 241.96. ^{1}H NMR (500 MHz, $CDCl_3$) δ 8.03 (d, 1H, Ar**H**), 7.57 (dd, 1H Ar**H**), 6.91 (d, 1H, Ar**H**), 4.51 (m, 4H, C(O)OC$\mathbf{H}_2$C$\mathbf{H}_2$O). ^{13}C NMR (126 MHz, $CDCl_3$) δ 167.72 (**C**(O)OR), 154.09, 137.99, 136.17, 123.06, 120.57, 115.06 (Ar), 71.07 (C(O)OCH_2**C**H_2O), 65.78 (C(O)O**C**H_2CH_2O).

6.11 Synthesis of P2HEB

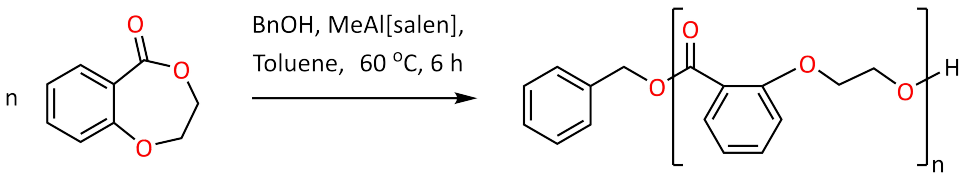

Following a modified literature procedure,[113] 2,3-DHB (1.05 g, 6.38 mmol), MeAl[salen] (42.9 mg, 0.09 mmol) and BnOH (9.4 μL, 0.09 mmol) were dissolved in toluene (0.3 mL) in an ampoule. The mixture was heated at 60 °C for six hours.

The polymerisation was quenched with 10 % dichloromethane in methanol (0.5 mL) and precipitated in cold methanol to afford an off-white solid. ^{1}H NMR (500 MHz, $CDCl_3$) δ 7.72 (dd, 1H, Ar**H**), 7.35 (dd, 1H Ar**H**), 6.94–6.86 (m, 2H, Ar**H**), 5.29 (s, 2H, PhC$\mathbf{H}_2$O) 4.55 (t, 2H, C(O)OC$\mathbf{H}_2$CH_2O), 4.25 (t, 2H, C(O)OCH_2C$\mathbf{H}_2$O). ^{13}C NMR (126 MHz, $CDCl_3$) δ 166.10 (**C**(O)OR), 158.56, 133.67, 131.87, 120.96, 120.81, 114.18 (Ar), 67.37 (C(O)OCH_2**C**H_2O), 62.97 (C(O)O**C**H_2CH_2O).

6.12 Synthesis of Polymers 1 to 4

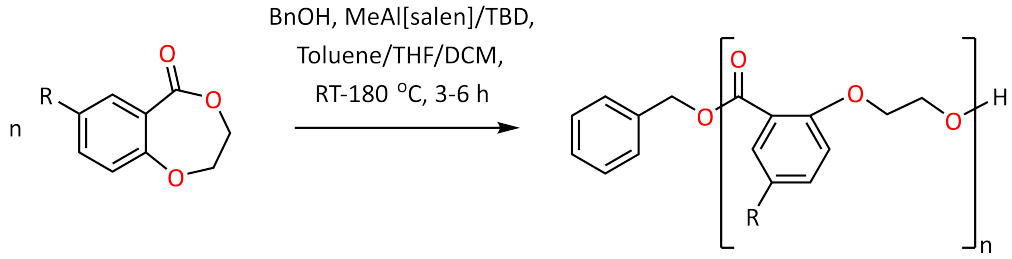

R= Me (Polymer **1**), OMe (Polymer **2**), F (Polymer **3**), Br (Polymer **4**)

Following a modified literature procedure,[113,136] the respective monomer (2.74 mmol), MeAl[salen] (9.8 mg, 0.018 mmol), BnOH (1.8 μL, 0.018 mmol) and toluene (0.1 - 0.3 mL) were added to an ampoule with a stirrer bar. The reaction was heated at 60 °C for six hours. The polymerisation was quenched with 1 mL of a 5 % methanol in dichloromethane solution and precipitated in cold methanol to afford an off-white solid.

6.12.1 Polymer 1

: ^{1}H NMR (500 MHz, $CDCl_3$) δ 7.53 (d, 1H, Ar**H**), 7.15 (dd, 1H Ar**H**), 6.83 (dd, 1H, Ar**H**), 5.28 (s, 2H, PhC$\mathbf{H}_2$O), 4.54 (t, 2H, C(O)OC$\mathbf{H}_2$CH_2O), 4.25 (dt, 2H, C(O)OCH_2C$\mathbf{H}_2$O), 2.22 (s, 3H, ArC$\mathbf{H}_3$). ^{13}C NMR (126 MHz, $CDCl_3$) δ 166.35 (**C**(O)OR), 156.12, 134.46, 132.42, 130.75, 120.91, 115.03 (Ar), 68.03 (C(O)OCH_2**C**H_2O), 63.39 (C(O)O**C**H_2CH_2O), 20.65 (Ar**C**H_3).

6.12.2 Polymer 2

: ^{1}H NMR (500 MHz, $CDCl_3$) δ 7.28 (d, 1H, Ar**H**), 6.92 (dd, 1H Ar**H**), 6.89 (d, 1H, Ar**H**), 5.28 (s, 2H, PhC$\mathbf{H}_2$O), 4.53 (t, 2H, C(O)OC$\mathbf{H}_2$CH_2O), 4.23 (t, 2H, C(O)OCH_2C$\mathbf{H}_2$O), 3.71 (s, 3H, ArOC$\mathbf{H}_3$). ^{13}C NMR (126 MHz, $CDCl_3$) δ 165.98 (**C**(O)OR), 154.17, 152.84, 122.14, 119.93, 117.54, 116.36 (Ar), 69.10 (C(O)OCH_2**C**H_2O), 63.71 (C(O)O**C**H_2CH_2O), 56.16 (ArO**C**H_3).

6.12.3 Polymer 3

: ^{1}H NMR (500 MHz, $CDCl_3$) δ 7.46 (dd, 1H, Ar**H**), 7.08 (m, 1H Ar**H**), 6.90 (dd, 1H, Ar**H**), 5.29 (s, 2H, PhC$\mathbf{H}_2$O), 4.56 (t, 2H, C(O)OC$\mathbf{H}_2$CH_2O), 4.25 (t, 2H, C(O)OCH_2C$\mathbf{H}_2$O). ^{13}C NMR (126 MHz, $CDCl_3$) δ 164.40 (**C**(O)OR), 155.66, 154.48, 121.68, 120.14, 118.17, 116.28 (Ar), 68.18 (C(O)OCH_2**C**H_2O), 63.28 (C(O)O**C**H_2CH_2O).

6.12.4 Polymer 4

: ^{1}H NMR (500 MHz, $CDCl_3$) δ 7.83 (m, 1H, Ar**H**), 7.45 (dq, 1H Ar**H**), 6.79 (d, 1H, Ar**H**), 5.29 (s, 2H, PhC$\mathbf{H}_2$O), 4.56 (t, 2H, C(O)OC$\mathbf{H}_2$CH_2O), 4.25 (t, 2H, C(O)OCH_2C$\mathbf{H}_2$O). ^{13}C NMR (126 MHz, $CDCl_3$) δ 163.90 (**C**(O)OR), 157.06, 136.27, 134.33, 126.29, 115.92 113.02 (Ar), 67.50 (C(O)OCH_2**C**H_2O), 63.09 (C(O)O**C**H_2CH_2O).

6.13 Synthesis of BnOH-initiated PLLA

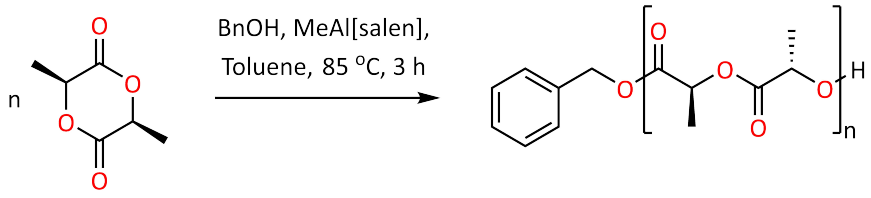

L-Lactide (2 g, 13.9 mmol), MeAl[salen] (108.4 mg, 0.2 mmol), and BnOH (20.6 μL, 0.2 mmol) were dissolved in toluene (13.8 mL) in an ampoule. The reaction was stirred for three hours at 85 °C prior to quenching with cold methanol followed by precipitation in cold methanol to afford the PLLA as a white solid. ^{1}H

NMR (500 MHz, $CDCl_3$) δ 5.16 (q, 1H, COOC**H**CH_3), 1.58 (d, 3H, COOCHC**H**$_3$). ^{13}C NMR (126 MHz, $CDCl_3$) δ 169.50 (**C**OOCHCH$_3$), 68.91 (COO**C**HCH$_3$), 16.54 (COOCH**C**H$_3$).

6.14 Synthesis of 1,3-propanediol initiated PLLA

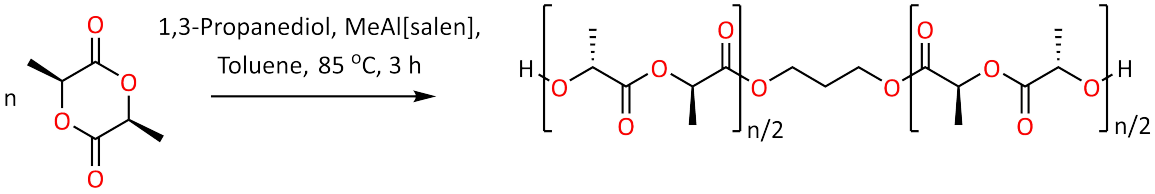

L-Lactide (2.5 g, 17.3 mmol), MeAl[salen] (271.1 mg, 0.5 mmol), and 1,3 propanediol (17.8 μL, 0.25 mmol) were dissolved in toluene (17.4 mL) in an ampoule. The reaction was stirred for three hours at 85 °C prior to quenching with cold methanol followed by precipitation in cold methanol to afford the PLLA as a white solid, ^{1}H NMR (500 MHz, $CDCl_3$) δ 5.16 (q, 1H, COOC**H**CH_3), 1.58 (d, 3H, COOCHC**H**$_3$). ^{13}C NMR (126 MHz, $CDCl_3$) δ 169.50 (**C**OOCHCH$_3$), 68.91 (COO**C**HCH$_3$), 16.53 (COOCH**C**H$_3$).

6.15 Synthesis of P2HEB-PLLA diblock copolymer

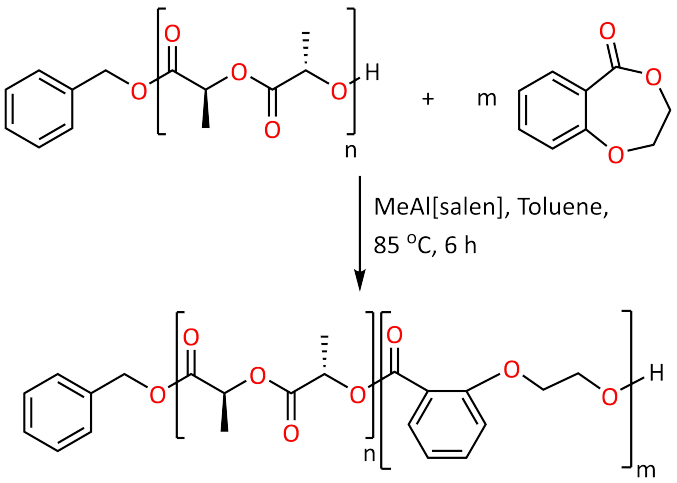

Homopolymer PLLA (0.3 g, 0.033 mmol), 2,3 DHB (0.38 g, 2.32 mmol), and MeAl[salen] (18.2 mg, 0.033 mmol) were dissolved in THF (0.3 mL) in an ampoule. The reaction was stirred for six hours at 66 °C prior to quenching with 10 % dichloromethane in methanol (0.1 mL) followed by precipitation in cold methanol to afford the diblock copolymer as an off-white solid. ^{1}H NMR (500 MHz, $CDCl_3$) δ 7.76 (t, 0.11H, Ar**H**), 7.38 (m, 0.11H Ar**H**), 6.93 (m, 0.22H, Ar**H**), 5.16 (q, 1H, C(O)C**H**(CH_3)O), 4.57 (t, 0.22H, C(O)OC**H**$_2$$CH_2$O), 4.28 (t, 0.22H, C(O)OCH_2C**H**$_2$O). ^{13}C NMR (126 MHz, $CDCl_3$) δ 169.80 (**C**(O)CH(CH_3)O), 166.10 (**C**(O)OR), 158.56, 133.67, 131.87, 120.96, 120.81, 114.18 (Ar), 68.86 (C(O)**C**H(CH_3)O), 67.37 (C(O)OCH_2**C**H_2O), 62.97 (C(O)O**C**$H_2$$CH_2$O). 16.60 (C(O)CH(**C**$H_3$)O).

6.16 Synthesis of P2HEB-PLLA-P2HEB triblock copolymer

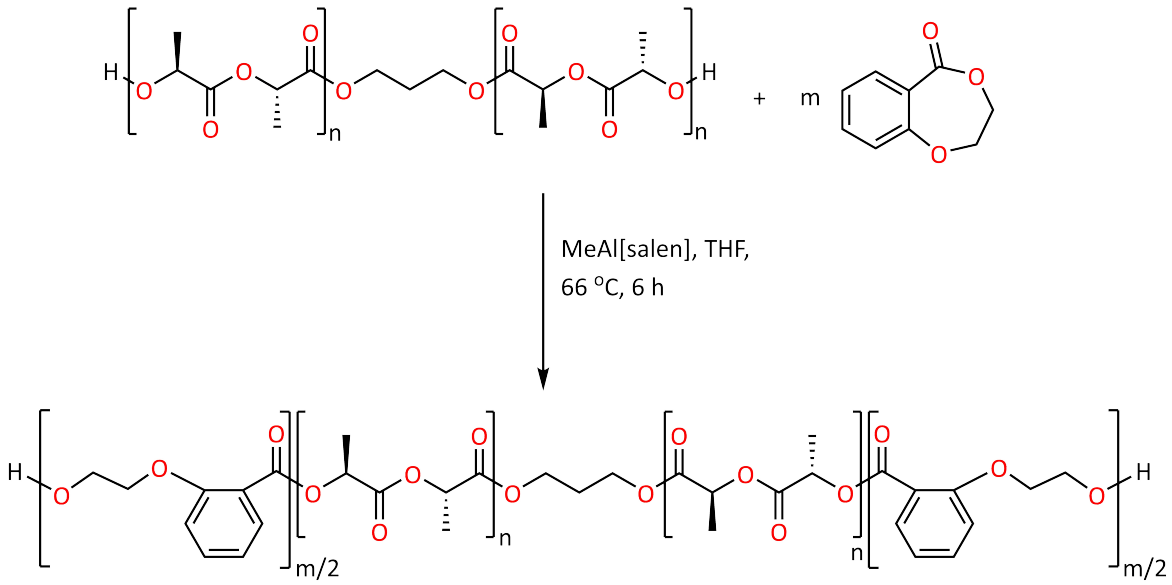

Diol homopolymer PLLA (1.4 g, 0.15 mmol), 2,3 DHB (1.7 g, 10.5 mmol), and MeAl[salen] (82.01 mg, 0.15 mmol) were dissolved in THF (0.3 mL) in an ampoule. The reaction was stirred for six hours at 66 °C prior to quenching with 10 % dichloromethane in methanol (0.1 mL) followed by precipitation in cold methanol to afford the triblock copolymer as an off-white solid. ^{1}H NMR (500 MHz, $CDCl_3$) δ 7.76 (m, 0.12H, Ar**H**), 7.38 (dd, 0.12H Ar**H**), 6.93 (m, 0.29H, Ar**H**), 5.16 (q, 1H, C(O)C**H**(CH_3)O), 4.57 (m, 0.29H, C(O)OC**H**$_2$$CH_2$O), 4.28 (m, 0.29H, C(O)OCH_2C**H**$_2$O). ^{13}C NMR (126 MHz, $CDCl_3$) δ 169.80 (**C**(O)CH(CH_3)O), 166.10 (**C**(O)OR), 158.56, 133.67, 131.87, 120.96, 120.81, 114.18 (Ar), 68.86 (C(O)**C**H(CH_3)O), 67.37 (C(O)OCH_2**C**H_2O), 62.97 (C(O)O**C**$H_2$$CH_2$O). 16.60 (C(O)CH(**C**$H_3$)O).

6.17 Degradation Studies

6.17.1 Preparation of P2HEB polymer films

P2HEB (0.50 g) of molecular weight 40,000 and 80,000 g mol^{-1} were dissolved in 6 mL of chloroform and pipetted, avoiding bubble deposition, onto a PTFE plate with a diameter of 7.4 mm. The PTFE plate was covered with a glass lid and placed on a balance to allow even evaporation of the solvent to form a film of 0.1 mm thickness.

6.17.2 Enzymatic degradation of P2HEB

Following a modified literature procedure,[16] the respective polymer films (either 1 cm^2 or cut to weigh a maximum of 12 mg) were placed in separate vials consisting of Tris-HCl buffer (5 mL, 50 mM, pH 8.6) and 1 mg of proteinase K. The vials were placed in an incubator at 37 °C on a rotary shaker set to 250 rpm. The study was carried out over 60 hours, analysing three separate replicates of each film every 12 hours. Analysis was carried out by removing the film from the buffer solution, rinsing it with distilled water and drying in vacuum at room temperature over phosphorus pentoxide until constant mass was obtained. The degradation was analysed by ^{1}H NMR spectroscopy and GPC.

6.17.3 Catalytic degradation of P2HEB

Polymers **1** to **4** and P2HEB of different molecular weights (0.0045 mmol) and MeAl[salen] (0.0045 mmol) were dissolved in toluene (0.003 M) in an ampoule. The ampoule was heated to 70 °C or 110 °C for 6 to 24 hours. Kinetic studied were perfomed on the Bruker Asance 400 MHz spectrometer in a Youngs tap NMR tube.

6.18 Blend preparation

PLLA/P2HEB blends were prepared via solvent-casting. 100/0, 80/20, 60/40, 50/50, 40/60, 20/80 and 0/100 compositions were dissolved in chloroform at a concentration of 10 % (w/w) with vigorous magnetic stirring for 60 min. The resulting

mixtures were placed onto a PTFE plate and dried at 30 °C for 96 h in an oven. 150 μm thick films were obtained.

6.19 Characterisation

6.19.1 Differential scanning calorimetry (DSC)

The thermal transitions of the polymers, copolymers and blends were determined using a Mettler Toledo DSC 822e calorimeter under nitrogen atmosphere (30 mL min^{-1}). Samples of 7 to 13 mg were sealed in an aluminium pan,heated at a rate of 10 °C min^{-1} (from -50 °C) and held at temperatures above T_m (for each polymer) for two minutes to remove the previous thermal history. Samples were then cooled again to -50 °C and a subsequent heating scan at 10 °C min^{-1} was applied. Additionally, when cooling, crystallization treatments were applied to the samples; non-isothermal crystallization by cooling the polymers and holding them at a crystallisation temperature for 300 min prior to cooling them to -30 °C.

6.19.2 Thermogravimetric analysis (TGA)

Thermal degradation of polymers, copolymers and blends were studied through thermal gravimetric analysis (TGA METTLER TOLEDO 822e) in alumina pans under nitrogen atmosphere (20 mL min^{-1}). Samples (8 to 12 mg) were heated from room temperature up to 500 °C at 2, 5, 10 and 20 °C min^{-1}.

6.19.3 Dynamic Mechanical Analysis (DMA)

DMA was performed on a DMA/SDTA861 analyser (Mettler- Toledo) in tensile mode and shear mode. 150 to 200 μm thick samples (4 mm wide and 5.5 mm long) were obtained through solvent-casting. Curves displaying storage modulus (E') and the energy loss (tan δ) were recorded as a function of temperature at a heating rate of 3 °C min^{-1}, a frequency of 1 Hz and displacement of or 0.4 % strain.

6.19.4 UV-Vis spectroscopy (UV-Vis)

UV-Vis absorption spectra were recorded with a Shimadzu MultiSpec-1501 spectrophotometer. Total transmittance experiments have been analysed in the range of 190 to 800 nm with a sampling interval of 1 nm and 25 accumulations. Approximately 150 μm thick films were obtained via solvent-casting using chloroform.

6.19.5 Wide angle X-Ray diffraction (WAXD)

X-ray powder diffraction patterns were measured using a Bruker D8 Advance diffractometer equipped with a Cu tube, Ge(111) incident beam monochromator (λ = 1.5406 Å) (fixed slit 1 mm) and a Sol-X energy dispersive detector (fixed slit 0.06 mm). The sample was mounted on a zero background silicon wafer embedded in a generic sample holder. Data were collected from 5 to 50 ° 2 θ (step size = 0.02 and time per step = 100 s, total time 60 h) at RT. A fixed divergence and antiscattering slit (1 °) giving a constant volume of sample illumination was used. The high temperature X-ray patterns of the sample was registered on a Bruker D8 Advance diffractometer operating at 30 kV and 20 mA, equipped with a Cu tube (λ = 1.5418 Å), a Vantec-1 PSD detector, and an Anton Parr HTK2000 high-temperature furnace with a direct sample heating Pt sample holder. The powder patterns were recorded in 2 θ steps of 0.033 ° in the $5 \leq 2\,\theta \leq 38$ range. The sample was measured heating and cooling in the 30 - 250 °C range, each 2 °C at 10 °C min^{-1}.

6.19.6 Morphology

SEM images were obtained via the Hitachi S-4800 field emission scanning electron microscope (FE-SEM) at an acceleration voltage of 5 kV. Before characterisation, cryogenic fractured surfaces were gold-coated (15 nm thick layer) using an Emitech K550X sputter coater.

AFM images were analysed using a Dimension ICON atomic force microscope (AFM) from Bruker (Bruker Corporation, Coventry, UK). Experiments were carried out in tapping mode with an integrated silicon tip/cantilever.

Bibliography

[1] J. Scheirs, *Modern Styrenic Polymers: Polystyrenes and Styrenic Copolymers*, John Wiley and Sons Inc, 2003.

[2] K. Mulder and M. Knot, *Technol. Soc.*, 2001, **23**, 265–286.

[3] R. M. Ogorkiewicz, *Engineering Properties of Thermoplastics*, John Wiley and Sons Inc, 1970.

[4] www.acs.org/content/acs/en/education/whatischemistry/landmarks/bakelite.html, Date Accessed: 07/08/2019.

[5] D. Walton and P. Lorimer, *Polymers*, Oxford University Press, Oxford, 2005, p. 154.

[6] B. T. Ho, T. K. Roberts and S. Lucas, *Crit. Rev. Biotechnol.*, 2017, **38**, 308–320.

[7] D. W. Van Krevelen, in *Properties of polymers their correlation with chemical structure: Their numerical estimation and prediction from additive group contributions*, Elsevier Science Bv, 2009, ch. Chapter 2, p. 1030.

[8] https://www.statista.com/statistics/282732/global-production-of-plastics-since-1950/, Date Accessed: 16/01/2019.

[9] R. Geyer, J. R. Jambeck and K. L. Law, *Sci. Adv.*, 2017, **3**, e1700782.

[10] https://edition.cnn.com/2018/03/21/health/ocean-plastic-intl/index.html, Date Accessed: 16/01/2019.

[11] F. La Mantia and A. Correnti, *Prog. Rubber. Plast. Re.*, 2003, **19**, 135–142.

[12] G. Dodbiba and T. Fujita, *Physical Separation in Science and Engineering*, 2004, **13**, 165–182.

[13] T. E. Parliament, *Directive (EU) 2018 of the european parliament and of the council*, http://data.consilium.europa.eu/doc/document/PE-11-2018-INIT/en/pdf, Date Accessed: 15/07/2019.

[14] *EU ambassadors approve new rules on waste management and recycling*, https://www.consilium.europa.eu/en/press/press-releases/2018/02/23/eu-ambassadors-approve-new-rules-on-waste-management-and-recycling/pdf, Date Accessed: 17/01/2019.

[15] A. Frydrych, Z. Florjanczyk, M. Charazinska and M. Kakol, *Polym. Degrad. Stab.*, 2016, **132**, 202–212.

[16] T. Ohkita and S. H. Lee, *J. Appl. Polym. Sci.*, 2006, **100**, 3009–3017.

[17] M. J. L. Tschan, E. Brulé, P. Haquette and C. M. Thomas, *Polym. Chem.*, 2012, **3**, 836–851.

[18] V. Mitova, G. Grancharov, C. Molero, A. M. Borreguero, K. Troev and J. F. Rodriguez, *J. Macromol. Sci. A*, 2013, **50**, 774–795.

[19] S. Ray and R. P. Cooney, *Thermal Degradation of Polymer and Polymer Composites*, Elsevier, 2018, pp. 185–206.

[20] E. Yousif and R. Haddad, *SpringerPlus*, 2013, **2**, 398.

[21] M. A. Elsawy, K. H. Kim, J.-W. Park and A. Deep, *Renew. Sust. Energ. Rev.*, 2017, **79**, 1346–1352.

[22] U. Witt, T. Einig, M. Yamamoto, I. Kleeberg, W.-D. Deckwer and R.-J. Müller, *Chemosphere*, 2001, **44**, 289–299.

[23] C. Bastioli, *Handbook of Biodegradable Polymers*, Smithers Rapra Press, 2005.

[24] J. Rydz, W. Sikorska, M. Kyulavska and D. Christova, *Int. J. Mol. Sci.*, 2014, **16**, 564–596.

[25] J. N. Hoskins and S. M. Grayson, *Polym. Chem.*, 2011, **2**, 289–299.

[26] H. R. Kricheldorf, *Chemosphere*, 2001, **43**, 49–54.

[27] J. P. L. David Walton, *Polymers*, Oxford Univesrsity Press, 2001.

[28] L. W. McKeen, in *The Effect of Creep and Other Time Related Factors on Plastics and Elastomers*, Elsevier, 2009, pp. 115–165.

[29] M. Vert, S. M. Li, G. Spenlehauer and P. Guerin, *J. Mater. Sci. Mater. M.*, 1992, **3**, 432–446.

[30] W. H. Carothers and J. A. Arvin, *J. Am. Chem. Soc.*, 1929, **51**, 2560–2570.

[31] T. J. Matray, R. J. Twieg and J. L. Hedrick, in *Step-Growth Polymers for High-Performance Materials*, American Chemical Society, 1996, pp. 266–275.

[32] W. F. Su, *Principles of Polymer Design and Synthesis*, Springer Berlin Heidelberg, 2013.

[33] T. Yokozawa, *J. Synth. Org. Chem. Jpn.*, 2002, **60**, 62–73.

[34] K. M. Nampoothiri, N. R. Nair and R. P. John, *Bioresour. Technol.*, 2010, **101**, 8493–8501.

[35] W. A. Ma, L. Wang and Z. X. Wang, *Dalton Trans.*, 2011, **40**, 4669–4677.

[36] M. Okada, H. Sumitomo, M. Atsumi and H. K. Hall, *Makromol. Chem-M. Symp.*, 1991, **42-3**, 355–364.

[37] B. D. Ulery, L. S. Nair and C. T. Laurencin, *J. Polym. Sci. Pol. Phys.*, 2011, **49**, 832–864.

[38] G. Scott, *Biodegradable Polymers for Industrial Applications*, Elsevier, 1st edn., 2005, p. 552.

[39] H. Seyednejad, A. H. Ghassemi, C. F. van Nostrum, T. Vermonden and W. E. Hennink, *J. Control. Release*, 2011, **152**, 168–176.

[40] Y. Ikada and H. Tsuji, *Macromol. Rapid Commun.*, 2000, **21**, 117–132.

[41] O. Nuyken and S. Pask, *Polymers*, 2013, **5**, 361–403.

[42] B. Rieger, A. Künkel, G. W. Coates, R. Reichardt, E. Dinjus and T. A. Zevaco, *Synthetic Biodegradable Polymers*, Springer Berlin Heidelberg, 2012.

[43] A. P. Dove, *ACS Macro Lett.*, 2012, **1**, 1409–1412.

[44] K. Makiguchi, S. Kikuchi, K. Yanai, Y. Ogasawara, S. Sato, T. Satoh and T. Kakuchi, *J. Polym. Sci. Pol. Chem.*, 2014, **52**, 1047–1054.

[45] K. Makiguchi, T. Satoh and T. Kakuchi, *Macromolecules*, 2011, **44**, 1999–2005.

[46] F. Stassin, O. Halleux and R. Jerome, *Macromolecules*, 2001, **34**, 775–781.

[47] V. W. Dittrich and R. C. Schulz, *Angew. Makromol. Chem.*, 1971, **15**, 109–126.

[48] O. Dechy-Cabaret, B. Martin-Vaca and D. Bourissou, *Chem. Rev.*, 2004, **104**, 6147–6176.

[49] Teranish.K, M. Iida, T. Araki, Yamashit.S and H. Tani, *Macromolecules*, 1974, **7**, 421–427.

[50] R. A. Gross, Y. Zhang, G. Konrad and R. W. Lenz, *Macromolecules*, 1988, **21**, 2657–2668.

[51] A. Hamitou, T. Ouhadi, R. Jerome and P. Teyssie, *J. Polym. Sci. Pol. Chem.*, 1977, **15**, 865–873.

[52] K. A. Winship, *Adverse Drug React. Toxicol. Rev.*, 1988, **7**, 19–38.

[53] J. W. Kramer, E. B. Lobkovsky and G. W. Coates, *Org. Lett.*, 2006, **8**, 3709–3712.

[54] K. Masutani and Y. Kimura, in *PLA Synthesis. From the Monomer to the Polymer*, ed. A. Jimenez, M. Peltzer and R. Ruseckaite, Royal Soc Chemistry, Cambridge, 2015, pp. 3–36.

[55] X. Y. Zhang, G. O. Jones, J. L. Hedrick and R. M. Waymouth, *Nat. Chem.*, 2016, **8**, 1047–1053.

[56] A. C. Albertsson and I. K. Varma, *Biomacromolecules*, 2003, **4**, 1466–1486.

[57] B. Gao, R. L. Duan, X. Pang, X. Li, Z. Qu, Z. H. Tang, X. L. Zhuang and X. S. Chen, *Organometallics*, 2013, **32**, 5435–5444.

[58] N. Spassky, M. Wisniewski, C. Pluta and A. L. Borgne, *Macromol. Chem. Phys.*, 1996, **197**, 2627–2637.

[59] N. S. V. Vincens, A. Le Borgne, *Makromol. Chem. Macromol. Symp.*, 1991, **47**, 285–291.

[60] P. G. Cozzi, *Chem. Soc. Rev.*, 2004, **33**, 410–421.

[61] M. Wisniewski, A. L. Borgne and N. Spassky, *Macromol. Chem. Phys.*, 1997, **198**, 1227–1238.

[62] P. A. Cameron, D. Jhurry, V. C. Gibson, A. J. P. White, D. J. Williams and S. Williams, *Macromol. Rapid Commun.*, 1999, **20**, 616–618.

[63] E. D. Cross, L. E. N. Allan, A. Decken and M. P. Shaver, *J. Polym. Sci. Pol. Chem.*, 2013, **51**, 1137–1146.

[64] J. P. MacDonald, M. Sidera, S. P. Fletcher and M. P. Shaver, *Eur. Polym. J.*, 2016, **74**, 287–295.

[65] W. H. Carothers, G. L. Dorough and F. J. van Natta, *J. Am. Chem. Soc.*, 1932, **54**, 761–772.

[66] D. Garlotta, *J. Polym. Environ.*, 2001, **9**, 63–84.

[67] T. Chandy, G. S. Das, R. F. Wilson and G. H. R. Rao, *J. Appl. Polym. Sci.*, 2002, **86**, 1285–1295.

[68] T. G. Park, M. J. Alonso and R. Langer, *J. Appl. Polym. Sci.*, 1994, **52**, 1797–1807.

[69] R. Zhang and P. X. Ma, *Macromol. Biosci.*, 2004, **4**, 100–111.

[70] S. I. Moon, C. W. Lee, M. Miyamoto and Y. Kimura, *J. Polym. Sci. Pol. Chem.*, 2000, **38**, 1673–1679.

[71] M. F. C. de Andrade, P. M. S. Souza, O. Cavalett and A. R. Morales, *J. Polym. Environ.*, 2016, **24**, 372–384.

[72] H. Urayama, S. I. Moon and Y. Kimura, *Macromol. Mater. Eng.*, 2003, **288**, 137–143.

[73] M. P. Shaver and D. J. A. Cameron, *Biomacromolecules*, 2010, **11**, 3673–3679.

[74] T. M. Ovitt and G. Coates, *J. Polym. Sci. Pol. Chem.*, 2000, **38**, 4686–4692.

[75] Z. Zhong, P. J. Dijkstra and J. Feijen, *J. Am. Chem. Soc.*, 2003, **125**, 11291–11298.

[76] W. Zhao, Y. Wang, X. Liu, X. Chen, D. Cui and E. Y. X. Chen, *Chem. Commun.*, 2012, **48**, 6375–6377.

[77] D. Rasselet, A. Ruellan, A. Guinault, G. Miquelard-Garnier, C. Sollogoub and B. Fayolle, *Eur. Polym. J.*, 2014, **50**, 109–116.

[78] M. Kaci, A. Benhamida, L. Zaidi, N. Touati and C. Remili, in *Ecosustainable Polymer Nanomaterials for Food Packaging*, CRC Press, 2013, pp. 281–312.

[79] M. A. Elsawy, K. H. Kim, J.-W. Park and A. Deep, *Renew. Sust. Energ. Rev.*, 2017, **79**, 1346–1352.

[80] S. H. Lee, I. Y. Kim and W. S. Song, *Macromol. Res.*, 2014, **22**, 657–663.

[81] M. Jamshidian, E. A. Tehrany, M. Imran, M. Jacquot and S. Desobry, *Comprehensive Reviews in Food Science and Food Safety*, 2010, **9**, 552–571.

[82] V. M. Pathak and Navneet, *Bioresources and Bioprocessing*, 2017, **4**, 1 –31.

[83] H. Pranamuda, Y. Tokiwa and H. Tanaka, *Appl. Environ. Microbiol.*, 1997, **63**, 1637–1640.

[84] S. Sukkhum and V. Kitpreechavanich, *New Insight into Biodegradation of Poly (L-Lactide), Enzyme Production and Characterization*, InTech, 2011.

[85] Y. Ikura and T. Kudo, *J. Gen. Appl. Microbiol.*, 1999, **45**, 247–251.

[86] K. Nakamura, *J. Exp. Psychol. Anim. B*, 2001, **27**, 345–353.

[87] A. Jarerat, H. Pranamuda and Y. Tokiwa, *Macromol. Biosci.*, 2002, **2**, 420–428.

[88] X. Qi, Y. Ren and X. Wang, *Int. Biodeter. Biodegr.*, 2017, **117**, 215–223.

[89] V. Vichaibun and M. Chulavatnatol, *ScienceAsia*, 2003, **29**, 297.

[90] D. F. Williams, *Eng. Med.*, 1981, **10**, 5–7.

[91] Y. Oda, A. Yonetsu, T. Urakami and K. Tonomura, *J. Polym. Environ.*, 2000, **8**, 29–32.

[92] T. Q. Liu, T. L. Simmons, D. A. Bohnsack, M. E. Mackay, M. R. Smith and G. L. Baker, *Macromolecules*, 2007, **40**, 6040–6047.

[93] J. Rieger, *J. Therm. Anal.*, 1996, **46**, 965–972.

[94] I. Oral, H. Guzel and G. Ahmetli, *Polym. Bull.*, 2011, **67**, 1893–1906.

[95] S. H. Wilen, C. B. Kremer and I. Waltcher, *J. Chem. Educ.*, 1961, **38**, 304.

[96] Y. Otake, T. Kobayashi, H. Asabe, N. Murakami and K. Ono, *J. Appl. Polym. Sci.*, 1995, **56**, 1789–1796.

[97] J. Wunsch, *Polystyrene - Synthesis, Production and Applications*, Rapra Technology Ltd, 1999.

[98] A. Buchard, D. R. Carbery, M. G. Davidson, P. K. Ivanova, B. J. Jeffery, G. I. Kociok-Kohn and J. P. Lowe, *Angew. Chem. Int. Ed.*, 2014, **53**, 13858–13861.

[99] S. A. Cairns, A. Schultheiss and M. P. Shaver, *Polym. Chem.*, 2017, **8**, 2990–2996.

[100] J. R. Whinfield and J. T. Dickson, *Polymeric Linear Terephthalic Esters*, 1949, https://patents.google.com/patent/US2465319.

[101] H. Webb, J. Arnott, R. Crawford and E. Ivanova, *Polymers*, 2012, **5**, 1–18.

[102] S. Venkatachalam, G. Shilpa, V. Jayprakash, R. Prashant, R. Krishna and K. Anil, in *Polyester*, InTech, 2012, p. 75 to 98.

[103] https://www.plasticseurope.org/en/resources/publications/274-plastics-facts-2017, Date Accessed: 18/06/2019.

[104] D. Paszun and S. Tadeusz, *Ind. Eng. Chem. Res.*, 1997, **36**, 1373–1383.

[105] X. Han, W. Liu, J. W. Huang, J. Ma, Y. Zheng, T. P. Ko, L. Xu, Y. S. Cheng, C. C. Chen and R. T. Guo, *Nat. Commun.*, 2017, **8**, 2 – 6.

[106] S. Yoshida, K. Hiraga, T. Takehana, I. Taniguchi, H. Yamaji, Y. Maeda, K. Toyohara, K. Miyamoto, Y. Kimura and K. Oda, *Science*, 2016, **351**, 1196–1199.

[107] H. P. Austin, M. D. Allen, B. S. Donohoe, N. A. Rorrer, F. L. Kearns, R. L. Silveira, B. C. Pollard, G. Dominick, R. Duman, K. E. Omari, V. Mykhaylyk, A. Wagner, W. E. Michener, A. Amore, M. S. Skaf, M. F. Crowley, A. W. Thorne, C. W. Johnson, H. L. Woodcock, J. E. McGeehan and G. T. Beckham, *Proc. Nat. Acad. Sci.*, 2018, **115**, E4350–E4357.

[108] H. Seo, S. Kim, H. F. Son, H.-Y. Sagong, S. Joo and K.-J. Kim, *Biochem. Bioph. Res. Co.*, 2019, **508**, 250–255.

[109] S. W. Lee, M. Ree, C. E. Park, Y. K. Jung, C. S. Park, Y. S. Jin and D. C. Bae, *Polymer*, 1999, **40**, 7137–7146.

[110] A. E. Tonelli, *J. Polym. Sci. Pol. Phys.*, 2002, **40**, 1254–1260.

[111] R. C. Y. Liu, J. Lusztyk, M. A. McAllister, T. T. Tidwell and B. D. Wagner, *J. Am. Chem. Soc.*, 1998, **120**, 6247–6251.

[112] R. Koch, R. J. Blanch and C. Wentrup, *J. Org. Chem.*, 2014, **79**, 6978–6986.

[113] J. P. MacDonald and M. P. Shaver, *Polym. Chem.*, 2016, **7**, 553–559.

[114] T. L. Church, Y. D. Y. L. Getzler and G. W. Coates, *J. Am. Chem. Soc.*, 2006, **128**, 10125–10133.

[115] M. Mulzer, W. C. Ellis, E. B. Lobkovsky and G. W. Coates, *Chem. Sci.*, 2014, **5**, 1928.

[116] Y. Tamai, H. Yoshiwara, M. Someya, J. Fukumoto and S. Miyano, *J. Chem. Soc., Chem. Commun.*, 1994, 2281–2282.

[117] T. Hattori, Y. Suzuki, O. Uesugi, S. Oi and S. Miyano, *Chem. Commun.*, 2000, 73–74.

[118] M. Hmamouchi and R. E. Prudhomme, *J. Polym. Sci. A1*, 1991, **29**, 1281–1291.

[119] R. Aumann and H. Ring, *Angew. Chem. Int. Ed.*, 1977, **16**, 50–50.

[120] M. Mulzer, B. T. Whiting and G. W. Coates, *J. Am. Chem. Soc.*, 2013, **135**, 10930–10933.

[121] Y. Kamiya, K. Kawato and H. Ohta, *Chem. Lett.*, 1980, **42**, 1549–1552.

[122] A. Cowell and J. K. Stille, *J. Am. Chem. Soc.*, 1980, **102**, 4193–4198.

[123] H. Li, A. Spannenberg, H. Neumann, M. Beller and X.-F. Wu, *Chem. Commun.*, 2014, **50**, 2114–2116.

[124] C. A. Rose and K. Zeitler, *Org. Lett.*, 2010, **12**, 4552–4555.

[125] N. U. Hofsløkken, L. Skattebøl, F. Johansson, S. K. Bertilsson, P. G. Andersson, J. Møller, A. Senning, X.-K. Yao, H.-G. Wang, J. P. Tuchagues and M. Ögren, *Acta Chem. Scand.*, 1999, **53**, 258–262.

[126] G. Casiraghi, G. Casnati, G. Puglia, G. Sartori and G. Terenghi, *J. Chem. Soc. Perk. T. 1*, 1980, 1862.

[127] L. P. Hammett, *J. Am. Chem. Soc.*, 1937, **59**, 96–103.

[128] D. H. McDaniel and H. C. Brown, *J. Org. Chem.*, 1958, **23**, 420–427.

[129] H. H. Jaffe, *Chem. Rev.*, 1953, **53**, 191–261.

[130] M. Lewis, C. Bagwill, L. K. Hardebeck and S. Wireduaah, *Computational and Structural Biotechnology Journal*, 2012, **1**, e201204004.

[131] N. Grimblat, A. M. Sarotti, T. S. Kaufman and S. O. Simonetti, *Org. Biomol. Chem.*, 2016, **14**, 10496–10501.

[132] S. Saito, in *Comprehensive Organometallic Chemistry III*, Elsevier, 2007, pp. 245–296.

[133] M. O. Miranda, Y. DePorre, H. Vazquez-Lima, M. A. Johnson, D. J. Marell, C. J. Cramer and W. B. Tolman, *Inorg. Chem.*, 2013, **52**, 13692–13701.

[134] A. I. Ojeda-Amador, A. J. Martínez-Martínez, A. R. Kennedy and C. T. O'Hara, *Inorg. Chem.*, 2016, **55**, 5719–5728.

[135] P. McKeown, J. Brown-Humes, M. G. Davidson, M. F. Mahon, T. J. Woodman and M. D. Jones, *Dalton Trans.*, 2017, **46**, 5048–5057.

[136] E. Lizundia, V. A. Makwana, A. Larraaga, J. L. Vilas and M. P. Shaver, *Polym. Chem.*, 2017, **8**, 3530–3538.

[137] C. Hagiopol, in *Reference Module in Materials Science and Materials Engineering*, Elsevier, 2016, ch. N/A, p. N/A.

[138] A. D. Jenkins, P. Kratochvíl, R. F. T. Stepto and U. W. Suter, *Pure Appl. Chem.*, 1996, **68**, 2287–2311.

[139] H. Feng, X. Lu, W. Wang, N. Kang and J. Mays, *Polymers*, 2017, **9**, 494.

[140] M. Chanda, *Introduction to Polymer Science and Chemistry: A Problem-Solving Approach, Second Edition*, CRC Press, 2013.

[141] M. Jamshidian, E. A. Tehrany, M. Imran, M. Jacquot and S. Desobry, *Compr. Rev. Food Sci. Food Saf.*, 2010, **9**, 552–571.

[142] R. A. Gross and B. Kalra, *Science*, 2002, **297**, 803–807.

[143] G. Sabbatier, A. Larraaga, g. A. A. Guay B, J. Fernandez, F. Di val, B. Durand, J. R. Sarasua and G. t. Laroche, *Macromol. Biosci.*, 2015, **15**, 1392–1410.

[144] J. K. Oh, *Soft Matter*, 2011, **7**, 5096.

[145] O. Jeon, S. H. Lee, S. H. Kim, Y. M. Lee and Y. H. Kim, *Macromolecules*, 2003, **36**, 5585–5592.

[146] C. M. Zhang, T. L. Zhai, L. S. Turng and Y. Dan, *Ind. Eng. Chem. Res.*, 2015, **54**, 9505–9511.

[147] E. Stirling, Y. Champouret and M. Visseaux, *Polym. Chem.*, 2018, **9**, 2517–2531.

[148] S.-R. Z. Ru-Min Wang, *Polymer Matrix Composites and Technology*, Woodhead Pub, 2011.

[149] E. Lizundia, J. L. Vilas and L. M. León, *Carbohydr. Polym.*, 2015, **123**, 256–265.

[150] E. Lizundia, J. L. Vilas, A. Sangroniz and A. Etxeberria, *Eur. Polym. J.*, 2017, **91**, 10–20.

[151] J. Ahmed, S. K. Varshney and F. Janvier, *J. Therm. Anal. Calorim.*, 2014, **115**, 2053–2061.

[152] J. Dai, H. Bai, Z. Liu, L. Chen, Q. Zhang and Q. Fu, *RSC Adv.*, 2016, **6**, 17008–17015.

[153] G. Pound-Lana, J.-M. Rabanel, P. Hildgen and V. C. F. Mosqueira, *Eur. Polym. J.*, 2017, **90**, 344–353.

[154] M. Harada, K. Iida, K. Okamoto, H. Hayashi and K. Hirano, *Polym. Eng. Sci.*, 2008, **48**, 1359–1368.

[155] X. Lu, J. Q. Zhao, X. Y. Yang and P. Xiao, *Polym. Test.*, 2017, **60**, 58–67.

[156] Y. K. Dasan, A. H. Bhat and F. Ahmad, *Carbohydr. Polym.*, 2017, **157**, 1323–1332.

[157] K. Chavalitpanya and S. Phattanarudee, *Energy Proced.*, 2013, **34**, 542–548.

[158] S. M. Davachi, *Carbohydr. Polym.*, 2017, **155**, 336–344.

[159] X. Hao, J. Kaschta, Y. Pan, X. Liu and D. W. Schubert, *Polymer*, 2016, **82**, 57–65.

[160] V. A. Makwana, E. Lizundia, A. Larrañaga, J. L. Vilas and M. P. Shaver, *Green Materials*, 2018, **6**, 85–96.

[161] S. Li, A.Girard, H. Garreau and M.Vert, *Polym. Degrad. Stabil.*, 2001, **71**, 61–67.

[162] Z. X. Zhao, L. Yang, Y. F. Hu, Y. He, J. Wei and S. M. Li, *Polym. Degrad. Stab.*, 2007, **92**, 1769–1777.

[163] S. Koltzenburg, M. Maskos and O. Nuyken, *Polymere: Synthese, Eigenschaften und Anwendungen*, Springer-Verlag GmbH, 2013.

[164] R. J.Muller, H. Schrader, J. Profe, K. Dresler and W. D. Deckwer, *Macromol. Rapid Commun.*, 2005, **26**, 1400–1405.

[165] L. H. Sperling, *Introduction to Physical Polymer Science*, Blackwell Science Publishing, 2006, vol. 78, p. 845.

[166] S. Rastogi, D. R. Lippits, G. W. M. Peters, R. Graf, Y. Yao and H. W. Spiess, *Nat. Mater.*, 2005, **4**, 635–641.

[167] D. Jauffre, O. Lame, G. Vigier and F. Dore, *Macromolecules*, 2008, **41**, 9793–9801.

[168] C. Romain, B. Heinrich, S. B. Laponnaz and S. Dagorne, *Chem. Commun.*, 2012, **48**, 2213.

[169] S. Yamazaki, M. Hikosaka, A. Toda, I. Wataoka and F. Gu, *Polymer*, 2002, **43**, 6585–6593.

[170] T. F. L. McKenna, A. D. Martino, G. Weickert and J. B. P. Soares, *Macromol. React. Eng.*, 2010, **4**, 40–64.

[171] J. L. Carvalho, S. L. Cormier, N. Lin and K. Dalnoki Veress, *Macromolecules*, 2012, **45**, 1688–1691.

[172] S. Andjelić and R. Scogna, *J. Appl. Polym. Sci.*, 2015, **132**, 1–15.

[173] V. T. Popa and E. Segal, *J. Therm. Anal. Calorim.*, 2002, **69**, 149–161.

[174] R. O. Ebewele, *Polymer Science and Technology*, CRC Press, 2000.

[175] A. Larranaga, S. Petisco and J. R. Sarasua, *Polym. Degrad. Stab.*, 2013, **98**, 1717–1723.

[176] B. V. Kokta, J. L. Valade and W. N. Martin, *J. Appl. Polym. Sci.*, 1973, **17**, 1–19.

[177] A. Q. Gu, Z. L. Yu and Y. B. Li, *J. Appl. Polym. Sci.*, 2009, **114**, 911–918.

[178] R. M. Wellen and E. L. Canedo, *Polym. Test.*, 2014, **40**, 33–38.

[179] K. Król-Morkisz and K. Pielichowska, in *Polymer Composites with Functionalized Nanoparticles*, Elsevier, 2019, pp. 405 – 435.

[180] E. Lizundia, P. Susana and S. Jose-Ramon, *J. Mech. Behav. Biomed. Mater.*, 2012, **17**, 242–251.

[181] J. Fernandez, A. Larranaga, A. Etxeberria and J. R. Sarasua, *J. Mech. Behav. Biomed. Mater.*, 2014, **35**, 39–50.

[182] P. Scherrer, *Nachrichten von der Gesellschaft der Wissenschaften zu Göttingen, Mathematisch-Physikalische Klasse*, 1918, **2**, 98–100.

[183] A. Rudin and P. Choi, in *The Elements of Polymer Science & Engineering*, Elsevier, 2013, pp. 149–229.

[184] E. Erbas, Kiziltas, A., Kiziltas, S., C. Bollin and D. J. Gardner, *Carbohydr. Polym.*, 2015, **127**, 381–389.

[185] B. Cullity and S. Stock, *Elements of X-ray Diffraction, Third Edition*, Prentice-Hall, 2001.

[186] http://www.ccdc.cam.ac.uk, Date Accessed: 06/05/2017.

[187] H. M. Rietveld, *J. Appl. Crystallogr.*, 1969, **2**, 65–71.

[188] J. R. Carvajal, *Phys. B Condens. Matter*, 1993, **192**, 55–69.

[189] J. R. Carvajal, *Commission On Powder Diffraction (IUCr)*, 2001, **26**, 12–19.

[190] W. E. Donath, *J. Chem. Phys.*, 1963, **39**, 2685–2688.

[191] L. T. Lim, R. Auras and M. Rubino, *Prog. Polym. Sci.*, 2008, **33**, 820–852.

[192] E. Lizundia and A. Larraaga, *RSC Adv.*, 2016, 11943–11951.

[193] J. Fernandez, A. Etxeberria and J.-R. Sarasua, *RSC Adv.*, 2016, **6**, 3137–3149.

[194] K. N. Turhan and Şahbaz F., *Polym. Int.*, 2001, **50**, 1138–1142.

[195] R. Auras, B. Harte and S. Selke, *Macromol. Biosci.*, 2004, **4**, 835–864.

[196] E. Lizundia and L. Ruiz-Rubio, *J. Appl. Polym. Sci.*, 2016, **132**, 42426.

[197] R. A. Auras, L. T. Lim, S. E. M. Selke and H. Tsuji, *Poly(lactic acid): Synthesis, Structures, Properties, Processing, and Applications*, John Wiley & Sons, Inc, 2010, p. 528.

[198] Z. Hu and E. Reichmanis, *J. Polym. Sci., Part A: Polym. Chem.*, 2011, **49**, 1155–1162.

[199] J. Gutierrez, S. Carrasco Hernandez, H. S. Barud, R. L. Oliveira, R. A. Carvalho, A. C. Amaral and A. Tercjak, *Carbohydr. Polym.*, 2017, **165**, 437–443.

[200] M. Narayanan, S. Loganathan, R. B. Valapa, S. Thomas and T. O. Varghese, *Int. J. Biol. Macromol.*, 2017, **99**, 37–45.

[201] H. C. Kim, S. M. Park and W. D. Hinsberg, *Chem. Rev.*, 2010, **110**, 146–177.

[202] M. J. Kristo, in *Handbook of Radioactivity Analysis*, Elsevier, 2012, pp. 1281–1304.

[203] Y. Yan, in *Metals for Biomedical Devices*, Elsevier, 2010, pp. 178–201.

[204] R. M. Dorin, H. Sai and U. Wiesner, *Chem. Mater.*, 2014, **26**, 339–347.

[205] L. Rueda-Larraz, B. F. Arlas, A. Tercjak, A. Ribes, I. Mondragon and A. Eceizaa, *Eur. Polym. J.*, 2009, **45**, 2096–2109.

[206] H. Wang, P. Yang, R. Zhu and Y. Gu, *RSC Adv.*, 2016, **6**, 15271–15278.

[207] A. A. Aydin and V. Ilberg, *Carbohydr. Polym.*, 2016, **136**, 441–448.

[208] E. Lizundia, F. Gmez-Galvn, L. Prez, L. M. Len Alvarez and J. L. Vilas, *Carbohydr. Polym.*, 2016, **144**, 25–32.

[209] A. Morro, F. Catalina, T. Corrales, J. L. Pablos, I. Marin and C. Abrusci, *Carbohydr. Polym.*, 2016, **149**, 68–76.

[210] E. Lizundia, A. Oleaga, A. Salazar and J. R. Sarasua, *Polymer*, 2012, **53**, 2412–2421.

[211] H. Tsuji, Y. Tezuka, S. K. Saha, M. Suzuki and S. Itsuno, *Polymer*, 2005, **46**, 4917–4927.

[212] E. Lizundia, E. Meaurio, J. M. Laza and J. L. Vilas, *Mat. Sci. Eng. C*, 2015, **50**, 97–106.

[213] V. Ojijo, *ACS Appl. Mater. Inter.*, 2012, **4**, 6690–6701.

[214] M. Rizzuto, A. Mugica, M. Zubitur, D. Caretti and A. J. Muller, *CrystEngComm*, 2016, **18**, 2014–2023.

[215] Y. Li, L. Liu, Y. Shi, F. Xiang, T. Huang, Y. Wang and Z. Zhou, *J. Appl. Polym. Sci.*, 2011, **121**, 2688–2698.

[216] J. Rehbein, S. M. Ruser and J. Phan, *Chem. Sci.*, 2015, **6**, 6013–6018.